

AD-A141 236

MODELLING OF IONOSPHERIC IRREGULARITIES AND TOTAL  
ELECTRON CONTENT(U) EMMANUEL COLL BOSTON MASS PHYSICS  
RESEARCH DIV S BASU ET AL. DEC 83 AFGL-TR-84-0032

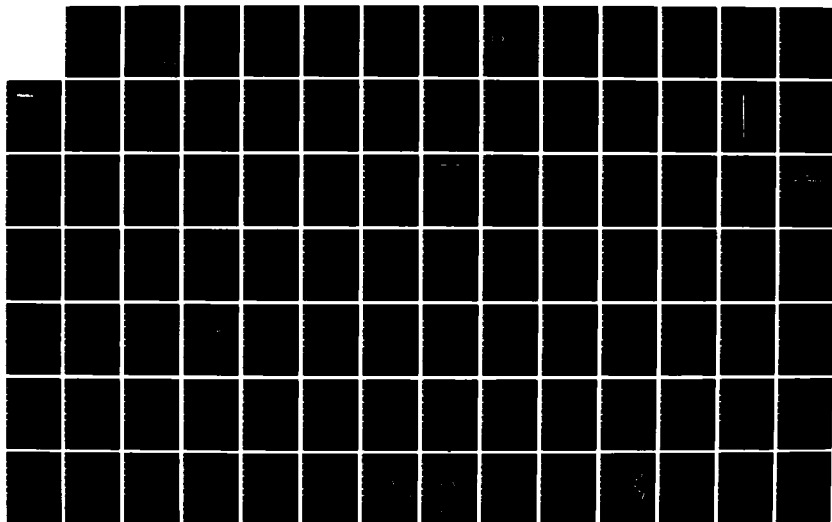
1/2

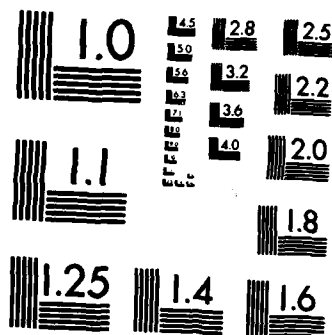
UNCLASSIFIED

F19628-81-K-0011

FFG 4/1

NL





MICROCOPY RESOLUTION TEST CHART  
NATIONAL BUREAU OF STANDARDS-1963-A

12

AFGL-TR- 84-0032

MODELLING OF IONOSPHERIC IRREGULARITIES AND TOTAL ELECTRON CONTENT

Santimay Basu  
Sunanda Basu  
Patricia Doherty  
Eileen MacKenzie  
M.P. Hagan

AD-A141 236

The Trustees of Emmanuel College  
400 The Fenway  
Boston, Massachusetts 02115

Final Report  
14 November 1980 - 13 November 1983

December 1983

Approved for public release; distribution unlimited

DTIC FILE COPY

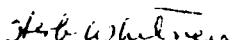
AIR FORCE GEOPHYSICS LABORATORY  
AIR FORCE SYSTEMS COMMAND  
UNITED STATES AIR FORCE  
HANSCOM AFB, MASSACHUSETTS 01731


DTIC  
ELECTE  
MAY 21 1984  
S B

84 05 21 001

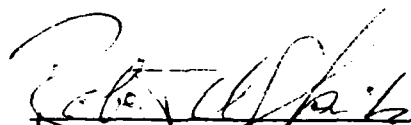
This report has been reviewed by the ESD Public Affairs Office (PA) and is releasable to the National Technical Information Service (NTIS).

This technical report has been reviewed and is approved for publication

  
HERBERT WHITNEY  
Ionospheric Physics Branch  
Ionospheric Physics Division

  
HERBERT C. CARLSON, JR., CHIEF  
Ionospheric Physics Branch  
Ionospheric Physics Division

FOR THE COMMANDER

  
ROBERT A. STRIVANEK  
ACTING DIRECTOR  
Ionospheric Physics Division

Qualified requestors may obtain additional copies from the Defense Technical Information Center. All other should apply to the National Technical Information Service.

If your address has changed, or if you wish to be removed from the mailing list, or if the addressee is no longer employed by your organization, please notify AFGL/DAA, Hanscom AFB, MA 01731. This will assist us in maintaining a current mailing list.

Do not return copies of this report unless contractual obligations or notices on a specific document requires that it be returned.



Unclassified

MIL-STD-847A  
31 January 1973

SECURITY CLASSIFICATION OF THIS PAGE (When Data Entered)

REPORT DOCUMENTATION PAGE		READ INSTRUCTIONS BEFORE COMPLETING FORM
1. REPORT NUMBER AFGL-TR- 84-0032	2. GOVT ACCESSION NO. <b>AD A44 4236</b>	3. RECIPIENT'S CATALOG NUMBER
4. TITLE (and Subtitle) <i>Modelling of Ionospheric Irregularities and Total Electron Content</i>		5. TYPE OF REPORT & PERIOD COVERED <i>Final</i> <i>14 Nov 80 - 13 Nov 83</i>
7. AUTHOR(s) <i>Santimay Basu Patricia Doherty</i> <i>Sunanda Basu Eileen MacKenzie</i> <i>M.P. Hagan</i>		6. PERFORMING ORG. REPORT NUMBER
9. PERFORMING ORGANIZATION NAME AND ADDRESS <i>Emmanuel College</i> <i>Physics Research Division</i> <i>400 The Fenway, Boston MA 02115</i>		8. CONTRACT OR GRANT NUMBER(s) <i>F19628-81-K-0011</i>
11. CONTROLLING OFFICE NAME AND ADDRESS <i>Air Force Geophysics Laboratory</i> <i>Hanscom AFB MA 01731</i> <i>Contract Monitor: Herbert E. Whitney/PHP</i>		10. PROGRAM ELEMENT PROJECT, TASK AREA & WORK UNIT NUMBERS <i>62101F</i> <i>4643AAAB</i>
14. MONITORING AGENCY NAME & ADDRESS (if different from Controlling Office)		12. REPORT DATE <i>December 1983</i>
		13. NUMBER OF PAGES <i>139</i>
		15. SECURITY CLASS. (of this report) <i>Unclassified</i>
		15a. DECLASSIFICATION DOWNGRADING SCHEDULE
16. DISTRIBUTION STATEMENT (of this Report)  <i>Approved for Public Release; Distribution Unlimited</i>		
17. DISTRIBUTION STATEMENT (of the abstract entered in Block 20, if different from Report)		
18. SUPPLEMENTARY NOTES  <i>This work was partially sponsored by the Defense Nuclear Agency, Subtask I25AAXHX, Space Division, Project 2029, and the Air Force Office of Scientific Research, Task 2311G2.</i>		
19. KEY WORDS (Continue on reverse side if necessary and identify by block number)  <i>See other side</i>		
20. ABSTRACT (Continue on reverse side if necessary and identify by block number)  <i>See other side</i>		

DD FORM 1473 EDITION OF 1 NOV 55 IS OBSOLETE

Unclassified  
SECURITY CLASSIFICATION OF THIS PAGE (When Data Entered)

Unclassified

SECURITY CLASSIFICATION OF THIS PAGE (When Data Entered)

- |                              |                              |
|------------------------------|------------------------------|
| 19. VHF/UHF & GHz amplitude  | Ionospheric heating          |
| scintillation                | Underdense heating           |
| Phase scintillation          | Overdense heating            |
| F-region irregularities      | Generation mechanisms        |
| Equatorial irregularities    | Total Electron Content (TEC) |
| Satellite in-situ            | Power spectra                |
| Radar backscatter            | Electron content depletions  |
| High-latitude irregularities | Low-energy electron          |
| Scintillation modelling      | precipitation                |
|                              | Artificial irregularities    |

20. Ionospheric irregularity and total electron content studies have been conducted near the equator, at midlatitudes and at high latitudes. F-region irregularities near the equator are viewed from the concept of the temporal structure of UHF scintillations and the electron content depletions associated with VHF, UHF and GHz scintillations. Near the equatorial anomaly crest, the solar cycle effect on GHz scintillation and the depolarization of VHF satellite signals are probed along with electron density irregularities using in-situ data coupled with VHF/GHz scintillation. Occurrence of nighttime VHF scintillation in the Indian sector near the anomaly is addressed.

In the midlatitude sector, coordinated incoherent scatter radar, total electron content and scintillation measurements are studied in the investigation of the generation of km-scale irregularities while spatial variability of total electron content is analyzed in the Mediterranean region.

At high latitudes, in-situ measurements provide the opportunity for scintillation modelling while low-energy electron precipitation measurements have been correlated with scintillations/TEC in the auroral oval.

The nature of ionospheric irregularities generated by high-power, high-frequency heating has also been investigated and shown to vary between two sites studied.

Unclassified

SECURITY CLASSIFICATION OF THIS PAGE (When Data Entered)

## TABLE OF CONTENTS

	Page
SUMMARY	1
The temporal structure of intensity scintillations near the magnetic equator	3
Ionospheric electron content depletions associated with amplitude scintillations in the equatorial region	12
VHF amplitude scintillations and associated electron content depletions as observed at Arequipa, Peru	16
Microwave equatorial scintillation intensity during solar maximum	27
Depolarization of VHF geostationary satellite signals near the equatorial anomaly crests	34
High resolution topside in-situ data of electron densities and VHF/GHz scintillations in the equatorial region	45
Occurrence of nighttime VHF scintillations near the equatorial anomaly crest in the Indian sector	58
Generation of kilometer scale irregularities during the midnight collapse at Arecibo	62
Spatial variability of total electron content in the eastern Mediterranean region	72
The role of in-situ measurements in scintillation modelling	92
Coordinated measurements of low-energy electron precipitation and scintillations/TEC in the auroral oval	102
Artificial irregularities generated by ionospheric heating and their effects of transionospheric propagation	117
Coordinated study of subkilometer and 3-m irregularities in the F region generated by high-power HF heating at Arecibo	126

## SUMMARY

Ionospheric irregularity and total electron content studies have been conducted near the equator, at midlatitudes and at high latitudes. The nature of ionospheric irregularities generated by high-power high-frequency heating has also been investigated.

Near the equator the major emphasis has been elucidation of the differences in the character of large (i.e., TEC) and small ( $\sim 1$  km) scale variation at the magnetic equator vis-a-vis the Appleton anomaly crests. By comparing the shortest correlation length transverse to the propagation path at both these locations, it is found that the correlation length at the equator is a factor of 5 larger than that at the anomaly crest thereby indicating the much weaker strength of scattering at the equator. The TEC depletions at the equator are found to maximize during the vernal equinox which is also the period of the largest GHz scintillation occurrence. It was also shown that large scintillation patches at VHF are associated with frequency spread on ionograms, but no TEC depletions during the December solstice under high sunspot conditions.

At the Appleton anomaly crest it was found that saturated 1.54 GHz scintillations occur routinely in the early evening hours when ambient F-region densities are very high. Usually at such times intense and fast fluctuations in Faraday rotation angles are found to occur as a consequence of depolarization due to diffractive scattering by small scale ( $< 200$  m) density irregularities which are also responsible for the GHz scintillations. Further, the in-situ structure of such large amplitude irregularities is found to have a 2-component spectrum with the spectral break occurring around a scale-length of 1 km. Continuous scintillation observations at the Appleton anomaly crest in the Indian longitude sector show remarkable increase in irregularity occurrence at the equinoxes with increasing solar activity.

At midlatitudes near Arecibo the occurrence of irregularities was found to be associated with gradients in TEC caused by the midnight collapse of the F-region. Similar gradients are seen at Haifa, Israel

The high-latitude environment was found to be always populated by km-scale irregularities according to the in-situ data from the Atmosphere Explorer-D satellite. A special class of these irregularities near the equatorward edge of the diffuse aurora was found to be associated with soft electron precipitation and to give rise to enhanced TEC and intense phase and amplitude scintillations.

DTIC  
ELECTE  
MAY 21 1984

SECRET  
ACU  
DIED

## The temporal structure of intensity scintillations near the magnetic equator

Santimay Basu

Emmanuel College, Boston, Massachusetts 02115

H. E. Whitney

Air Force Geophysics Laboratory, Hanscom Air Force Base, Massachusetts 01731

(Received April 5, 1982; revised October 22, 1982; accepted October 22, 1982.)

The temporal structure of weak and strong intensity scintillations observed with a geostationary satellite at 249 MHz near the magnetic equator is studied. It is shown that for weak intensity scintillations, the power spectra exhibit an asymptote immediately beyond the Fresnel frequency, which signifies a power law variation of power spectral density with frequency yielding spectral indices ranging between  $-3$  and  $-3.5$ . By the use of simultaneous irregularity drift measurements, it is found that the power law portion of the spectrum for weak scintillations is caused by  $F$  region irregularities in the scale length range of about 700 m to 100 m. On the other hand, for strong intensity scintillations, the asymptote signifies a somewhat higher spectral index ranging between  $-3$  and  $-4.5$ . Considering both weak and strong scintillations, an average spectral index of  $-3.5$  is obtained which is found to be consistent with the average one-dimensional in situ spectral index for irregularities with scale lengths less than 1 km. In addition, it is shown that for strong intensity scintillations, a substantial decrease of the correlation time occurs which is dictated not only by the increased strength of scattering but by the increased irregularity drift as well. At 249 MHz the shortest correlation length transverse to the propagation path is found to be about 70 m near the magnetic equator. This is a factor of 5 larger than the corresponding value obtained away from the equator near the crest of the equatorial anomaly at Ascension Island.

### INTRODUCTION

In the postsunset hours, near the magnetic equator, intense  $F$  region irregularities of electron density, encompassing a scale length range of tens of kilometers to tens of centimeters, are often encountered [Basu and Basu, 1981; Ossakow, 1981; Kelley and McClure, 1981]. The irregularities, covering nearly 5 decades of scale length range, develop suddenly within an hour of ground sunset and decay near midnight, with the erosion of the shorter scale irregularities taking place prior to those of the larger scales [Basu et al., 1978, 1980]. As a result, VHF-UHF radio waves from geostationary satellites during their passage through the intense irregularity environment are strongly scattered in the early evening hours but suffer only weak scattering in the postmidnight period when the irregularity intensity is greatly reduced. Consequently, a receiver on the ground re-

cords a sudden onset of intense fluctuations of amplitude and phase in the evening and registers a gradual decay of the fluctuations in the postmidnight hours. Continuous scintillation measurements with geostationary satellites thus offer an opportunity to study the nature of signal fluctuations under varying scattering conditions.

In this paper we shall study the temporal structure of intensity fluctuations observed at Ancon, Peru (dip  $2^\circ\text{N}$ ) by the use of the 249 MHz transmissions from the near-geostationary satellite LES 9. For geostationary satellite observations, the temporal structure of intensity scintillations is dictated by the integrated electron density deviation, the power spectrum of the irregularities, and their drift speed. Satellite in situ data when combined with other supporting data on irregularity layer thickness indicate that the integrated electron density deviation in the scale length range of tens of kilometers to a few hundred meters may vary by 2-3 orders of magnitude from inside to the outside of an irregularity patch. From satellite and rocket in situ measurements, the power

Copyright 1983 by the American Geophysical Union.

Paper number 2S1699.

0048-6604/83/030263-09\$08.00

The U.S. Government is authorized to reproduce and sell this report. Permission for further reproduction by others must be obtained from the copyright owner.

spectrum of the nighttime *F* region equatorial irregularities have also been studied. The irregularity spectra can, in general, be characterized by a power law form but considerable variations of the spectral character are noted [Basu *et al.*, 1980, 1983; Livingston *et al.*, 1981; Rino *et al.*, 1981]. Further, on many occasions, the spectral description of the irregularity structure becomes invalid [Wernik *et al.*, 1980]. Finally, during the period of scintillation activity, the eastward drift speed of the equatorial irregularity changes. In the course of a single night the drift speed may change from 200 m/s in the evening to 50 m/s late at night giving rise to a factor of 4 variation. Thus owing to the variation of the parameters that characterize equatorial irregularities, the temporal structure of intensity scintillations is expected to undergo considerable change in the course of a single night. In particular, the wide variation of the power spectral density of the irregularities is expected to control to a large extent the intensity scintillation structure.

To characterize the structure of scintillating signals in statistical terms, the power spectra of intensity scintillations are computed. The theory of weak scintillations is well developed and, in this framework, the power spectra of intensity scintillations can be simply related to the spectra of ionospheric irregularities [Cronyn, 1970; Crane, 1976]. Recently, coordinated scintillation and in situ irregularity measurements have been performed in the equatorial region [Basu *et al.*, 1980, 1983; Livingston *et al.*, 1981; Rino *et al.*, 1981] which have allowed a direct comparison of the irregularity structures predicted from scintillation measurements with those measured by in situ probes. In contrast to weak scintillations, a few attempts have been made to develop the multiple scatter theory appropriate to strong ionospheric scintillations [Yeh *et al.*, 1975] and the results of asymptotic or numerical computations have only been obtained for the case of deeply modulated phase screen, i.e., strong single scattering with assumed forms of irregularity spectra [Rino, 1980; Booker and MajidiAhi, 1981]. Yet, near-saturated intensity scintillations at frequencies as high as UHF are routinely observed in the equatorial region during the nighttime and persist for several hours. In view of the paucity of results on the structure of strong intensity scintillation in the equatorial irregularity environment, we have focused our attention on this type of scintillation as obtained from continuous scintillation measurements with geostationary satellites near the

magnetic equator. We shall examine these results in the context of our recently improved knowledge of irregularity structures and current theoretical work that predicts the structure of strong ionospheric scintillations.

## RESULTS AND DISCUSSION

Figures 1-4 show a sequence of four 3-min scintillation data segments along with their spectra, acquired during the development phase of equatorial irregularities. Each of the spectra exhibits a flat low-frequency end and a linear roll-off portion in the high-frequency region. The modulation structure around 9 Hz visible in all spectra from Ancon is not ionospheric in origin but is introduced by the tape recorder. To avoid aliasing of this structure with ionospheric fluctuations, a data sampling rate of 36 Hz was used. It may be noted that the increase in the level of scintillation from the weak-scatter limit ( $S_4 = 0.5$  in Figure 1) to the level of strong scattering ( $S_4 = 0.92$  in Figure 4) leads to an increase in the width of the power spectra. Since the power spectrum and the correlation time are transform pairs, this increase in spectral width corresponds to a reduction of correlation time. The correlation times that reduce the autocorrelation coefficient to 0.5 in Figures 1-4 are 4.6 s, 4.1 s, 3.6 s, and 2.6 s, respectively. Thus the correlation time reduces with increasing  $S_4$  index [Crane, 1976; Umeki *et al.*, 1977a; Whitney and Basu, 1977; Rino and Owen, 1981]. It should be noted, however, that for geostationary satellite observations the autocorrelation interval can decrease not only with an increase in the strength of scattering but also with an increase in the irregularity drift speed. We shall presently show that the variation of the irregularity drift speed was negligible during the 12-min period corresponding to Figures 1-4. Thus the observed effect is indeed caused by strong scattering. Yeh *et al.* [1975] first investigated the problem theoretically for the ionospheric case and obtained numerical results to illustrate this effect of strong scattering on the spatial correlation of intensity scintillation.

The irregularity drift speed was determined by making scintillation measurements with a pair of receivers spaced over an east-west baseline of 366 m. The time delays which give maximum correlation between the pair of scintillation records were determined every 3 min and were combined with the known length of the baseline to derive the drift speed. Since the magnetic declination of this location is only

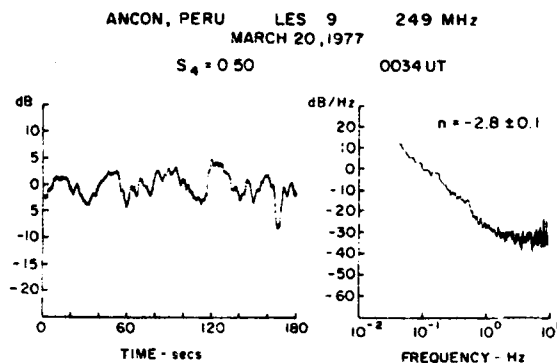


Fig. 1. A 3-min data sample and its spectrum obtained at Ancon from LES 9 starting at 0034 UT on March 20, 1977, during the developing phase of equatorial irregularities. The normalized second central moment  $S_4$  and the spectral index  $n$  of the roll-off portion are indicated in the diagram.

6°E, the measured drift corresponds very closely to the drift in the magnetic E-W direction and any contamination by the drift in the N-S direction is negligible. The drift speed, so measured, is called 'apparent' drift because no allowance is made for the effect of anisotropy or any changes in the diffraction pattern as it moves. However, it is not possible to measure reliably the true velocity near the magnetic equator where the correlation lengths in the N-S direction is 100 times more than the E-W direction [Briggs and Golley, 1968; Koster *et al.*, 1966].

The top panel in Figure 5 shows the variation of the apparent horizontal E-W drift with universal time, and the bottom panel shows the variation of the cross correlation coefficient. The breaks in the top panel correspond to periods of time when the cross correlation coefficient became lower than 0.5 and rendered the drift measurement unreliable.

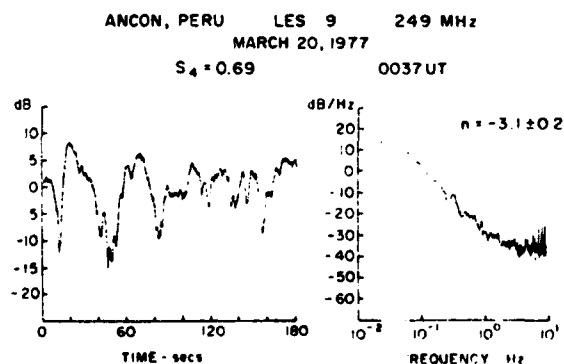


Fig. 2. Same as in Figure 1 except that the data start at 0037 UT.

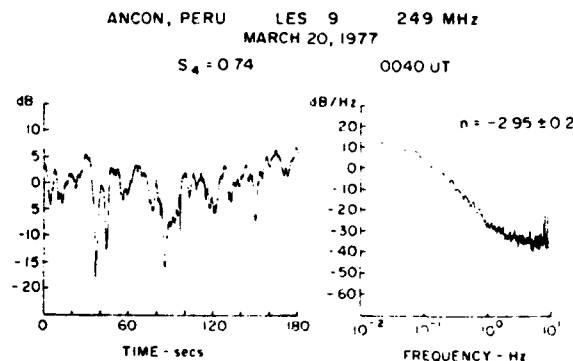


Fig. 3. Same as in Figure 1 except that the data start at 0040 UT.

The drop in the cross correlation coefficient is probably due to either a change in the irregularity structure or velocity turbulence in the early evening hours. The top panel shows a considerable variation of the irregularity drift speed between the early and the late evening periods. From Figure 5, we can now substantiate the earlier statement that between 0037 UT and 0043 UT the drift speed did not vary appreciably. In fact, a maximum variation of 15% around an average value of 70 m/s is observed.

In order to illustrate the effect of the variation of the drift speed on the temporal structure of intensity scintillation, we show a data segment and the corresponding spectrum in Figure 6 and compare it with Figure 4. Both data sets represent similar  $S_4$  index but under very different drift conditions. The spectrum in Figure 6 corresponds to a correlation time of 0.83 s as compared to 2.61 s for the spectrum shown in Figure 4, indicating a factor of 3 variation in correlation time at substantially the same level of  $S_4$  index. If we refer to Figure 5, we find that Figure 4

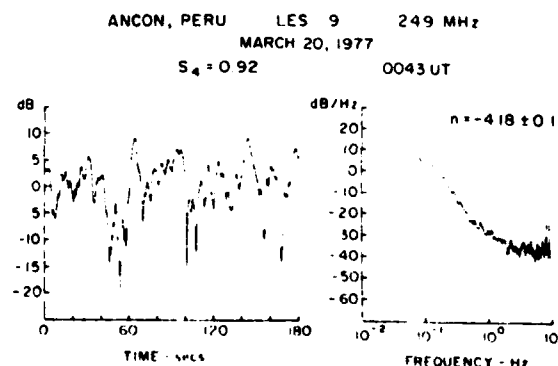


Fig. 4. Same as in Figure 1 except that the data start at 0043 UT.



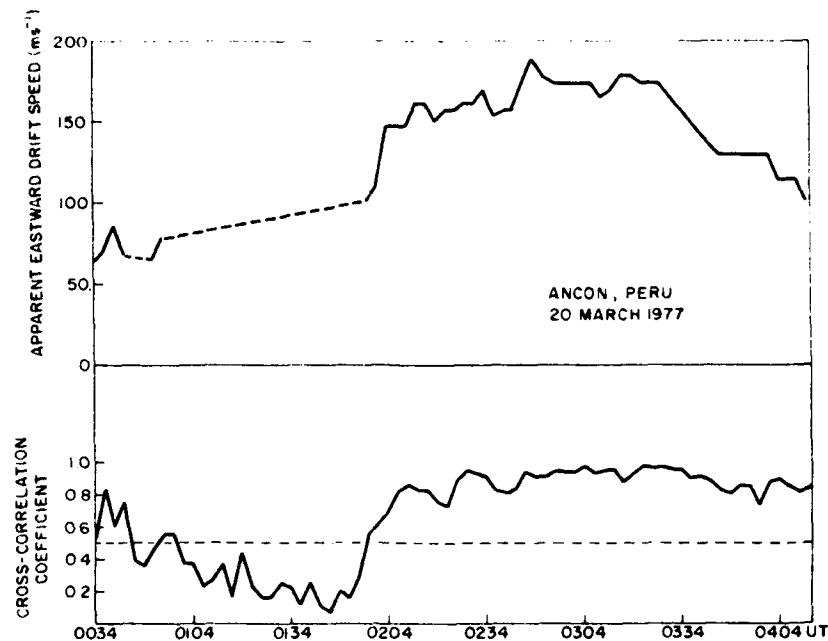


Fig. 5. Irregularity drift velocity and cross correlation coefficient measured by the spaced receiver technique, using LES 9 transmissions at 249 MHz on March 20, 1977. The E-W baseline was 366 m.

corresponds to a period when the drift was 70 m/s, whereas Figure 6 corresponds to a drift of 160 m/s, a factor of approximately 2.5 increase. Thus the observed decrease in correlation time under a similar level of scintillation is explained largely by considering the variation of the irregularity drift.

In order to study the effect of the strength of scattering on spatial correlation, on a statistical basis, we

obtained the product of the autocorrelation interval and the component of the E-W drift speed in a direction orthogonal to the propagation path. In Figure 7 we show the variation of the transverse spatial correlation distance with  $S_4$  index from data obtained on the night of March 6-7, 1978, at the same location. The observations on this night were selected as they provide a more uniform coverage of the range of  $S_4$  values. The decrease of transverse spatial correlation length with increasing  $S_4$  index in the strong scatter regime ( $S_4 > 0.5$ ) is evident as depicted by the best fit straight line. The scatter of the points around the best fit line is within the bounds of the variance estimates of the cross correlation function utilized to obtain the drift speed as well as the variance of the correlation time. It should be mentioned here that the correlation time under strong scattering has also a dependence on the irregularity spectral index. For strong turbulence, the correlation time reduces with increased spectral index if the outer scale is large compared to the Fresnel radius  $(\lambda z)^{1/2}$ ,  $\lambda$  being the wavelength of scintillation measurement and  $z$  the height of the irregularities [Rino, 1980; Booker and MajidiAhi, 1981]. Rino and Owen [1981] have studied the problem with the orbiting Wideband satellite data and demonstrated that the theoretical fit to the

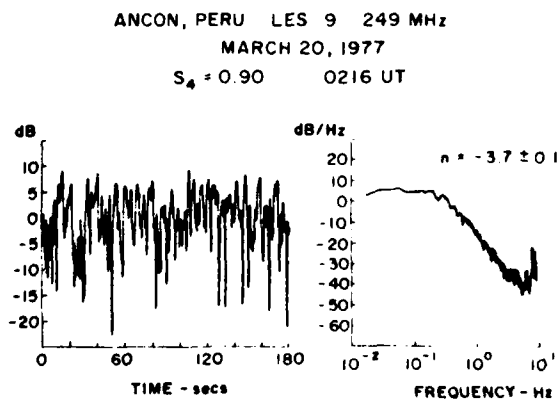


Fig. 6. Same as in Figure 1 except that the data start at 0216 UT. Note that the flat low-frequency portion extends to 0.2 Hz, showing the effects of decorrelation due to increased drift velocity.

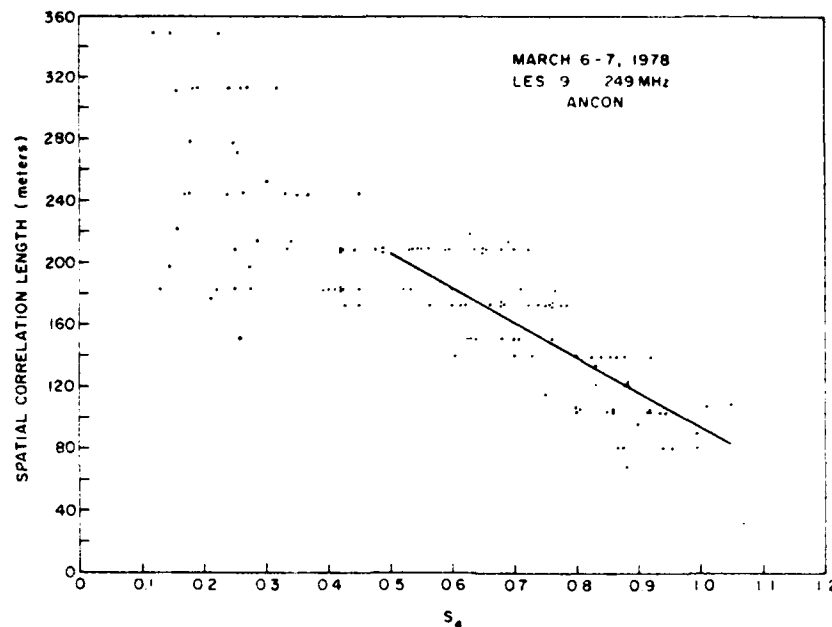


Fig. 7. Variation of spatial correlation length  $\rho_s$  transverse to the propagation path with  $S_4$  index. In the strong scatter regime ( $S_4 > 0.5$ ),  $\rho_s$  decreases with increasing  $S_4$ , as indicated by the best fit straight line.

experimentally observed loss of the temporal correlation of strong intensity scintillations with the phase turbulent strength is greatly improved when the variation of the spectral index and the effects of wave front curvature for low-altitude satellites are considered. The variability of the irregularity spectral index that may contribute to the scatter in Figure 7 will be shown later.

In view of the considerable interest in the relationship between the temporal structure of scintillations and the spatial structure of ionospheric irregularities [Basu *et al.*, 1980, 1983; Livingston *et al.*, 1981; Rino *et al.*, 1981], we shall study, in the following paragraphs, the form of the power spectra of intensity scintillations and compare the results with the available information on irregularity structures. We have already shown the power spectra of five data segments, each of 3 min duration, in Figures 1-4 and Figure 6. The linear roll-off portions of the spectra depicting the variation of power spectral density (PSD) with frequency  $f$  on a log-log scale indicate a power law variation  $f^n$  of PSD with frequency. The power law index  $n$  is determined from the slopes of the best fit straight line in the frequency range of 0.1-0.6 Hz in Figures 1-4 and the range of 0.4-2 Hz in Figure 6, where the roll-off does not commence before 0.3 Hz. The value of the index  $n$  is indicated

on each spectra. Figures 1-3 indicate a power law index in the vicinity of  $-3$ , whereas in Figures 4 and 6, which correspond to  $S_4 \sim 1$ , the index approaches a value of  $-4$ . We shall show later that on a statistical basis, it is difficult to conclude if there exists a pronounced and systematic variation of  $n$  with  $S_4$  index at the Ancon station which is situated close to the magnetic equator.

An unmistakable evidence of steepening of the roll-off portions of intensity spectra for strong scintillations has, however, been obtained recently from measurements made near the crest of the equatorial anomaly [Basu *et al.*, 1983]. During the recent solar maximum period, the nighttime  $F$  region ionization density at the crest was found to be at least a factor of 3-4 higher than that at the magnetic equator, creating a much higher strength of turbulence at such stations as compared to those near the magnetic equator. At Ascension Island, so strong was the integrated electron density deviation that even the 1.54 GHz transmission from the Marisat satellite was driven to saturation ( $S_4 \sim 1$ ). Under such conditions, the flat low-frequency part of the intensity scintillation spectra at 257 MHz extended to frequencies as high as 3 Hz, yielded extremely steep slopes ( $f^{-4}$ ) over the linear roll-off portions, and provided correlation lengths as small as 15 m in a direction trans-

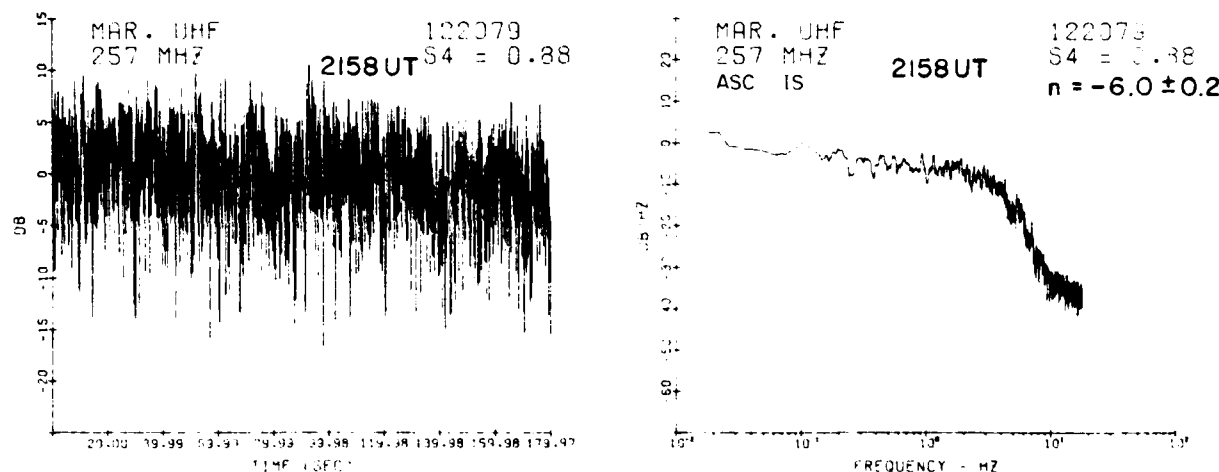


Fig. 8. A 3-min sample and its spectrum obtained at Ascension Island from Marisat between 2158 and 2201 UT on December 20, 1979. Note the extreme steepness of the spectral slope.

verse to the propagation path. One such data sample and the corresponding spectrum are shown in Figure 8. It should be noted that the data in this diagram were acquired by a different tape recorder which did not introduce the modulation structure around 9 Hz present in Ancon data.

Figures 9–11 indicate a sequence of three data segments and their spectra acquired at Ancon between 0337 UT and 0346 UT on March 20, 1977. This period corresponds to the end of scintillation activity on this night, when the equatorial irregularities decay slowly providing weak scintillation data for a period of hours. The features of weak intensity scintillations are best studied in this period due to their longer duration in contrast to the early evening period when weak activity persists for not more than a few minutes.

The set of spectra in Figures 9–11 illustrates the characteristics of weak scintillations. Each spectrum yields a maximum power spectral density at the Fresnel frequency  $f_{FR}$ , which corresponds in the frequency domain to the Fresnel radius  $(\lambda z)^{1/2}$  in the spatial domain [Cronyn, 1970]. The slopes of the best fit straight line (between 0.1 and 0.6 Hz) to the high-frequency ( $f > f_{FR}$ ) roll-off portion of the spectra indicate a spectral index of  $n \sim -3.5$ , whereas in the low-frequency region ( $f < f_{FR}$ ), a spectral index of  $n \sim 1$  is obtained. From a determination of the irregularity drift speed transverse to the propagation path computed from Figure 5, it is found that the Fresnel frequencies in these diagrams correspond to a Fresnel radius of about 650 m, which agrees very well with the value determined from the frequency of measurement and 350 km altitude of the irregu-

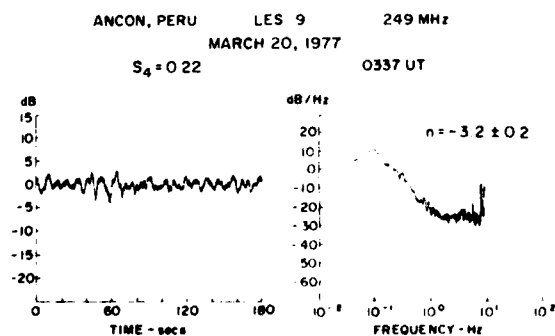


Fig. 9. Same as in Figure 1 except that the data start at 0337 UT. Note  $f^{-1}$  dependence at the low-frequency end and  $f^{-3.5}$  roll-off for conditions of weak intensity scintillations.

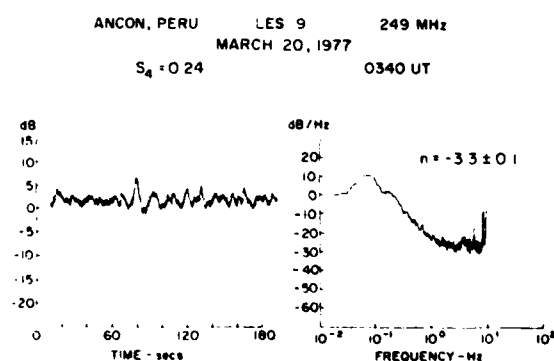


Fig. 10. Same as in Figure 1 except that the data start at 0340 UT.

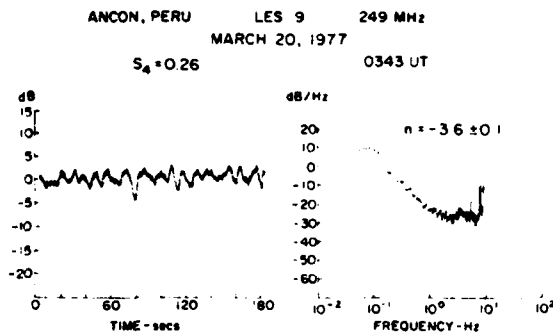


Fig. 11. Same as in Figure 1 except that the data start at 0343 UT.

larities. Thus the high-frequency asymptotes in the set of power spectra shown in Figure 9-11 correspond to irregularities in the scale length range of  $\sim 700$  m to  $\sim 100$  m.

In Figure 12, we examine on a statistical basis the variation of spectral index  $n$  with  $S_4$  from all measurements made on the night of March 20, 1977. It may be noted that most of the points are scattered between  $n = -3$  and  $-4$ , yielding an average value of  $n \sim -3.5$ . In addition, a small trend of increasing spectral slope with increasing  $S_4$  may be observed.

The asymptotic spectral index  $n$  of intensity scintil-

lations is expected to be greater than the one-dimensional irregularity spectral index  $n_1$  by unity, i.e.,  $|n| = |n_1| + 1$ . It should be noted that this relationship is based on the assumption that the three-dimensional power law type of irregularity spectrum is nonseparable, i.e., the spectrum in any of the three orthogonal directions is not independent [Cronyn, 1970]. In the absence of satellite in situ data over the observing location on this night, we examined the high-resolution (35 m) in situ electron density data obtained by the AE-E satellite and their spatial spectra obtained the night after (i.e., on March 21, 1977) as discussed by Basu *et al.* [1980]. A study of 34 spatial spectra of turbulent type of electron density variations having irregularity amplitudes  $\Delta N/\bar{N}$  between 1 and 20% ( $\Delta N$  being the electron density deviation and  $\bar{N}$  being the average electron density) revealed that a spectral partitioning into two domains corresponding to irregularity scale lengths  $\Lambda < 1$  km and  $\Lambda > 1$  km is necessary. It was found that although the spectral indices in both domains vary from sample to sample, similar to the scatter of  $n$  in Figure 12, the average value of the one-dimensional spectral index in the large scale length range ( $\Lambda > 1$  km) is  $n_{11} \sim -1.5$ , whereas at short scale length ( $\Lambda < 1$  km) the average spectral index is  $n_{s1} \sim -2.8$ . Since the intensity scintillations at 249

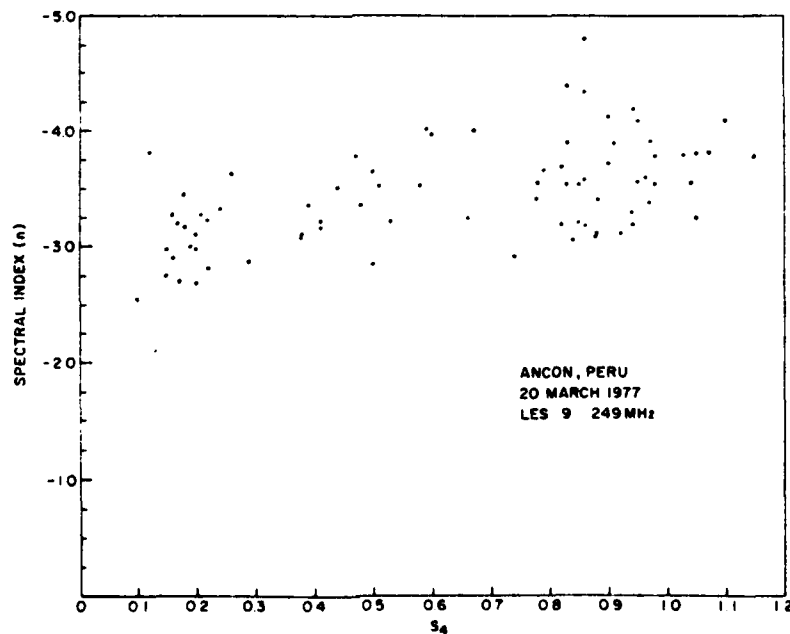


Fig. 12. Variation of spectral index  $n$  with  $S_4$  index. Note the increasing trend of  $n$  with increase of  $S_4$ .

MHz are caused by the short-scale irregularities, the spectral index of intensity scintillations is expected to be  $n \sim -3.8$ . The average value of  $n \sim -3.5$  obtained from Figure 12 is thus in very good agreement with the predicted value, particularly because the in situ data refers to a fixed altitude, whereas the intensity scintillation is an integrated effect. Recent analysis of in situ data at Ascension Island indicates that the most probable value of the one-dimensional spectral index lies between  $-3$  and  $-3.5$  [Basu *et al.*, 1982]. It is not known if the greater value of the spectral index at this location as compared to the equator is a result of the difference in longitude or the difference in solar activity between 1979 and 1977.

We have noted earlier that there exists in Figure 12 a small trend of increasing  $n$  with the increase of  $S_4$ . Whitney and Basu [1977] performed scintillation measurements at 137 MHz and 360 MHz from the nearby Huancayo station and reported steeper slopes of the frequency spectra at 137 MHz compared to the slopes at 360 MHz, when the lower frequency was driven into the strong scintillation regime and the higher frequency remained in the weak scintillation regime. It seems that the small trend in Figure 12 could have been more pronounced if the observing frequency were lower than 249 MHz. It should be noted that earlier theoretical and experimental work indicated  $n$  should remain the same for both weak and strong scintillations [Rumsey, 1975; Marians, 1975; Umeki *et al.*, 1977b]. Recently, numerical computations of strong scintillations [Rino, 1980; Booker and MajidiAhi, 1981] indicate that in a very strongly turbulent power law irregularity environment the asymptotic spectral index of intensity scintillations becomes steeper if the one-dimensional irregularity power law index exceeds a value of 2. Such spectral steepening is often observed in 250 MHz scintillation data obtained near the crest of the equatorial anomaly as discussed in Basu *et al.* [1983]. We have shown one such sample in Figure 8. The preponderance of such cases of steepening observed at 250 MHz near the anomaly crest compared to the equator is probably due to the high ambient ionization density ( $\sim 3 \times 10^{12} \text{ m}^{-3}$ ) prevalent near the crest of the anomaly during the solar maximum period as compared to a value of about  $5 \times 10^{11} \text{ m}^{-3}$  near the equator during solar minimum. For the same level of irregularity amplitude, the electron density deviation is thus a factor of 6 higher at the crest than near the equator.

## SUMMARY

The temporal structure of intensity scintillations observed with a geostationary satellite at 249 MHz near the magnetic equator studied in the paper may be summarized as follows.

The asymptotic portion of the spectra of weak intensity scintillations at 249 MHz near the magnetic equator corresponds to irregularity scale lengths covering 700 m to 100 m at  $F$  region heights. Considering both weak and strong scintillations, an average asymptotic spectral index of  $n \sim -3.5$  is obtained which relates quite well to the observed average one-dimensional irregularity spectral index  $n_{\perp 1} \sim -2.8$  at scale lengths shorter than 1 km. The steepening of the spectral slope of strong scintillations at 249 MHz is minimal near the magnetic equator due to low ambient ionization density at  $F$  region heights. The effect may be noticeable at a lower frequency of observation near the magnetic equator or at 250 MHz in a stronger irregularity environment such as the crest of the equatorial anomaly in the Ascension Island sector during the solar maximum period.

The decrease of correlation interval in geostationary satellite observations arises from both an increase of the strength of scattering as well as a variation of the irregularity drift speed, the latter undergoing at least a factor of  $\sim 4$  variation in the course of a night. At 249 MHz, the smallest transverse spatial correlation length is observed to be  $\sim 70$  m near the magnetic equator. We have shown that correlation lengths as small as 15 m at the same frequency are obtained in a much stronger irregularity environment existing at Ascension Island, which is situated near the crest of the equatorial anomaly.

*Acknowledgments.* The efforts of Bedford Research Associates on computer processing of the scintillation data to obtain the signal statistics is gratefully acknowledged. We wish to thank C. I. Rino and Sunanda Basu for helpful comments on the manuscript. The AE-E in situ data were kindly made available to us by J. P. McClure and W. B. Hanson. The work at Emmanuel College was supported by Air Force Geophysics Laboratory contract F-19628-81-K-0011.

## REFERENCES

- Basu, S., and Su-Basu (1981). Equatorial scintillations—A review, *J. Atmos. Terr. Phys.*, **43**, 473.
- Basu, S., Su-Basu, J. Aarons, J. P. McClure, and M. D. Cousins (1978). On the coexistence of kilometer- and meter-scale irregularities in the nighttime equatorial  $F$  region, *J. Geophys. Res.*, **A3**, 4219.

- Basu, S., J. P. McClure, Su. Basu, W. B. Hanson, and J. Aarons (1980), Coordinated study of equatorial scintillation and in situ and radar observations of nighttime *F* region irregularities, *J. Geophys. Res.*, **85**, 5119.
- Basu, Su., S. Basu, J. P. McClure, W. B. Hanson, and H. E. Whitney (1983), High-resolution topside in situ data of electron densities and VHF/GHz scintillation in the equatorial region, *J. Geophys. Res.*, in press.
- Booker, H. G., and G. MajidiAhi (1981), Theory of refractive scattering in scintillation phenomena, *J. Atmos. Terr. Phys.*, **43**, 1199.
- Briggs, B. H., and M. G. Golley (1968), A test for dispersion in *F* region drifts observed by the radio star scintillation method, *J. Atmos. Terr. Phys.*, **30**, 963.
- Crane, R. K. (1976), Spectra of ionospheric scintillation, *J. Geophys. Res.*, **81**, 2041.
- Cronyn, W. M. (1970), The analysis of radio scattering and space probe observations of small-scale structure in the interplanetary medium, *Astrophys. J.*, **161**, 755.
- Kelley, M. C., and J. P. McClure (1981), Equatorial spread-*F*: a review of recent experimental results, *J. Atmos. Terr. Phys.*, **43**, 427.
- Koster, J. R., I. Katsriku, and M. Tete (1966), Studies of the equatorial ionosphere using transmissions from active satellites, *Annu. Summ. Rep. I*, Univ. of Ghana-Legon, Accra, Ghana.
- Livingston, R. C., C. L. Rino, J. P. McClure, and W. B. Hanson (1981), Spectral characteristics of medium-scale equatorial *F* region irregularities, *J. Geophys. Res.*, **86**, 2421.
- Marians, M. (1975), Computed scintillation spectrum for strong turbulence, *Radio Sci.*, **10**, 115.
- Ossakow, S. L. (1981), Spread-*F* theories—A review, *J. Atmos. Terr. Phys.*, **43**, 437.
- Rino, C. L. (1980), Numerical computations for a one-dimensional power law phase screen, *Radio Sci.*, **15**, 41.
- Rino, C. L., and J. Owen (1981), On the temporal coherence loss of strongly scintillating signals, *Radio Sci.*, **16**, 31.
- Rino, C. L., R. T. Tsunoda, J. Petriceks, R. C. Livingston, M. C. Kelley, and K. D. Baker (1981), Simultaneous rocket-borne beacon and in situ measurements of equatorial spread *F* Intermediate wavelength results, *J. Geophys. Res.*, **86**, 2411.
- Rumsey, V. H. (1975), Scintillations due to a concentrated layer with a power law turbulence spectrum, *Radio Sci.*, **10**, 107.
- Umeki, R., C. H. Liu, and K. C. Yeh (1977a), Multifrequency studies of ionospheric scintillations, *Radio Sci.*, **12**, 311.
- Umeki, R., C. H. Liu, and K. C. Yeh (1977b), Multifrequency spectra of ionospheric amplitude scintillations, *J. Geophys. Res.*, **82**, 2752.
- Wernik, A. W., C. H. Liu, and K. C. Yeh (1980), Model computations of radio wave scintillation caused by equatorial ionospheric bubbles, *Radio Sci.*, **15**, 559.
- Whitney, H. E., and S. Basu (1977), The effect of ionospheric scintillation on VHF/UHF satellite communications, *Radio Sci.*, **12**, 123.
- Yeh, K. C., C. H. Liu, and M. Y. Youakim (1975), A theoretical study of the ionospheric scintillation behavior caused by multiple scattering, *Radio Sci.*, **10**, 97.

IONOSPHERIC ELECTRON CONTENT DEPLETIONS ASSOCIATED WITH AMPLITUDE SCINTILLATIONS  
IN THE EQUATORIAL REGION

A. DasGupta<sup>1\*</sup>, J. Aarons<sup>1</sup>, J.A. Klobuchar<sup>1</sup>, Santimay Basu<sup>2</sup>, and A. Bushby<sup>3</sup>

<sup>1</sup>Air Force Geophysics Laboratory, Hanscom AFB, MA 01731

<sup>2</sup>Emmanuel College, Boston, MA 02115

<sup>3</sup>Instituto Geofísico del Peru, Huancayo, Peru

**Abstract.** The diurnal and seasonal behavior of the depletions in the ionospheric electron content, associated with amplitude scintillations measured at Arequipa, Peru for about one year around the recent solar maximum period, are presented. The seasonal variation shows asymmetrical equinoctial maxima, the February-April period having markedly higher occurrences. Amplitude scintillation measurements at 1.54 GHz and 257 MHz at the nearby magnetic equatorial station Huancayo, Peru also show a similar pattern. A comparison of the three sets of data indicates the simultaneous development of irregularities of different scale sizes and earlier erosion of the smaller scale irregularities.

Introduction

Multitechnique observations of ionospheric irregularities in the equatorial region have established that the irregularities in electron density distribution may occur over a height range of a few hundred kilometers in the F-region of the ionosphere. Such irregularities in the form of ionization depletions, sometimes having amplitudes as large as an order of magnitude of the ambient level, occupying an extended height range should have their signatures on the height integrated total electron content of the ionosphere at an equatorial station. Klobuchar et al. (1978) and Yeh et al. (1979a) have shown that the Faraday rotation technique can be used to observe ionospheric electron content depletions associated with amplitude scintillations of transionospherically propagated signals. Yeh et al. (1979b) have published results of observations on such depletions for a very limited period of about one month. Although the above papers have shown that the Faraday rotation data can be used for studying electron content perturbations, no long term study on the behavior of the ionization depletions associated with scintillations in the equatorial region has yet been reported. The purpose of this paper is to present the results of such measurements at an equatorial station Arequipa, Peru during a period of about one year (May 1979 through May 1980). The results combined with observations on amplitude scintillations of satellite signals in the VHF to microwave range have been used to obtain information on the nature and evolution of equatorial ionospheric irregularities.

\*NRC/NAS Senior Resident Research Associate on leave from the University of Calcutta, India.

Copyright 1982 by the American Geophysical Union.

Paper number 1L1879.  
0094-8276/82/001L-1879\$01.00

12

The U.S. Government is authorized to reproduce and sell this report. Permission for further reproduction by others must be obtained from the copyright owner.

Data

A polarimeter recording the Faraday rotation and the amplitude of the 137 MHz signal from ATS-3 has been in operation at Arequipa, Peru (16.4°S, 71.5°W, Geogr.; 9°S dip) since March 1979. The present paper is based on observations made during the one year period May 1979 - May 1980. The 400 km subionospheric point is approximately (14.5°S, 74.6°W, Geogr.; 2.5°S dip) and the satellite look angle has an elevation of about 46°. The measurements of amplitude scintillations of the 1.54 GHz and 257 MHz signals from the satellite Marisat (15°W) obtained at the nearby magnetic equatorial station Huancayo, Peru (12°S, 75°W, Geogr.; 2°N dip) have been used for comparison. The 400 km subionospheric point in this case is (11°S, 68.5°W, Geogr.; 2.5°N dip) and the elevation angle is 20° looking almost directly towards the east. It may be noted that the observations reported in this paper cover a period when the average monthly Zurich sunspot number  $R_z$  was very high (> 163).

Results

Figure 1 shows the percentage occurrences of electron content depletions of amplitude  $1 \times 10^{16}$  el/m<sup>2</sup> or more. The limited sensitivity of polarimeter records at stations near the magnetic equator does not permit accurate observations of depletions with smaller amplitude. Since the dynamical behavior of the F-region around sunset is controlled by E-region conductivity (Rishbeth, 1971; Fejer et al., 1979), E-region (110 km) sunset and sunrise times at the subionospheric location are shown in the diagram. The pre-midnight diurnal and the equinoctial seasonal maxima are evident. There is practically no occurrence of depletions in May-July months. The most remarkable feature is the much higher occurrences around the February-April equinox as compared to those for September-October months.

Basu et al. (1980) have published the first long term observations of microwave scintillations near the magnetic equator at Huancayo during the solar minimum years 1975-1976. They have shown that the microwave scintillations also have seasonal maxima during the equinoxes. A comparison of the occurrence patterns of the depletions of Figure 1 and simultaneous amplitude scintillations at 1.54 GHz at the nearby magnetic equatorial station Huancayo (Figure 2) reveals some very interesting features. The seasonal variation of microwave scintillations with a scintillation index of 3 dB or more shows equinoctial maxima, with practically no occurrence in June-July and less than 5 percent occurrence for

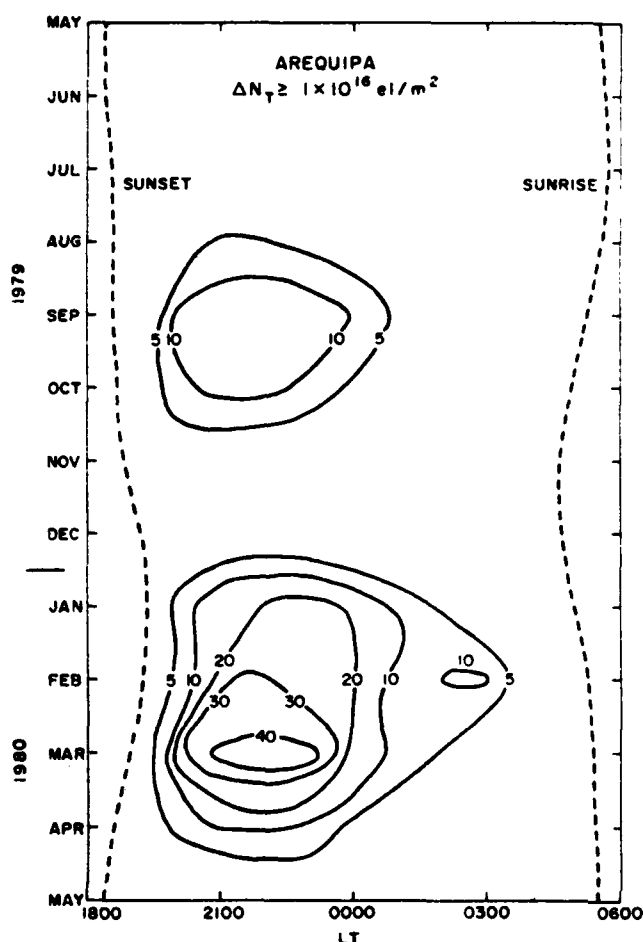


Figure 1. Monthly percentage occurrence contours of ionospheric electron content depletions  $\geq 1 \times 10^{16}$  el/m<sup>2</sup> at Arequipa during May 1979 - May 1980.

December solstice. An asymmetric seasonal behavior, similar to that of the ionization depletions illustrated in Figure 1, emerges in this case also. The seasonal pattern of microwave scintillations observed earlier during solar minimum condition does not show such pronounced asymmetry. The depletions, however, persist into post-midnight hours, whereas scintillation is mostly confined to pre-midnight periods.

The electron content depletions are signatures of irregularities of scale sizes of a few tens of km. On the other hand, scintillations in the VHF range are most effectively produced by irregularities having scale sizes of about a km. Irregularities in the scale size range from a km to several km should also show some correspondence. This is established from a comparison of Figures 1 and 3. An actual comparison of the percentage occurrence patterns of electron content depletions at Arequipa and amplitude scintillations at 257 MHz obtained simultaneously at Huancayo (scintillation index 20 dB or more) also shows a remarkable similarity, with pronounced equinoctial asymmetry and considerable occurrences during post-midnight hours. The asymmetric equinoctial maxima has not been reported earlier. It should also be mentioned that a selection of the scintillation index at a lower level might result

in a different type of seasonal behavior. For example, if the occurrence statistics are studied for 6 or 10 dB levels at 257 MHz or even for saturated scintillations at 137 MHz, a December solstice maximum is observed, although the asymmetric equinoctial behavior is still evident.

#### Discussions

Simultaneous observations of electron content depletions and scintillations at VHF and microwaves in the equatorial region indicate the nature and evolution of the equatorial ionospheric irregularities. The ionization depletions may be taken as the manifestation of tens of km scale irregularities occupying a considerable vertical range around the F-region, whereas km scale irregularities are responsible for VHF scintillations. Scintillations in the GHz range are most effectively produced by irregularities having scale sizes of a few hundred meters, corresponding to the Fresnel dimension at the observing frequency. During the initial phase of development in the post-sunset hours, irregularities of different scale sizes coexist. In the late phase during post-midnight hours the overall strength of the irregularities is eroded, the smaller scale irregularities decaying earlier

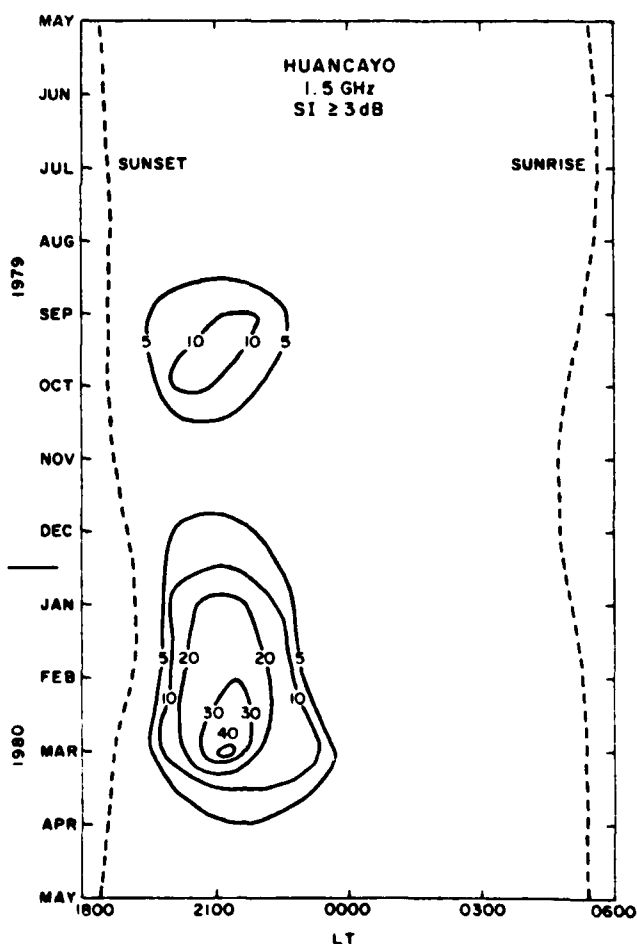


Figure 2. Monthly percentage occurrence contours of scintillations at 1.54 GHz ( $SI \geq 3$  dB) observed at Huancayo.



(Basu et al., 1978; Basu et al., 1980). From co-located measurements of scintillations and VHF and GHz and of high resolution in-situ data, Basu et al. (1981) have found that during early evening hours very sharp density gradients within large scale depletions are associated with VHF and GHz scintillations. The role of sharp density structures in causing GHz scintillations has been discussed by Wernik et al. (1980). In the late phase, when the GHz scintillation is absent, with the VHF channel still exhibiting saturation, the sharpness of the small scale structures inside the large scale density depletions is diminished. More or less similar behavior of VHF and GHz scintillations as well as electron content depletions during pre-midnight hours is along the expected lines. The continuation of VHF scintillations and depletions beyond midnight is due to the longer lifetimes of the larger scale irregularities. The occurrences of VHF scintillations near the pre-sunrise period may be related to weaker irregularities in a number of magnetic field tubes intercepted by the oblique satellite ray path. Observation of ionization depletions smaller than  $\approx 1 \times 10^{16}$  el/m<sup>2</sup> is, however, not possible due to the limited sensitivity of the Faraday rotation technique near the magnetic equator.

The asymmetry of the seasonal dependence of scintillations as well as electron content depletions, between the two equinoxes during solar

maximum conditions, has not been previously reported. An asymmetry in the equinoctial electron content values, have been reported from a number of mid-latitude stations in both northern and southern hemispheres for high solar activity conditions (Titheridge, 1973; Essex, 1977). The higher electron content values have been suggested to be caused by a change in the global circulation pattern or by a change in the vertical drift pattern (Titheridge, 1973). It may be noted that no such observation has yet been reported from equatorial stations, where electrodynamic drift plays the dominating role. Observations on the behavior of equinoctial electron content and detailed statistics of electron content perturbations associated with scintillations in the equatorial region will be published elsewhere.

In the last two years, high levels of amplitude scintillations at microwave frequencies ( $> 20$  dB at 1.54 GHz) have frequently been observed at locations like Ascension Island situated near the crest of the Appleton anomaly (Aarons et al., 1981). The Faraday rotation records at VHF often exhibit fast polarization fluctuations, induced by depolarization effect due to scattering from power-law type irregularities (Lee et al., 1982), when intense amplitude scintillations are observed. The long term behavior of these fluctuations and associated scintillations, particularly for high solar activity conditions, are yet to be established. Although such intense microwave scintillations and fast polarization fluctuations are not encountered at Huancayo and Arequipa, it would be interesting to compare the present results with those at stations like Ascension Island.

**Acknowledgment.** We thank Sunanda Basu for many helpful comments.

#### References

- Aarons, J., H.E. Whitney, E. MacKenzie, and S. Basu, Microwave equatorial scintillation intensity during the current solar maximum, *Radio Sci.*, **16**, 939, 1980.
- Basu, S., Sunanda Basu, J. Aarons, J.P. McClure, and M.D. Cousins, On the co-existence of kilometer and meter-scale irregularities in the nighttime equatorial F-region, *J. Geophys. Res.*, **83**, 4219, 1978.
- Basu, S., J.P. McClure, Sunanda Basu, W.B. Hanson, and J. Aarons, Coordinated study of equatorial scintillation and in-situ and radar observations of nighttime F-region irregularities, *J. Geophys. Res.*, **85**, 5119, 1980.
- Basu, Sunanda, S. Basu, J.P. Mullen, and A. Bushby, Long-term 1.5 GHz amplitude scintillation measurements at the magnetic equator, *Geophys. Res. Lett.*, **7**, 259, 1980.
- Basu, Sunanda, S. Basu, J.P. McClure, W.B. Hanson, and H.E. Whitney, Spatially and temporally co-located measurements of GHz/VHF scintillation and in-situ irregularity spectra near Ascension Island, Paper presented at the Spring Meeting of American Geophysical Union, Baltimore, 1981.
- Essex, E., Equinoctial variations in the total electron content of the ionosphere at northern and southern hemisphere stations, *J. Atmos. Terr. Phys.*, **39**, 645, 1977.

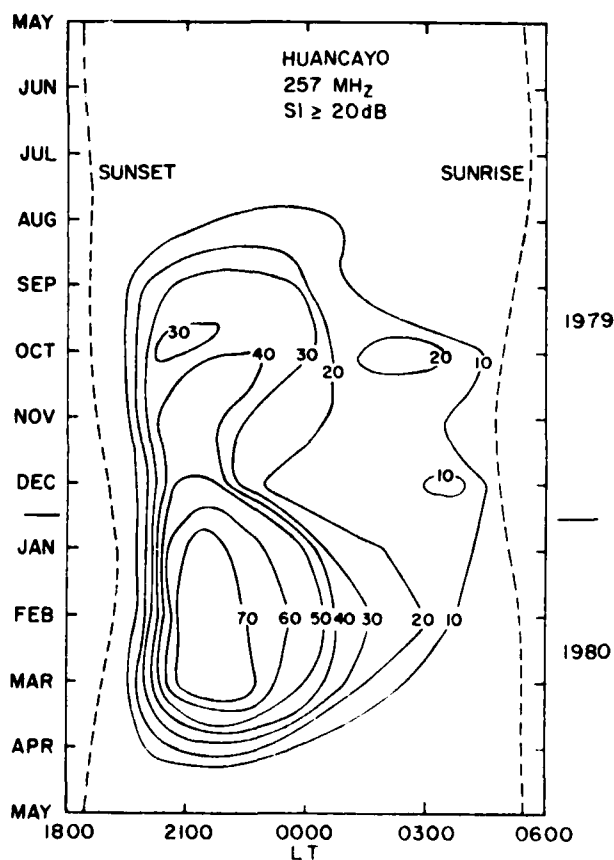


Figure 3. Monthly percentage occurrence contours of scintillations at 257 MHz ( $SI \geq 20$  dB) observed at Huancayo.

- Fejer, B.G., D.T. Farley, R.F. Woodman, and C. Calderon, Dependence of equatorial F-region vertical drifts on season and solar cycle, J. Geophys. Res., **84**, 5792, 1979.
- Klobuchar, J.A., J. Aarons, E. Weber, L. Lucena, and M. Mendillo, Total electron content changes associated with equatorial irregularity plumes, Paper presented at the National Radio Science Meeting, URSI, Boulder, CO, Nov. 6-9, 1978.
- Lee, M.C., A. DasGupta, J.A. Klobuchar, S. Basu, and S. Basu, Depolarization of VHF geostationary satellite signals near the equatorial anomaly crests, Radio Sci., 1982 (in press).
- Rishbeth, H., Polarization fields produced by winds in the equatorial F-region, Planet. Space Sci., **19**, 357, 1971.
- Titheridge, J.E., The total electron content of the southern mid-latitude ionosphere, 1965-1971, J. Atmos. Terr. Phys., **35**, 981, 1973.
- Wernik, A.W., C.H. Liu, and K.C. Yeh, Model computations of radio wave scintillation caused by equatorial ionospheric bubbles, Radio Sci., **15**, 559, 1980.
- Yeh, K.C., H. Soicher, C.H. Liu, and E. Bonelli, Ionospheric bubbles observed by the Faraday rotation method at Natal, Brazil, Geophys. Res. Lett., **6**, 473, 1979a.
- Yeh, K.C., H. Soicher, and C.H. Liu, Observations of equatorial ionospheric bubbles by the radio propagation method, J. Geophys. Res., **84**, 6589, 1979b.

(Received November 3, 1981;  
accepted November 30, 1981.)

## VHF amplitude scintillations and associated electron content depletions as observed at Arequipa, Peru

A. DASGUPTA,\*† J. SANTIMAY BASU,† J. AARONS,‡ J. A. KLOBUCHAR,\* SUNANDA BASU† and A. BUSHBY§

\*Air Force Geophysics Laboratory, Hanscom Air Force Base, MA 01731, U.S.A., †Emmanuel College, 400 The Fenway, Boston, MA 02115, U.S.A., ‡Department of Astronomy, Boston University, Boston, MA 02215, U.S.A., §Instituto Geofísico del Perú, Huancayo, Peru

(Received in final form 14 July 1982)

**Abstract**—Results of observations on occurrences and behavior of 137 MHz VHF amplitude scintillations and associated ionospheric electron content depletions obtained at Arequipa, Peru (16.4°S, 71.5°W, geogr.; 9°S dip) during the recent solar maximum period 1979–1980 are presented. The seasonal variation of scintillations shows the usual deep minimum during May–July and a prominent maximum in December, when scintillations also persist for a long period of time, sometimes even beyond sunrise. Ionospheric irregularities have been found to occur in distinct patches whose extent varies with season. During the December solstice the average VHF scintillation patch duration is about 6 h, while numerous patches of much shorter duration are observed in equinoctial months. The depletions in the height integrated ionospheric electron content associated with scintillations have a typical duration of 10–15 min and amplitude less than  $5 \times 10^{16}$  el m<sup>-2</sup>, although depletions with an amplitude as large as  $20 \times 10^{16}$  el m<sup>-2</sup> and with a duration of more than 30 min are sometimes encountered. The pre-midnight amplitude scintillations and associated electron content depletions could be identified with range type spread-F, as established earlier, while the association of post-midnight VHF scintillations with frequency type spread-F is found to be a special feature observed during years of very high solar activity. The seasonal dependence of irregularity patch dimensions is examined in terms of variations of drifts in the post-sunset equatorial ionosphere.

### 1. INTRODUCTION

Since the launching of the first artificial satellite, measurement of amplitude scintillations of trans-ionospheric signals has been one of the most widely used techniques for studying ionospheric irregularities. From the point of view of occurrence and nature, it is now well established that the irregularities in the equatorial region, covering about  $\pm 15^\circ$  of latitude around the magnetic equator, have some definite characteristics. They are found to be embedded in cloudlike patches having an east-west extent in the range of tens to hundreds of kilometers and a magnetic field-aligned north-south dimension of a few thousand kilometers. Coordinated measurements with other techniques, such as *in situ*, radar backscatter and airglow, have shown that the patches are regions of depleted ionization (BASU and BASU, 1981 and references therein). The depletions may occur over a considerable height range and sometimes have amplitudes as large as orders of magnitude of the ambient ionization level (McCLURE *et al.*, 1977). Such intense depletions should have their signatures on the height integrated ionospheric total electron content (TEC). YERBAH-AMANKWAH and KOSTER (1972)

reported large changes of the Faraday rotation angle of the received transionospheric signal associated with amplitude scintillations at Legon, Ghana. KAUSHIKA and DE MENDONCA (1974) reported a similar phenomenon from São Paulo, Brazil but they had no simultaneous amplitude records. Only recently, it has been definitely shown that simultaneous measurements of amplitude scintillations and Faraday rotation of a linearly polarized transionospheric signal can be used for investigations of equatorial TEC depletions, frequently referred to as 'bubbles', in a very simple and inexpensive manner (KLOBUCHAR *et al.*, 1978; YEH *et al.*, 1979a).

The use of the above technique is, however, limited to certain locations within the equatorial irregularity belt. It is difficult to detect the presence of bubbles in the Faraday rotation records obtained at equatorial stations like Huancayo and Legon, which are situated virtually on the magnetic equator. Close to the magnetic equator, because of near-transverse propagation and the low value of the so-called M-factor (YEH and GONZALES, 1960), only very large amplitude depletions could be observed. On the other hand, at locations near the crests of the equatorial anomaly, VHF Faraday rotation records often exhibit fast and intense fluctuations during periods of amplitude scintillations (KLOBUCHAR and AARONS, 1980;

\*NRC/NAS Senior Resident Research Associate on leave from the University of Calcutta, India.

DASGUPTA and MAITRA, 1980) and the fluctuations are often too fast and intense to render the data useful; at times even the concept of Faraday rotation is not valid, due to a depolarization effect caused by scattering from small-scale power law type density irregularities (LEE *et al.*, 1982). Because of the above two reasons, stations situated off the magnetic equator but not near the anomaly crests, such as Natal in Brazil and Arequipa in Peru, with a magnetic dip of about  $10^\circ$  and a propagation angle sufficiently different from the quasitransverse case offer a compromise. The purpose of this paper is to present results of observations on scintillations and associated depletions in total ionization obtained at Arequipa, Peru, which is located in between the magnetic equator and the Appleton anomaly crest in the American longitude sector. The emphasis is on a systematic study of morphology of irregularity patches and electron content depletions and their dependence on season. It should be pointed out that, because of a considerable longitudinal variation, some results and conclusions presented in this paper may not apply to other longitudes.

## 2. DATA

A polarimeter recording the amplitude and Faraday rotation angle of the 137 MHz VHF signal from the satellite ATS-3 has been in operation at Arequipa ( $16.4^\circ\text{S}$ ,  $71.5^\circ\text{W}$ , geogr.;  $9^\circ\text{S}$  dip), Peru since March 1979. The subionospheric point at 400 km height corresponds to ( $14.5^\circ\text{S}$ ,  $74.6^\circ\text{W}$ , geogr.;  $2.5^\circ\text{S}$  dip) approximately. The period of observation covered in this paper is May 1979–May 1980. The data pertain to a very high level of solar activity around the recent solar maximum period. The average monthly Zurich sunspot number for the reporting period was 163, with the highest value of 188.4 observed in September 1979.

## 3. RESULTS

### 3.1. Morphology of scintillations

The diurnal and seasonal variations of scintillations in the equatorial region are now well established, at least in the American and African sectors. The seasonal dependence of VHF amplitude scintillations is characterized by a deep minimum in the May–July period and a broad maximum from October to April. However, if the frequency of the signal is in the gigahertz band, such as the 1.54 GHz Marisat observations from Huancayo, the broad maximum breaks up into two equinoctial maxima (BASU *et al.*, 1980; DASGUPTA *et al.*, 1982). Observations at different frequencies, in the VHF to L-band range, at Huancayo during 1979–1980

show that the March equinox of 1980 was characterized by an unusually strong equatorial scintillation activity (DASGUPTA *et al.*, 1982). This difference in pattern is in all likelihood related to the overall strength of the irregularities, the equinoxes probably having more intense irregularities than the solstices. Figure 1 shows the percentage occurrence contours of VHF scintillations ( $S_I > 6\text{ dB}$ ) at Arequipa. Although a level of 6 dB has been selected in this case, the occurrence pattern remains more or less unchanged even for saturated scintillations ( $\sim 20\text{ dB}$ ). Scintillation at VHF has been found to be commonly saturated when it occurs, excepting some infrequent cases around sunrise. Since the F-region dynamics are controlled to a large extent by the E-region electric field, the 110 km sunset and sunrise times at the subionospheric location are also shown in the figure. It is observed that the occurrence around December is not only the highest but also persists for longer periods during the night, sometimes even beyond sunrise. On the other hand, during the equinoxes scintillation is mainly a pre-midnight phenomenon. There are remarkable differences also, as we shall discuss later, in some of the related parameters between the solstice and equinoxes.

### 3.2. Irregularity patches

Equatorial irregularities usually occur in field-aligned cloudlike patches, having both north–south as well as east–west extents. The patches may be either discrete or overlapping and, when developed, they drift from west to east. The east–west drift velocity ranges from 30 to 300  $\text{m s}^{-1}$ , with an average of 100–150  $\text{m s}^{-1}$  (WOODMAN, 1972; BASU *et al.*, 1977; YEH *et al.*, 1981). Assuming a typical value of drift velocity an idea about the east–west spatial dimension can be obtained from temporal observations with geostationary satellites. From observations with geostationary as well as orbiting satellite beacons and airglow measurements, it has been found that the equatorial irregularity patches become more discrete with decreasing east–west dimensions as one moves away from the equator (SINCLAIR and KELLEHER, 1969; BHAR *et al.*, 1970; WEBER *et al.*, 1980; AARONS *et al.*, 1980). AARONS *et al.* (1980) discussed in detail the nature and behavior of irregularity patches at two locations, one near the magnetic equator and the other near the Appleton anomaly crest, based on data for one year. However, AARONS *et al.* (1980) made no attempt to obtain a seasonal dependence of the patch characteristics. It is apparent from earlier observations that the patch dimensions may vary with season. We will present here the seasonal dependence of the east–west extent of irregularity patches at Arequipa.

Scintillations as observed at Arequipa at 137 MHz

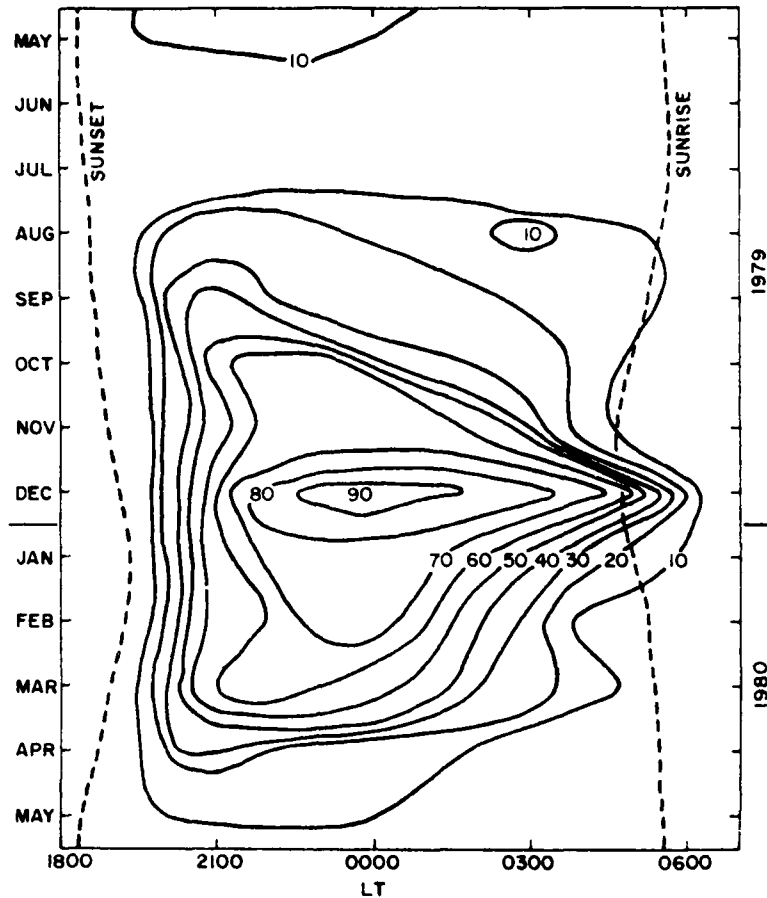


Fig. 1. Percentage occurrence contours of scintillation ( $SI > 6$  dB) at 137 MHz. The 110 km sunset and sunrise times at the 400 km subionospheric location are also shown.

occur in patches reaching saturation within a couple of minutes of onset. During the pre-midnight hours the decay of scintillations is also generally abrupt. In the post-midnight periods, however, the decay is often gradual, with fading rates becoming considerably slower. As a function of season, there is a remarkable difference in the east-west horizontal extents of the patches. During the equinoxes the scintillation patches are numerous with short periods of tens of minutes of scintillations interspersed with absolutely quiet intervals. On the other hand, the December solstice months are characterized by scintillations for extended periods lasting several hours during a single night. Figure 2(a) shows the monthly occurrence of the total number of patches along with the total hours of scintillations, indicated by the numbers at the top of the bars. On average, the December patch has a duration of about 6 h, while in September it is about 1 h. Assuming an east-west drift speed of  $100 \text{ m s}^{-1}$ , these correspond

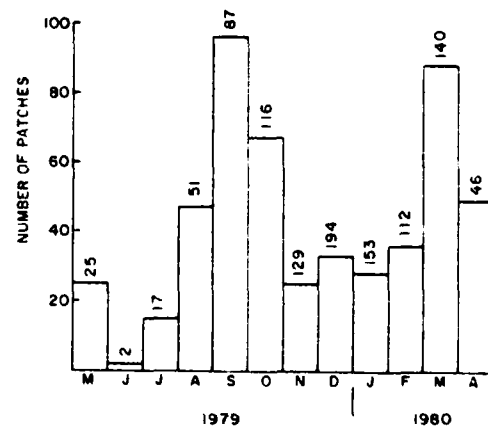


Fig. 2(a). Occurrence of VHF scintillation patches as a function of months. The numbers at the top of the bars are the corresponding total hours of scintillations.

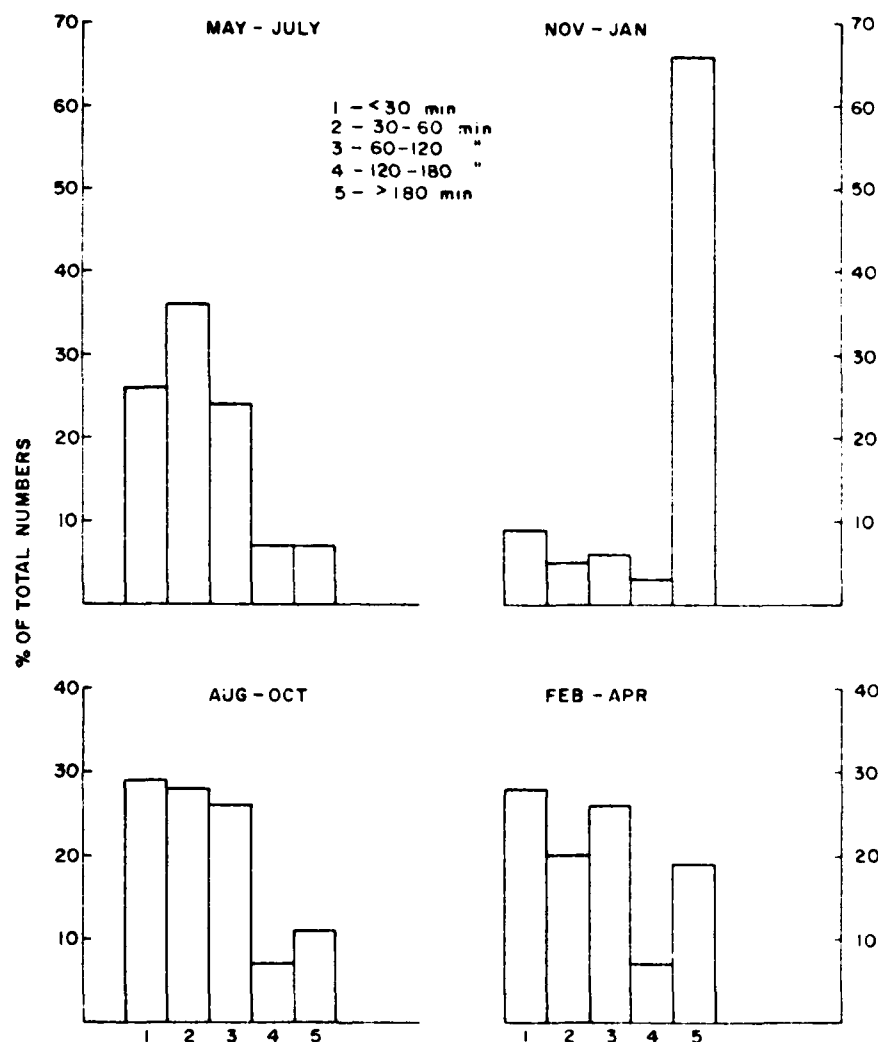


Fig. 2(b). Histograms showing the distribution of patch duration for different seasons.

to about 2000 and 350 km, respectively. If the apparent drift velocity varies with season and local time, the above estimates should be modified accordingly. During the two equatorial irregularity campaigns in March 1977 and 1978 in the American sector, it has been observed that, with a higher solar activity, the apparent drift velocity of the irregularities increases and persists for a longer period into the post-midnight hours (BASU, private communication, 1982). Further, as the satellite look angle in the present case is off-zenith and off-meridian (elevation  $43^\circ$  and azimuth  $302^\circ$ ) the ray path may, however, encounter irregularities in a number of field tubes (i.e. more than one patch) and an individual patch may actually have dimensions less

than that indicated by the observed duration of scintillations. Figure 2(b) shows the distribution of a scintillation patch duration for different seasons, following the categorization in AARONS *et al.* (1980). The enormously longer duration in the December solstice is also obvious in this diagram.

### 3.3. Ionospheric electron content depletion

YEH *et al.* (1979b) have described the characteristics, such as amplitude and duration, of the electron content depletions associated with scintillations obtained at Natal for a period of about one month only. From Areqipa the diurnal and seasonal behavior of the TEC depletions covering a one year period around the recent

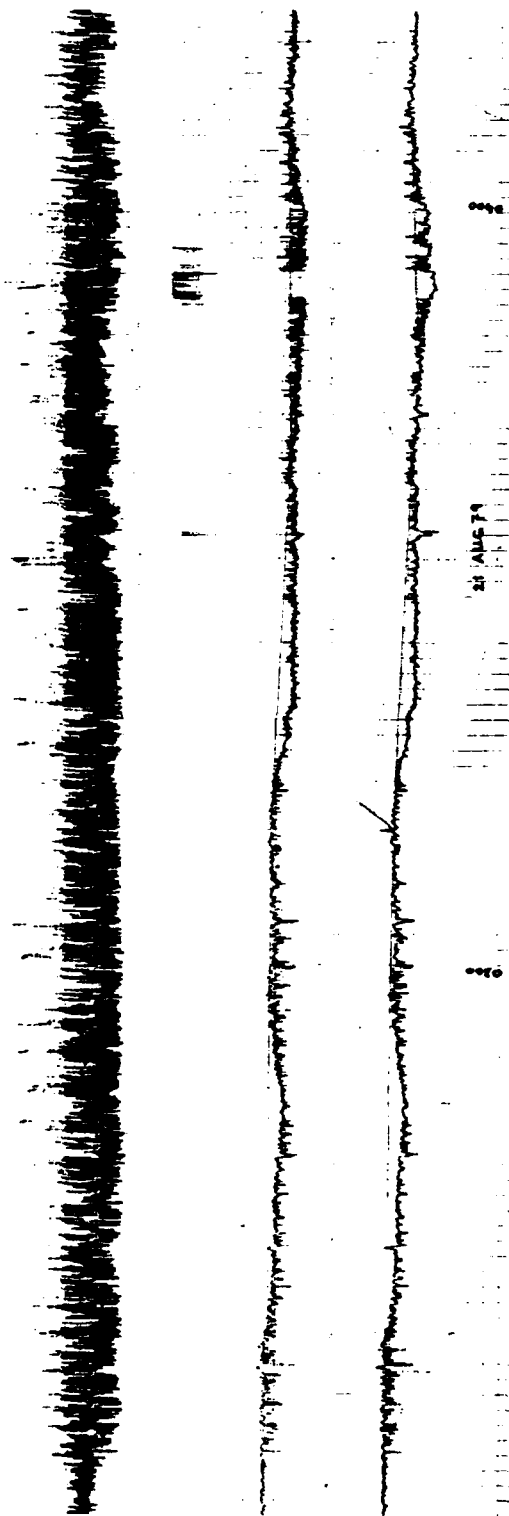


Fig. 3. A section of the polarimeter record at Arequipa exhibiting three depletions within a single scintillation patch. The channel at the top shows the amplitude of the 137 MHz signal and the other two channels correspond to the Faraday polarization angle of the signal, with one shifted from the other by  $90^\circ$ . The response of the amplitude channel is limited by the very fast amplitude scintillation rate. The large spikes are due to a local interference. Universal time hours are indicated.

solar activity maximum have recently been reported (DASGUPTA *et al.*, 1982). Both at Natal and Arequipa the depletions have been found to occur essentially during the pre-midnight hours. The seasonal pattern at Arequipa is similar to that of the 1.54 GHz microwave scintillations observed at the nearby equatorial station Huancayo. At Natal YEH *et al.* (1979b) observed that the electron content depletions have a typical duration of 8–10 min and amplitude of 1–4 TEC units (1 TEC unit =  $1 \times 10^{16}$  el m<sup>-2</sup>).

Two interesting features have been noted during examination of amplitude scintillation and Faraday polarization records simultaneously. The presence of the depletions is always accompanied with a very fast amplitude scintillation fading rate, as has been reported by YEH *et al.* (1979b). Frequently, particularly during the pre-midnight period there may be a series of bubbles occurring within a single scintillation patch. Figure 3 shows a section of a polarimeter record with a number of electron content depletions within a single 137 MHz VHF scintillation patch. It may be observed that the amplitude fading rate is very high, as indicated by the smudged trace, and the amplitude scintillation is limited by the response time of the system.

Figure 4(a) shows the occurrences of electron content depletions with amplitude 1 TEC unit or more as a

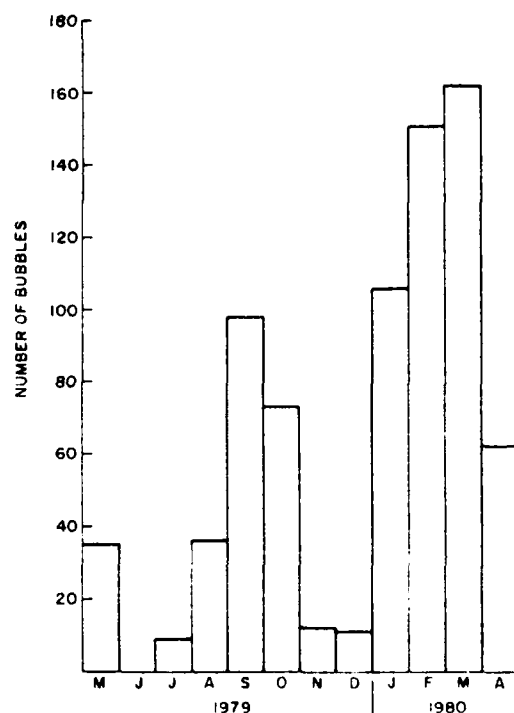


Fig. 4(a). Occurrence of electron content depletions as a function of months

function of individual months. An accurate observation of a smaller depletion amplitude is difficult due to the limited sensitivity of the polarimeter records near the magnetic equator. It is found that the depletion occurrence has a maxima during the equinoctial months, the March equinox having a much higher number than September. As mentioned earlier, the March equinox is characterized by an unusually strong equatorial scintillation activity also (DASGUPTA *et al.*, 1982). A comparison with Figs 1 and 2 indicates that during the December solstice continuous scintillations at VHF may be present for several hours with practically no detectable depletions. On the contrary, the equinoctial months are characterized by narrower discrete patches with considerable integrated ionization depletions. Figures 4(b) (d) show the nature of electron content depletions observed at Arequipa in different seasons. It is evident that the majority of depletions have an amplitude of less than 5 TEC units and the most probable duration is 10–15 min. However, there are occasions when depletions of amplitude as large as 20 TEC units and with a duration of 30 min or more are encountered. It is also observed that there is practically no seasonal dependence of depletion amplitude and duration. In terms of ambient ionization level there is an indication that the percentage depletion is slightly higher in December than that in the equinoxes. No definite relationship between depletion amplitude and duration could be established.

More recently, TYAGI *et al.* (1982) reported observations on changes in ionospheric electron content associated with amplitude scintillations obtained at Natal, Brazil during the one year period from September 1978 to August 1979. A portion of their observing period overlaps that of the present study. A prominent nighttime secondary diurnal peak during the equinoxes, similar to that observed by TYAGI *et al.* (1982), occurs at Arequipa. The average amplitude and duration of the TEC depletions are nearly the same at both Natal and Arequipa. However, in contrast to their observations, we did not find any systematic change in the average signal amplitude during periods of strong scintillations and TEC changes. Also, we found no TEC enhancements associated with scintillations. We believe that the increases in TEC during periods of slower amplitude scintillation fading do not occur, and those reported for Natal, Brazil by TYAGI *et al.* (1982), as they say, "may be affected by the subjective approach". The TEC depletions and enhancements should be determined in the context of the overall background TEC variations during the night, as shown in Fig. 3 of TYAGI *et al.* (1982). The length of the sample record of their Fig. 5, in which they purport to show TEC depletions as well as enhancement accompanying



## AREQUIPA 'BUBBLE' DURATION

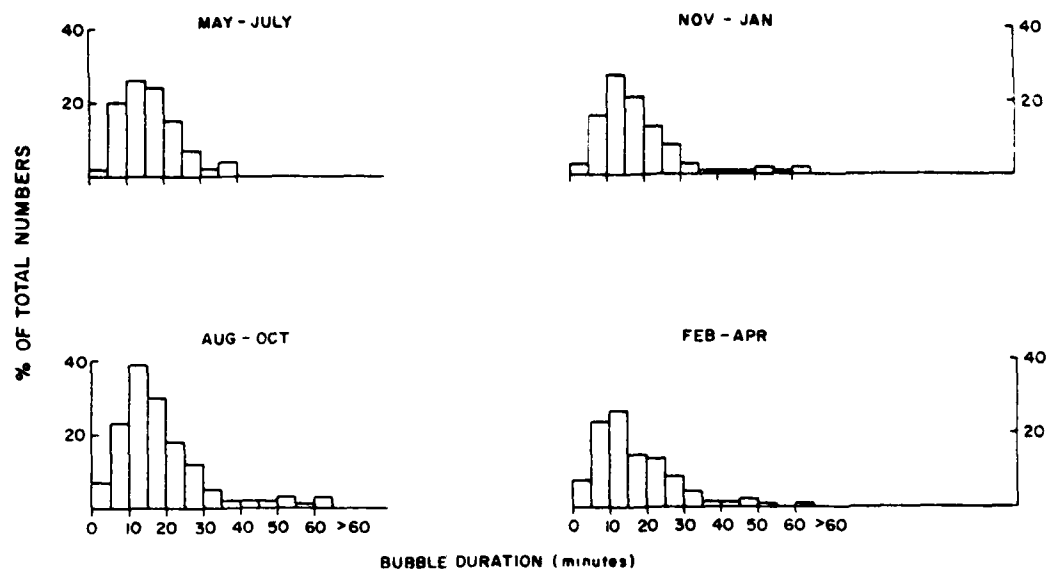


Fig. 4(b). Distribution of total content depletions with duration.

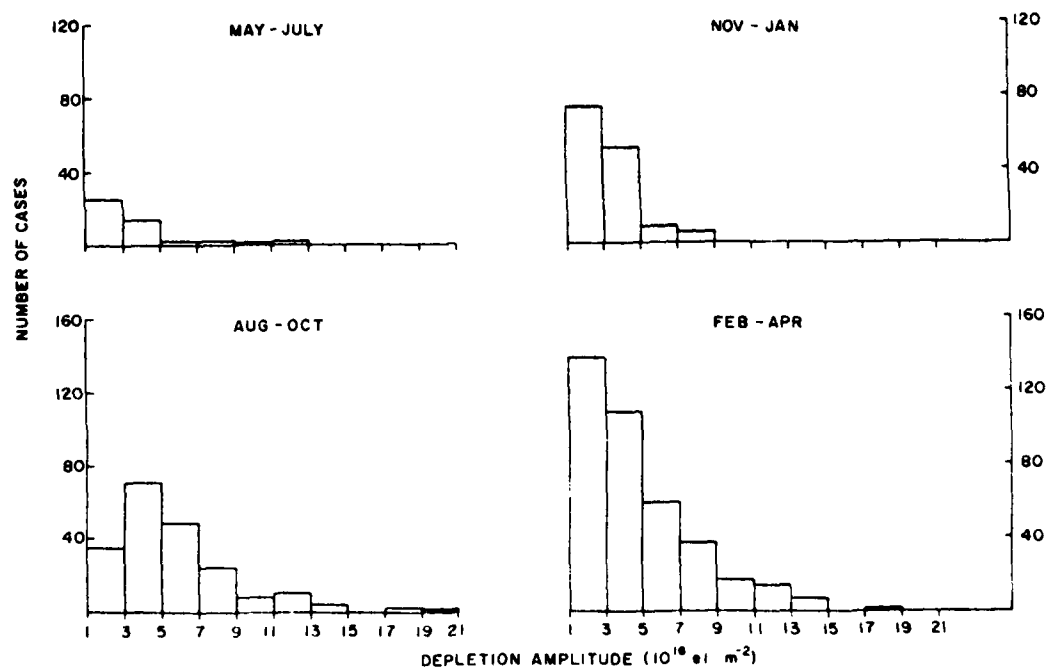


Fig. 4(c). Distribution of total content depletions with depletion amplitude.

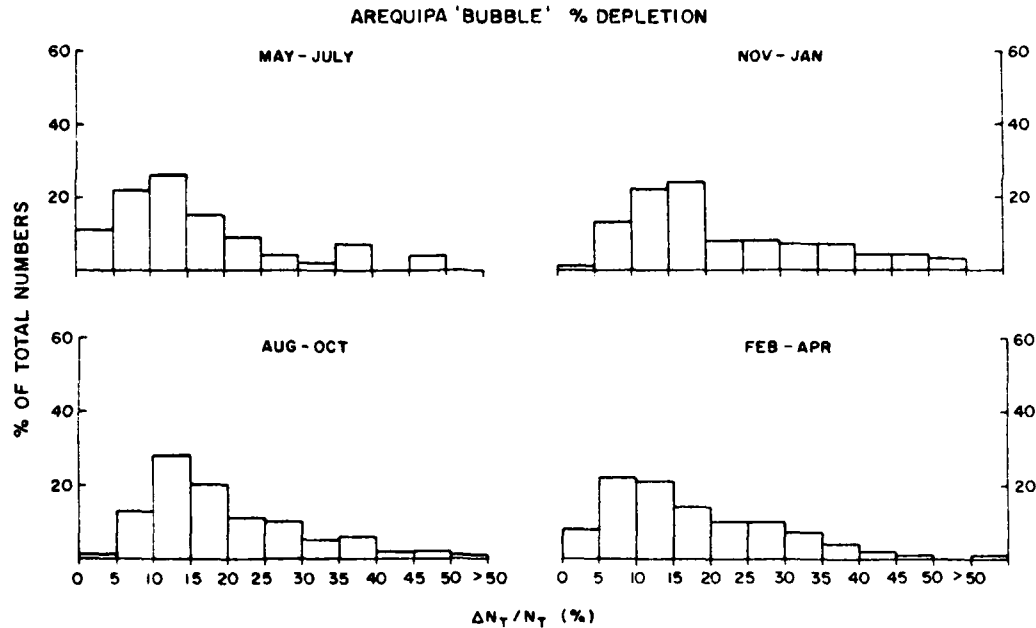


Fig. 4(d). Distribution of total content depletion as a function of percentage depletion about the ambient total content level.

scintillation during a 45 min interval, is not long enough for an independent judgement of their definition of enhancement. We prefer to believe that the entire period had depleted TEC values, with greater depletions occurring during periods of faster amplitude scintillations. The sample enhancement record presented in their Fig. 6 does not show any accompanying amplitude channel, nor is the record long enough to show the longer term background TEC changes during that night. Other techniques, such as the rocket and satellite *in situ* measurements (McCLURE *et al.*, 1977) and radar measurements (TSUNODA, 1980) have not detected any density enhancement relative to the background. Theoretical studies (HUDSON, 1978; SZUSZCZEWICZ, 1978) also indicate why TEC enhancements are unlikely to occur.

#### 4. DISCUSSION

The results presented in this paper cover the morphology of scintillations at VHF observed at Arequipa around the recent solar maximum. The regular features of scintillations, such as the diurnal, seasonal and geomagnetic control, are similar to those already established at Huancayo. The higher scintillation occurrence at VHF during the December solstice is in contrast to the equinoctial seasonal maxima at 1.54 GHz and may be due to the seasonal dependence

of the overall strength of equatorial irregularities. VHF amplitude scintillation at 137 MHz is caused by irregularities of scale size of about 1 km, while microwave scintillation at 1.54 GHz is due to irregularities of a few hundred meters scale size (about 450 m in the present case), corresponding to their respective Fresnel dimensions. During the equinoxes the equatorial irregularities may be intense and the irregularities over the scale size range of a few hundred meters to a few kilometers may be strong enough to cause scintillations at VHF as well as microwaves. In the December solstice, with a relatively weaker overall level, the kilometer scale irregularities may still have sufficient strength to cause scintillations at VHF but the smaller scales will have little power spectral density to affect the microwaves.

The difference in the diurnal and seasonal behavior of electron content depletions and VHF amplitude scintillation occurrences may be related to the strength of the irregularities and the type of associated spread-*F*. Electron content depletions at Arequipa and amplitude scintillations in the *L*-band at the nearby equatorial station at Huancayo have been found to have pronounced maxima during pre-midnight hours of the equinoxes (DASGUPTA *et al.*, 1982). The effect is not so pronounced at a lower frequency of 257 MHz, while at 137 MHz the seasonal variation of scintillation occurrence has a maximum in the December solstice, with

considerable occurrences during the post-midnight period. During the December solstice 137 MHz amplitude scintillation patches of several hours duration are obtained without detectable electron content depletions. LIVINGSTON (1980) also observed a systematic difference in the occurrence statistics of equatorial VHF and *L*-band scintillations.

RASTOGI (1980a) has observed that during solar maximum years range type spread-*F* occurrence at Huancayo has its maximum during the pre-midnight hours of equinoctial months, while frequency type spread-*F* maximum occurs around midnight hours of the December solstice. If the electron content depletions are taken as indications of large amplitude irregularities extended over a certain height range, a corrugation in the spatial distribution of the *F*-region electron density may be visualized. Such a configuration will give rise to range spread echoes with multiple traces on ionograms during the pre-midnight hours, in association with electron content depletions and microwave scintillations. On the other hand, relatively weak and thin irregularity layers, manifested in the form of frequency type spread-*F*, may cause moderate

to intense scintillations at VHF with no signatures on electron content or microwave signal amplitude.

For the period under investigation, the occurrence of spread-*F* as indicated by the parameter *F* in the scaled values of  $f_oF_2$  at Huancayo shows a pattern similar to that of VHF scintillations. An actual examination of the Huancayo ionosonde data for December 1979 shows that the spread-*F* during its onset phase in the post-sunset hours is of range type. In the course of a couple of hours, there is a transformation to the frequency type. During the post-midnight hours the spread-*F* is mainly of frequency type and quite a few cases of intense, even saturated, scintillations at VHF could be identified with frequency type spread-*F*. Figure 5 shows the hourly occurrence patterns of the two types of spread-*F* and 137 MHz amplitude scintillations during December 1979. It is evident that during the post-midnight hours the spread-*F* is essentially of frequency type and the VHF scintillations generally follow the occurrence pattern of the above. RASTOGI (1980b) and RASTOGI and AARONS (1980) observed that strong VHF scintillations are generally associated with range type spread-*F*, while during frequency spread VHF

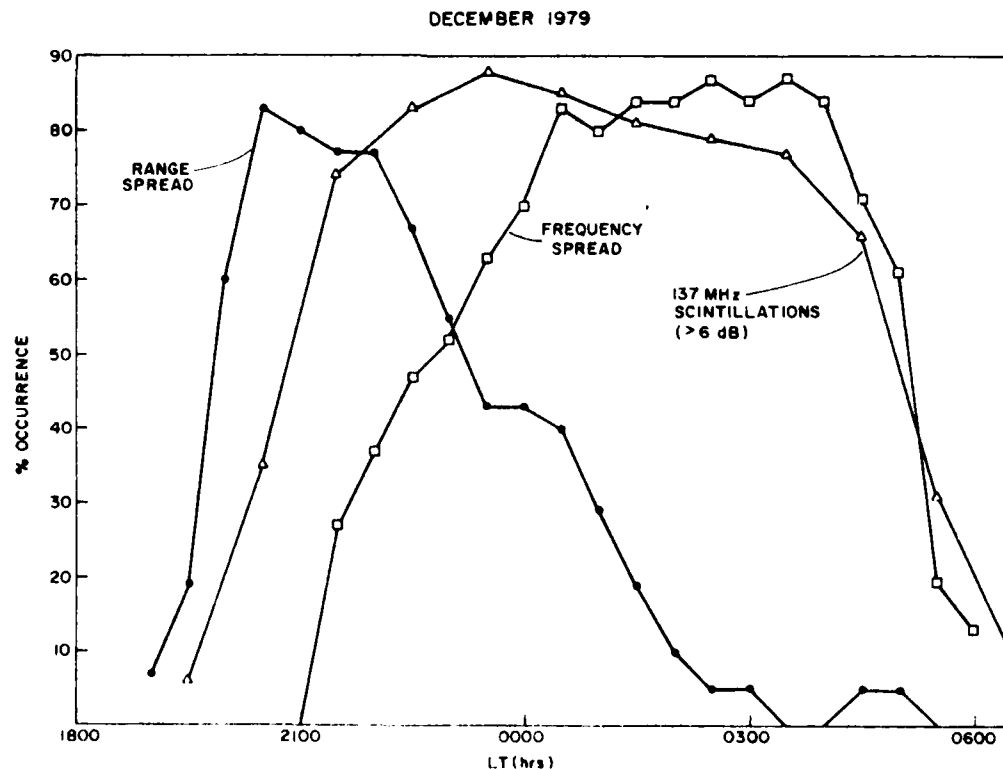


Fig. 5. Occurrences of range and frequency types of spread-*F* at Huancayo and 137 MHz scintillations at Arequipa during December 1979.

scintillations were practically absent. The above features were obtained during solar minimum conditions, when the *F*-region ambient ionization was low. The present results pertain to a period characterized by an unusually high level of solar activity, and, as a consequence, a much higher value of *F*-region ionization. A higher ambient ionization will result in a larger electron density deviation of the irregularities, for the same percentage deviation. A typical *foF2* value of 7 MHz with a frequency spread ( $\Delta f$ ) = 0.5 MHz corresponds to a density deviation  $\Delta n = n(2\Delta f)/foF2 = 8.5 \times 10^{10} \text{ el m}^{-3}$  (WRIGHT *et al.*, 1977). For the above value of  $\Delta n$ , the level of amplitude scintillation may be estimated provided the form of the irregularity spectrum is known (RUFENACH, 1975). With *in situ* measurements, the irregularity waveform encountered during the post-midnight period in the presence of frequency spread on ionograms is found to be sinusoidal with scale length  $\sim 1 \text{ km}$  (McCLURE, private communication, 1982), leading to a Gaussian form of irregularity spectrum. If we assume that the irregularities with the above value of  $\Delta n$  are distributed over a layer thickness of 25 km (which may generally be considered to be a thin layer), then they can give rise to near-saturated scintillations at 137 MHz. Thus, moderate to intense levels of scintillations at VHF may be observed with frequency spread under very high levels of solar activity, in contrast to the cases reported for solar minimum years.

The seasonal dependence of east-west dimensions of the irregularity patches has not been reported before. This paper clearly establishes that the equinoctial patches are more in number but with narrower east-west extent, compared to the much wider patches during the December solstice. The above feature together with the observed seasonal dependence of electron content depletion and microwave scintillation occurrences, with maxima during the equinoxes, indicates that the irregularities corresponding to the equinoctial and December solstice months belong to

different classes and also possibly to different initiating mechanisms. Atmospheric gravity waves have been suggested to be the most likely seed mechanism for the generation of equatorial *F*-region irregularities (ROTTGER, 1978; BOOKER, 1979). However, the seasonal dependence of gravity wave characteristics in the equatorial region is yet to be reported. The period of a gravity wave effect is a function of the difference between the zonal thermospheric wind and plasma drift velocities (KELLEY *et al.*, 1981). If the above difference is dependent on season, with the two velocities differing significantly in equinoxes, the equinoctial irregularity patches should be numerous with narrower east-west extents.

Further, the dynamical behavior of the equatorial *F*-region ionosphere is largely controlled by the *E*-region electric field. The magnitude and the time of pre-reversal enhancement of the *F*-region  $\mathbf{E} \times \mathbf{B}$  vertical drift around the sunset time have a strong seasonal dependence. From Jicamarca radar observations, it has been established that, around solar maximum years, the difference between the drift reversal time and the *E*-region sunset is maximum during the December solstice months (FEJER *et al.*, 1979). In addition, although there is considerable day-to-day variability, an examination of the above data also shows that the width of the pre-reversal peak of vertical drift is greater in December than in other seasons. A broader peak of upward drift might result in a perturbation of large horizontal scale, in a process analogous to the tidal wave modes in the upper atmosphere. ABDU *et al.* (1981) have also recently reported that the occurrence of frequency type spread-*F* on ionograms may be associated with a broader pre-reversal peak of the  $\mathbf{E} \times \mathbf{B}$  drift.

*Acknowledgement* - The ionosonde data were obtained from the World Data Center-A for Solar-Terrestrial Physics, NOAA/EDIS, Boulder, Colorado.

## REFERENCES

- |   |      |  |
|---|------|--|
| AARONS J., MULLEN J. P., WHITNEY H. E. and MACKENZIE E. M.            | 1980 | <i>J. geophys. Res.</i> <b>35</b> , 139.       |
| ABDU M. A., BITTENCOURT J. A. and BATISTA I. S.                       | 1981 | <i>J. geophys. Res.</i> <b>86</b> , 11443.     |
| BASU S. and BASU S.   | 1981 | <i>J. atmos. terr. Phys.</i> <b>43</b> , 473.  |
| BASU S., BASU S., MULLEN J. P. and BUSHBY A.                          | 1980 | <i>Geophys. Res. Lett.</i> <b>7</b> , 259.     |
| BASU S., BASU S., MULLEN J. P., LAHOZ C., BUSHBY A. and WOODMAN R. F. | 1977 | <i>J. atmos. terr. Phys.</i> <b>39</b> , 1251. |
| BHAR J. N., DASGUPTA A. and BASU S.                                   | 1970 | <i>Radio Sci.</i> <b>5</b> , 939.              |
| BOOKER H. G.  | 1979 | <i>J. atmos. terr. Phys.</i> <b>41</b> , 501.  |
| DASGUPTA A., AARONS J., KLOBUCHAR J. A., BASU S. and BUSHBY A.        | 1982 | <i>Geophys. Res. Lett.</i> <b>9</b> , 147.     |

- DASGUPTA A. and MAITRA A. 1980 *Advances in Space Exploration, COSPAR Series* (Edited by A. P. MITRA) Vol. 8, p. 209. Pergamon Press, Oxford.
- FEJER B. G., FARLEY D. T., WOODMAN R. F. and CALDERON C. 1979 *J. geophys. Res.* **84**, 5792.
- HUDSON M. K. 1978 *J. geophys. Res.* **83**, 3189.
- KAUSHIKA N. D. and DE MENDONCA F. 1974 *Planet. Space Sci.* **22**, 1331.
- KELLEY M. C., LARSEN M. F., LAHOZ C. and MCCLURE J. P. 1981 *J. geophys. Res.* **86**, 9087.
- KLOBUCHAR J. A. and AARONS J. 1980 *Alta Freq.* **49**, 345.
- LEE M. C., DASGUPTA A., KLOBUCHAR J. A., BASU S. and BASU S. 1982 *Radio Sci.* **17**, 399.
- LIVINGSTON R. C. 1980 *Radio Sci.* **15**, 801.
- MCCLURE J. P., HANSON W. B. and HOFFMAN J. F. 1977 *J. geophys. Res.* **82**, 2650.
- RASTOGI R. G. 1980a *J. atmos. terr. Phys.* **42**, 593.
- ROTTGER J. 1978 *J. atmos. terr. Phys.* **40**, 1103.
- RUFENACH C. L. 1975 *Radio Sci.* **10**, 155.
- SINCLAIR J. and KELLEHER R. F. 1969 *J. atmos. terr. Phys.* **31**, 201.
- SZUSZCZEWICZ E. P. 1978 *J. geophys. Res.* **83**, 2665.
- TSUNODA R. T. 1980 *J. atmos. terr. Phys.* **42**, 743.
- TYAGI T. R., YEH K. C., TAURIANEN A. and SOICHER H. 1982 *J. geophys. Res.* **87**, 2525.
- WEBER E. J., BUCHAU J. and MOORE J. G. 1980 *J. geophys. Res.* **85**, 4631.
- WOODMAN R. F. 1972 *Space Res.* **12**, 969.
- WRIGHT J., MCCLURE J. P. and HANSON W. B. 1977 *J. geophys. Res.* **82**, 548.
- YEBOAH-AMANKWAH D. and KOSTER J. R. 1972 *Planet. Space Sci.* **20**, 395.
- YEH K. C. and GONZALES V. H. 1960 *J. geophys. Res.* **65**, 3209.
- YEH K. C., SOICHER H., LIU C. H. and BONELLI E. 1979a *Geophys. Res. Lett.* **6**, 473.
- YEH K. C., SOICHER H. and LIU C. H. 1979b *J. geophys. Res.* **84**, 6589.
- YEH A. C., MULLEN J. P., MEDEIROS J. R., DASILVA R. F. and MEDEIROS R. T. 1981 *J. geophys. Res.* **86**, 7527.
- Reference is also made to the following unpublished material:*
- KLOBUCHAR J. A., AARONS J., WEBER E., LUCENA L. and MENDILLO M. 1978 Paper G.4, U.S. National Radio Science Meeting, U.S. National URSI, Boulder, Colorado, 6-9 November.
- RASTOGI R. G. 1980b Proc. COSPAR/URSI Symp. Scientific and engineering uses of satellite radio beacons, Warsaw, Poland, 19-23 May, Polish Scientific Publishers, p. 215.
- RASTOGI R. G. and AARONS J. 1980 Pre-print, AFGL.

## Microwave equatorial scintillation intensity during solar maximum

Jules Aarons and Herbert E. Whitney

Air Force Geophysics Laboratory, Hanscom Air Force Base, Bedford, Massachusetts 01731

Eileen MacKenzie and Santimay Basu

Emmanuel College, Boston, Massachusetts 02115

(Received September 12, 1980; revised December 24, 1980; accepted December 29, 1980)

A comparison of scintillation levels at 1.5 GHz made from the Appleton anomaly region of the magnetic equator and from the region close to the magnetic equator (termed the electrojet latitudes) showed increased *F* region irregularity intensity over the anomaly region during years of high sunspot number. Peak to peak fading greater than 27 dB was noted from Ascension Island (through a dip latitude of 17°) in the anomaly region while only 7-9 dB from Natal, Brazil, and Huancayo, Peru, were noted, the last two paths being close to the magnetic equator. The hypothesis advanced is that the dominant factor responsible for the intense gigahertz scintillation is the traversal of the propagation path through the anomaly region. During years of high sunspot numbers the high levels of  $\Delta N$  constituting the *F* region irregularity structure are due to (1) very high electron density in the anomaly region (compared to the electrojet region) and (2) the late appearance of these high electron densities (to 2200 local time) in the anomaly region. The patches or plumes of irregularities seen in the postsunset time period then produce high  $\Delta N$ ; scintillation excursions are proportional to this parameter. The postulation of vertical irregularity sheets in the patches was examined to determine the possibility of this being an important factor in the difference between electrojet and anomaly scintillation levels. Older gigahertz data from the sunspot maximum years 1969-1970 were reanalyzed, and more recent observations from other studies were also reviewed. It was found that through the anomaly region, high scintillation indices were noted at a variety of azimuths of the propagation path rather than just along a path closely aligned with the magnetic meridian. A more complete evaluation of the geometrical factor, which must be of considerable importance in determining the absolute value of the scintillation intensity, awaits further observations.

### INTRODUCTION

In recent years a variety of methods have been used to probe and measure *F* layer irregularities in the equatorial region [Aarons, 1977; Basu and Kelley, 1979]. One method is to record transionospheric scintillation of satellite signals in the VHF to microwave frequency range.

This paper will contrast levels of scintillation activity at *L* band (1541 MHz in this case) which were relatively low when a satellite beacon was observed through latitudes close to the magnetic equator (Natal, Brazil, and Huancayo, Peru) and very high when the same satellite beacon was observed nearly overhead at Ascension Island through a region near the peak of the equatorial anomaly. The differences in scintillation intensity was recorded during the peak of solar activity in

1979 and 1980. The equatorial or Appleton anomaly shows during noontime a distinct trough of electron density in the bottomside and topside ionosphere at the magnetic dip equator with crests of ionization at ~15°-20° north and south dip latitudes. We shall discuss later that the *F* region ionization near Ascension Island exhibits a latitudinal variation similar to the daytime Appleton anomaly in the postsunset hours during the solar maximum period.

**Measurements.** The Air Force Geophysics Laboratory, in cooperation with various groups, records scintillation activity of the MARISAT beacon, transmitting at UHF (257 MHz) and at *L* band (1541 MHz) at three sites near the magnetic equator. The sites are listed in Table 1 along with the coordinates of the 400-km subionospheric intersection point, the dip latitude of this point, and the propagation angle (i.e., the angle between the path to the satellite and the lines of force of the earth's magnetic field) and the ground elevation and azimuth angles of

Copyright © 1981 by the American Geophysical Union

Paper number IS0036.  
0048-6604/81/0910-0036\$01.00

TABLE 1. Geometry of primary observations

Station	Elevation angle	Azimuth angle	Propagation angle	400-km subionospheric		Approximate dip latitude
				latitude	longitude	
Huancayo, Peru	20°	83°	85°	11°S	68.5°W	2.5°N
Natal, Brazil	65°	75°	84°	5.6°S	33.7°W	5.5°S
Ascension Island	80°	356°	52°	7.4°S	14.4°W	17°S

the path to the satellite. Figure 1 is a map with geographic latitudes and dip latitudes plotted. This tracing was taken from the Defense Mapping Agency map of the 1975 epoch of magnetic inclination. The isoclinic lines are the results of a spherical harmonic analysis to degree and order 12.

**Magnetic equator observations.** In a recent paper, Basu *et al.* [1980a] have analyzed the *L* band observations made from Huancayo, Peru. Data have been taken at this site over a period of 3 years. During that time no fluctuation greater than 8 dB peak to peak was recorded. In the month of December 1979, a period of intensive and common measurements at the three sites being contrasted in this paper, scintillation activity maximum was 6.8 dB at Huancayo. Viewing of MARISAT from this site was done almost perpendicular to the field lines, that is, at an azimuth of 83° through a dip latitude of 2.5°N, as shown in Table 1.

Similar observations have been made recently at Natal, Brazil, in cooperation with the Federal University of the Northern Rio Grande. This site

viewed MARISAT at 65°, a higher elevation angle than that of the Huancayo observations. The viewing of the satellite was also across the field lines, that is, at an azimuth of 75°. Scintillations greater than 8 dB were not detected during the December period.

In December 1979 a 10-ft (~3-m) antenna was put into operation at Ascension Island for both *L* band and UHF. Over several hours on many nights some scintillations exceeded 27 dB peak to peak (Figure 2) at 1541 MHz. These fades reached the noise level of the equipment. Calibrated and consistent measurements have been made since that time which show hours of such intense activity during the December–March period. Figure 3 gives the percentage of occurrence of scintillation activity at 1541 MHz greater than 20 dB for *Kp* = 0–3 and *Kp* = 3+ to 9 during January–February 1980. The highest percentage of occurrence of >20 dB for *Kp* = 0–3 was ~42% with ~23% for *Kp* = 3+ to 9. It might be noted that in accord with Aarons *et al.* [1980b] during these months, increased magnetic activity inhibits scintillation. Ascension Island was viewing MARISAT close to the magnetic meridian plane at an elevation of 80° during these observations.

Statistics of the *L* band scintillations observed at Huancayo, during February–March 1980, show a 16% occurrence of scintillation of >3 dB in the time period 0000–0400 UT (~1900–2300 LT) with no scintillation of >6.8 dB even during those times. The data are clear; that is, for Ascension the scintillation activity is considerably higher than for the two sites near the magnetic equator during the same periods of time. While the intersection longitudes of Ascension and Natal are somewhat separated, they are, by global standards, quite close and are expected to behave according to the pattern of their longitudinal sector [Aarons *et al.*, 1980b].

Although the data contrasts are clear, a problem exists in interpreting the observations; the Ascension Island observations were taken with the propagation path near the magnetic meridian, while those

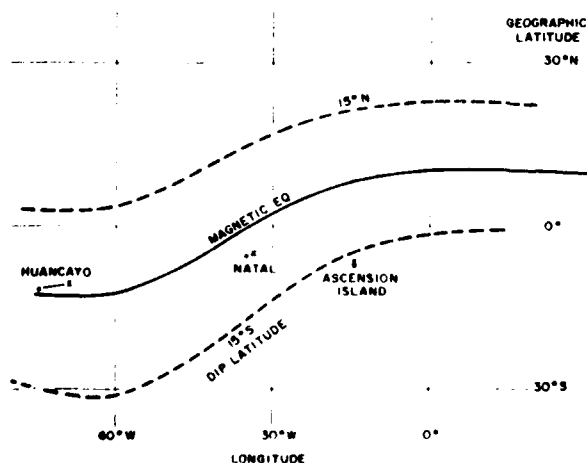


Fig. 1. Map of equatorial region in the 0°–70°W longitude region using the 1975 epoch of the Defense Mapping Agency magnetic inclination map for magnetic parameters.

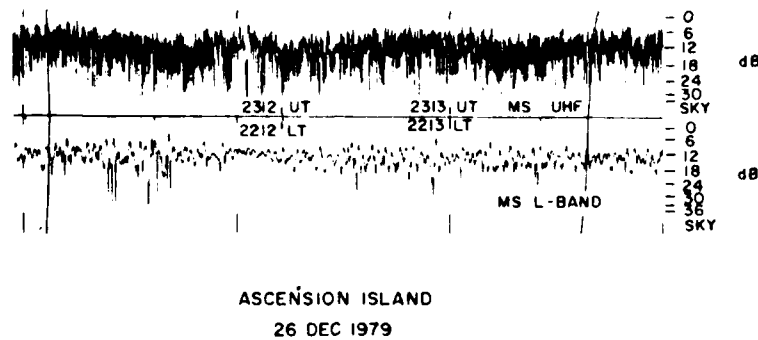


Fig. 2. Sample of both UHF and L band data recorded at Ascension Island during December 1979 to January 1980. Note excursions of  $\geq 27$  dB on both UHF and L band channels.

at Natal and Huancayo were not. However, the Ascension Island 400-km intersection is in the anomaly region (a dip latitude of  $17^\circ$ ), while the Natal and Huancayo intersections are close to the magnetic equator. In this paper we shall attempt to weigh the relative importance of these two factors.

#### THE IRREGULARITY STRUCTURE AND ITS GEOMETRY

The configuration of the patch containing the small-scale irregularities which has emerged from optical and radio measurements and from in situ probing is that of an elongated structure extending several thousand kilometers north and south of the magnetic equator [Weber *et al.*, 1980; Aarons *et al.*, 1980a; Basu *et al.*, 1980b].

Within the highly elongated patch it is possible to contemplate various models for the irregularities

producing the scintillations. If a 10:10:1 irregularity model of vertical sheets is assumed (10 magnetic N-S, 10 vertical in the magnetic meridian plane, and 1 unit magnetic E-W), then a pronounced maximum will result from pure geometrical considerations for observations made along the magnetic meridian (S. Basu, private communication, 1980). This effect will enhance or minimize the amplitude scintillation value depending on the magnetic azimuth of the ray path. The postulation of vertical sheets has been based on the correlation lengths of plasma bubbles in the vertical direction obtained by numerical simulation techniques [Zalesak and Ossakow, 1980].

Using the basic formulation of a program developed by Mikkelsen *et al.* [1978] for high-latitude irregularity enhancement due to geometry, the scintillation intensity ( $S_4$ ) for the propagation path from Ascension for a vertical sheet (10:10:1) is a factor of 0.98 relative to observations made immediately overhead of the station. The factor for the same postulated configuration using the geometry appropriate to Natal is 0.14 (an increase of  $S_4$  ASC/ $S_4$  NATAL of 7). Therefore the 10:10:1 sheets might account for a large portion of the ratio of Ascension to Natal levels. The geometrical situation for Huancayo is very similar to that for Natal.

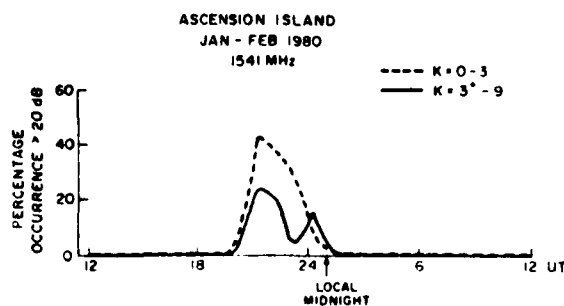


Fig. 3. Percentage occurrence of L band scintillations of  $\geq 20$  dB at Ascension Island during January-February 1980. Observations are segmented into quiet ( $K_p = 0-3$ ) and disturbed ( $K_p = 3+$  to 9) magnetic conditions.

#### HIGH SUNSPOT NUMBER AND SCINTILLATION INTENSITY

Measurements at 137 and 250 MHz have shown that the occurrence of scintillation is greater in the same season for years of high versus years of low sunspot activity [Aarons *et al.*, 1978]. However, absolute levels cannot be measured at these two



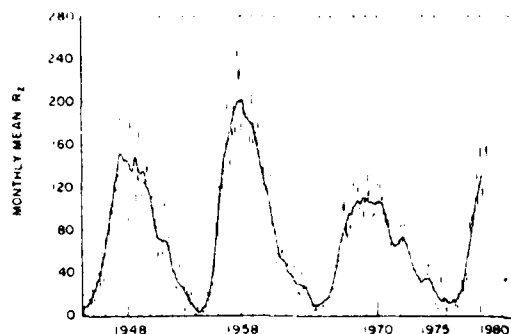


Fig. 4. Plot of mean Zurich sunspot numbers from 1944 to 1980.

frequencies with the morphological studies made, since both strong scattering and saturation of the signal-to-noise levels of the equipment took place frequently. Therefore in order to assess the role of high sunspot number, we shall confine our remarks to frequencies above 1 GHz including data at 2.2–4 GHz where signals are not saturated, that is, do not show fading down to noise. It might be noted that peak to peak fading of 3 dB at 4 GHz is equivalent to fading of 18 dB at 1.5 GHz if a frequency dependence of  $f^{-1.5}$  holds [Whitney, 1974]. This conversion is applicable to weak scattering, which, admittedly, may not be involved here.

Fang *et al.* [1978] states that 'Gigahertz ionospheric scintillations follow the sunspot cycle. For years with sunspot number less than 30, scintillations at 4 GHz with magnitudes over 2 dB were never observed at INTELSAT earth stations.' For the purposes of relating various measurements we have plotted sunspot number in Figure 4 for recent years.

For the sake of outlining our hypothesis we have divided the equatorial region into 'electrojet' latitudes and 'anomaly' latitudes. Electrojet latitudes are taken to be in the range of 5°N to 5°S magnetic dip latitude, while anomaly latitudes are on either side of the electrojet latitudes, falling off beyond 15°–20° dip latitude. Anomaly peaks may be relatively narrow in latitude. The hypothesis advanced for higher scintillation levels in the anomaly latitudes during this period of high sunspot number is that electron density levels and time of maximum electron density at these latitudes primarily account for the greater scintillation intensities at Ascension than at Natal or Huancayo. It is believed that the differences in intensity are related to the following:

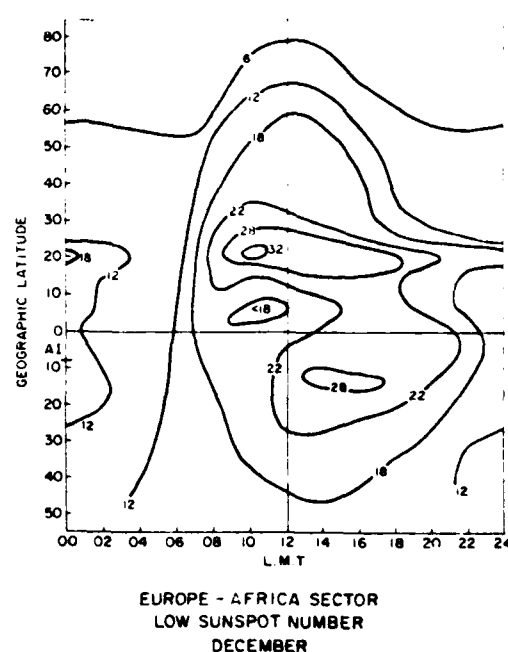


Fig. 5. Map of MUF (3000)  $F_2$  (December) in Europe-Africa zone derived from observations during years of low solar flux [Rawer, 1963].

(1) the equatorial anomaly produces higher electron density values in high sunspot number years than in years of low solar activity and (2) the occurrence of maximum electron density for anomaly latitudes is near sunset in the years of high sunspot number and in the afternoon in years of low solar activity.

To illustrate these two points, we have reproduced diagrams from Rawer [1963] for MUF (3000)  $F_2$  in the Europe-Africa zone for the month of December for years of low sunspot number (Figure 5) and for years of high sunspot number (Figure 6). These contour maps are derived from observations rather than a model. They indicate that during years of high sunspot number the peak of the MUF (3000)  $F_2$  in the southern hemisphere is 36 MHz and that in low sunspot years the peak is 28 MHz. The time of peak MUF is 1800–2200 LT during high sunspot number years and 1300–1700 LT during low solar activity years. MUF 3000 ( $F_2$ ) is related to  $foF_2$ . Ascension Island belongs between the American sector and the Europe-Africa sector, but the ionospheric path to the satellite is through the Appleton anomaly.

Observations of total electron content were taken at Ascension Island by J. A. Klobuchar (private

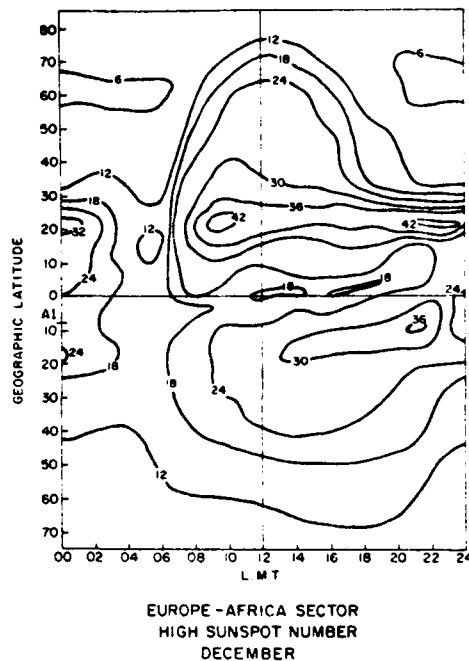


Fig. 6. Map of MUF (3000)  $F_2$  (December) in Europe-Africa zone derived from observations during years of high solar flux [Rawer, 1963].

communication, 1980) during the December 1979 to February 1980 time period. The propagation path (to the satellite, SIRIO) corresponded almost exactly with that to MARISAT. Two maxima were seen during the months examined, one at 1830 LT and the second at 2100–2200 LT, corresponding well with the times of maxima given in Figure 6.

During the December period, observations were made with AE-E using the retarding potential analyzer (W. B. Hanson, private communication, 1980). The value of  $N$  was greater by an order of magnitude in the anomaly region than near the magnetic equator. The ratio ( $\Delta N/N$ ) was of the same order of magnitude in both regions. Scintillation intensity, which is proportional to  $\Delta N$ , would then be expected to be greater in the anomaly region.

#### EARLIER OBSERVATIONS

Since the Ascension Island data could not resolve the question of the importance of the geometrical versus the latitudinal variables, it was thought worthwhile to reexamine older data to try to resolve the question.

Between November 1969 and June 1970, when

a high sunspot number of  $\sim 120$  was reported, observations were made of an S band (2.2 GHz) transponder on the moon [Christiansen, 1971] from Ascension Island with both earth- and moon-based signals in this frequency range. Scintillations as large as 20 and 25 dB on the two-way path, ground to transponder and return, were noted. In addition, Canary Island observations from high dip latitudes on the other side of the magnetic equator were also disturbed. Guam observations (at a different longitude) showed shorter periods of lower-intensity scintillations during this time. No other stations on the magnetic equator made observations.

In order to utilize the Christiansen data to their maximum extent, they were reanalyzed to determine if high scintillation levels were predominantly a function of azimuth (the vertical sheet model predicts maximum index at an azimuth of  $\sim 340^\circ$ ) or if high levels were noted at all azimuths of the moon's path as observed from Ascension Island. Figure 7 is a plot of azimuths when scintillation was greater than 10 dB for the 2200-MHz two-way path. Approximately 45 days of data were available.

The results are fairly conclusive. High-intensity scintillation occurs at all azimuths. The levels of scintillation were high at many azimuths (elevation angles were greater than  $25^\circ$  in all of the data illustrated).

Similar results were noted for the Canary Island observations of 2.2-GHz signals. Fewer data are available, but scintillations to 25 dB were recorded at a variety of azimuths. While the data point to

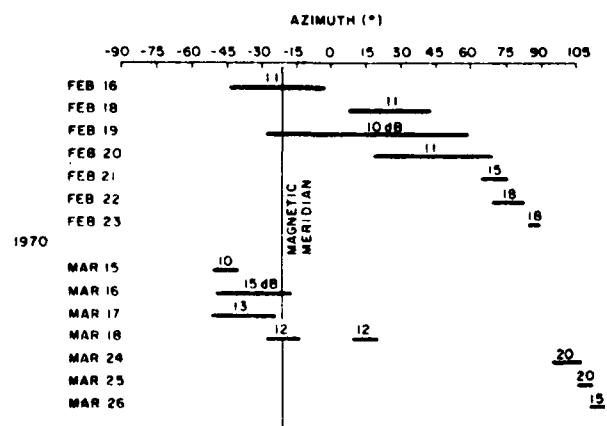


Fig. 7. Azimuths of 2.2-GHz lunar observations of Christiansen, 1970, with maximum decibel excursions for each grouping.

high scintillation intensities in the anomaly region, they still fail to evaluate the geometrical contribution to the intensity at any single observation point.

An interesting set of observations at 4 GHz was made in March–May 1971 from Longonot, Kenya, through a subionospheric dip latitude of  $\sim 14^\circ\text{S}$  by Skinner *et al.* [1971]. They reported that 'scintillation fading of amplitude up to 4 dB in carrier level has frequently been observed at Longonot at night during the months of March, April and May 1971 on signals received from five stations.' The azimuth to the satellite was approximately  $90^\circ$ . Another station, Arvi, India, situated at  $10^\circ$  dip latitude (N) showed only 'weak to moderate scintillation fading on several nights' for the same period. Arvi, India, observed the satellite at an azimuth of  $\sim 210^\circ$ , considerably closer to the magnetic meridian plane than the azimuth from Longonot.

More recently, similar results of high scintillation activity were noted by Fang [1980] at Hong Kong. He recorded 9-dB fluctuations on the 4-GHz COMSAT downlink to Hong Kong at azimuths of  $\sim 105^\circ$  (the Pacific Ocean satellite) and  $252^\circ$  (the Indian Ocean satellite) for periods of up to an hour. Thus high values were noted almost perpendicular to the magnetic meridian.

#### DISCUSSION

From theoretical studies [Basu and Kelley, 1979, and references therein] it seems most likely that the generation of the irregularity bubbles commences at or near the magnetic equator. Once formed, the irregularities in the patch below 600 km would not be observed at Ascension. The field lines of the irregularities below 600 km terminate at the 200-km level at latitudes lower than those of the Ascension propagation path. One effect of increased solar sunspot number is to raise the height of the more intense irregularities [Aarons *et al.*, 1980a] as seen on the Jicamarca backscatter.

Increased solar activity does produce higher electron densities in the *F* region, as shown by the long-term sounder observations, the total electron content (TEC), and the in situ data. If the effect of irregularity formation acts on a percentage basis, then the high sunspot years should show increased scintillation levels at gigahertz frequencies at electrojet and anomaly latitudes. This has been seen at electrojet latitudes (Huancayo) where a comparison of September–October 1977 *L* band data with

September–October 1979 data showed higher intensities in 1979, the higher solar activity year. In addition, Fang's statement indicates that the increase is a general increase.

It is almost impossible to compare absolute values of the moon transponder data at 2.2 GHz, the Kelleher observations at 4 and 6 GHz, the Fang Hong Kong recordings at 4 GHz, and the Ascension Island observations at 1.5 GHz. It is clear, however, that the scintillation levels at Huancayo, Natal, and Guam are lower than levels observed from anomaly latitudes.

While the scintillation intensities during years of high sunspot number are higher in the anomaly regions than those in the electrojet sector, the contribution of geometry of the irregularity model to intensity levels has not been established.

#### CONCLUSIONS

The basic conclusion is that during years of high sunspot activity the absolute value of irregularity intensity increases, particularly in the anomaly region. Ascension Island observations showed fades of greater than 27 dB peak to peak while stations near the magnetic equator were recording values of 7 and 9 dB for isolated fluctuations. At a variety of azimuths, Christiansen reported scintillations in a two-way path at 2.2 GHz of up to 25 dB. At azimuths considerably off the magnetic meridian, Skinner *et al.* [1971] showed appreciable scintillation at 4 GHz. Recently, during years of very high sunspot number, Fang has observed over periods of more than an hour scintillations of 9 dB at Hong Kong at 4 GHz.

In several sets of observations reviewed, azimuths of the propagation path were close to east or west; high scintillation values were found. However, the contribution of geometry to scintillation intensity must be assessed in further experiments. During 1981 there will be an opportunity to view *L* band beacons of the Global Positioning System satellite program at varying geometries from Ascension Island. It is expected that the level of the activity will be adequate to assess the geometrical contribution.

*Acknowledgments.* The authors would like to thank the following for taking and reducing the observations: the Instituto Geofísico del Perú at Huancayo, the Federal University of the Northern Rio Grande at Natal, and the Eastern Space and Missile Center at Ascension. We would also like to thank Sunanda

Basu for many conversations relative to the role of geometry and latitude in gigahertz scintillation levels and J. A. Klobuchar for his initial observations of the *L* band transmissions.

## REFERENCES

- Aarons, J. (1977), Equatorial scintillations: A review, *IEEE Trans. Antennas Propag.*, *AP-25*(5), 729-736.
- Aarons, J., E. MacKenzie, and K. Bhavnani (1978), Equatorial and high latitude empirical models of scintillation levels, paper presented at Conference on Operational Modelling of the Aerospace Propagation Environment, Adv. Group for Aeronaut. Res. and Dev., North Atl. Treaty Organ., Ottawa.
- Aarons, J., J. P. Mullen, H. E. Whitney, and E. M. MacKenzie (1980a), The dynamics of equatorial irregularity patch formation, motion, and decay, *J. Geophys. Res.*, *85*(A1), 139-149.
- Aarons, J., J. P. Mullen, J. R. Koster, R. F. daSilva, J. R. Medeiros, R. T. Medeiros, A. Bushby, J. Pantoja, J. Lanat, and M. R. Paulson (1980b), Seasonal and geomagnetic control of equatorial scintillations in two longitude sectors, *J. Atmos. Terr. Phys.*, *42*, 861-866.
- Basu, S., and M. C. Kelley (1979), A review of recent observations of equatorial scintillations and their relationship to current theories of *F* region irregularity generation, *Radio Sci.*, *14*(3), 471-485.
- Basu, S., S. Basu, J. P. Mullen, and A. Bushby (1980a), Long-term 1.5 GHz amplitude scintillation measurements at the magnetic equator, *Geophys. Res. Lett.*, *7*(4), 259-262.
- Basu, S., J. P. McClure, S. Basu, W. B. Hanson, and J. Aarons (1980b), Coordinated study of equatorial scintillation, in situ, and radar observations of nighttime *F* region irregularities, *J. Geophys. Res.*, *85*(A10), 5119-5130.
- Christiansen, R. M. (1971), Preliminary report of S-band propagation disturbance during ALSEP mission support, *Rep. X-861-71-239*, Goddard Space Flight Center, Greenbelt, Md.
- Fang, D. J. (1980), 4/6 GHz ionospheric scintillation measurements, paper presented at Conference on Propagation Effects in Space/Earth Paths, Adv. Group for Aeronaut. Res. and Dev., North Atl. Treaty Organ., London.
- Fang, D. J., D. J. Kennedy, and C. Devieux (1978), Ionospheric scintillations at 4/6 GHz and their system impact, paper presented at IEEE Electronics and Aerospace Systems Convention, Inst. of Electr. and Electron. Eng., Arlington, Va.
- Mikkelsen, I. S., J. Aarons, and E. Martin (1978), Geometrical considerations of 136 MHz amplitude scintillation in the auroral oval, *J. Atmos. Terr. Phys.*, *40*, 479-483.
- Rawer, K. (1963), F2 layer ionization, in *Advances in Upper Atmosphere Research*, edited by B. Landmark, Pergamon, New York.
- Skinner, N. J., R. F. Kelleher, J. B. Hacking, and C. W. Benson (1971), Scintillation fading of signals in the SHF bands, *Nature London Phys. Sci.*, *232*(26), 19-21.
- Weber, E. J., J. Buchau, and J. G. Moore (1980), Airborne studies of equatorial *F* layer irregularities, *J. Geophys. Res.*, *85*(A9), 4631-4641.
- Whitney, H. E. (1974), Notes on the relationship of scintillation index to probability distributions and their uses for system design, *Rep. AFCRL-TR-74-0004*, Air Force Cambridge Res. Lab., Bedford, Mass.
- Zalesak, S. T., and S. L. Ossakow (1980), Nonlinear equatorial spread *F*: Spatially large bubbles resulting from large horizontal scale initial perturbations, *Memo. Rep. 4154*, Naval Res. Lab., Washington, D. C.

## Depolarization of VHF geostationary satellite signals near the equatorial anomaly crests

M. C. Lee

Regis College Research Center, Weston, Massachusetts 02193

A. Das Gupta<sup>1</sup> and J. A. Klobuchar

Air Force Geophysics Laboratory, Hanscom Air Force Base, Massachusetts 01731

S. Basu and S. Basu

Emmanuel College, Boston, Massachusetts 02115

(Received June 24, 1981; revised September 9, 1981; accepted September 9, 1981.)

The nighttime polarization fluctuations of linearly polarized 136 MHz satellite signals received at Ascension Island, located near the southern crest of the equatorial anomaly, have been shown to be the manifestation of depolarization effect due to the diffractive scattering by small-scale ( $<200$  m) density irregularities with power law spectra. The theory can explain its coexistence with  $L$  band scintillation. The absence of this phenomenon at equatorial locations off the anomaly crests is attributed to two factors: (1) the ambient plasma densities are relatively low, and (2) the propagation angles of satellite signals are more nearly perpendicular to the geomagnetic field.

### 1. INTRODUCTION

Intense and fast fluctuations in Faraday rotation angles have been observed from low-orbit satellite beacon signals transmitting on 20 MHz by Parthasarathy and Reid [1959], Yeh and Swenson [1959], and Roger [1965], on 40 MHz by Kent [1959], and on 54 MHz by McClure [1964]. Kaushika and de Mendonca [1974] observed that the Faraday rotation angle of the 137-MHz VHF signals from a geostationary satellite sometimes exhibited fluctuations of relatively slower periods, ranging from a few seconds to about an hour, when the local ionosonde showed spread  $F$  echoes at the low-altitude station of Sao Jose dos Campos (24°S dip), Brazil. Recently, Klobuchar and Aarons [1980] and Das Gupta and Maitra [1980] have reported intense and fast fluctuations of the Faraday rotation angles, in association with strong and fast amplitude scintillation, respectively, from Ascension Island (31°S dip) and Calcutta (32°N dip), both situated near the crests of the equatorial anomaly.

Similar observations of fast fluctuations of Faraday rotation angles associated with strong, fast amplitude scintillation have been observed as far away from the equator as Delhi (44°N dip), India (Y. V. Somayajulu, private communication, 1981), but they have not been seen at Arequipa (7.9°S dip), Peru, located near the geomagnetic equator, nor have they been reported by Yeh *et al.* [1979a, b], in observations taken at Natal (7.9°S dip), Brazil.

In our observations from Ascension Island, we have noted the coexistence of Faraday polarization fluctuations with strong  $L$  band amplitude scintillation. They appear together during the postsunset hours and disappear at the same time near or after midnight. Saturated 136 MHz amplitude scintillations with a fast fading rate are always seen during the observations of Faraday polarization fluctuations. A sample record is shown in Figure 1. In an experiment at Ascension Island in December 1979, we separately recorded the amplitude of the left-hand circular and right-hand circular components of 136-MHz signals from the SIRIO geostationary satellite observed at 80° elevation transmitting nominally linearly polarized waves. We found that, during the times of strong, fast amplitude fading when polarization fluctuations occur, there was a loss of correlation of the opposite

<sup>1</sup>NAS/NRC Senior Resident Research Associate on leave from the University of Calcutta, India.

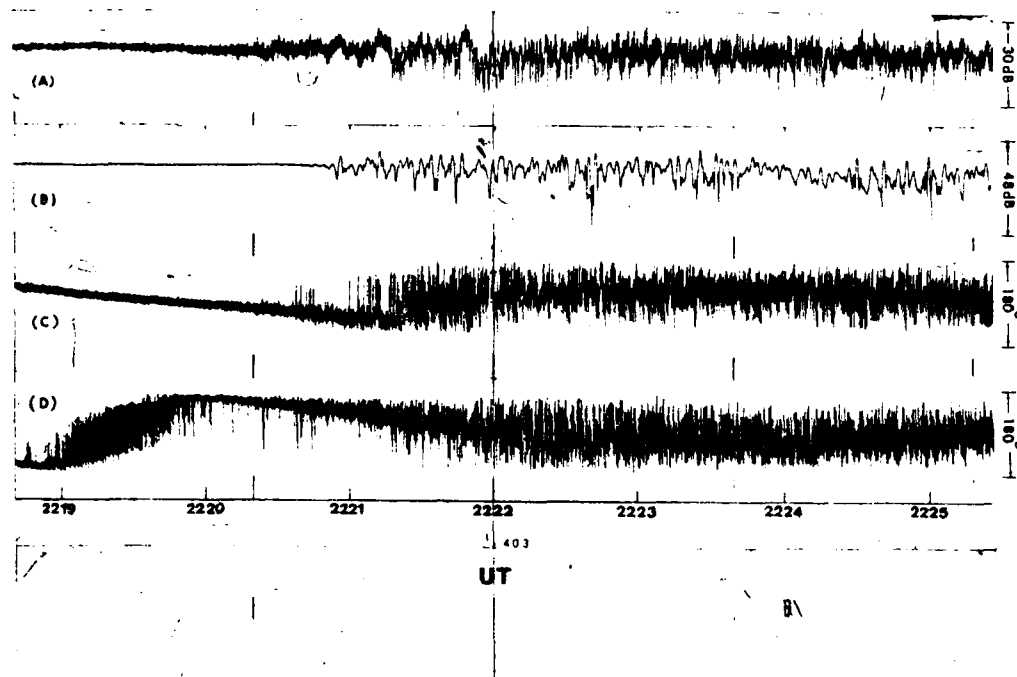


Fig. 1. Sample data of the geostationary satellite signals received at Ascension Island on January 2, 1980. Channels (A) and (B) show the amplitude scintillation of the 136-MHz signals transmitted from SIRIO and that of the *L* band (1.541 GHz) transmitted from MARISAT 1, respectively. Shown in channels (C) and (D) are the Faraday rotation measurements of 136-MHz signals in a ramp format with one channel displaced by 90° relative to the other. Intense and fast polarization fluctuations make the last two channels almost undistinguishable.

sense circularly polarized wave components (i.e., ordinary and extraordinary modes), indicating that, during those times, the concept of simple Faraday rotation was not valid at our observation frequency. It is the purpose of this paper to explain the reasons for those observations and to suggest why polarization fluctuations of VHF radio waves have not been observed very near the magnetic equator.

Ionospheric density irregularities are responsible for the irregular fluctuations in the Faraday rotation angles of satellite signals. We believe that the polarization fluctuations as shown in Figure 1 indicate the depolarization of linearly polarized transionospheric satellite signals. Two mechanisms have been suggested for interpreting the polarization fluctuations of HF satellite signals, specifically, at the frequency of 20 MHz. One concerned the effect of refraction imposed by large spatial inhomogeneities that give rise to large path separation of the ordinary and extraordinary modes, and, consequently, these two characteristic components of a linearly polarized signal can

scintillate independently [Roger, 1965]. The other one proposed by Yeh and Liu [1967] is the process of wave scattering by density irregularities. Induced fluctuations in Faraday rotation angles due to this scattering may cause depolarization effect on the linearly polarized satellite signals.

In Roger's mechanism, it is the ray path separation of the two modes but not the density irregularities that is primarily investigated for the polarization fluctuations of satellite signals. The magnitude of path separation, which is large enough to decorrelate the two modes, is estimated roughly as  $\Delta r = l / \langle (\Delta\phi)^2 \rangle^{1/2}$ , where  $l$  is the scale size of density irregularities, and  $\langle (\Delta\phi)^2 \rangle^{1/2}$  is the rms phase variation of the signals. Roger assumed that  $l = 1$  km,  $\langle (\Delta\phi)^2 \rangle^{1/2} = 2$  rad for 20-MHz signals and obtained  $\Delta r = 0.5$  km. The current in situ data, however, indicate a power law type of irregularity power spectrum encompassing scale sizes from meters to tens of kilometers. Moreover, Roger's mechanism cannot be used in the case of concern here to explain the close relationship of polari-

zation fluctuations with  $L$  band scintillations and others.

By contrast, no significant path separation of ordinary and extraordinary modes is necessary in Yeh and Liu's mechanism. The wave scattering by density irregularities is considered to be the principal process responsible for the polarization fluctuations of satellite signals. Nevertheless, Yeh and Liu's theory cannot be extended to the case of VHF signals concerned, as explained later. As a matter of fact, density irregularities with Gaussian spectra, as assumed in Yeh and Liu's theory, turn out to be ineffective in causing the depolarization of VHF satellite signals.

Along the line of Yeh and Liu's approach, we show that the polarization fluctuations of linearly polarized 136-MHz satellite signals is the manifestation of depolarization effect due to the diffractive scattering by small-scale ( $<200$  m) density irregularities with power law spectra. The absence of this phenomenon at equatorial locations off the anomaly crests is attributed to two factors: (1) the ambient plasma densities are relatively low, and (2) the propagation angles of satellite signals are more nearly perpendicular to the geomagnetic field. It can be shown that these two factors lead to the requirement of rather unrealistically large fractional fluctuations of ionization density for the depolarization of VHF signals to be seen at other equatorial locations.

This paper is organized as follows. The theory of single wave scattering by density irregularities is presented in section 2. In section 3, the variances of phase shift, field amplitude ratio, the Faraday rotation fluctuations, and the induced field component of transionospheric signals are formulated and evaluated for density irregularities of both power law and Gaussian types. Interpretation of observations and discussion are given in section 4.

## 2. TRANSIONOSPHERIC WAVE SCATTERING BY DENSITY IRREGULARITIES

For simplicity, density irregularities are modeled as a uniform mean square fractional fluctuations of ionization density  $\langle(\Delta N/N)^2\rangle$  within a slab of ionization in the  $F$  region of mean density  $N$ . A linearly polarized wave transmitted from a geostationary satellite  $S$  is received on the ground at zenith angle  $\chi$ .

The center of the coordinate system is chosen to be located at the geostationary satellite  $S$  as illustrated in Figure 2. In Figure 2,  $Z_0$  represents the distance between the satellite and the receiver.  $a$  represents

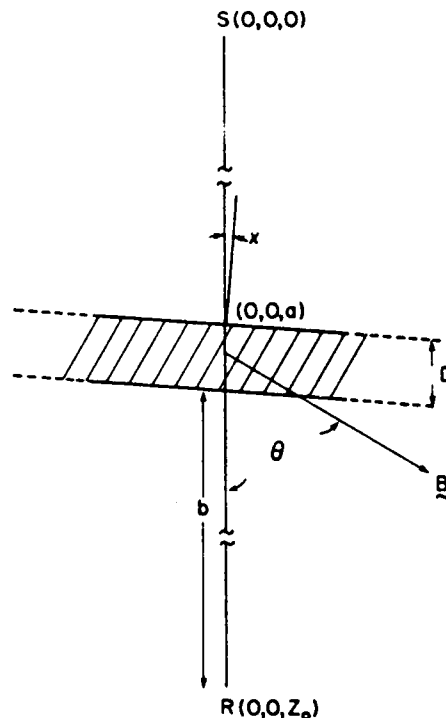


Fig. 2. Geometry of the transionospheric propagation concerned. The center of the coordinate system is located at the geostationary satellite  $S$ .  $Z_0 = 35,000$  km,  $a = 34,300$  km,  $b = 500$  km,  $D = 200$  km,  $\theta = 52^\circ$ , and  $\chi = 10^\circ$ .

that between the satellite and the topside of density irregularities,  $b$  represents that between the receiver and the bottomside of density irregularities,  $D$  represents the thickness of the slab, and  $\theta$  represents the propagation angle. The unscattered ray path within the density irregularities is  $D \sec \chi$ . In the case of concern here,  $Z_0 = 35,000$  km,  $b = 500$  km,  $D = 200$  km,  $a = 34,300$  km,  $\theta = 52^\circ$ , and  $\chi = 10^\circ$  are assumed.

For quasi-longitudinal propagation in the ionosphere, the refractive index of electromagnetic waves can be approximated as

$$n^2 \approx 1 - \tilde{f}_N^2(1 \pm \tilde{\Omega}_L) \quad (1)$$

at frequencies large compared with the electron gyrofrequency, where  $\tilde{f}_N^2 = f_N^2/f^2$ , i.e., the squared ratio of the ambient plasma frequency to the wave frequency,  $\tilde{\Omega} = \Omega/f$ , i.e., the ratio of the electron gyrofrequency to the wave frequency, and  $\tilde{\Omega}_L = \tilde{\Omega} \cos \theta$ . The plus and minus signs in (1) refer, respectively, to the extraordinary and ordinary waves that are the

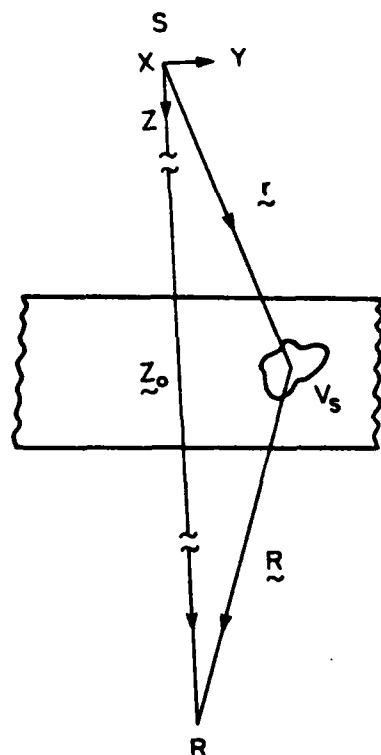


Fig. 3. Geometry of the wave scattering by density irregularities.

two characteristic modes of a linearly polarized wave in the ionosphere.

Since the refractive index  $n$  is defined as  $kc/\omega$ , expression (1) can be written as

$$k_o = k(1 + \epsilon) \quad k_x = k(1 - \epsilon)$$

as the wave numbers of the ordinary and extraordinary waves, respectively, where  $\epsilon$  defined as  $\tilde{f}_N^2 \Omega_e / 2(1 - \tilde{f}_N^2)$  has a small value ( $\sim 10^{-4}$ ) for the VHF propagation in the ionospheric  $F$  region, and  $k = (\omega/c)(1 - \tilde{f}_N^2)^{1/2}$  is the wave number in an isotropic medium (i.e.,  $\epsilon = 0$ ).

In the far-field approximation, the wave fields of these two modes received at a distance of  $r$  from the source are given, respectively, by

$$\mathbf{E}_{io}(r) = (E/r)(\hat{x} + i\hat{y}) \exp[i(\omega t - k_o r)] \quad (2)$$

and

$$\mathbf{E}_{ix}(r) = (E/r)(\hat{x} - i\hat{y}) \exp[i(\omega t - k_x r)] \quad (3)$$

The summation of (2) and (3) yields the field of the linearly polarized spherical wave received at the same

location. That is,

$$\mathbf{E}_R(r) = (2E/r)[\hat{x} \cos(\epsilon kr) + \hat{y} \sin(\epsilon kr)] \cdot \exp[i(\omega t - kr)] \quad (4)$$

showing that the polarization vector of the linearly polarized wave is rotated by an angle of  $\epsilon kr = (1/2)(k_o - k_x)r$  known as the Faraday rotation.

In the presence of density irregularities, namely  $\tilde{f}_N^2 = \langle \tilde{f}_N^2 \rangle + \Delta \tilde{f}_N^2$  (where  $\langle \tilde{f}_N^2 \rangle$  corresponds to the mean ionization density and  $\Delta \tilde{f}_N^2$  corresponds to the density irregularities), an additional change of Faraday rotation angle is introduced by wave scattering from density irregularities. Since satellite signals are received at a high elevation angle and the wavelength is assumed to be much shorter than the scale sizes of the most intense density irregularities concerned, wave reflection and the refraction due to horizontal stratification may be neglected. Only the forward scattering is considered here.

Let us first consider the scattering of ordinary waves by density irregularities. The incident electric field at scatterer  $V_s$  (see Figure 3) is represented by  $\mathbf{E}_{io} = (\mathbf{E}_o/r) \exp[i(\omega t - k_o r)]$ . For single forward scattering with small angles of deviation, the resultant field ( $\mathbf{E}_s$ ) of the scattered waves received at  $R(O, O, Z_0)$  is approximately given by

$$\mathbf{E}_s = -\frac{Z_0 \omega^2}{4\pi c^2} \left\{ \left( \frac{\mathbf{E}_o}{Z_0} \right) \exp[i(\omega t - k_o Z_0)] \right. \\ \left. \cdot \int_V d^3r \frac{\Delta \tilde{f}_N^2(r) \exp[-ik_o(r + R - Z_0)]}{Rr} \right\} \quad (5)$$

where  $V$  is the total volume of density irregularities. The total field of ordinary waves received at  $R(O, O, Z_0)$  is composed of the unscattered and the scattered parts, i.e.,

$$\mathbf{E}_{RO}(Z_0) = [\mathbf{E}_o(Z_0)/Z_0] \exp[i(\omega t - k_o Z_0)] \\ \cdot \left\{ 1 - \frac{Z_0 \omega^2}{4\pi c^2} \cdot \int_V d^3r \frac{\Delta \tilde{f}_N^2(r) \exp[-ik_o(r + R - Z_0)]}{Rr} \right\} \quad (6)$$

If the scattered waves are weak compared with the unscattered waves, (6) may be also expressed as

$$\mathbf{E}_{RO}(Z_0) \approx \mathbf{E}_o(Z_0) \exp(-i\phi_o) \quad (7)$$

This means that weak wave scattering by density irregularities introduces a complex phase shift into the original wave. Expanding the exponential function in



(7) to the first order of  $\phi_n$  and equating it to (6) yields

$$\phi_o = -i \frac{Z_0}{4\pi} \frac{\omega^2}{c^2} \int_V d^3r \frac{\Delta \tilde{f}_N^2(r) \exp[-ik_o(r+R-Z_0)]}{Rr} \quad (8)$$

The phase shift ( $\phi_x$ ) of extraordinary waves due to weak scattering by density irregularities can be similarly obtained as

$$\phi_x = -i \frac{Z_0}{4\pi} \frac{\omega^2}{c^2} \int_V d^3r \frac{\Delta \tilde{f}_N^2(r) \exp[-ik_x(r+R-Z_0)]}{Rr} \quad (9)$$

The field of the linearly polarized waves received at  $R(O, O, Z_0)$  is, therefore, given by

$$\mathbf{E}'_R = \mathbf{E}_{io}(Z_0) \exp(-i\phi_o) + \mathbf{E}_{ix}(Z_0) \exp(-i\phi_x) \quad (10)$$

which reduces to (4) in the absence of density irregularities.

A new  $xy$  coordinate plane is so chosen that the new  $x$  axis coincides with the polarization vector of the unscattered linearly polarized wave at  $R(O, O, Z_0)$ , i.e., (4) is expressed as

$$\mathbf{E}_R(Z_0) = (2E/Z_0) \exp[i(\omega t - kZ_0)] \hat{x} \quad (11)$$

In this new system of coordinates, expression (10) assumes the following form

$$\mathbf{E}'_R(Z_0) = (2E/Z_0) \exp[i(\omega t - kZ_0)] \exp[-i(\phi_o + \phi_x)/2] \cdot \left[ \hat{x} \cos\left(\frac{\phi_o - \phi_x}{2}\right) + \hat{y} \sin\left(\frac{\phi_o - \phi_x}{2}\right) \right] \quad (12)$$

a comparison between (11) and (12) shows that density irregularities cause phase shift, amplitude variation, and Faraday rotation of the linearly polarized waves. An induced field component along the  $y$  axis can be visualized to be associated with the induced Faraday rotation and to result in the depolarization of the linearly polarized waves. They are summarized as follows.

**Phase shift**

$$\Delta\phi = \text{Re} \left( \frac{\phi_o + \phi_x}{2} \right) = -\frac{Z_0}{4\pi} \frac{\omega^2}{c^2} \int_V d^3r \frac{\Delta \tilde{f}_N^2(r)}{Rr} \cdot \cos[\epsilon k(r+R-Z_0)] \sin[k(r+R-Z_0)] \quad (13)$$

**Amplitude variation**

$$\ln \left( \frac{E'_R}{E_R} \right) = \text{Im} \left( \frac{\phi_o + \phi_x}{2} \right) = -\frac{Z_0}{4\pi} \frac{\omega^2}{c^2} \int_V d^3r \frac{\Delta \tilde{f}_N^2(r)}{Rr} \cdot \cos[\epsilon k(r+R-Z_0)] \cos[k(r+R-Z_0)] \quad (14)$$

**Faraday rotation**

$$\Delta\Omega = \frac{\phi_o - \phi_x}{2} = -\frac{Z_0}{4\pi} \frac{\omega^2}{c^2} \int_V d^3r \frac{\Delta \tilde{f}_N^2(r)}{Rr} \cdot \exp[-ik(r+R-Z_0)] \sin[\epsilon k(r+R-Z_0)] \quad (15)$$

**Change of polarization vector**

$$\frac{E_y}{E_x} = \tan \left( \frac{\phi_o - \phi_x}{2} \right) = -\frac{Z_0}{4\pi} \frac{\omega^2}{c^2} \int_V d^3r \frac{\Delta \tilde{f}_N^2(r)}{Rr} \cdot \exp[-ik(r+R-Z_0)] \sin[\epsilon k(r+R-Z_0)] \quad (16)$$

for  $|\phi_o - \phi_x| < 1$  rad. As noted in (8) and (9),  $\phi_o$  and  $\phi_x$  are in general complex, the real parts of which correspond to phase shifts, and the imaginary parts of which indicate changes in logarithmic amplitudes of wave fields. Therefore, the induced Faraday rotation angles ( $\Delta\Omega$ ) and the polarization vector change ( $E_y/E_x$ ) have complex values as expressed in (15) and (16), respectively. Physically, it means that  $\Delta\Omega$  and ( $E_y/E_x$ ) result from the differential phase shift (i.e.,  $\text{Re}(\phi_o - \phi_x)$ ) and the differential changes in logarithmic amplitudes of ordinary and extraordinary modes. The spatial averages of  $\Delta\phi$ ,  $\ln(E'_R/E_R)$ ,  $\Delta\Omega$ , and ( $E_y/E_x$ ) are zeroes; their variances, which are of main physical interest, are not, however.

### 3. VARIANCES OF $\Delta\phi$ , $\ln(E'_R/E_R)$ , $\Delta\Omega$ , AND ( $E_y/E_x$ )

Let us first evaluate the induced Faraday rotation (15) or the change of polarization vector (16) for  $|\phi_o - \phi_x| < 1$  rad, i.e.,

$$I = -\frac{Z_0}{4\pi} \frac{\omega^2}{c^2} \int_V d^3r \frac{\Delta \tilde{f}_N^2(r)}{Rr} \cdot \exp[-ik(r+R-Z_0)] \cdot \sin[\epsilon k(r+R-Z_0)] \quad (17)$$

In the system of coordinates (see Figure 3) used to evaluate (17),  $r = (x^2 + y^2 + z^2)^{1/2}$  and  $R = [(Z_0 - z)^2 + x^2 + y^2]^{1/2}$ . Since  $Z_0, Z_0 - z \gg (x^2 + y^2)^{1/2}$  is assumed, therefore,  $r \approx z + (x^2 + y^2)/2z$  and  $R \approx (Z_0 - z) + (x^2 + y^2)/2(Z_0 - z)$  lead to

$$r + R - Z_0 = (x^2 + y^2)Z_0/2z(Z_0 - z) \quad (18)$$

Equation (18) is used to substitute for  $(r + R - Z_0)$  in (17), and  $Rr$  in (17) is simply replaced by  $z(Z_0 - z)$ . These approximations are based on the assumption that the outer scale of density irregularities responsible for the depolarization effect is small compared with the distance between the altitude of density irregularities and the receiver. This assumption also

assures forward scattering with small angles of deviation.

The variance of  $\Delta\Omega$  or  $(E_v/E_r)$  over space can be, therefore, approximated as

$$\begin{aligned} \langle |I|^2 \rangle &= \frac{Z_0^2 \omega^2}{16\pi^2 c^2} \int_V d^3r_1 \int_V d^3r_2 \frac{\langle (\Delta f_N^2(\mathbf{r}_1)) (\Delta f_N^2(\mathbf{r}_2))^* \rangle}{z_1 z_2 (Z_0 - z_1)(Z_0 - z_2)} \\ &\cdot \cos \left[ \frac{k(x_1^2 + y_1^2)Z_0}{2z_1(Z_0 - z_1)} - \frac{k(x_2^2 + y_2^2)Z_0}{2z_2(Z_0 - z_2)} \right] \\ &\cdot \sin \left[ \frac{\epsilon k(x_1^2 + y_1^2)Z_0}{2z_1(Z_0 - z_1)} \right] \sin \left[ \frac{\epsilon k(x_2^2 + y_2^2)Z_0}{2z_2(Z_0 - z_2)} \right] \end{aligned} \quad (19)$$

where  $\langle (\Delta f_N^2(\mathbf{r}_1)) (f_N(\mathbf{r}_2))^* \rangle$  is the autocorrelation function of density irregularities. To carry out the integration in (19), it is convenient to make the following coordinate transformation:

$$\begin{aligned} \xi &= x_1 - x_2 & \eta &= y_1 - y_2 & \zeta &= z_1 - z_2 \\ X &= 1/2(x_1 + x_2) & Y &= 1/2(y_1 + y_2) \\ Z &= 1/2(z_1 + z_2) \end{aligned} \quad (20)$$

Integrating (19) over  $X$  and  $Y$  from  $-\infty$  to  $+\infty$  leads to

$$\begin{aligned} \langle |I|^2 \rangle &= \frac{k^2}{16\pi(1 - \langle X \rangle)^2} \int_a^{a+D\sec\chi} dZ \int_{-D\sec\chi}^{D\sec\chi} d\zeta \\ &\cdot \int_{-\infty}^{\infty} d\eta \int_{-\infty}^{\infty} d\xi \langle (\Delta f_N^2(\mathbf{r}_1)) (\Delta f_N^2(\mathbf{r}_2))^* \rangle \\ &\cdot \{2G(0) \sin[G(0)(\xi^2 + \eta^2)] - G(\epsilon) \sin[G(\epsilon)(\xi^2 + \eta^2)] \\ &- G(-\epsilon) \sin[G(-\epsilon)(\xi^2 + \eta^2)]\} \end{aligned} \quad (21)$$

where

$$G(t) = Z_0 k \{ 2\zeta(2Z - Z_0) + 4t[ZZ_0 - Z^2 - (\zeta/2)^2] \}^{-1}$$

where

$$t = 0, \pm \epsilon$$

The form of the autocorrelation function has to be determined for the further evaluation of (21). Two types of power spectra are assumed for density irregularities: (1) power law type and (2) Gaussian type, which have been seen to be associated respectively with the early and the late phases of density irregularities in the observation of satellite scintillation [Basu *et al.*, 1980].

For simplicity, density irregularities are assumed to be generated by spatially homogeneous processes. The autocorrelation functions, therefore, depend only

on the coordinate differences  $\xi = x_1 - x_2$ ,  $\eta = y_1 - y_2$ , and  $\zeta = z_1 - z_2$ . Moreover, only statistically isotropic density irregularities are considered. In this case the autocorrelation functions are only functions of  $(\xi^2 + \eta^2 + \zeta^2)^{1/2}$ .

### 3.1. Density irregularities with power law spectra

For isotropic density irregularities of power law type, the autocorrelation function is taken to be

$$\begin{aligned} \langle (\Delta f_N^2(\mathbf{r}_1)) (\Delta f_N^2(\mathbf{r}_2))^* \rangle &= \langle (\Delta f_N^2)^2 \rangle \\ &\cdot \exp[-l^{-1}(\xi^2 + \eta^2 + \zeta^2)^{1/2}] \end{aligned}$$

where  $\langle (\Delta f_N^2)^2 \rangle$  corresponds to the mean square fluctuations of ionization density and  $l$  is the correlation length. The integration in (21) over  $\xi$  and  $\eta$  can be conveniently evaluated with the transformation of  $(\xi, \eta)$  into the polar coordinates  $(r, \phi)$ , namely,

$$\begin{aligned} \int_{-\infty}^{\infty} d\xi \int_{-\infty}^{\infty} d\eta G \exp[-l^{-1}(\xi^2 + \eta^2 + \zeta^2)^{1/2}] \\ \cdot \sin[G(\xi^2 + \eta^2)] = \pi \int_0^{\infty} dr \\ \cdot \exp[-l^{-1}(|G|)^{1/2}(r + |G|\zeta^2)^{1/2}] \sin(r) \end{aligned} \quad (22)$$

Although the general analytic solution of (22) cannot be obtained, an approximate form that is appropriate for the case of  $kl \gg 1$  is shown in the appendix to be

$$\begin{aligned} \int_0^{\infty} dr \exp[-l^{-1}(|G|)^{1/2}(r + |G|\zeta^2)^{1/2}] \sin(r) \\ \approx \exp(-l^{-1}|\zeta|)(1 - l^{-1}|G|^{-1/2}) \end{aligned} \quad (23)$$

Since  $Gl^2 \sim kl \gg 1$ , the second term in parentheses of (23) is less than the first one by an order of  $(kl)^{1/2}$ . However, if the second term in (23) is neglected, the integration in (21) over  $\xi$  and  $\eta$  cancels and thus  $\langle |I|^2 \rangle = 0$ . This indicates that the depolarization of satellite signals, if any, is a second order ionospheric effect.

Using the identity of integration given by (23), (21) yields

$$\begin{aligned} \langle |I|^2 \rangle &= \frac{k^2 \langle (\Delta f_N^2)^2 \rangle}{16(1 - \langle \bar{f}_N^2 \rangle)^2} \int_a^{a+D\sec\chi} dZ \\ &\cdot \int_{-D\sec\chi}^{D\sec\chi} d\zeta l^{-1} [2(2Z - Z_0)/Z_0 k]^{1/2} \\ &\cdot \{ |\zeta| + 2(ZZ_0 - Z^2 - (\zeta/2)^2)/(2Z - Z_0) \}^{1/2} \end{aligned}$$

$$+ \{[\zeta - \epsilon 2(ZZ_0 - Z^2 - (\zeta/2)^2)/(2Z - Z_0)]^{1/2} - 2\zeta^{1/2}\} \exp(-l^{-1}|\zeta|) \quad (24)$$

It is quite clear in (24) that  $\langle |l|^2 \rangle = 0$  if the terms involving  $\epsilon$  in the integrand are much less than  $\zeta$ . We assume that  $\epsilon 2[ZZ_0 - Z^2 - (\zeta/2)^2]/(2Z - Z_0) \sim 2\epsilon d$  is comparable to  $\zeta \leq l$ , where  $d$  is the distance between the receiver and the mean altitude of density irregularities. Then

$$l \sim 2\epsilon d = 2d(f_N/f)^2(\Omega/f)(1 - f_N^2/f^2)^{-1} \cos \theta \quad (25)$$

can be used to determine the outer scales of irregularities that are responsible for the 136-MHz Faraday polarization fluctuations.

Neglecting  $\zeta$  in the braces of (24) and replacing the limits of integration  $\pm D \sec \chi$  by  $\pm \infty$ , since  $D \gg l$ , we can easily carry out the integration of (24) over  $\zeta$  and obtain

$$\langle |l|^2 \rangle = \frac{k^2 \langle (\Delta f_N^2)^2 \rangle}{2(1 - \langle f_N^2 \rangle)^2} \int_a^{a+D \sec \chi} dZ \left[ \frac{\epsilon Z(Z_0 - Z)}{Z_0 K} \right]^{1/2} \quad (26)$$

Because  $a \gg D$ , the integral in (26) can be simply represented by the product of the interval of integration and the integrand wherein all  $Z$ 's are replaced by  $Z_m$ , where  $Z_m$  is the distance between the satellite and the mean altitude of density irregularities. We finally obtain the following result

$$\langle |l|^2 \rangle = \frac{k \langle (\Delta N/N)^2 \rangle \langle f_N^2 \rangle^2}{2(1 - \langle f_N^2 \rangle)^2} (\epsilon k d)^{1/2} D \sec \chi \quad (27)$$

During the current solar maximum period, total electron contents (TEC's) as large as 100 units ( $1 \text{ unit} = 10^{16} \text{ m}^{-2}$ ) have been frequently measured at Ascension Island. This indicates a large  $F_2$  maximum plasma density  $N_m$  ( $= 100 \text{ units}/250 \text{ km} \sim 4.1 \times 10^{12} \text{ m}^{-3}$ , where 250 km is the assumed slab thickness of the ionosphere), namely, a large ambient plasma frequency ( $\sim 18 \text{ MHz}$ ). Ionograms obtained at Ascension Island from airborne measurements also indicate large  $f_0 F_2$  between 16 MHz and 20 MHz (E. Weber and J. Moore, private communication, 1981).

If  $f_N = 18 \text{ MHz}$ ,  $\Omega_e = 1.5 \text{ MHz}$ , and  $d = 600 \text{ km}$  are used in (25), the polarization fluctuations of 136-MHz satellite signals received at Ascension Island ( $\theta = 52^\circ$ ) turns out to be caused by density irregularities with an 'outer scale length' of  $< 200 \text{ m}$ . It is interesting to note that recent rocket [Rino *et al.*, 1981] and satellite in situ [Basu *et al.*, 1981] measurements at  $F$  region heights show a break in spectral slope generally around several hundred meters.

Therefore, the outer scale length so termed here may refer to that portion of irregularity power spectrum.

At Ascension Island, the Faraday rotation measurements were made at an elevation angle of  $80^\circ$ , namely,  $\chi = 10^\circ$  in (27). If the thickness of density irregularities is taken to be 200 km and the ambient plasma frequency is taken to be 18 MHz, (27) shows that 0.33% rms fractional fluctuations of ionization density can cause appreciable polarization fluctuations of 136-MHz signals, i.e.,  $\langle |l|^2 \rangle^{1/2} = 0.1$ , and that 1.65% ionization density fluctuations may result in large depolarization effect, i.e.,  $\langle |l|^2 \rangle^{1/2} = 0.5$ .

Similarly,  $\langle (\Delta \Phi)^2 \rangle$  and  $\langle 1n(E_r/E_e)^2 \rangle$  can be derived from (13) and (14), respectively, as

$$\langle (\Delta \Phi)^2 \rangle = 4r_e^2 N^2 \langle (\Delta N/N)^2 \rangle \lambda^2 D \sec \chi / (1 - \langle f_N^2 \rangle) \quad (28)$$

and

$$\langle [1n(E_r/E_e)]^2 \rangle = \frac{\langle (\Delta f_N^2)^2 \rangle}{(1 - \langle f_N^2 \rangle)^2} D k \sec \chi (k d)^{1/2} \quad (29)$$

where  $l$  represents the scale sizes of density irregularities that cause the phase fluctuation of VHF satellite signals,  $r_e$  ( $\sim 2.82 \times 10^{-15} \text{ m}$ ) is the classical electron radius, and  $\lambda$  the wavelength of VHF signals.

### 3.2. Density irregularities with Gaussian spectra

$$\langle (\Delta f_N^2(\mathbf{r}_1) \Delta f_N^2(\mathbf{r}_2))^* \rangle = \langle (\Delta f_N^2) \rangle \exp[-l^{-2}(\xi^2 + \eta^2 + \zeta^2)] \quad (30)$$

is the autocorrelation function used to represent the density irregularities with Gaussian spectra. In situ measurements indicate that Gaussian spectra are associated with the late developed phase of irregularities with a correlation length of 1 km [Basu *et al.*, 1980]. Therefore,  $l$  is taken to be 1 km in (30). Substituting (30) into (21) and integrating with respect to  $\xi$  and  $\eta$ , we obtain

$$\langle |l|^2 \rangle = \frac{k^2 \langle (\Delta f_N^2)^2 \rangle}{16(1 - \langle f_N^2 \rangle)^2} \int_a^{a+D \sec \chi} dZ \int_{-\infty}^{\infty} d\xi \exp(-l^{-2}\xi^2) \{2F(0) - F(\epsilon) - F(-\epsilon)\} \quad (31)$$

where

$$F(t) = \left\{ 1 + \left[ \frac{2\zeta(ZZ_0 - Z_1)}{Z_0 k l^2} \pm 4t \frac{(ZZ_0 - Z^2 - (\zeta/2)^2)}{Z_0 k l^2} \right]^2 \right\}^{-1} \quad (32)$$

where  $t = 0, \pm \epsilon$ .

Since  $2\zeta(ZZ - Z_0)/Z_0kl^2$  is of the order of  $2/kl \sim 7.0 \times 10^{-4}$  and  $4\epsilon Z(Z_0 - Z)/Zkl^2$  of the order of  $4\epsilon d/kl^2 \sim 5.0 \times 10^{-5}$ ,  $F(0)$  and  $F(\pm\epsilon)$  have the general expression of  $(1 + \delta^2)^{-1}$  with  $\delta \ll 1$ , which can be well approximated as  $(1 - \delta^2)$ . The expression in the braces of (31) is, consequently, simplified to be  $2[4\epsilon Z(Z_0 - Z)/Zkl^2]^2$ . Straightforward integration of (31) over  $\zeta$  and  $Z$  leads to

$$\langle |I|^2 \rangle = 4^{-1} \pi^{1/2} (\langle \Delta N/N \rangle^2) (1 - \bar{f}_N^2)^{-2} (\bar{f}_N^2)^4 (\bar{\Omega})^2 d^2 l^{-3} D \cdot \sec \chi \cos^2 \theta \quad (33)$$

Substituting into (33) the same parameters as used in the case of power law type irregularities shows that unrealistically large density fluctuations are required for causing the polarization fluctuations of 136-MHz signals, namely  $\langle (\Delta N/N)^2 \rangle^{1/2} = 843\%$  for  $\langle |I|^2 \rangle^{1/2} = 0.1$  and  $\langle (\Delta N/N)^2 \rangle^{1/2} = 4215\%$  for  $\langle |I|^2 \rangle = 0.5$ . A reasonable ionospheric density depletion ( $\langle (\Delta N/N)^2 \rangle^{1/2}$ ) with Gaussian spectra is about a few percentage points, say 5%. According to (33), the ambient plasma frequency must be as high as 65 MHz so that the Gaussian type of irregularities is able to cause the appreciable depolarization (i.e.,  $\langle |I|^2 \rangle^{1/2} = 0.1$ ) of 136-MHz signals. Such a high ionospheric plasma frequency is, however, unrealistic under the normal conditions.

The derivation of  $\langle (\Delta \Phi)^2 \rangle$  and  $\langle \ln(E'_R/E_R)^2 \rangle$  can be easily done in the case of Gaussian type irregularities. They are

$$\langle (\Delta \Phi)^2 \rangle = \frac{\pi^{1/2} l \lambda^2 r_e^2 N^2 \langle (\Delta N/N)^2 \rangle}{4(1 - \langle \bar{f}_N^2 \rangle)^2} \{J(0) + J(1)\} \quad (34)$$

and

$$\langle [\ln(E'_R/E_R)]^2 \rangle = \frac{\pi^{1/2} l \lambda^2 r_e^2 N^2 \langle (\Delta N/N)^2 \rangle}{4(1 - \langle \bar{f}_N^2 \rangle)^2} \{J(0) - J(1)\} \quad (35)$$

where

$$J(x) = \int_a^{a+D \sec \chi} dz \{1 + [x 4Z(Z_0 - Z)/Z_0kl^2]^2\}^{-1}$$

where

$$x = 0, 1$$

Equations (34) and (35) can be reduced, respectively, from the (26) and (27) of Yeh and Liu [1967], wherein  $J(\epsilon)$  reduces to  $J(0)$ , since  $\epsilon \sim 10^{-4}$  for the 136-MHz wave propagation.

#### 4. DISCUSSION AND CONCLUSION

In this paper, wave scattering by density irregularities with power law spectra has been proposed as the process for causing the intense and fast fluctuations of the SIRIO 136-MHz signals received at Ascension Island. Based on the above analysis, the following things can be understood: (1) the nature of density irregularities that result in the polarization fluctuations of satellite signals, (2) why the polarization fluctuations of 136-MHz signals has a close correlation with the occurrence of the  $L$  band scintillation, (3) why the polarization fluctuations of 136-MHz signals has only been seen at locations near the equatorial anomaly crests, and (4) the frequency limit beyond which density irregularities will not affect significantly the polarization vector of satellite signals.

We have already shown that the polarization fluctuations of 136-MHz satellite signals result from the wave scattering by density irregularities whose power spectra exhibit power law rather than Gaussian distribution. In situ measurements [Basu *et al.*, 1980] show that, while density irregularities have relatively flat power spectra obeying a power law slope in their early phase, density irregularities in their late phase are seen to have a sharp slope essentially characteristic of a Gaussian distribution. This indicates that, during the change of power spectra from power law to Gaussian types, relatively short-scale (say, less than 1 km) density irregularities decay. As shown in (25), the polarization fluctuations of 136-MHz satellite signals turns out to be caused by those short-scale density irregularities with an outer scale length less than about 200 m.

Density irregularities with scale lengths of a few hundreds of meters are responsible for the  $L$  band scintillation. Therefore, the  $L$  band scintillation is not expected during the late phase of density irregularities characterized with Gaussian spectra, indicating the decaying of short-scale density irregularities. Observations of the 257-MHz scintillation at Ascension Island in the presence and absence of the  $L$  band scintillation, indeed, indicate the characteristic increasing of the correlation lengths of the 257-MHz signals [Basu *et al.*, 1981]. That both the  $L$  band scintillation and the polarization fluctuations of the 136-MHz signals are caused by relatively short-scale density irregularities is likely to account for the coexistence of these two phenomena.

The ambient plasma density ( $N$ ) and the propagation angle ( $\theta$ ) are the most location dependent param-

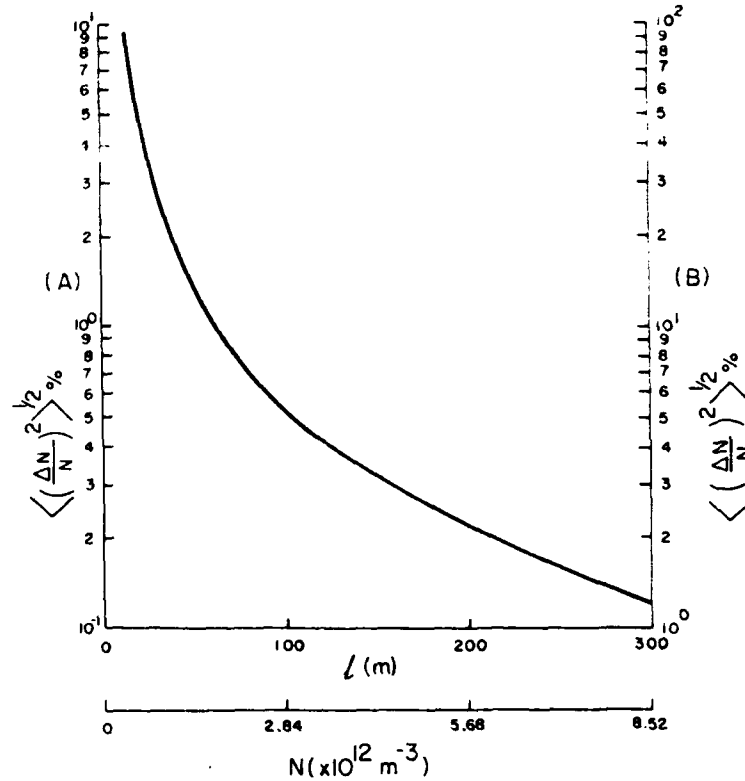


Fig. 4. Fractional fluctuations  $\langle (\Delta N/N)^2 \rangle^{1/2}$  of the plasma density  $N$  versus the outer scale lengths  $l$  of density irregularities or the ambient plasma density  $N$ , as required to cause the polarization fluctuations of 136-MHz satellite signals at Ascension Island. Scale (A) for  $\langle |f|^2 \rangle^{1/2} = 0.1$ , scale (B) for  $\langle |f|^2 \rangle^{1/2} = 1.0$ .

eters. As mentioned before, the ambient plasma density measured at locations near the Appleton anomaly crests may be larger than those at other equatorial locations by a factor of 2–4 during the solar maximum period [Rastogi, 1966; Aarons *et al.*, 1981]. Let us look at the possibility of observing the 136-MHz polarization fluctuations near the magnetic equator, e.g., Natal, Brazil (geographic coordinate 5.85°S, 35.23°W, 9.6°S dip).

The propagation angle at Natal is about 80° (cf. 52° at Ascension Island). If the ambient plasma frequency at Natal is taken to be 10 MHz (cf. 18 MHz at Ascension Island),  $f_N^2 \cos \theta$  obtained at Natal is less than that at Ascension Island by a factor of 11.5. Therefore, according to  $l \propto f_N^2 \cos \theta$  in (25), the density irregularities causing the polarization fluctuations of 136 MHz signals at Natal, if any, have an outer scale shorter than 20 m (cf. 200 m at Ascension Island). On the other hand, since the ratio of  $f_N^2 (\cos \theta)^{1/2}$  at Natal to that at Ascension Island is 35.6,  $\langle |f|^2 \rangle \propto$

$\langle (\Delta N/N)^2 \rangle f_N^5 (\cos \theta)^{1/2}$  in (27) requires that  $\langle (\Delta N/N)^2 \rangle$  at Natal be larger than that at Ascension Island by 35.6 times to cause the same level of 136-MHz polarization fluctuations, i.e.,  $\langle (\Delta N/N)^2 \rangle^{1/2} = 10\%$  for  $\langle |f|^2 \rangle^{1/2} = 0.5$ . This example shows clearly that low ambient plasma densities and large propagation angles at the magnetic equator make it impossible to observe the polarization fluctuations of 136-MHz satellite signals at equatorial locations except near the anomaly crests.

In (25),  $l \propto f_N^2 \propto N$  indicates that, in an environment of high ambient plasma density, density irregularities with longer scale lengths can also be involved in producing the polarization fluctuations of satellite signals. Eliminating  $f_N$  from (25) and (27) yields

$$\langle (\Delta N/N)^2 \rangle^{1/2} = C \langle |f|^2 \rangle^{1/2} l^{-5/4} \quad (36)$$

where  $C = 4(\Omega/f)dk^{-3/4}(D \sec \chi)^{-1/2} \cos \theta \sim 16.5$  for the assumed ionospheric conditions at Ascension

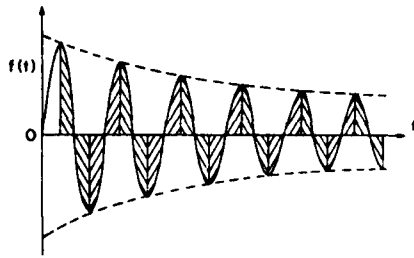


Fig. 5. Plot of  $f(t) = \exp[-l^{-1}(|G|)^{-1/2}(t + |G|\zeta^2)^{1/2}] \sin(t)$  for  $Gl^2 \gg 1$ . The unhatched area represents approximately the integration of  $f(t)$  over  $t$  from 0 to  $\infty$ .

Island:  $d = 600$  km,  $D = 200$  km,  $\Omega = 1.5$  MHz,  $f = 136$  MHz,  $\theta = 52^\circ$ , and  $\chi = 10^\circ$ . It is clear from the plotting of (36) in Figure 4 that, in the presence of density irregularities, high ambient plasma density provides the favorable environment for the VHF polarization fluctuations to occur. This may explain why the polarization fluctuations of 136-MHz signals has been frequently observed at Ascension Island during the current solar maximum period.

For illustration, the frequency limit beyond which density irregularities cannot cause significant polarization fluctuations of satellite signals is loosely defined as that at which  $(|l|^2)^{1/2} = 0.1$  requires 1% of density fluctuation under the aforesaid ionospheric condition. This frequency is determined as 235 MHz from (27), and the outer scale length of density irregularities is determined as 28 m from (25).

It should be pointed out that the theory of single wave scattering discussed in this paper cannot explain the observed saturated amplitude scintillations of 136-MHz signals. It is well known that the saturation of VHF amplitude scintillation is attributed to multiple scattering. Therefore, deductions of the present theory for the amplitude scintillation may not be true. The validity of single scatter approximation as applied to the problem of polarization fluctuations can be justified [Lee, 1981]. Multiple scattering is expected to give rise to the saturation of polarization fluctuations in the presence of large density irregularities. However, the effect of multiple scattering does not impose significant quantitative changes in the results derived from the theory of single wave scattering. Simple analyses presented in this paper turn out to be adequate for the understanding of the 136-MHz polarization fluctuations and associated phenomena.

#### APPENDIX: AN APPROXIMATE SOLUTION OF $\int_0^\infty dt \exp[-l^{-1}(|G|)^{-1/2}(t + |G|\zeta^2)^{1/2}] \sin(t)$

For  $Gl^2 \sim kl$ , which is much greater than one as assumed, the integrand in (22), i.e.,  $\exp[-l^{-1}(|G|)^{-1/2}(t + |G|\zeta^2)^{1/2}] \sin(t)$  can oscillate for many cycles before it dies out. As illustrated in Figure 5, only the unhatched area does not vanish and represent the approximate integration of (22).

Integration by parts twice in (22) yields

$$\begin{aligned} & \int_0^\infty dt \exp[-l^{-1}(|G|)^{-1/2}(t + |G|\zeta^2)^{1/2}] \sin(t) \\ &= \exp(-l^{-1}|\zeta|) - \int_0^\infty dt \sin(t) \frac{\partial^2}{\partial t^2} \\ & \quad \cdot \exp[-l^{-1}(|G|)^{-1/2}(t + |G|\zeta^2)^{1/2}] \end{aligned} \quad (A1)$$

Since  $\exp[-l^{-1}(|G|)^{-1/2}(t + |G|\zeta^2)^{1/2}]$  vanishes effectively at distances of the order of the correlation length, the double differentiation of  $\exp[-l^{-1}(|G|)^{-1/2}(t + |G|\zeta^2)^{1/2}]$  with respect to  $t$  may be approximated by

$$\begin{aligned} & \max \{ \exp[-l^{-1}(|G|)^{-1/2}(t + |G|\zeta^2)^{1/2}] / G^2 t^4 \\ &= \exp(-l^{-1}|\zeta|) / G^2 t^4 \end{aligned} \quad (A2)$$

$\sin(t)$  in (A1) may be represented approximately by the parabolic function  $(t)^{1/2}$ . The integral in (A1) can therefore be approximated as

$$\begin{aligned} & \int_0^\infty dt \sin(t) \frac{\partial^2}{\partial t^2} \exp[-l^{-1}(|G|)^{-1/2}(t + |G|\zeta^2)^{1/2}] \\ & \approx |G|l^2 \cdot (|G|l^2)^{1/2} \cdot \exp(-l^{-1}|\zeta|) / G^2 t^4 \\ &= \exp(-l^{-1}|\zeta|) / (|G|)^{1/2} l \end{aligned} \quad (A3)$$

Substituting (A3) into (A1) leads to the approximate form of (22) for  $Gl^2 \gg 1$ , namely,

$$\begin{aligned} & \int_0^\infty dt \sin(t) \exp[-l^{-1}(|G|)^{-1/2}(t + |G|\zeta^2)^{1/2}] \\ & \approx \exp(-l^{-1}|\zeta|) [1 - l^{-1}(|G|)^{-1/2}] \end{aligned} \quad (A4)$$

Indeed, that the approximate form in (A4) carries the right functional relationship with  $G$  and  $l$  is confirmed by the exact integration in (22) for  $\zeta = 0$ .

**Acknowledgments.** Comments from C. L. Rino and K. C. Yeh are greatly appreciated. This work was supported by AFGL contract F19628-80-C-0016 at Regis College Research Center and by AFGL contract F19628-81-K-0011 at Emmanuel College. This

paper was presented at the AGU 1981 spring meeting held at Baltimore, Maryland, May 25-29, 1981.

## REFERENCES

- Aarons, J., H. E. Whitney, E. Mackenzie, and S. Basu (1981), Microwave equatorial scintillation intensity during the current solar maximum, *Radio Sci.*, **16**, 939-945.
- Basu, S., J. P. McClure, S. Basu, W. B. Hanson, and J. Aarons (1980), Coordinated study of equatorial scintillation and in situ and radar observations of nighttime *F* region irregularities, *J. Geophys. Res.*, **85**, 5119-5130.
- Basu, S., S. Basu, J. P. McClure, W. B. Hanson, and H. E. Whitney (1981), Spatially and temporally co-located measurements of GHz/VHF scintillation and in situ irregularities spectra near Ascension Island (abstract), *Eos Trans. AGU*, **62**, 347.
- Das Gupta, A., and A. Maitra (1980), VHF satellite signal scintillation near the edge of the equatorial ionospheric irregularity belt, *Adv. Space Explor.*, **8**, 209-212.
- Kaushika, N. D., and F. de Mendonca (1974), Nighttime fluctuations (scintillations) in Faraday rotation angle of VHF signals from geostationary satellites, *Planet. Space Sci.*, **22**, 1331-1334.
- Kent, G. S. (1959), High frequency fading observed on the 40 Mc/s wave radiated from artificial satellite 1957 $\alpha$ , *J. Atmos. Terr. Phys.*, **16**, 10-20.
- Klobuchar, J. A., and J. Aarons (1980), Studies of equatorial irregularity patches using SIRIO VHF transmissions, *Alta Freq.*, **49**, 345-349.
- Lee, M. C. (1981), Faraday polarization fluctuations of transionospheric propagation, *J. Geophys. Res.*, **86**, in press.
- McClure, J. P. (1964), Polarization measurements during scintillation of radio signals from satellites, *J. Geophys. Res.*, **69**, 1445-1447.
- Parthasarathy R., and G. C. Reid (1959), Signal strength recordings of the satellite 1958 82 (Sputnik III) at College, Alaska, *Proc. Inst. Radio. Eng.*, **47**, 78-79.
- Rastogi, R. G. (1966), The equatorial anomaly in the *F2* region of the ionosphere, *J. Inst. Telecommun. Eng. New Delhi*, **12**, 245-256.
- Rino, C. L., R. T. Tsunoda, J. Petriceks, R. C. Livingston, M. C. Kelley, and K. D. Baker (1981), Simultaneous rocket-borne beacon and in situ measurements of equatorial spread *F*: Intermediate wavelength results, *J. Geophys. Res.*, **86**, 2411-2420.
- Roger, R. S. (1965), The effect of scintillations on the polarization of satellite transmissions near 20 Mc/s, *J. Atmos. Terr. Phys.*, **27**, 335-348.
- Yeh, K. C., and C. H. Liu (1967), Wave propagation in a random medium with anisotropic background, *IEEE Trans. Antennas Propag.*, **AP-15**, 539-542.
- Yeh, K. C., and C. W. Swenson (1959), The scintillation of radio signals from satellites, *J. Geophys. Res.*, **64**, 2281-2286.
- Yeh, K. C., H. Soicher, and C. H. Liu (1979a), Observations of equatorial ionospheric bubbles by the radio propagation method, *J. Geophys. Res.*, **84**, 6589-6594.
- Yeh, K. C., H. Soicher, C. H. Liu, and E. Bonelli (1979b), Ionospheric bubbles observed by the Faraday rotation method at Natal, Brazil, *Geophys. Res. Lett.*, **6**, 473-475.

# High Resolution Topside In Situ Data of Electron Densities and VHF/GHz Scintillations in the Equatorial Region

SUNANDA BASU AND SANTIMAY BASU

*Emmanuel College, Boston, Massachusetts 02115*

J. P. McCLURE AND W. B. HANSON

*University of Texas at Dallas, Richardson, Texas 75080*

H. E. WHITNEY

*Air Force Geophysics Laboratory, Hanscom AFB, Massachusetts 01731*

Coordinated in situ measurements of high-resolution (spatial resolution 35 m) irregularity structures in the topside ionosphere using the retarding potential analyzer (RPA) on the AE-E satellite and scintillation measurements using the geostationary satellite Marisat transmissions at 257 MHz and 1.54 GHz from Ascension Island were made in December, 1979 during the recent solar maximum period. The in situ irregularity spectra could be classified into two categories: those having or not having spectral breaks. The first category of spectra is characterized by two spectral indices: one above and the other below a scale-length that lies typically between 500 m and 1 km. The spectral index in the long scale-length end (10 km to  $\sim 1$  km) varies between  $-1$  to  $-1.5$ , whereas the index in the short scale-length end ( $\sim 1$  km to 70 m) is between  $-3$  to  $-3.5$ . In the second category, the power law spectral index of the irregularities ranges between  $-2$  to  $-2.5$  over the entire scale-length range of 70 m to 10 km. The in situ measurements reveal that in the early evening hours, the E-W gradient scale-lengths can be as small as 35 m, the sampling interval of the RPA instrument. In the pre-midnight and post-midnight hours, the gradient scale length becomes larger, but scale lengths of several hundred meters are frequently encountered. The temporal variation of 1.54-GHz scintillation magnitudes are found to track the E-W bubble structure, scintillations being minimum when the ray traverses the center and large when it crosses the eastern and western walls of the bubble. On the other hand, scintillations at 257 MHz remain saturated during an encounter with a bubble and focussing is often observed, but the autocorrelation interval tracks the bubble structure, being large when the ray path is deep within the bubble where the perturbation is weaker. The power spectra of weak 1.54-GHz scintillations are found to be consistent with the predictions of weak scatter theory based on irregularities having the observed in situ spectra. Significant differences are noted in the spectra of strongly scattered 257-MHz scintillations. In this case the decorrelation bandwidth extends beyond 1 Hz, and the spectral slope of the transitional portion of the spectrum becomes as steep as  $-6$ . The moderate to strong GHz scintillations sometimes show a dual slope power spectrum with the lower frequencies exhibiting a slope of  $-1.5$  and the higher frequencies showing a slope of  $-5.5$ . The observations of steep structures in irregularities with scale-length of a few hundred meters near midnight, implying relatively slow erosion of sharp gradients are discussed in terms of plasma processes in the topside ionosphere.

## 1. INTRODUCTION

The subject of nighttime equatorial  $F$  region irregularities received a tremendous boost when the collisional Rayleigh-Taylor instability with field-line integration was proposed [Balsley *et al.*, 1972; Haerendel, 1974] to explain the occurrence of irregularities on both the bottomside and topside of the equatorial  $F$  region. Since then an enormous amount of new information on multi-technique experiment, theory and numerical simulations of these irregularities have become available. In this rapidly developing field, reviews having various theoretical and/or experimental orientations followed in quick succession [Farley, 1974; Aarons, 1977, 1982; Basu and Kelley, 1977, 1979; Fejer and Kelley, 1980; Ossakow, 1979, 1981; Kelley and McClure, 1981; Basu and Basu, 1981; Yeh and Liu, 1982]. While there is agreement now on some of the basic facts regarding generation of these irregularities and their effects on radiowave propagation, many details regarding the nature of irregularity waveforms in the  $F$  region and their spectral forms remain unsolved. For instance, high-resolution ( $\sim 35$  m sam-

pling interval) satellite in situ data have shown that in the early phase, the bottomside irregularity spectra exhibit shallow slopes due to steep spatial structures, whereas in the late phase erosion of these steep structures lead to spectra with steeper slopes [Basu *et al.*, 1980]. High-resolution ( $\sim 15$  m) rocket data were the first to show that under certain conditions the vertical wave number spectrum has different spectral slopes in different scale length regimes [Rino *et al.*, 1981; Kelley *et al.*, 1982]. Livingston *et al.* [1981] showed that while the average one-dimensional index for intermediate scale ( $\sim$  several tens of km to few km) equatorial irregularities is near  $-2$ , it varies systematically with changing perturbation strength. Earlier measurements, on the other hand, generally associated a uniform  $k^{-2}$  one-dimensional in situ irregularity wave number spectrum with equatorial spread  $F$  from satellite data [Dyson *et al.*, 1974] and with bottomside spread  $F$  using rocket data [Kelley *et al.*, 1976; Morse *et al.*, 1977]. Moreover, theoretical analyses of the nonlinear saturation of the collisional Rayleigh-Taylor instability also predict a  $k^{-2}$  spectral density function [Chaturvedi and Ossakow, 1977]. In fact, any electron density data that is dominated by steep structures will give rise to a power law spectrum with a  $k^{-2}$  slope [Costa and Kelley, 1978].

The rocket measurements presented by Rino *et al.* [1981]

Copyright 1983 by the American Geophysical Union.

Paper number 2A1738.  
0148-0227/83/002A-1738\$5.00



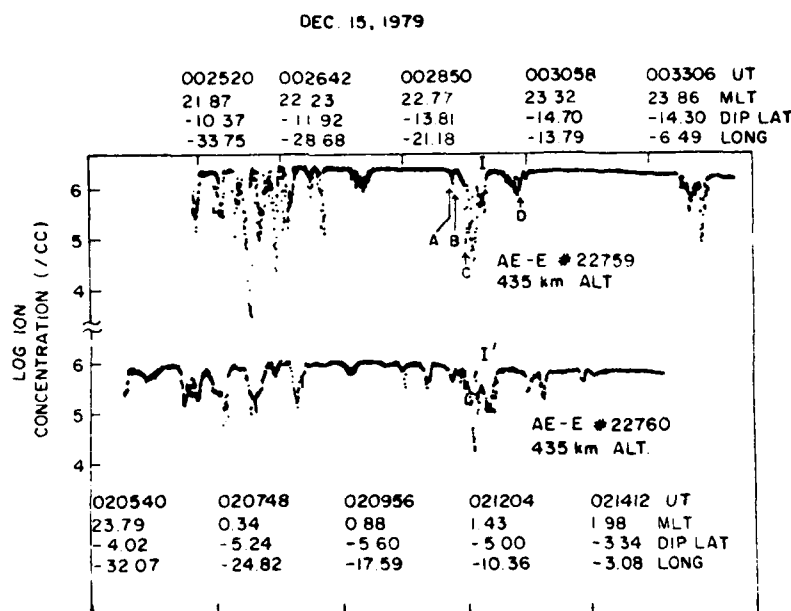


Fig. 1. Ion concentration data obtained by the ion-drift meter on board Atmosphere Explorer-E during orbits 22759 and 22760 in the Ascension Island longitude sector on December 15, 1979. The depletions or bubbles marked I and I' represent the same structure detected at two different local times. The points marked A, B, C, D are shown in high resolution in Figures 4a-4d. The magnetic local time (MLT), dip latitude (DIP LAT), and geographic longitude (LONG) for the two orbits are indicated at the top and bottom respectively.

and Kelley *et al.* [1982] while providing information on both topside and bottomside spectra were confined to data obtained from a brief, single data set. The rocket was moreover launched near local midnight into conditions that can be characterized as an equatorial spread *F* decay phase [Rino *et al.*, 1981]. The satellite measurements [Basu *et al.*, 1980], though made during various phases of irregularity evolution, were at relatively low altitudes ( $\sim 270$  km) and thus probably sampled only the bottomside in the early phase of irregularity generation when the equatorial *F* layer has been raised by electrodynamic forces. The object of the current paper is to present a fairly large number of high resolution AE-E retarding potential analyzer (RPA) measurements [Hanson *et al.*, 1973] of irregularity waveforms and their spectra near the *F* peak and in the immediate topside obtained during the current solar maximum period in December 1979 at an altitude of 435 km. It is these regions containing the highest plasma density that mostly affect radio wave propagation channels in the microwave frequency range. We were fortunate enough on one occasion to observe a patch of scintillation at 1.54 GHz from Ascension Island (dip lat  $14.4^\circ$ S) centered near the exact time that the AE-E satellite passed very close to the ionospheric intersection point of the scintillation ray path [Basu *et al.*, 1981]. Thus we are able to present for the first time coordinated measurements of GHz intensity scintillation spectra and corresponding topside irregularity spectra. The AE-E data were obtained as part of a special coordinated experiment at Ascension Island when the Air Force Geophysics Laboratory Airborne Ionospheric Observatory was also making airglow measurements with TV all-sky imaging photometers at 6300 Å and 7774 Å [Weher *et al.*, 1982]. The imaging system was able to follow the individual depletions or bubbles [McClure *et al.*, 1977] observed by AE-E for several hours so that by using successive orbits of AE-E data we were able to follow the spectral evolution associated with the long-lived individual bubbles. The plan of this paper is to present the in situ AE-E measurements in section 2 followed

by the coordinated GHz/VHF scintillations in section 3. These results are discussed in section 4. The implications of the in situ measurements on scintillation theory and short-scale irregularity generation are pointed out.

## 2. IN SITU MEASUREMENTS

We shall discuss the high-resolution ( $\sim 35$ -m sampling) retarding potential analyzer ion density measurements obtained during four AE-E orbits in the vicinity of Ascension Island during the coordinated campaign referred to above. To put the high-resolution measurements in perspective the AE-E low-resolution ( $\sim 4$  km) ion-drift meter plots of ion densities are shown in Figures 1 and 2. In the *F* region, because of charge neutrality the ion densities are essentially equal to the electron densities. All 4 orbital tracks (orbit numbers 22759, 22760, 22790, and 22791) are plotted on a map of the region in Figure 3 (almost all ocean except Ascension Island itself) to show the relative positions of the tracks with respect to the magnetic equator and the scintillation observation subionospheric (at 400-km altitude) point ( $7.4^\circ$ S;  $14.4^\circ$ W) indicated as ASC IS (MAR) for the Ascension Island site looking at the Marisat satellite parked at  $15^\circ$ W.

The slight discrepancies in the dip latitude numbers between Figures 1 and 2 when compared with Figure 3 arise from the fact that the former two diagrams use the dip latitude as obtained at the height of the satellite AE-E, while the latter diagram uses dip latitudes as obtained at the surface of the earth. A short explanation is necessary regarding the manner in which Figures 1 and 2 have been put together. Figure 1 has been constructed by lining up a specific bubble marked I and I' on the two AE-E orbits occurring on the night of December 15. The identity of the bubble on the two orbits was established by the continuous tracking of the airglow depletion associated with the bubble first seen at 0030 UT on the Ascension Island meridian by the airborne 6300 Å all sky TV imaging photome-

DEC 17, 1979

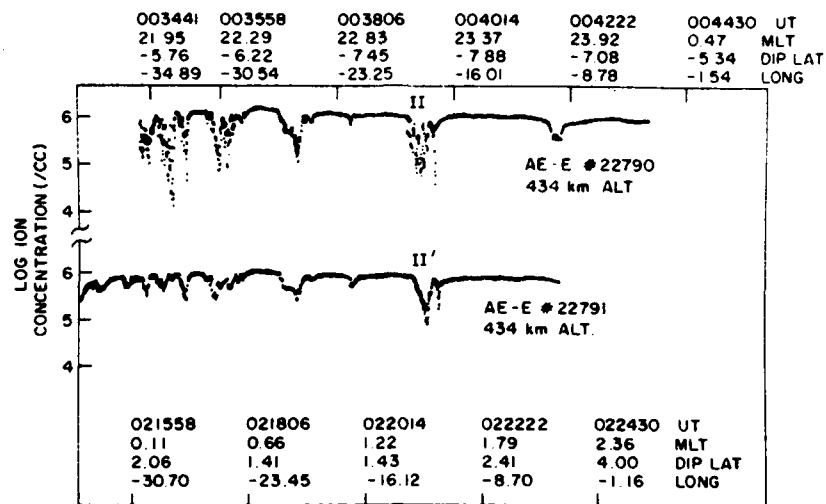


Fig. 2. The same as in Figure 1 but for orbits 22790 and 22791 on December 17, 1979. The depletions or hubbles marked II and II' represent the same structure on this night.

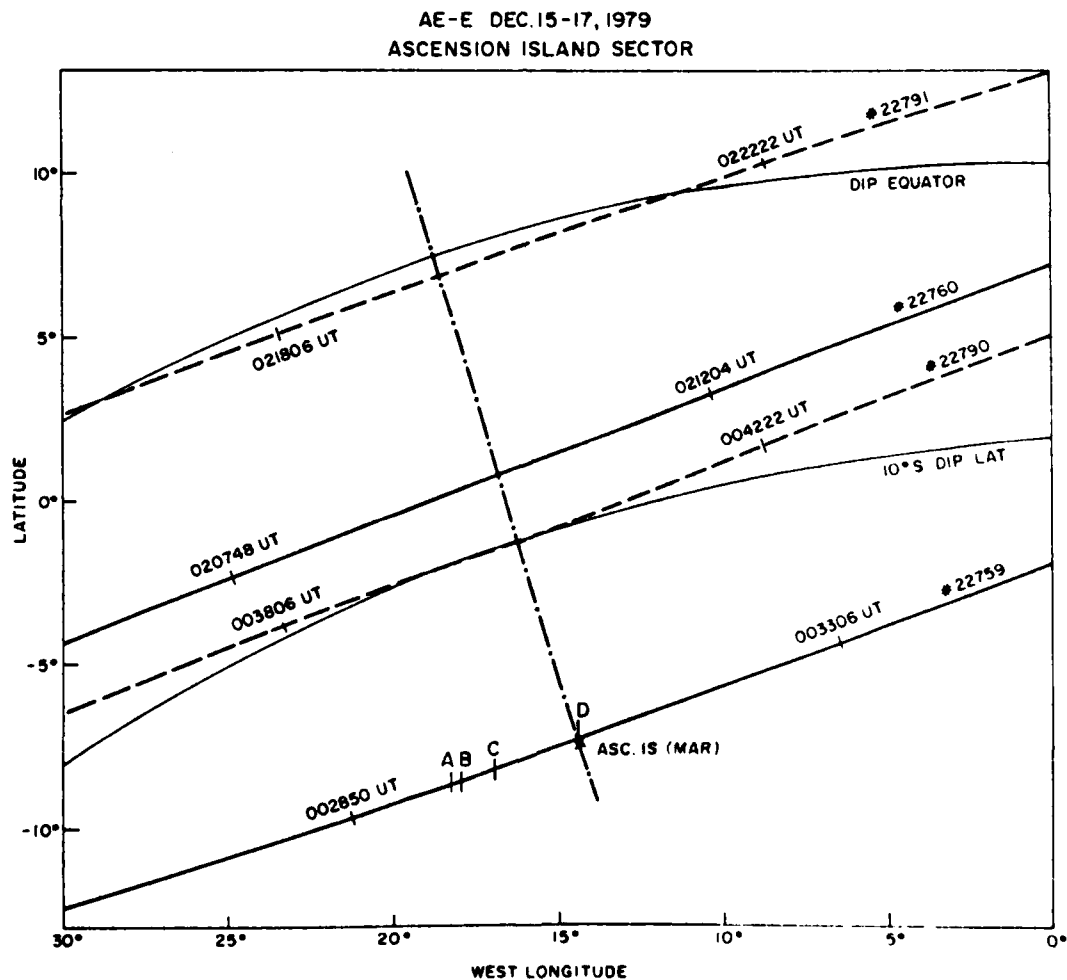


Fig. 3. AE-E orbits 22759, 22760, 22790, and 22791 shown on a map of the Ascension Island longitude sector. The point marked ASC IS (MAR) locates the sub-ionospheric (400 km) intersection of the ray path from the Marisat satellite located at 15°W to Ascension Island. The points A, B, C, and D are those shown in Figure 1. The projection of the magnetic field line through Ascension Island is shown for an altitude of 430 km by the chain line.

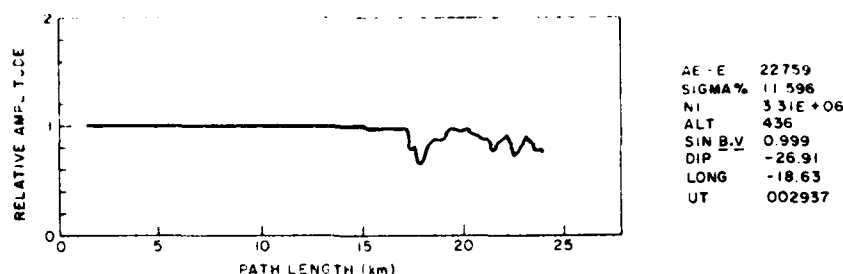


Fig. 4a. A 3-s sample of high-resolution RPA data of relative amplitudes obtained on AE-E orbit 22759 near point A indicated on Figure 1. The irregularity amplitude (SIGMA), the ion concentration (NI) at the beginning of the data interval, the satellite altitude (ALT), the sine of the angle between the magnetic field (B) and the satellite velocity (V) vectors, the dip angle (DIP), geographic longitude (LONG), and the universal time (UT) are indicated on the diagram. Note the sharp gradient at the western edge of bubble marked I.

ter [Weber *et al.*, 1982]. An exactly similar method was used in constructing Figure 2 where the bubbles II and II' were aligned, the bubble (II) tracked in this case appearing first at 0040 UT. On both nights the AE-E orbits were essentially circular at 435-km altitude.

Two features are immediately apparent from these diagrams. One is that the earlier local time bubbles tend to be more highly structured and the second is that fewer bubbles are observed (i.e., there are larger undisturbed regions between them) as one moves to higher  $I$  shells or away from the dip equator. Further, by combining with Figure 3, one notes that the ambient densities are higher for the orbits that are closer to the southern crest of the Appleton anomaly than those which pass near the magnetic equator. It has been shown earlier that the Appleton anomaly persists late into the evening hours in this longitude sector [Aarons *et al.*, 1981]. As far as scintillations are concerned, the AE orbits occurred at such a time that we can match up a specific bubble with a specific scintillation patch only in the midnight to post midnight sectors.

The rest of this section will be concerned with a discussion of the high-resolution waveforms and spectra that were obtained from the orbits shown in Figures 1 and 2. The high-resolution spectra were obtained from 3-s samples of  $N_i$  data from the RPA at a sampling interval of 4.45 ms, which is approximately equal to 35 m along the orbital track. These four orbits provided 260 such samples (not contiguous, because they were separated by  $\sim 3$ -s samples of various other RPA observations of thermal plasma parameters). Of the 260 samples, approximately 125 samples contained irregularity amplitudes  $\Delta N/N > 1\%$ , while 135 samples had lower levels of fluctuations. Most of these latter samples came from in-between bubble regions (cf. Figures 1 and 2) that appear smooth on the low-resolution plots.

A sequence of four 3-s RPA samples of irregularity waveforms between 0029:37–0030:50 UT on December 15 associated with significant irregularity amplitudes on orbit 22759 are shown in Figures 4a–4d. These refer to the positions marked A, B, C, and D, respectively, on both the low-resolution AE orbit shown in Figure 1, as well as on the map in Figure 3. This particular set was chosen because of the spatial proximity of the satellite orbit to the subionospheric point of the scintillation measurements that will be discussed in the next section. Figures 4b–4d also contain spectra of  $\Delta N/N$  computed from the respective data samples. Figure 4a clearly shows that the satellite entered the edge of the irregular region to the west of the Ascension Island subionospheric point. The existence of this edge within the 3-s sample makes it nonstationary and hence

unsuitable for spectral analysis. It was chosen primarily to show the boundary between a stable and an unstable region in the topside ionosphere. The very high unperturbed ambient ion density of  $3.3 \times 10^6 \text{ cm}^{-3}$  shows that AE-E was near  $h_{\text{max}}F$  or in the immediate topside of the  $F$  region. The aircraft digisonde showed that the bottom of the  $F$  region at Ascension Island was 250 km at this time (cf. Figure 3 of Weber *et al.* [1982]). The relative amplitude in the diagram signifies  $\Delta N/N$ , where  $\Delta N$  is the change in ion concentration from the ion concentration ( $N$ ) at the beginning of a 3-s interval. The numbers at the top right-hand side of the diagram denote the square root of the variance from the least-squares linear trend of the data expressed as a percentage (SIGMA%), the ion concentration per  $\text{cm}^{-3}$  (NI) at the beginning of the 3-s interval, the angle between the satellite velocity (V) and magnetic field vector (B), as well as the parameters that signify the satellite altitude and location.

The second sample (lower panel of Figure 4b) was obtained 6 s later and shows structure on the walls of the bubble (since the density of  $1.9 \times 10^6 \text{ cm}^{-3}$  at the starting point of the data is so close to the ambient value). It is such structure that is most probably responsible for the scintillation at GHz frequencies as was also hypothesized earlier by Costa and Kelley [1976]. To obtain the spectrum shown in the top panel, the data illustrated in the lower panel of Figure 4b was linearly detrended, and the zero mean time series of positive and negative fluctuations  $\Delta N$  from the trend line was obtained. The percentage fluctuations of  $\Delta N/N$ ,  $N$  being derived from the trend line, was subjected to spectral analysis by both the fast Fourier transform (FFT) and maximum entropy (MEM) methods. The FFT program was the same as the one used earlier by Dyson *et al.* [1974]. The spectra were normalized such that the integral of the fluctuation power  $\int S(f) df$  over the observed frequency range equals the variance of the original time series of  $\Delta N/N$ . The frequency ( $f$ ) scale was converted to irregularity scale length ( $\Lambda$ ) by using the relation  $\Lambda = v/f$ , where  $v$  is the satellite velocity. In view of its geophysical importance, we shall illustrate the power spectra in terms of irregularity wavelength. The dots indicate the spectral estimates obtained by the FFT technique, and the solid line represents the MEM spectrum. It should be kept in mind that the above spectrum obtained from in situ data is a one-dimensional power spectrum of  $\Delta N/N$ . The spectrum seems fairly typical of the kind seen in the topside when moderate to large amplitude irregularities are observed. The characteristic feature is a break in the spectrum that is most likely to occur at an irregularity scale-length between 500 m and 1 km. In this particular case the break occurs at 1 km with a slope  $p_1 = 0$

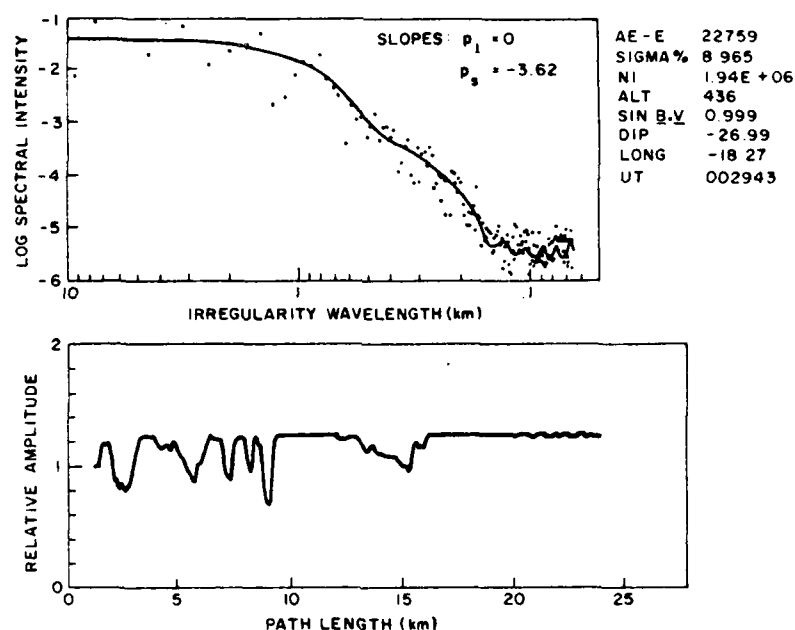


Fig. 4b. The lower panel is the same as in Figure 4a except for 3-s sample near point B on Figure 1. The upper panel shows a power spectrum of the linearly detrended data corresponding to the 3-s sample shown obtained by the FFT (dots) and maximum entropy (solid lines) techniques. Note the structure on the bubble wall that gives rise to a power spectrum with two spectral slopes, a long scale-length spectral index  $p_1 = 0$ , and short scale length spectral index  $p_2 = -3.62$ , with the spectral break occurring at a scale length of 1 km.

between 10 km and 1 km and a slope  $p_2 = -3.6$  between 1 km and 70 m as derived by linear least squares fit to the MEM spectral estimates.

The third sample (Figure 4c) shows irregularity waveforms and spectrum observed at point C near the center of the depletion 12 s after the sample shown in Figure 4b. The waveforms shown are not spectacular because of the compressed linear scale having increments of 5N between tick marks. Thus the

structures observed near the 20 km mark are extremely sharp indeed. The effect of such sharp steplike structures on spectra has been discussed by *Costa and Kelley* [1978]. In fact the relative amplitude varies so fast that it is difficult to estimate a gradient scale length  $L = [(1/N)(dN/dX)]^{-1}$  and only approximate upper bounds  $\sim 200$  m can be quoted. The spectrum, probably because it is so dominated by sharp structures, shows a uniform slope of  $-2.4$  over the entire scale length range with

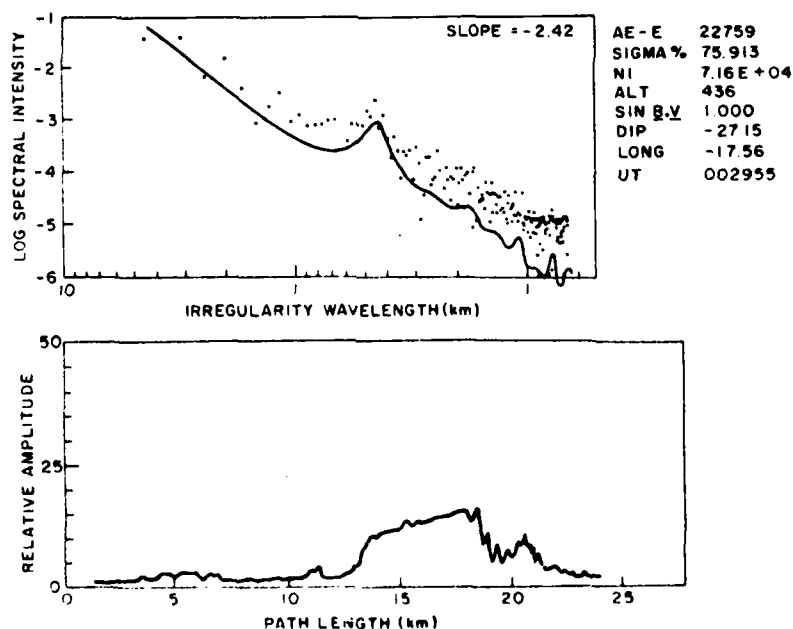


Fig. 4c. The same as in Figure 4a except for 3-s sample near point C on Figure 1. Note the low-density deep within the bubble and the steep gradients that provide a spectrum defined by a single spectral index with a spectral bump near a scale length of 500 m.

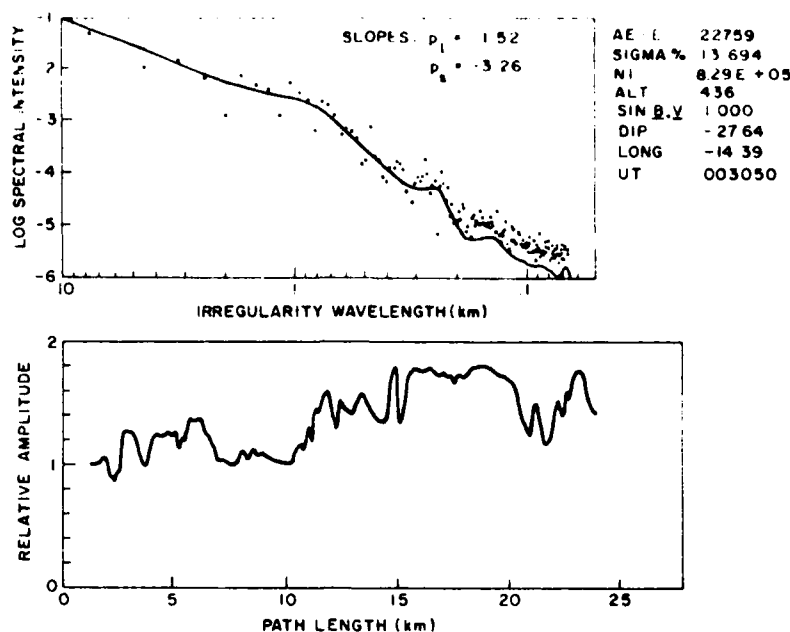


Fig. 4d. The same as in Figure 4a except for 3-s sample near point D on Figure 1. Note that this sample is exactly colocated with the subionospheric point for observation of the Marisat satellite from Ascension Island. The power spectrum is defined by two spectral slopes with  $p_1 = -1.52$  and  $p_2 = -3.26$ .

the superposition of a bump centered at 500 m. The irregularity amplitude is very large but the ambient density is so low within the first 18 km of path length, that scintillations at GHz frequencies are expected to decrease when the ray path is aligned with such depletions as will be shown in the next section. Further, the fact that such small gradient scale lengths are experimentally observed (also cf. Kelley *et al.* [1982]) has important implications for short scale irregularity generation and eventual decay of such sharp structures in the plasma. We shall discuss these points later in the paper.

The last data and spectral sample exhibited in Figure 4d is almost exactly matched in latitude and longitude with the subionospheric point of the scintillation observations of Marisat from Ascension Island as shown in Figure 3. Further, from Figure 1 and a consideration of ambient densities we see that this data was obtained from within a shallow bubble that has densities only a factor of 4 reduced from the ambient. The spectrum is as 'typical' as one can find in a large body of topside in situ data as the slopes  $p_1 = -1.5$  and  $p_2 = -3.3$  exactly match the most probable values determined from the statistical study to be presented below. Some sharp structures still exist in the data ( $L_N \sim 200$  m), and we know from coordinated scintillation measurements that such irregularity waveforms give rise to GHz scintillation.

A limited statistical study was made of the 125 samples with  $\Delta N/N > 1\%$  obtained during the 4 orbits shown in Figures 1 and 2. The idea was to determine the most probable scale length at which the break in the slope occurs such as in Figures 4b and 4d and to estimate the respective slopes on either side of the break. Of the total number, approximately 40 spectra had no breaks and were similar to the one shown in Figure 4c. Figure 5 shows a histogram of the percentage occurrence of scale length  $\Lambda_b$  at which a break in the spectral slopes occurs in the remaining 85 samples. The most probable scale-length is between 500 m to 1 km and a full two-thirds of all samples show a break at less than 1.5 km. Not a single spectrum was

observed for which  $\Lambda_b$  was less than 500 m even though the spectral range extends to 70 m. Since there is considerable interest in the scale length at which the break occurs, we made a further study of the range between 500 m and 1 km and found the percentage occurrence evenly split between 500–750 m and 750 m–1 km. Since the satellite is travelling perpendicular to the magnetic meridian plane ( $\sin B \cdot V = 1$ ), these are actual cross-field scale lengths.

The histograms for the percentage occurrence of  $p_1$ , the long scale length spectral index and  $p_2$ , the short scale length spectral index, are shown in Figures 6 and 7. The top panels in each case show the distributions when all the samples (including those without a marked break) are considered while the bottom panels show the distribution when only the spectra containing breaks are considered. Since those without breaks are mostly caused by steep edges and are, therefore, characteristic of data that lack stationarity, we shall only discuss the bottom panels of Figures 6 and 7. While there is quite a bit of variability in the

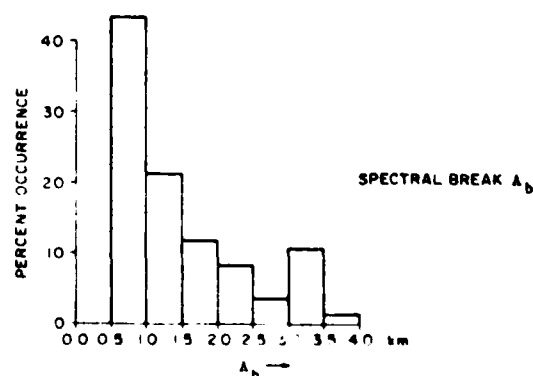


Fig. 5. Histogram showing percentage occurrence of spectral break,  $\Lambda_b$ , as a function of irregularity scale length observed during the four AE-F orbits shown in Figure 1.

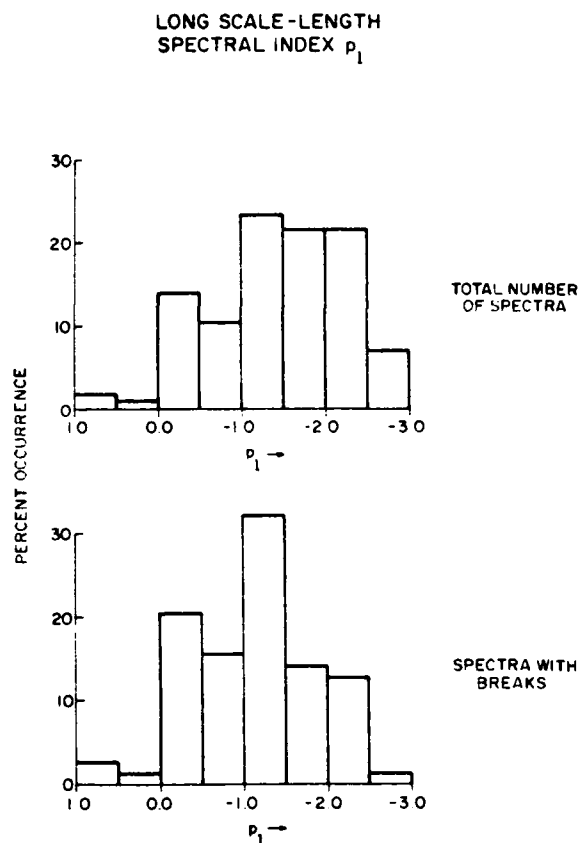


Fig. 6. Histogram showing the percent occurrence of different values of long scale length spectral index  $p_l$ . The top panel shows the occurrence distribution when all samples with and without breaks are considered, while the lower panel shows the occurrence when only those with significant spectral breaks are considered.

observed slopes, a  $p_l$  value of  $-1$  to  $-1.5$  and a  $p_s$  value between  $-3$  to  $-3.5$  seems to best describe a large fraction of the data set.

As mentioned in the introduction, the all sky TV imaging photometer was able to track a specific bubble on both nights. Thus we were able to compare the spectral characteristics of the same bubble between approximately 0030 UT and 0212 UT on December 15 that are marked I and I' in Figure 1. Similarly, we were also able to compare the features between 0038 UT and 0220 UT on December 17 which are marked II and II' in Figure 2. Actually we did not find any significant changes in spectral shape that we could relate to the age of the bubble within this 100-min time span around local midnight. On both nights, we were obviously comparing 2 topside bubbles. What differed from pre-midnight to post-midnight phase was the average rms electron density deviation associated with each bubble. Thus the 0030 UT bubble on December 15 was characterized by an average  $\langle \Delta N \rangle$  of  $1.7 \times 10^5 \text{ cm}^{-3}$  (obtained by averaging 8 RPA samples within the feature marked I), whereas the 0212 UT bubble was characterized by an average  $\langle \Delta N \rangle$  of  $5.4 \times 10^4 \text{ cm}^{-3}$ . That is, the electron concentration deviation had become a third of its initial value in approximately 100 min. The corresponding numbers for the bubble observed at two different times on December 17 are  $8.5 \times 10^4 \text{ cm}^{-3}$  and  $2.7 \times 10^4 \text{ cm}^{-3}$ . Again a reduction to one-third the initial value is observed in 100 min. It is instructive to note that the 0030 UT bubble on December 15 had GHz scintillation associated with

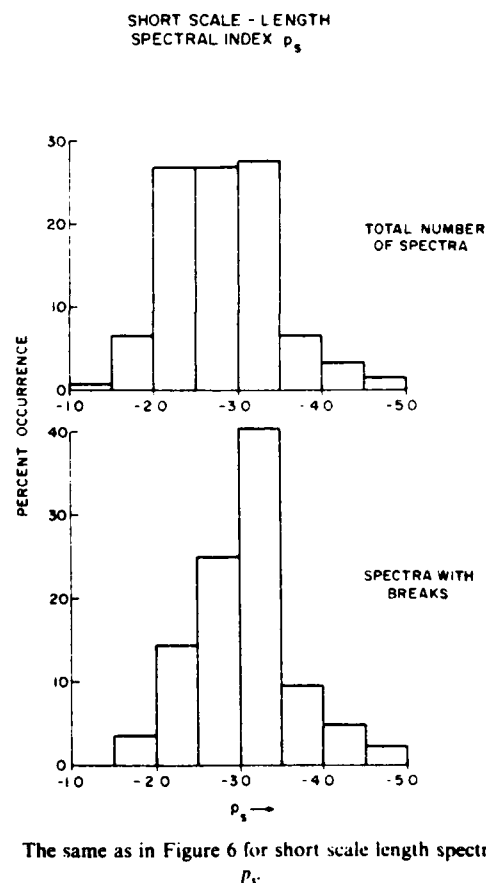


Fig. 7. The same as in Figure 6 for short scale length spectral index  $p_s$ .

it while the 0038 UT bubble on December 17 had only 257 MHz scintillation associated with it, consistent with its reduced magnitude of average  $\langle \Delta N \rangle$ .

The bubbles in the pre-midnight and post-midnight time frame (discussed above) seem to belong to an intermediate stage in the decay phase when topside spectral forms remain preserved while the decay of both the spectral intensity of the irregularities and the background concentration takes place. When the spatial structure of the bubbles in this stage are compared with those detected earlier in the evening, much sharper gradients are encountered in the early phase and will be discussed in section 4. Basu *et al.* [1980] discussed such erosion of irregularity structures between the early evening hours when extremely large spatial gradients are observed and the later stage, which is characterized by much shallower gradients.

### 3. VHF/GHz SCINTILLATION MEASUREMENTS

The 257 MHz and the 1.5 GHz  $L$  band scintillation measurements made by using the geostationary Marisat satellite on the night of December 14-15 from Ascension Island are shown in the top panel of Figure 8. The normalized second central moment of signal intensity  $S_2$ , as defined by Briggs and Parkin [1963], is used to provide a measure of the scintillations. The sub-ionospheric point (at 400 km altitude) for the measurements and its position with respect to the AE orbits are shown in Figure 3. The measurements are made at an elevation angle of  $80^\circ$  in the magnetic meridian plane. The dramatic sudden onset of the first patch occurs in the pre-midnight period at 2000 LT (LT = UT - 1 hour). On this night, two GHz scintillation patches were observed in association with saturated

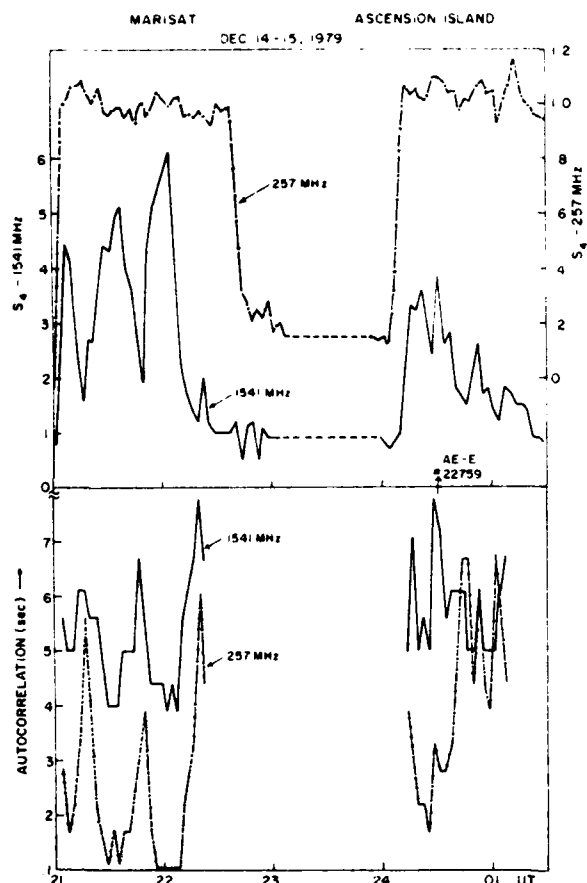


Fig. 8. The upper panel shows the temporal variation of 257- and 1541-MHz scintillation observations from Marisat recorded at Ascension Island on the night of December 14-15, 1979. The second scintillation patch was caused by the eastward drift of the bubble marked I on Figure 1. The existence of focussing at 257 MHz ( $S_4 > 1$ ) is clearly evident for this patch. The two lower panels show the autocorrelation interval  $\tau$  for 50 percent decorrelation observed at 1541 MHz (solid line) and 257 MHz (chain line). The one to one inverse correlation between increase of  $S_4$  at 1541 MHz and decrease of  $\tau$ , particularly at 257 MHz, is noteworthy.

VHF scintillation patches. The VHF scintillations show frequent effects of focussing [Singleton, 1970] with the  $S_4$  index often achieving values of 1.1. There was a somewhat weaker third VHF scintillation patch at 0400 UT on December 15 without any measurable GHz scintillation being associated with it and is thus not shown. The  $L$  band signal from Marisat is unfortunately subject to intensity changes usually on the order of 1 dB and is expected to affect the signal statistics during very weak scintillations. Tests on this data channel were carried out and it was found that the effect on even the weak scintillation spectra are minimal, except possibly at the very low frequency end. However, it is for this reason that dotted lines are used in between patches during periods of very weak scintillations to indicate possible contamination due to the level changes of the signal.

The AE satellite transit over Ascension Island occurred at 0030 UT when the second VHF/GHz patch was being observed as indicated in Figure 8. The in situ data provide irregularity amplitude ( $\Delta N/N$ ) at one fixed altitude along the propagation path while scintillation effects are caused by the integrated electron density deviation and hence becomes weighted heavily by structures that exist near the  $F$  peak. In this particular case,

judging by the in situ ambient density level of  $3 \times 10^6 \text{ cm}^{-3}$ , it is obvious that the satellite was sampling the irregularity structures that were primarily responsible for this scintillation patch. It is unfortunate that we do not have one to one correspondence between the first patch and AE data. The AE satellite at the earlier local time was in the Brazilian longitude sector. However, it is quite clear from the evening portions of the data shown in Figure 1 that the more intense GHz scintillations are associated with bubbles having large depletions that are immersed in a background of high ambient electron density. The high-elevation Ascension Island scintillation measurement with the GHz frequency also allows us to establish for the first time that what looks like one saturated (i.e.,  $S_4 \geq 1$ ) scintillation patch at 257 MHz is made up of several smaller bubbles with considerable structure associated with the walls. The GHz scintillation is reduced when the ray path in the  $F$  region goes through the center of such bubbles as the integrated electron density deviation is greatly reduced there, but obviously it is still adequate to cause saturated scintillations at the lower frequencies. In fact, the observation of  $S_4$  indices greater than unity indicating effects of focussing has important ramifications for the interpretation of scintillation spectra as will be discussed later. A further point to note is that we cannot, with the scintillation technique, at least, distinguish between differences in steepness at the eastern and western walls of bubbles as some radar studies have shown earlier [Tsunoda, 1981].

The two bottom panels of Figure 8 show the autocorrelation interval ( $\tau$ ) to 50% decorrelation at 1.5 GHz and 257 MHz. The 257 MHz scintillation was totally saturated (i.e.,  $S_4 \geq 1.0$ ) for the duration of both patches on December 14-15 as shown in the top panel. What is remarkable is that the GHz scintillation peaks and nulls are correlated one to one with decreased and increased values of  $\tau$ , respectively, on both frequencies. In fact, the correlation is even better with  $\tau$  determined from the 257-MHz signal. Thus the  $\tau$  values during strong scintillations provide much further insight into the strength of scattering, while no additional information can be obtained from the  $S_4$  index at 257 MHz (other than to note its complete saturation). For this night it seems that GHz scintillation is associated with  $\tau$  values smaller than 0.6 s at 257 MHz. This one to one relationship remains valid when  $S_4$  is moderately high and deteriorates somewhat at the end of the second patch on December 14-15 as the strength of scattering weakens considerably. This point will be further discussed in the next section.

The width of the bubble that gives rise to the second scintillation patch is 4.5° of longitude as measured by AE-E which is approximately 540 km at the altitude (435 km) of the satellite. The GHz scintillation event lasts for 60 mins at the  $S_4 > 1.5$  ( $SI = 2$  dB) level. From the above, the drift speed of the irregularity patch arising from the super-rotation of the nighttime equatorial  $F$  region [Rishbeth, 1971] is derived to be 150 m/s. This agrees well with the average velocity of 131 m/s derived by Weber *et al.* [1982] by tracking the bubble between 0030 to 0210 UT. When these drift speeds are combined with the  $\tau$  values quoted above, then we find that ground diffraction scales at 257 MHz have to be less than 90 m for measurable overhead GHz scintillations to occur. The agreement (between the drift velocities derived by the two techniques) further substantiates our earlier statement that the irregularity structures sampled by the AE-E satellite in an environment of high ambient ionization density ( $3 \times 10^6 \text{ cm}^{-3}$ ) was indeed responsible for the scintillation event observed on the ground.

The scintillation patch structure can be related well to the

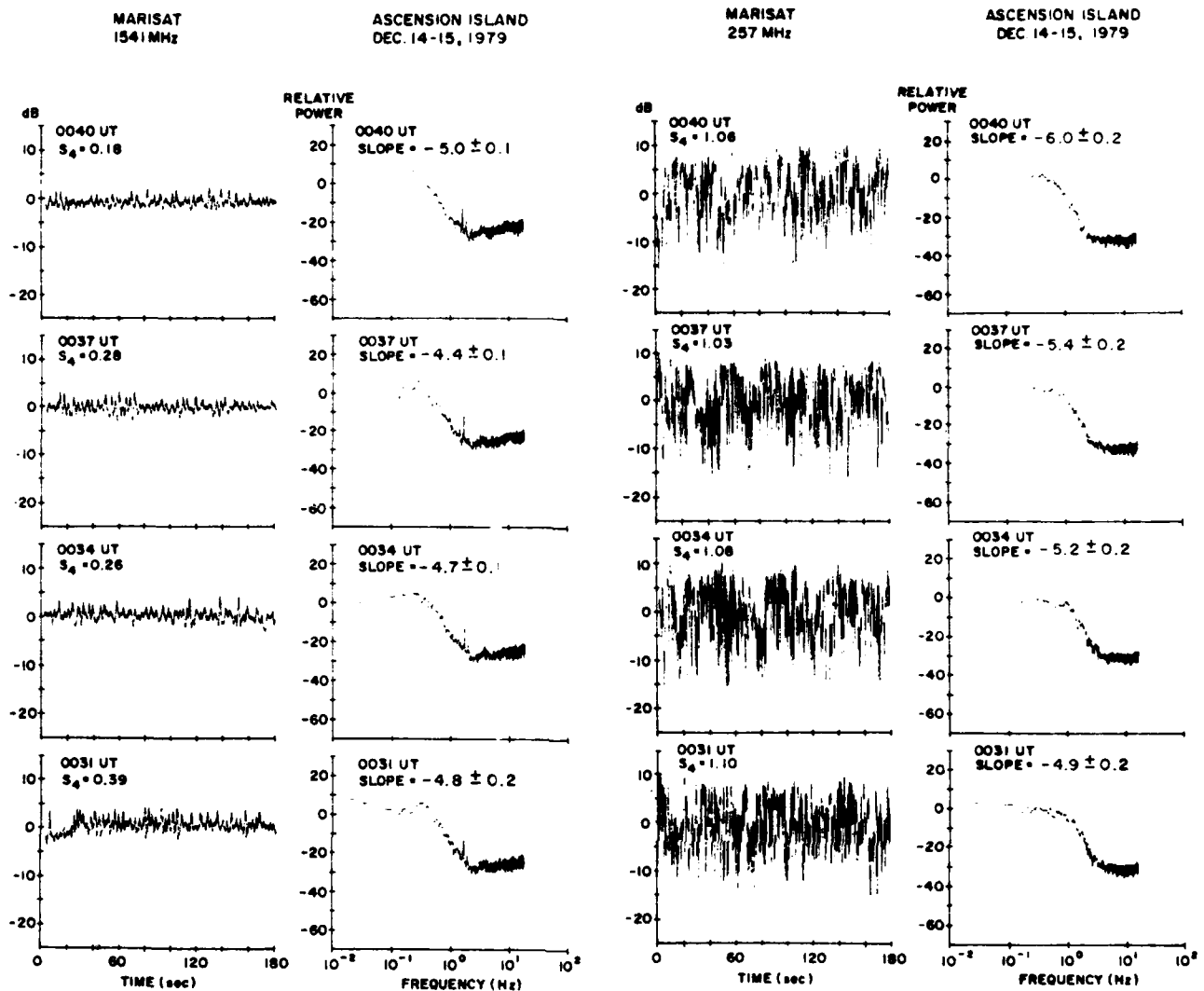


Fig. 9a

Fig. 9b

Fig. 9. (a) The left-hand panel shows four consecutive 3-min samples of 1541-MHz scintillations that were observed on December 14–15 when the AE-E satellite transited near the subionospheric location of the scintillation measurements. The right-hand panel shows the respective spectra obtained by the FFT technique. The Fresnel frequency of these weak scintillation spectra is near 0.3 Hz and the slope is approximately  $-4.5$  over the roll off portions between 0.5–1 Hz. The sharp spectral feature near 1.5 Hz is caused by the spin of the satellite. (b) Same as in Figure 9a except scintillations are on 257 MHz. The low frequencies show a filling in as compared to Figure 9a and the de-correlation bandwidth extends beyond 1 Hz. The slope over the roll-off portion between 1.5–2.5 Hz steepens to  $-5.5$ .

overall in situ bubble structure. For instance, during the eastward drift of the bubble (near 0030 UT on Figure 1) the scintillation onset (at 0015 UT on Figure 8) had been created by the eastern wall of the bubble. The part of the bubble immediately contiguous to this wall is quite shallow so that the drop-off in the scintillation intensity immediately prior to 0030 UT in Figure 8 is not emphasized. Then the deeper bubble comes into the ray path and we have a much larger falloff in the scintillation intensity at 0045 UT. We have mentioned earlier that the total scintillation patch width is consistent with the total bubble width on the basis of measured drift velocities for the night. Unfortunately, even though total electron content measurements were available at Ascension Island by using the Sirio satellite, which is located very close to Marisat, no estimate of the overall depletion can be made as the polarimeter records at 136 MHz are totally vitiated by fast polarization fluctuations as discussed by Lee *et al.* [1982]

The GHz scintillation spectra corresponding to four consecutive 3-min samples that are best time and space correlated with the in-situ AE data samples and spectra shown earlier are exhibited in Figure 9a. The  $S_4$  magnitudes are all in the weak intensity scatter regime at the GHz frequency. The spectra are fairly typical of those normally observed in the weak scattering regime. They all have a relatively flat to an  $f^{-1}$  at the low-frequency end and an  $f^{-4.5}$  dependence at the high-frequency end. The high-frequency spectral index was computed by linear least squares fit of the power spectral density estimates within the frequency interval 0.5 to 1.0 Hz, which includes the steepest portion of the spectrum. The frequency demarcating these two regimes is identified with the Fresnel frequency [Rufenach, 1975] and is close to 0.3 Hz for all the cases. With a  $150 \text{ m s}^{-1}$  drift this is equivalent to a scale-length of 500 m. This is close to the Fresnel dimension expected for overhead measurements at a frequency of 1.54 GHz. We have seen in section 2 that the



ASCENSION ISLAND  
DEC 16-17, 1979

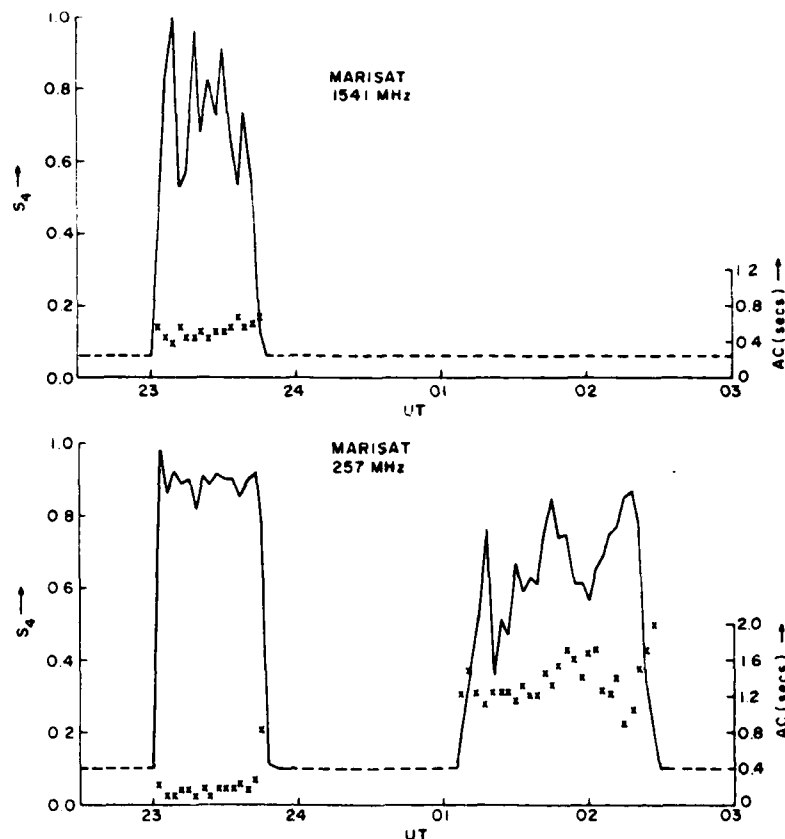


Fig. 10. The upper and lower panels show respectively the temporal variation of 1541 MHz and 257 MHz scintillations from Marisat recorded at Ascension Island on the night of December 16-17, 1979. The second scintillation patch at 257 MHz was caused by the eastward drift of the bubble marked II on Figure 2. The crosses on both panels represent the respective autocorrelation intervals  $\tau$  for 50% decorrelation.

break in the in situ spectra occurs at scale lengths  $> 500$  m. The roll off portions of the spectra under weak scatter conditions are thus expected to be consistent with  $p_s$ . We have found that the most probable value of  $p_s$  is between  $-3$  to  $-3.5$ . Thus given the uncertainties in the spectral measurements of both kinds the observed spectral slope of approximately  $f^{-4.5}$  is consistent with the predictions of weak scatter theory [Cronyn, 1970]. It should be noted that the narrow spectral peak at a frequency near 1.5 Hz is associated with the spin of the satellite.

The four corresponding VHF scintillation samples and their spectra are shown in Figure 9b. The scintillation magnitudes ( $S_4 > 1$ ) of all these samples place them in the focussing regime. The spectra all show a filling in of the low-frequency part and a spectral steepening of the roll off portions when compared with their respective GHz counterparts. The slopes in this case are obtained over the frequency interval of 1.5-2.5 Hz as the break point in the spectrum (which can no longer be identified with the Fresnel frequency) extends beyond 1 Hz. The ramifications of this Gaussian roll off together with the focussing effect observed will be discussed in the next section and an estimate of the phase perturbations under which such steepening occurs will be provided.

For comparison with the second night's in situ data, we show in Figure 10 the scintillations on 1.54 GHz and 257 MHz observed at Ascension Island on the night of December 16-17 and the respective autocorrelation intervals  $\tau$  to 0.5 decorrelation. On this night periods of saturated GHz scintillations are

observed in the premidnight period. Obviously the 257 MHz scintillations are driven far into saturation and the 18 Hz sampling rate is quite inadequate to resolve the variation of  $\tau$  with scattering strength as was done on the night of December 14-15. In Figure 10, in contrast to the situation shown in Figure 8, the  $S_4$  indices at VHF do not attain values greater than unity. The most likely reason is the inability of the receiving system to respond to the extremely fast fadings that limited the signal excursions and rendered the data unsuitable for spectral analysis. The AE transit 22790 occurs in the Ascension Island sector when the second 257 MHz scintillation patch was being observed and the one to one correspondence is with the bubble marked II in Figure 2. No GHz scintillation is associated with it in keeping with the reduced  $\langle \Delta N \rangle$  associated with this bubble as discussed in section 2. The  $\tau$  values pertaining to this second patch of the evening at 257 MHz varies between 0.9 and 1.8 s, which are approximately an order of magnitude larger than those associated with the first patch. This agrees with the earlier statement that measurable GHz scintillations are expected to be associated with  $\tau$  values smaller than 0.6 s. Incidentally, the average drift measured by optically tracking the 0040 bubble up to 0200 UT on the next AE orbit provides us with an eastward drift speed of  $128 \text{ m s}^{-1}$ , a value very close to that observed on December 14-15.

Finally, we present in Figure 11 four 3-min samples of saturated (samples 1 and 4) and moderate (samples 2 and 3) GHz scintillation data and their spectra. There are significant differ-

ences between these spectra and those presented in Figure 9a. The spectra show a two component structure with the spectral slope  $p_1$  being shallow ( $\sim -1.5$ ) between 0.25 to 0.55 Hz for samples 2 and 3 and between 0.25 and 0.85 Hz for samples 1 and 4. At higher frequencies up to 2 Hz the slopes  $p_2$  are quite steep, being  $\sim -5.5$ .

Since the spectral slopes remain the same under both moderate and strong scattering, it is tempting to associate this two-component scintillation spectrum with the two-component in situ spectrum discussed in section 2. However, if we assume the average drift speed of  $128 \text{ m s}^{-1}$  estimated by the airglow technique then the frequency of 0.25 Hz corresponds to  $\sim 500 \text{ m}$  scale length. Thus the entire two component structure is found to occur at scale lengths shorter than 500 m with the steepening being observed at scale lengths  $\sim 250 \text{ m}$  and shorter. The in situ data, on the other hand, generally shows the steepening to occur at scale lengths near 500 m. Further, only a small fraction ( $\sim 5\%$ , cf. Figure 7) shows steep in situ slopes between  $-4$  to  $-4.5$ , corresponding to the approximately  $-5.5$  slope observed in the scintillation data. The agreement between the

in situ and scintillation data can be improved, at least as far as the scale length of the break is concerned, if a higher drift velocity  $\sim 250 \text{ m s}^{-1}$  is assumed. Earlier spaced receiver drift measurements by Basu *et al.* [1980] have shown that a factor of 2 enhancement in E-W drifts is not uncommon, particularly in the evening hours. In this regard, we wish to point out that the two-component spectral structure is not always evident in Ascension Island GHz data, but in general the roll off portions can be described by a single steep slope varying between  $-5$  and  $-6$ .

#### 4. DISCUSSIONS

After attempting many equatorial campaigns with the collaboration of many different individuals and organizations, it is gratifying to note that we were finally able to obtain spatially and temporally correlated topside in situ irregularity and GHz scintillation data, in spite of Murphy's Law! This enabled us to make a careful comparison of the features of in situ spectra and unsaturated intensity scintillation spectra, the need for such a comparison having been recognized many years ago [Rufenach, 1975; Basu *et al.*, 1976].

The primary feature of the high-resolution topside in situ data that became apparent as a result of this study is the realization that the spectral form of the irregularities in the magnetic E-W direction, although power law, cannot be described by a single spectral index. A persistent break in the slopes is found between 500 m to 1.5 km with the longer scale lengths over a decade showing shallow slopes on the order of  $-1$  to  $-1.5$  and the shorter scales over a decade showing steeper slopes on the order of  $-3$  to  $-3.5$ . It is, indeed interesting to note that the irregularity spectra observed in the vertical direction during the rocket flight at Kwajalein also showed a similar break in the spectral slope at 500 m with the longer scales showing a spectral index of  $-1.5$  and the shorter scales exhibiting a steeper index of  $-3$  [Rino *et al.*, 1981]. Thus the two sets of measurements both obtained in planes perpendicular to the earth's magnetic field but one in a horizontal and the other in a vertical plane, gave similar results. The high resolution AE-E data was also extremely useful in demonstrating that spectra of weak intensity scintillations at 1.54 GHz obtained in a collocated volume could indeed map the in situ irregularity structures smaller than a km.

Livingston *et al.* [1981] had earlier used the low-resolution ( $\sim 2.6 \text{ km}$ ) AE-E data to do a comparative study of the in situ irregularity characteristics with those derived from the VHF/UHF phase scintillation measurements using the Wideband satellite. They found a systematic decrease in the spectral index with increasing perturbation strength. They also showed that the same systematic decrease of the spectral index with increasing perturbation strength was found in the measured phase spectral indices. In view of the two-component horizontal wave number spectrum discussed in this paper, the excellent agreement obtained between the phase spectral slope and the low-resolution in situ data by Livingston *et al.* can only be interpreted to mean that the Wideband phase measurements are sensitive to irregularities  $> 1 \text{ km}$ , even though Figure 1 of their paper shows that Wideband measurements cover irregularity scale lengths up to 100 m. No indication of the existence of a steeper slope at shorter scale lengths was obtained from the Wideband phase data. Indeed, Wideband equatorial phase spectral data have always shown slopes shallower than  $-3$  whatever the scattering condition (cf. Figure 1 of Rino [1979]). Thus it seems reasonable to conclude that even in the weak scatter regime (where contamination due to diffraction is not

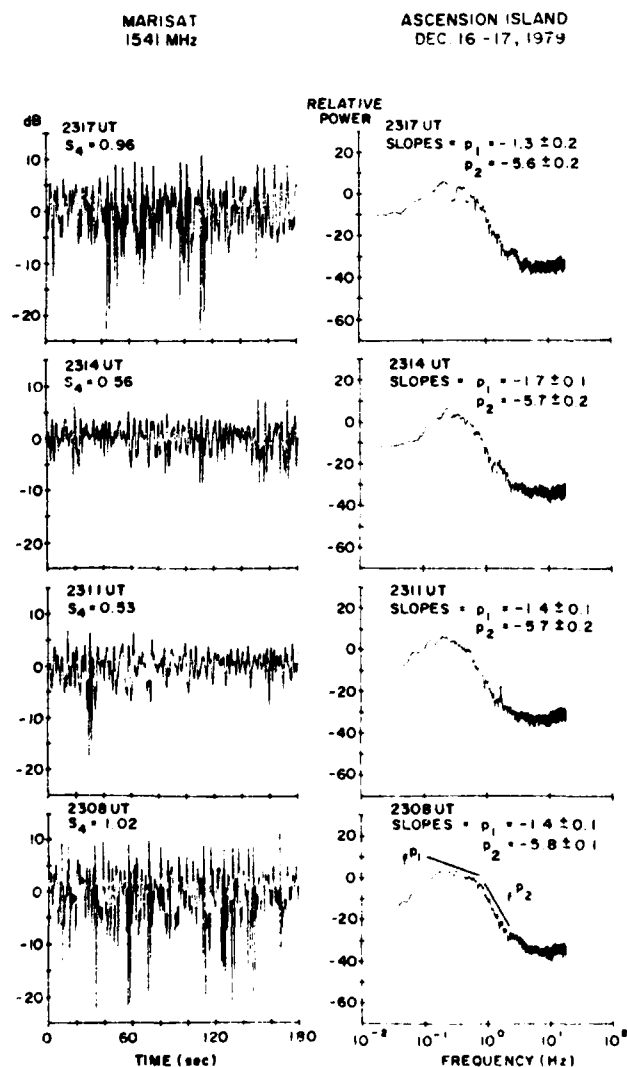


Fig. 11. Four consecutive 3-min samples of saturated (samples 1 and 4) and moderate (samples 2 and 3) 1541 MHz scintillations that were observed on the night of December 16–17, 1979, and their corresponding spectra obtained by the FFT technique. Two spectral slopes are observed with the low frequency slope  $p_1$  being  $\sim -1.5$  and the higher frequency slope  $p_2$  being  $\sim -5.5$ .

expected), the Wideband phase data can only map the large scale structures ( $> 1$  km) and cannot provide any information on density irregularities smaller than a km. Our current high resolution in situ and coordinated GHz scintillation measurements have shown that it is possible to map smaller scale structures with intensity scintillation data from geostationary satellites.

For the propagation community it may be of some interest to note that a study of the diffraction scales on the ground as obtained from the auto-correlation intervals provides a very good measure of the strength of scattering (as the irregularity drift speed variation is small over a few hours), even though the first-order statistics as represented by the  $S_4$  index is completely saturated. With simultaneous VHF and  $L$  band intensity scintillation data, we have shown how well the auto-correlation intervals of saturated 257-MHz scintillations track the variation of 1.54 GHz scintillation magnitude. In particular, we were able to show that the auto-correlation interval is reduced when the strength of scattering increases on walls of bubbles and vice versa deep within bubbles. On a statistical basis, *Rino and Owen* [1980], using orbiting satellites, and *Umeki et al.* [1977] and *Basu and Whitney* [1983], using geostationary satellite data, have shown that under conditions of strong scattering, the intensity coherence time is controlled by the perturbation strength, whereas in the weak scatter regime, the Fresnel dimension is the dominant factor.

We have shown that the in situ irregularity spectra in the equatorial region can be described by a spectral index  $\sim -3$  to  $-3.5$  at scale-lengths shorter than 1 km. For weak intensity scintillations at GHz frequencies, the scintillation spectra indicate a variation of the power spectral density (psd) with frequency ( $f$ ) as  $f^{-1}$  at frequencies below the Fresnel frequency ( $f_{FR}$ ) and  $f^{-4.5}$  at  $f > f_{FR}$ , which is consistent with the in situ data. We have also demonstrated that at Ascension Island, the irregularity environment is extremely intense and even the 1.54-GHz transmissions are driven into saturation. Under such conditions, both the 257 MHz and 1.54 GHz show the effects of focussing with the  $S_4$  index being as large as 1.2. The frequency spectra, particularly at 257 MHz, at such times indicate steepening of spectral slopes as high as  $f^{-6}$ . Recent numerical computations [*Rino*, 1980; *Booker and MajidiAhi*, 1981] for scattering by deeply modulated phase screens with power law type of irregularities indicate that the transition part of the spectral slope steepens and approaches a Gaussian form. We wish to emphasize that the observed level of phase perturbations computed from the in situ data does indeed achieve the high levels that are required for the Gaussian steepening to occur. For instance, using the background density level of  $3 \times 10^6 \text{ cm}^{-3}$  and an irregularity amplitude of 25% with an outer scale of 10 km as observed in the Ascension Island in situ data,  $\langle \Delta\phi^2 \rangle$ , the square of the phase perturbations exceeds  $10^3$  (radians) $^2$  at 257 MHz by using the equations developed by *Rino* [1979]. The numerical modeling efforts of *Booker and MajidiAhi* [1981], which predict steepening in the spectral roll off, are based on such high values of phase perturbation. Thus the observations of (1) steeply sloped in situ density spectrum ( $p_1$  steeper than  $-3$ ), (2) the existence of a focussing regime ( $S_4 > 1$ ), and (3) the Gaussian steepening of the transition portion of the intensity scintillation spectrum are all mutually consistent and follow theoretical and numerical computations [*Rino*, 1980; *Booker and MajidiAhi*, 1981].

Before concluding our discussions on scintillations we would like to draw the reader's attention to Figure 11, which illus-

trated four data samples corresponding to both moderate and strong GHz scintillations. Each spectrum is steeply sloped ( $p_2 \sim -6$ ), and some nonstationarity in the temporal structure may be noted. This data sample corresponds to the early evening period when the in situ data reveals the presence of steep spatial structures. It is very likely that such structures introduce the observed nonstationarity in the scintillation data and cause the two-component steeply sloped spectra. Further studies are currently being conducted with early evening in situ data and coordinated 3954- and 1541-MHz scintillation data to clarify this problem.

One of the features of possible interest to plasma physicists may be the extreme sharpness of the gradients that are observed in the data. While the near midnight bubble data that was discussed in detail showed gradient scale lengths on the order of 100 m, the early evening bubbles that almost certainly give rise to the saturated GHz scintillation showed gradient scale-lengths as small as the resolution of the instrument, namely 35 m. In their analysis of the lower hybrid drift instability, which had been invoked by *Huba et al.* [1978] and *Huba and Ossakow* [1979] to explain 1 m and 36 cm backscatter, *Sperling and Goldman* [1980] derived an instability criterion that depends on the ambient density, the gradient scale length, and the ion gyro radius of  $O^+$  ions, which is on the order of 5 m in the topside. Unfortunately, we do not have actual coordinated radar measurements to prove that such short scale lengths were indeed generated, but from the measurements presented here it seems that the instability relationship may often be satisfied within low-density bubbles and even on the sharp edges of relatively high-density walls of bubbles. This tends to indicate that the linear lower hybrid drift instability may explain the observed backscatter at the short scale lengths. *Kelley et al.* [1982], on the other hand, using data from the Plumex rocket, have shown that the data for  $L_N$  and plasma density are such that the plasma was just on the stable side of the lower hybrid drift wave marginal instability line.

The decay of the sharp gradients probably occurs through the anomalous diffusion process as pointed out by *Huba and Ossakow* [1981]. They used an expression for the anomalous collision frequency based on *Gary's* [1980] treatment of the anomalous transport properties associated with the collisionless universal drift instability and determined that the time scale for gradient scale lengths of  $L_N \leq$  several hundred meters to decay by this process would be of the order of minutes. The anomalous diffusion coefficient of the lower hybrid drift instability is substantially smaller than that of the universal drift instability and can be neglected [*Gary*, 1980]. *Huba and Ossakow* [1981] further point out that the radar backscatter observed irregularities ( $\leq 3$  m) themselves can disappear by either classical or anomalous diffusion. They also state that the scintillation causing irregularities ( $\sim 1$  km) cannot decay by either classical or anomalous diffusion because both require too much time ( $> 8$  hours). While anomalous diffusion seems to provide time scales that are generally in agreement with observations [*Basu et al.*, 1978], it is important to note that the bubble marked 1 on AE-E #22759 still had  $L_N \leq$  several hundred meters (actually  $< 200$  m) associated with it even though the local time is beyond 2300 LT. While we do not have definite proof regarding the time of its generation, it is probably fair to assume that generation took place close to 2100 LT. Thus quite sharp gradients can persist for, at least, a couple of hours. On the other end of the scale, kilometer-sized irregularities as explored by scintillation measurements once

generated certainly do not last more than 8 hours or until *E* region shorting takes place at sunrise (e.g., see Figure 10). Thus it seems that some mechanism other than diffusion is probably responsible for the decay of kilometer scale irregularities.

**Acknowledgments.** The work at Emmanuel College was partially supported by AFGL contract F19628-81-K-0011, and NASA grant 5419 under the AE Guest Investigator program. The work at the University of Texas at Dallas was supported by NSF grant ATM-80-07560 and NASA grants NGR 44-004-120 and NGL 44-004-130. The data at Ascension Island were acquired by J. A. Klobuchar. We thank J. Aarons and E. J. Weber for useful discussions and E. MacKenzie for help with the preparation of the manuscript.

The Editor thanks C. H. Liu and another referee for their assistance in evaluating this paper.

## REFERENCES

- Aarons, J., Equatorial scintillations: A review, *IEEE Trans. Antennas Propagat.*, AP-25, 729, 1977.
- Aarons, J., The global morphology of ionospheric scintillations, *Proc. IEEE*, 70, 360, 1982.
- Aarons, J., H. E. Whitney, E. MacKenzie, and S. Basu, Microwave equatorial scintillation intensity during solar maximum, *Radio Sci.*, 16, 939, 1981.
- Balsley, B. B., G. Haerendel, and R. A. Greenwald, Equatorial spread *F*: Recent observations and a new interpretation, *J. Geophys. Res.*, 77, 5625, 1972.
- Basu, S., and Su. Basu, Equatorial scintillations—A review, *J. Atmos. Terr. Phys.*, 43, 473, 1981.
- Basu, S., and H. E. Whitney, The temporal structure of intensity scintillations near the magnetic equator, *Radio Sci.*, 18, in press, 1983.
- Basu, S., Su. Basu, J. Aarons, J. P. McClure, and M. D. Cousins, On the coexistence of km- and m-scale irregularities in the nighttime equatorial *F* region, *J. Geophys. Res.*, 83, 4219, 1978.
- Basu, S., J. P. McClure, Su. Basu, W. B. Hanson, and J. Aarons, Coordinated study of equatorial scintillation, in situ and radar observations of nighttime *F* region irregularities, *J. Geophys. Res.*, 85, 5119, 1980.
- Basu, Su., and M. C. Kelley, Review of equatorial scintillation phenomena in light of recent developments in the theory and measurement of equatorial irregularities, *J. Atmos. Terr. Phys.*, 39, 1229, 1977.
- Basu, Su., and M. C. Kelley, A review of recent observations of equatorial scintillations and their relationship to current theories of *F* region irregularity generation, *Radio Sci.*, 14, 471, 1979.
- Basu, Su., S. Basu, and B. K. Khan, Model of equatorial scintillations from in situ measurements, *Radio Sci.*, 11, 821, 1976.
- Basu, Su., S. Basu, J. P. McClure, and W. B. Hanson, Spatially and temporally co-located measurements of GHz/VHF scintillation and in-situ irregularity spectra near Ascension Island (abstract), *Eos Trans. AGU*, 62, 347, 1981.
- Booker, H. G., and G. MajidiAhi, Theory of refractive scattering in scintillation phenomena, *J. Atmos. Terr. Phys.*, 43, 1199, 1981.
- Briggs, B. H., and I. A. Parkin, On the variation of radio star and satellite scintillations with zenith angle, *J. Atmos. Terr. Phys.*, 25, 339, 1963.
- Chaturvedi, P. K., and S. L. Ossakow, Nonlinear theory of the collisional Rayleigh-Taylor instability in equatorial spread *F*, *Geophys. Res. Lett.*, 4, 558, 1977.
- Costa, E., and M. C. Kelley, Calculations of equatorial scintillations at VHF and gigahertz frequencies based on a new model of the disturbed equatorial ionosphere, *Geophys. Res. Lett.*, 3, 677, 1976.
- Costa, E., and M. C. Kelley, On the role of steepened structures and drift waves in equatorial spread *F*, *J. Geophys. Res.*, 83, 4359, 1978.
- Cronyn, W. M., The analysis of radio scattering and space probe observations of small-scale structure in the interplanetary medium, *Astrophys. J.*, 161, 755, 1970.
- Dyson, P. L., J. P. McClure, and W. B. Hanson, In situ measurements of the spectral characteristics of ionospheric irregularities, *J. Geophys. Res.*, 79, 1497, 1974.
- Farley, D. T., Irregularities in the equatorial ionosphere: The Berkner Symposium, *Rev. Geophys. Space Phys.*, 12, 285, 1974.
- Fejer, B. G., and M. C. Kelley, Ionospheric irregularities, *Rev. Geophys. Space Phys.*, 18, 401, 1980.
- Gary, S. P., Wave particle transport from electrostatic instabilities, *Phys. Fluids*, 23, 1193, 1980.
- Haerendel, G., Theory of equatorial spread-*F*, Max-Planck Institut fur Phys. und Astrophys., Garching, West Germany, 1974.
- Hanson, W. B., D. R. Zuccaro, C. R. Lippincott, and S. Sanatani, The retarding potential analyzer on Atmosphere Explorer, *Radio Sci.*, 8, 333, 1973.
- Huba, J. D., and S. L. Ossakow, On the generation of 3-m irregularities during equatorial spread *F* by low-frequency drift waves, *J. Geophys. Res.*, 84, 6697, 1979.
- Huba, J. D., and S. L. Ossakow, Diffusion of small-scale density irregularities during equatorial spread *F*, *J. Geophys. Res.*, 86, 9107, 1981.
- Huba, J. D., P. K. Chaturvedi, and S. L. Ossakow, High-frequency drift waves with wavelengths below the ion gyroradius in equatorial spread *F*, *Geophys. Res.*, 5, 695, 1978.
- Kelley, M. C., and J. P. McClure, Equatorial spread-*F*: A review of recent experimental results, *J. Atmos. Terr. Phys.*, 43, 427, 1981.
- Kelley, M. C., G. Haerendel, H. Kappler, A. Valenzuela, B. B. Balsley, D. A. Carter, W. L. Ecklund, C. W. Carlson, B. Hausler, and R. Torbert, Evidence for a Rayleigh-Taylor type instability and upwelling of depleted density regions during equatorial spread *F*, *Geophys. Res. Lett.*, 3, 448, 1976.
- Kelly, M. C., R. Pfaff, K. D. Baker, J. C. Ulwick, R. Livingston, C. Rino, and R. Tsunoda, Simultaneous rocket probe and radar measurements of equatorial spread *F*—Transitional and short wavelength results, *J. Geophys. Res.*, 87, 1575, 1982.
- Lee, M. C., A. DasGupta, J. A. Klobuchar, S. Basu, and Su. Basu, Depolarization of VHF geostationary satellite signals near the equatorial anomaly crests, *Radio Sci.*, 17, 399, 1982.
- Livingston, R. C., C. L. Rino, J. P. McClure, and W. B. Hanson, Spectral characteristics of medium-scale equatorial *F* region irregularities, *J. Geophys. Res.*, 86, 2421, 1981.
- McClure, J. P., W. B. Hanson, and J. H. Hoffman, Plasma bubbles and irregularities in the equatorial ionosphere, *J. Geophys. Res.*, 82, 2650, 1977.
- Morse, F. A., B. C. Edgar, H. C. Koons, C. J. Rice, W. J. Heikkila, J. H. Hoffman, B. A. Tinsley, J. D. Winningham, A. B. Christensen, R. F. Woodman, J. Pomalaza, and N. R. Teixeira, Equion, an equatorial ionospheric irregularity experiment, *J. Geophys. Res.*, 82, 578, 1977.
- Ossakow, S. L., Ionospheric irregularities, *Rev. Geophys. Space Phys.*, 17, 521, 1979.
- Ossakow, S. L., Spread-*F* theories—A review, *J. Atmos. Terr. Phys.*, 43, 437, 1981.
- Rino, C. L., A power law phase screen model for ionospheric scintillation, I. Weak scatter, *Radio Sci.*, 14, 1135, 1979.
- Rino, C. L., Numerical computations for a one-dimensional power law phase screen, *Radio Sci.*, 15, 41, 1980.
- Rino, C. L., and J. Owen, The time structure of transionospheric radio wave scintillation, *Radio Sci.*, 15, 479, 1980.
- Rino, C. L., R. T. Tsunoda, J. Petriceks, R. C. Livingston, M. C. Kelley, and K. D. Baker, Simultaneous rocket-borne beacon and in situ measurements of equatorial spread *F*—Intermediate wavelength results, *J. Geophys. Res.*, 86, 2411, 1981.
- Rishbeth, H., Polarization fields produced by winds in the equatorial *F* region, *Planet. Space Sci.*, 19, 357, 1971.
- Rufenach, C. L., Ionospheric scintillation by a random phase screen: Spectral approach, *Radio Sci.*, 10, 155, 1975.
- Singleton, D. G., Saturation and focussing effects in radiostar and satellite scintillations, *J. Atmos. Terr. Phys.*, 32, 187, 1970.
- Sperling, J. L., and S. R. Goldman, Electron collisional effects of lower hybrid drift instabilities in the ionosphere, *J. Geophys. Res.*, 85, 3494, 1980.
- Tsunoda, R. T., Time evolution and dynamics of equatorial backscatter plumes, I. Growth phase, *J. Geophys. Res.*, 86, 139, 1981.
- Umeki, R., C. H. Liu, and K. C. Yeh, Multifrequency studies of ionospheric scintillations, *Radio Sci.*, 12, 311, 1977.
- Weber, E. J., H. C. Brinton, J. Buchau, and J. G. Moore, Coordinated airborne and satellite measurements of equatorial plasma depletions, *J. Geophys. Res.*, 87, 1050, 1982.
- Yeh, K. C., and C. H. Liu, Radio wave scintillations in the ionosphere, *Proc. IEEE*, 70, 324, 1982.

(Received April 19, 1982;  
revised October 8, 1982;  
accepted November 3, 1982.)

## Occurrence of nighttime VHF scintillations near the equatorial anomaly crest in the Indian sector

A. DasGupta<sup>1</sup> and A. Maitra

*Institute of Radio Physics and Electronics, University of Calcutta, Calcutta 700009, India*

Santimay Basu

*Emmanuel College, Boston, Massachusetts 02115*

(Received February 12, 1981; revised May 19, 1981; accepted May 19, 1981.)

The behavior of nighttime *F* region irregularities near the northern crest of the equatorial anomaly in the Indian sector has been investigated by using VHF amplitude scintillation measurements made at Calcutta (27°N dip subionospheric) during the period April 1977 through February 1980. With the increase in solar activity the occurrence of scintillations increases remarkably during the equinoxes and to a lesser extent during the December solstice, while the local summer occurrence shows little change. The observed patterns are assessed in terms of the variation of the *F* layer height with solar activity and upwelling motion of the depleted flux tubes associated with small scale irregularities. It is shown that the propagation path is more likely to intercept these equatorial irregularities during periods of high solar activity, while during periods of low solar activity the equatorial irregularities lie south of the propagation path.

### INTRODUCTION

In recent years there has been an increasing interest in the understanding of the physics of the nighttime *F* region irregularities near the magnetic equator [Basu and Kelley, 1979]. Even though a number of techniques have been used to explore the irregularities [Basu *et al.*, 1980], the measurement of scintillations of signals from satellites remains the most widely used method for the study of kilometer scale irregularities. In the context of the current experimental and theoretical investigations it is apparent that the equatorial *F* region plasma within an entire flux tube goes unstable and takes part in an upwelling motion [Anderson and Haerendel, 1979; Weber *et al.*, 1980]. As a result, the irregularities also occur north and south of the magnetic equator.

Most of the long-term observations have, however, been performed at locations like Huan-cayo and Legon, situated very close to the magnetic equator, and similar observations from stations off

the magnetic equator are lacking. Recently, an extremely high level (>20 dB at 1.54 GHz) of amplitude scintillation has been observed at Ascension Island (7.95°S, 14.4°W, 31.4°S dip), located near the southern crest of the well-known equatorial anomaly in *F2* ionization in the African zone [Aarons *et al.*, 1981]. Although the above results have focused attention on the problem, so far very few long-term scintillation observations have been reported from such locations. In this paper we present some results of 136-MHz amplitude scintillation measurements made during the 3-year period April 1977 through February 1980 at Calcutta (23°N, 88.5°E, 32° dip), which is situated virtually below the northern crest of the equatorial anomaly. We shall examine the seasonal variation of scintillation at this location during the above period and show that both the level of scintillations and the seasonal pattern are controlled by solar activity. This, as we shall discuss, may be related to the variation of the height of the *F2* layer at the magnetic equator with solar activity.

### DATA

A polarimeter of the type described by Eis *et al.* [1977] and received from the Air Force Geophysics Laboratory, Hanscom Air Force Base, Massachusetts, has been in operation at the

<sup>1</sup>Presently NRC/NAS senior resident research associate at the Air Force Geophysics Laboratory, Hanscom Air Force Base, Massachusetts 01731, on leave from the University of Calcutta.

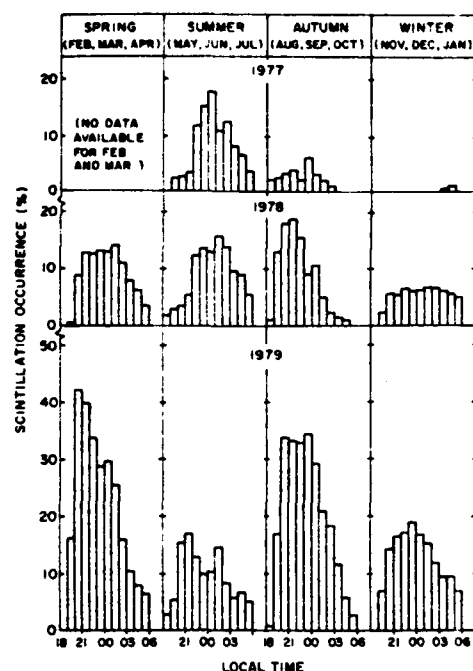


Fig. 1. Percentage occurrence of nighttime scintillations ( $SI \geq 3$  dB) at 136 MHz for different seasons.

Haringhata Field Station of the University of Calcutta. This was used to record the amplitude and polarization of the 136-MHz signal from the Japanese geostationary satellite ETS 2 since April 1977. This paper discusses the amplitude scintillations of the signal recorded by the polarimeter. The recording time constant of the system is 0.1 s and the dynamic range is about 22 dB. The scintillation index in decibels has been scaled manually every 15 min following the method outlined by *Whitney et al.* [1969]. The subionospheric point, namely, the intersection of the propagation path from the station to the ETS 2 satellite with the 400-km ionospheric height, occurred at  $21^\circ\text{N}$  and  $92^\circ\text{E}$  (dip  $27^\circ\text{N}$ ). This subionospheric position is to the immediate south of the northern crest of the equatorial anomaly. It should be noted that in this longitude sector the height of the 400-km subionospheric point maps along the earth's magnetic field to an altitude of 800 km above the magnetic equator.

## RESULTS AND DISCUSSION

Scintillations at Calcutta have varied considerably during the period April 1977 to February 1980 when

the level of solar activity changed greatly. During 1977, the scintillation index at 136 MHz generally ranged between 3 and 6 dB [*DasGupta and Maitra, 1980*] but in the later period the index attained levels exceeding 22 dB and was often limited by the dynamic range of the system.

Figure 1 shows the hourly percentage occurrence of nighttime scintillation (scintillation index ( $SI \geq 3$  dB) on a seasonal basis for 1977, 1978, and 1979. It is of interest to note that in 1977, a year of low solar activity, scintillations were observed mainly during the months of May–July. With the increase of solar activity during 1978, scintillations were also observed during the equinoxes (February–April and August–October) and the December solstice (November–January), in addition to the May–July period. In 1979, the year of recent maximum solar activity, the equinoctial occurrence of scintillations becomes much higher than that during the May–July period and the activity during November–January also registers some increase.

The effect of solar activity on the seasonal variation of scintillations is more clearly evident in Figure 2, which shows the nighttime occurrence of scintillations, ordered on a seasonal basis, as a function of the 10.7-cm solar flux. It may be noted that the occurrence during the June solstice remains virtually constant with increasing solar flux while the scintillation occurrences during the equinoxes and the December solstice increase with the 10.7-cm solar flux. It should be pointed out that

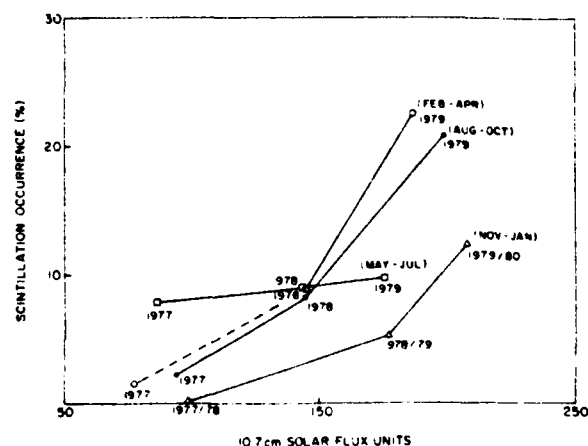


Fig. 2. Variation of percentage occurrence of scintillations with solar activity for different seasons. Vernal equinox of 1977 contains data for the month of April only.

the ATS 6 observations performed near the magnetic equator in this longitude sector during the solar minimum showed that nighttime scintillations occur during the equinoxes and the December solstice [Basu and Basu, 1981, and references therein]. Thus it appears that the equatorial irregularities with their characteristic seasonal pattern in the Indian sector are intercepted by the propagation path from Calcutta, located near the crest of the equatorial anomaly, only during the period of high solar activity. It should, however, be noted that the ATS 6 observations were made for only 1 year and these conclusions should be verified by long-term observations at the magnetic equator in the Indian sector.

Scintillations usually occur predominantly in the time period before local midnight during the equinoxes, while there is no such definite pattern for the other seasons. The temporal character of the equinoctial scintillations at 136 MHz has been observed to be patchy, the discrete patches lasting for a few tens of minutes interspersed with absolutely quiet periods. This character is very similar to that observed near the magnetic equator by Aarons *et al.* [1980a]. On the other hand, scintillations observed during the May–July period in all 3 years, 1977–1979, indicate absence of discrete patches and instead show one or two continuous periods of scintillation activity lasting for several hours. Scintillation patches in association with the depletions of total electron content or bubbles have been reported by Yeh *et al.* [1979] from their

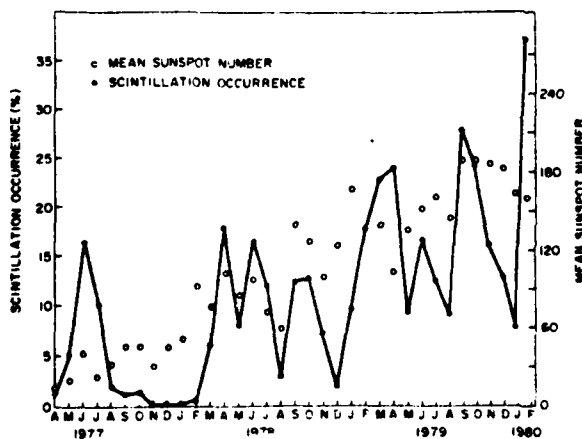


Fig. 3. Monthly variation of scintillation activity. The open circles show the monthly mean sunspot numbers.

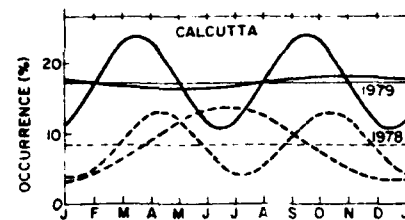


Fig. 4. Harmonic analysis of the monthly occurrence of nighttime scintillation during 1978 and 1979, shown by solid and dashed lines, respectively. The annual and semiannual components are shown around the corresponding mean or average values given by the straight lines.

observations at Natal. At the present location, the scintillation patches observed in the early evening hours are found to be associated with fast fluctuations of polarization when it becomes impossible to determine the total electron content. However, in the late phase, the polarization variations associated with the scintillation patches become slow; when analyzed, the variations indicate depletions of total electron content. Similar features of polarization fluctuations in association with scintillation patches have been obtained at Ascension Island, near the crest of the equatorial anomaly, during the recent period of maximum solar activity (J. A. Klobuchar, private communication, 1981).

Figure 3 shows the percentage of time the VHF signal scintillates ( $SI \geq 3$  dB) for the different months individually. The monthly mean sunspot numbers are also indicated in the diagram to facilitate the comparison of the scintillation pattern with solar activity. As discussed in the previous paragraph, a semiannual component corresponding to the equinoctial scintillations becomes progressively more prominent with the increase in the solar activity while the annual component identified with scintillation occurrence during the May–July period shows a decreasing trend relative to the semiannual component (Figure 4). The average occurrence of the dc component in 1979 is nearly double that in the previous year.

The emergence of an equinoctial component of scintillations as well as a secondary maximum during the December solstice at the crest of the (daytime) equatorial anomaly in  $F_2$  ionization during the period of high solar activity is very significant. This is in keeping with the seasonal variation of scintillations observed at the magnetic equator in the Indian

sector during solar minimum period [Krishnamoorthy *et al.*, 1979; Basu and Basu, 1981]. As mentioned earlier, the subionospheric locations of the present observations are mapped along the earth's magnetic field to an altitude of about 800 km above the magnetic equator. Should the *F* region irregularities above the magnetic equator extend to altitudes of 800 km and above, the kilometer scale irregularities at the magnetic equator are expected to be mapped down the field lines to the subionospheric location of the present observations. With increasing solar activity, the equatorial *F* region vertical drift velocity around sunset increases [Fejer *et al.*, 1979] and the height of the *F* region maximum in the postsunset hours typically attains altitudes of about 500 km. In the context of the current theories of the generation of nighttime equatorial irregularities and their upwelling motion [Scannapieco and Ossakow, 1976], irregularities near the magnetic equator may extend to altitudes above 800 km and get mapped down to intercept the propagation path from Calcutta. Thus the present station is able to record the seasonal pattern of the equatorial scintillation only during the years of high solar activity. During the period of low solar activity, scintillations which probably arise from mid-latitude irregularities are recorded only during the May–July period. As noted earlier, this component does not exhibit significant variation with solar activity.

Thus it seems that the scintillation occurrence at the crest of the equatorial anomaly in the Indian sector during the June solstice is due to mid-latitude irregularities whereas the scintillation occurrence during the equinoxes and the December solstice, observed only during the solar maximum, is equatorial in origin. Therefore the seasonal pattern of equatorial scintillation in the Indian sector is in keeping with that of the American and African sectors as reported by Aarons *et al.* [1980b] but is different from that observed at Kwajalein and Guam [Livingston, 1980; Aarons *et al.*, 1980b]. The ATS 6 observations performed near the magnetic equator in the Indian sector over a limited period during the solar minimum support the above conclusion [Krishnamoorthy *et al.*, 1979; Basu and Basu, 1981]. Long-term observations on the occurrence pattern of scintillation near the magnetic equator in the Indian sector are necessary to resolve this question unequivocally.

*Acknowledgments.* We wish to thank J. A. Klobuchar for

providing the AFGL polarimeter, with which the observations were made. We are grateful to J. Aarons for helpful discussions and to Sunanda Basu for a careful reading of the manuscript. Thanks are also due to R. K. De for help in the observational program.

## REFERENCES

- Aarons, J., J. P. Mullen, H. E. Whitney, and E. M. MacKenzie (1980a), The dynamics of equatorial irregularity patch formation, motion, and decay, *J. Geophys. Res.*, **85**, 139.
- Aarons, J., J. P. Mullen, J. R. Koster, R. F. daSilva, J. R. Medeiros, R. T. Medeiros, A. Bushby, J. Pantoja, J. Lanat, and M. R. Paulson (1980b), Seasonal and geomagnetic control of equatorial scintillations in two longitude sectors, *J. Atmos. Terr. Phys.*, **42**, 861.
- Aarons, J., H. E. Whitney, E. MacKenzie, and S. Basu (1981), Microwave equatorial scintillation intensity during solar maximum, *Radio Sci.*, **16**, 939–945.
- Anderson, D. N., and G. Haerendel (1979), The motion of depleted plasma regions in the equatorial ionosphere, *J. Geophys. Res.*, **84**, 4251.
- Basu, S., and S. Basu (1981), Equatorial scintillations—A review, *J. Atmos. Terr. Phys.*, **43**, 473.
- Basu, S., and M. C. Kelley (1979), A review of recent observations of equatorial scintillations and their relationship to current theories of *F*-region irregularity generation, *Radio Sci.*, **14**, 471.
- Basu, S., J. P. McClure, S. Basu, W. B. Hanson, and J. Aarons (1980), Coordinated study of equatorial scintillation and in situ and radar observations of nighttime *F* region irregularities, *J. Geophys. Res.*, **85**, 5119.
- DasGupta, A., and A. Maitra (1980), Scintillation of VHF satellite signals near the edge of the equatorial irregularity belt, in *Advances in Space Exploration*, vol. 8, *Low Latitude Aeronomical Processes*, edited by A. P. Mitra, p. 209, Pergamon, New York.
- Eis, K. E., J. A. Klobuchar, and C. Malik (1977), On the installation, operation, data reduction and maintenance of VHF electronic polarimeters for total electron content measurements, *Rep. AFGL-TR-77-0130*, Air Force Geophys. Lab., Hanscom Air Force Base, Mass.
- Fejer, B. G., D. T. Farley, R. F. Woodman, and C. Calderon (1979), Dependence of equatorial *F* region vertical drifts on season and solar cycle, *J. Geophys. Res.*, **84**, 5792.
- Krishnamoorthy, K., C. R. Reddi, and B. V. Krishnamurthy (1979), Nighttime ionospheric scintillations at the magnetic equator, *J. Atmos. Terr. Phys.*, **41**, 123.
- Livingston, R. C. (1980), Comparison of multifrequency equatorial scintillation: American and Pacific sectors, *Radio Sci.*, **15**, 801.
- Scannapieco, A. J., and S. L. Ossakow (1976), Nonlinear equatorial spread *F*, *Geophys. Res. Lett.*, **3**, 451.
- Weber, E. J., J. Buchau, and J. G. Moore (1980), Airborne studies of equatorial *F* layer ionospheric irregularities, *J. Geophys. Res.*, **85**, 4631.
- Whitney, H. E., J. Aarons, and C. Malik (1969), A proposed index for measuring ionospheric scintillation, *Planet. Space Sci.*, **17**, 1069.
- Yeh, K. C., H. Soicher, and C. H. Liu (1979), Observations of equatorial ionospheric bubbles by the radio propagation method, *J. Geophys. Res.*, **84**, 6589.



# Generation of Kilometer Scale Irregularities During the Midnight Collapse at Arecibo

SUNANDA BASU AND SANTIMAY BASU

*Emmanuel College, Boston, Massachusetts 02115*

S. GANGULY

*Department of Space Physics, Rice University, Houston, Texas 77001*

J. A. KLOBUCHAR

*Air Force Geophysics Laboratory, Hanscom Air Force Base, Massachusetts 01731*

Coordinated observations of the incoherent scatter radar at Arecibo, Puerto Rico, and total electron content/scintillation measurements made by using the 137-MHz transmissions from the geostationary satellite SMS 1 from the nearby station of Ramey are studied to determine the background ionospheric conditions necessary for the generation of kilometer scale irregularities in the midlatitude ionosphere. It is found that the well-known midnight descent or collapse of the *F* region known to occur in this part of the world is sometimes associated with increases in the bottomside electron content, as well as large scintillation events ( $\sim 10$  dB). From a measurement of vector ion velocities and electron densities during such events, it is determined that the scintillations occur in a region of eastward and northward electric fields coupled with a northward directed density gradient caused by the northward propagation of the midnight collapse. The role of possible plasma instability mechanisms, specifically the  $E \times B$  gradient drift instability and the Perkins instability, is discussed in the formation of the kilometer scale irregularities giving rise to VHF scintillations.

## 1. INTRODUCTION

From the analysis of 16 months' transionospheric propagation data taken near Arecibo, it was found by Kersley *et al.* [1980] that there are associations between nighttime enhancements and quasi-periodic fluctuations in total electron content (TEC) and the occurrence of amplitude scintillations. In particular, they observed a postmidnight peak in the occurrence of electron content increases, maximum wave activity, and largest scintillation activity. The motivation for the current study stems from these findings. Similar observations have been reported from Japan [Sinno and Kan, 1978; Fujita *et al.*, 1978], where larger scintillation events were observed most probably because of the field-aligned nature of their propagation path.

The postmidnight time frame of the above occurrences tends to focus one's attention immediately on the so-called midnight collapse of the *F* region [Nelson and Cogger, 1971], which is known to take place at Arecibo ( $18^\circ\text{N}$ ,  $50^\circ$  dip) at that time. Nelson and Cogger [1971], using radar data, were the first to point out that the height of the *F* layer typically decreases by 50–100 km after midnight at Arecibo. By using data from a chain of ionosondes, they further pointed out that the collapse starts first at latitudes equatorward of Arecibo and progresses northward at the rate of  $7.5^\circ$  of latitude per hour. A similar study based on ionosonde data was also made by Wright [1971], who determined that the midnight descent is associated with a poleward neutral wind. Later, Behnke and Harper [1973] and Harper [1973] showed that the midnight collapse was due to an abatement, and sometimes to a reversal, of the equatorward meridional neutral wind.

In recent years there has been a spate of multitechnique observations at or near Arecibo that have provided more infor-

mation on this nighttime dynamical feature. Airglow observations at Arecibo by Sobral *et al.* [1978] and Herrero and Meriwether [1980] show a northward propagation of airglow enhancements associated with the midnight collapse. Propagation velocities of 350 m/s were obtained that are consistent with the estimates of Nelson and Cogger [1971]. Harper [1979] utilized a limited amount of incoherent scatter radar measurements of ion drift velocities to infer that the change in direction of wind velocities determined by Behnke and Harper [1973] and Harper [1973] formed part of a regular semidiurnal tidal oscillation in the meridional wind at *F* region heights. He suggested that the midnight collapse of the *F* region is due to the existence of these semidiurnal winds and interpreted Sobral *et al.*'s [1978] measurements of the northward propagation of airglow enhancements as being also related to the tidal origin of the collapse. It is interesting to note that as early as 1952, Mitra [1952] discussed the semidiurnal tidal origin of the midnight descent of the *F* region at low-latitude stations.

Evidence for the existence of a midnight pressure bulge at the equator [Hedin *et al.*, 1974; Walker, 1980] has come from in situ measurements, which could explain the midnight reversal of the meridional wind. The Atmosphere Explorer E (AE-E) satellite has clearly shown the existence of a midnight temperature maximum and the associated change in the wind direction [Spencer *et al.*, 1979]. Mayr *et al.* [1979] have presented a theoretical analysis that shows that the pressure bulge results from semidiurnal and higher order modes of the tidal field. The semidiurnal tide in the *F* region is the result of a tidal wave propagation upward from the lower atmosphere and a wave generated in situ by ion drag interaction between the dominant diurnal mode and the diurnally varying ion density. Strong cancellation between these two sources is responsible for the variability of the phenomenon.

While there is a wealth of information on the large-scale dynamics of the *F* region near Arecibo, information on kilo-

Copyright © 1981 by the American Geophysical Union.

Paper number 1A0825.  
0148-0227/81/0015-0760\$01.00

62

The U.S. Government is authorized to reproduce and sell this report. Permission for further reproduction by others must be obtained from the copyright owner.

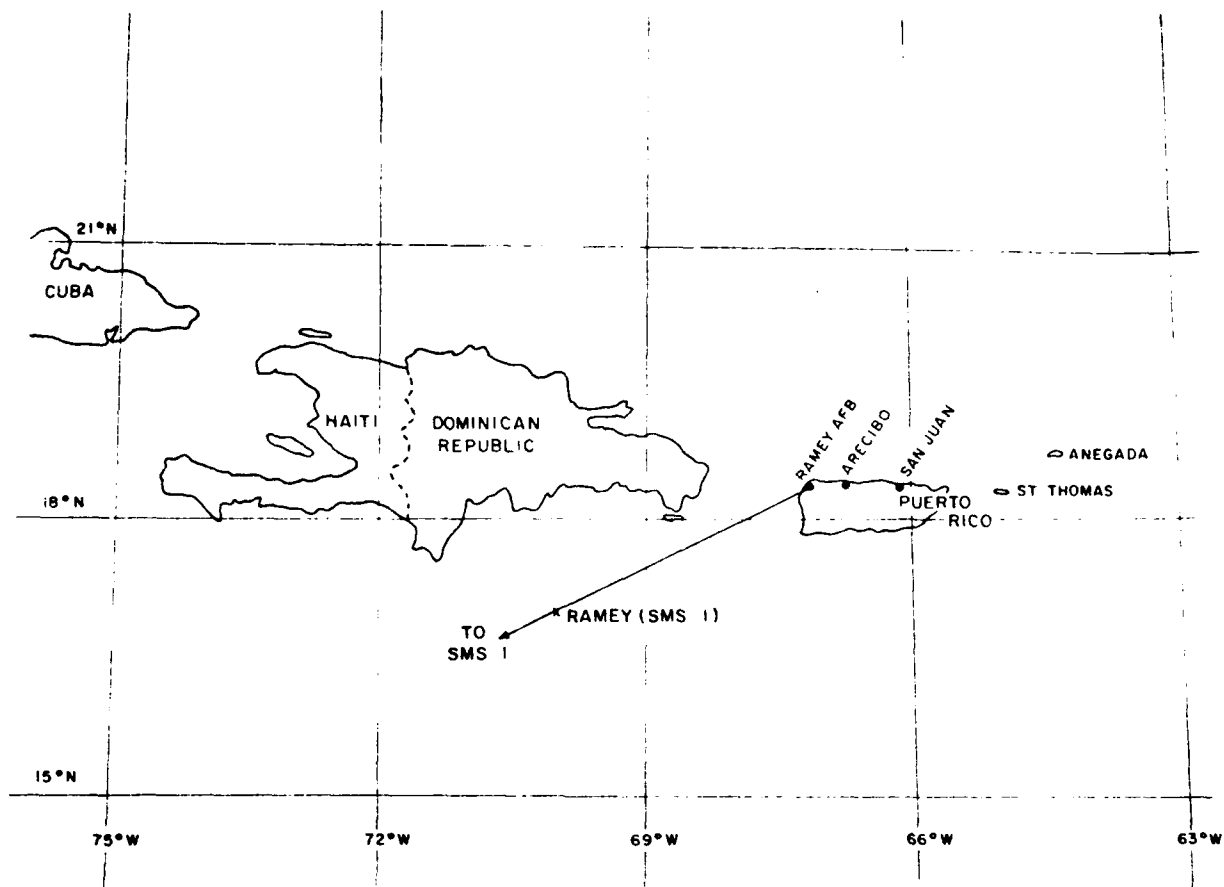


Fig. 1. Geometry of incoherent scatter radar at Arecibo and TEC/scintillation observations with SMS 1 from Ramey.

meter scale irregularities is quite sparse. Mathews and Harper [1972] made incoherent scatter radar observation of spread  $F$  producing ionospheric structures during the course of one night at Arecibo. They came to the conclusion that the main spread  $F$  event near midnight, during which the total electron content (obtained by integrating the radar profiles) increased considerably, was caused by tilts in the ionosphere. We will provide information that such spread  $F$  events are definitely associated with kilometer scale irregularities, as tilts alone cannot explain our coordinated scintillation measurements. Indirect evidence for the existence of plasma instabilities near Arecibo was provided by Behnke [1979], who found that sometimes the nocturnal  $F$  region over Arecibo has well defined bands where the  $F$  region as a whole is alternately high and low. He suggested that these bands are manifestations of the so-called Perkins instability [Perkins, 1973]. However, no actual information on the concomitant generation of small-scale irregularities was discussed in the paper.

The objective of the current investigation is to utilize radar measurements of electron densities and vector ion velocities in conjunction with TEC and VHF scintillation measurements by using a geostationary satellite to determine the background conditions necessary for the production of small-scale irregularities. The necessity for making such coordinated measurements was pointed out in the work of Basu [1978], in which she discussed how radar measurements could help identify specific instability mechanisms. The idea is to determine whether proper conditions exist in the nighttime ionosphere

near Arecibo for the growth of plasma instabilities that could explain the scintillation measurements.

## 2. OBSERVATION

The geometry of these coordinated measurements is given in Figure 1. A polarimeter at 137 MHz [Eis *et al.*, 1977] to record the Faraday rotation of the plane of polarization of signals from geostationary satellites was operated by the Global Air Weather Service at Ramey (18.5°N, 67.1°W). The satellite being observed was SMS 1, located at 105°W. On a routine basis, the magnetic field factor at a fixed altitude of 420 km was used to convert the Faraday rotation angle into TEC. It has been shown that under most conditions this yields the content up to an altitude of 2000 km with an accuracy of  $\pm 5\%$  [Titheridge, 1972]. The scintillation index was computed in decibels by following the method of Whitney *et al.* [1969]. The 350-km subionospheric point pertaining to these measurements is at 17.3°N, 70.2°W, giving rise to north-south and east-west separation of approximately 100 km and 300 km, respectively, from Arecibo, where the incoherent scatter measurements were made.

Observations made with the Arecibo incoherent scatter radar on three nights will be discussed in this initial report. During these nights, ion velocity measurements were conducted in the  $F$  region by pointing the Arecibo antenna beam at an angle of 15° to the zenith and rotating it to three azimuth positions in a manner similar to that discussed by Behnke and Harper [1973]. More details on the measurement technique

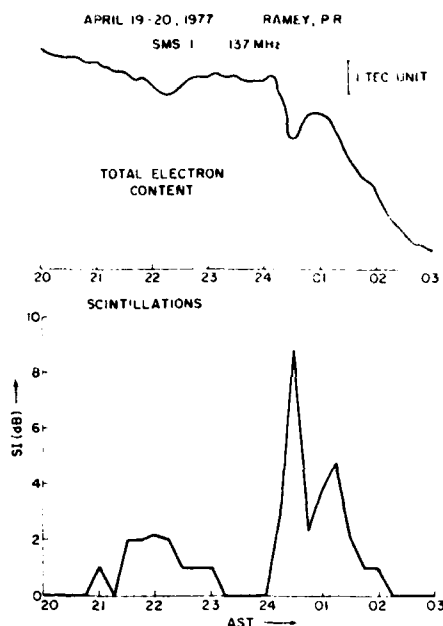


Fig. 2. TEC and scintillation measurements at 137 MHz on April 19-20, 1977.

are available in a manual by Harper and Ganguly [1977]. Together with the ion velocity measurements obtained with a height resolution of 35 km and time resolution of 45 min, electron density profiles were measured with a height resolution of 3.6 km and a time resolution of approximately 15 min.

### 3. RESULTS

#### a. Data of April 19-20, 1977

Coordinated TEC/scintillation observations at Ramey and incoherent scatter observations at Arecibo were available for April 19-20, 1977. The relative variation of Ramey TEC ob-

tained in the routine manner indicated in section 2 and scintillation index in decibels observed that night are shown in Figure 2 as a function of Atlantic Standard Time (AST). It should be noted that a change of 1 TEC unit represents a change of  $10^{16} \text{ el m}^{-2}$  in a vertical column. The fall in the TEC after sunset is interrupted at 2200 AST by a wavelike perturbation. At 2400 AST a rapid drop in TEC is observed, which is followed by an increase at 0100. We shall show later that most of the increase in TEC is apparent and is caused by the midnight collapse of the F region. The scintillation activity is weak, less than 2 dB between 2100 and 2300 AST. The Arecibo ionograms for the night show large sporadic E activity with  $f_s E$ , reaching as high as 6 MHz at 1945 AST. The weak scintillations seem to be associated with the transition in the E character from blanketing to nonblanketing at frequencies above 2.5 MHz. Our major interest, however, is the relatively large amplitude fluctuation of 9 dB found to occur in the postmidnight phase in association with the gradients in TEC as monitored by the Faraday rotation technique. At this time Arecibo ionograms show well developed frequency-type midlatitude spread F.

To compare the TEC behavior at Ramey with the radar measurements at Arecibo, we show in Figure 3 the equidensity contours obtained from incoherent scatter density measurements at 15-min intervals. Wavelike perturbations similar to those observed in TEC data are seen in the 2200-2400 local time period, followed by a precipitous drop in  $h_m$  commencing shortly after midnight that is identified with the collapse of the F region. The marked descent of the F layer and the decrease of its thickness is reproduced as the steep gradient in the Ramey TEC data at midnight. The large scintillation event observed on this night seems to be related to this steep gradient. The apparent postmidnight TEC increase associated with the clear enhancement in peak density is a result of the collapse, as will be shown later.

A comparison is made in Figure 4 between the TEC measurements obtained by the polarimeter at Ramey and the con-

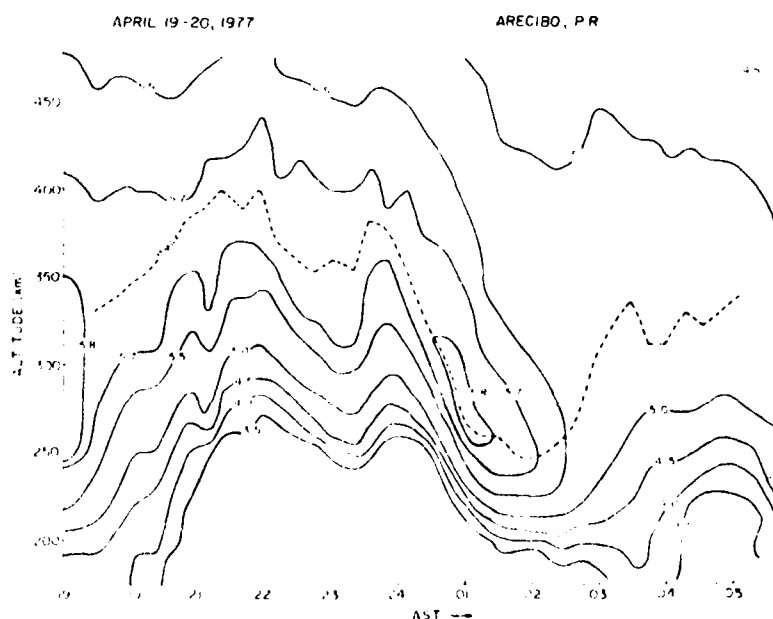


Fig. 3. Electron density contours obtained by incoherent scatter radar observations on April 19-20, 1977.

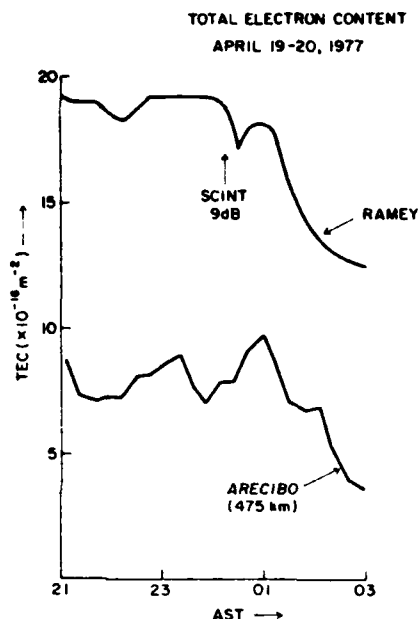


Fig. 4. A comparison of TEC obtained by the numerical integration of electron density contours shown in Figure 3 with that obtained by the polarimeter technique with a constant magnetic field factor at Ramey on April 19-20, 1977.

tent obtained by integrating the electron density profiles up to 475 km. The Ramey TEC is computed every 15 min on an absolute scale (as opposed to the 5-min time resolution plot of relative change of TEC shown in Figure 2) to make the temporal resolution compatible with the Arecibo profiles, which are obtained with a 15-min time resolution. In the pre-midnight hours there may be some suggestion of an equatorward wave propagation as observed by Kersley *et al.* [1980], since the TEC perturbations seem to start earlier at Arecibo. This is more clearly observed on the night of November 16-17, 1976, which we will discuss later. However, the midnight collapse and the resultant TEC increase seem to occur simultaneously within the accuracy of the measurements. The north-south separation of the two stations is only 100 km, and if the poleward propagation of the midnight descent is of the order of 350 m/s as determined by Sobral *et al.* [1978], then only a 5-min delay is expected at Arecibo, which would be impossible to detect with a 15-min averaging process.

The interesting aspect of these observations is the increase in the integrated electron densities up to 475 km as a result of the midnight descent of the *F* region. At first glance, one would expect that in the absence of production, a decrease of density should result from the downward motion of the *F* layer, which carries the ionization into regions of higher loss. To study this point further, we show in Figure 5 the temporal variation of the vertical velocity  $V_z$ , measured by the radar at different altitudes. The approximate uncertainty in  $V_z$  is of the order of 5 m/s as indicated in our diagram (Figure 5) [Harper and Ganguly, 1977]. It is apparent that the plasma at higher altitudes in the postmidnight period is descending at a faster rate than the plasma at lower altitudes, with the result that the plasma tends to pile up in the region of the peak and below it [Mahajan and Saxena, 1976]. In the following paragraph, we shall attempt to show that the increase of TEC implied by the polarimeter is merely a result of the plasma pileup at lower altitudes caused by the collapse.

It may be recalled that the Faraday rotation  $\Omega$  in radians for a one-way passage through the ionosphere is given in mks units by

$$\Omega = \frac{2.36 \times 10^4}{f^2} \int_0^\infty (B \cos \theta \sec \chi) N dh \quad (1)$$

where  $B$  is the local magnetic flux density (in  $\text{Wb m}^{-2}$ ),  $\theta$  is the angle between radio wave normal and magnetic field direction, and  $\chi$  is the angle between wave normal and vertical [Rishbeth and Garriott, 1969]. Conventionally, the magnetic field factor is evaluated at a fixed altitude and taken outside the integral for the determination of TEC. As was mentioned earlier, Titheridge [1972] has shown that the use of a fixed altitude of 420 km yields, for most purposes, the TEC up to 2000 km with an error of  $\pm 5\%$ . By using the fixed altitude of 420 km, the increase in TEC shown in Figure 4 between 0030 and 0100 is 1 TEC unit, which is approximately a 5% increase. In Figure 6 the plot of magnetic field factor  $B \cos \theta \sec \chi$  against altitude is shown for the Ramey station when observing in the direction of SMS 1 at  $105^\circ\text{W}$ . The figure indicates that the field factor increases by 5% per 100-km decrease in the altitude of the centroid of ionization distribution. Between 0030 and 0100 AST, the height of the *F* region maximum decreases from 325 km to 250 km. If the shape of the ionization distribution remains unaltered during this period, the centroid of ionization distribution will be depressed in altitude by the same amount as the *F* region maximum, namely 75 km, which will account for a 4% increase in the value of the field factor. As a result, the TEC increase of 5% derived under the assumption of a constant height of 420 km for the centroid is reduced to

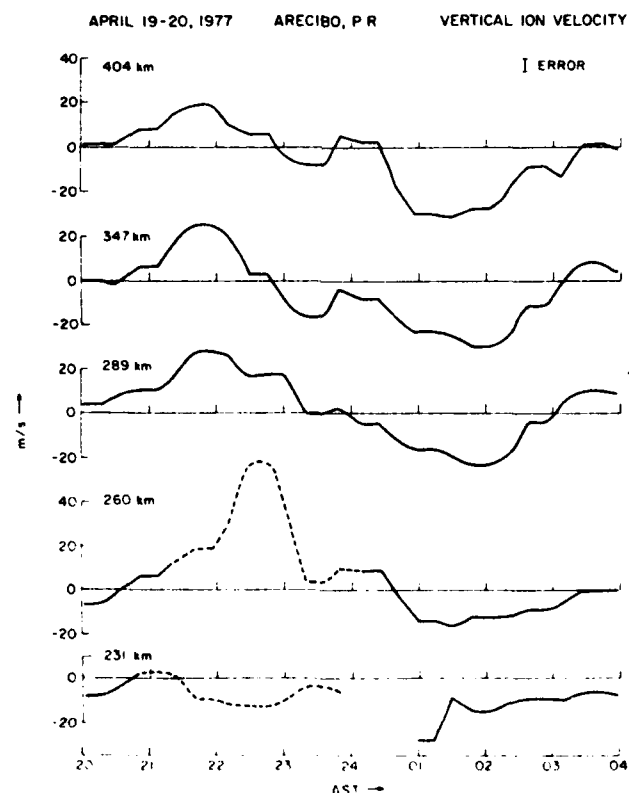


Fig. 5. Variation of vertical ion velocities with altitude at Arecibo on April 19-20, 1977. Dotted lines indicate signal-to-noise ratio  $< 2$ .

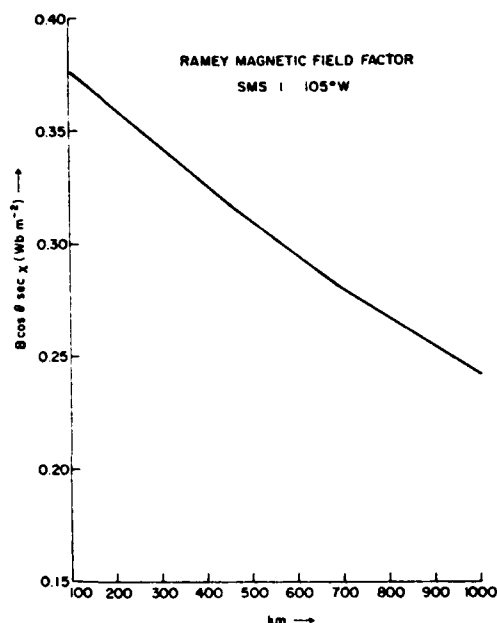


Fig. 6. The variation of the magnetic field factor  $B \cos \theta \sec \chi$  with altitude for Ramey when viewing SMS 1 at  $105^\circ\text{W}$ .

only 1% when its height variation is considered. In this context, we note that the increase in the integrated density to 475 km as obtained from the radar observations implies that there is a redistribution of plasma during this period of time rather than an actual increase in the integrated content up to 2000 km.

By determining the net difference between the quantity  $\text{TEC}_{\text{Ramey}} - \text{TEC}_{\text{Arecibo}}$  (after correcting the Ramey TEC for height changes as discussed above) at two specific times, for instance 0030 and 0100, it is possible to compute the vertical flux into the ionosphere at an altitude of 475 km. By using this procedure, one obtains  $7 \times 10^{12} \text{ m}^{-2} \text{ s}^{-1}$  for the flux into the ionosphere during the period 0030–0100 AST. This flux is the product of the density at 475 km and the vertical velocity  $V_z$  at the same altitude. Since the measured density at 475 km is  $10^{11} \text{ m}^{-3}$  (cf. Figure 3), we obtain for  $V_z$  at 475 km a value of  $70 \text{ m s}^{-1}$ , which is about a factor of 2 higher than the radar measurements of  $V_z$  at 475 km at the same time. Considering the 100 km north-south separation of the TEC measurements

and the Arecibo radar, this agreement is fairly good. The TEC related computations are presented to provide the reader with a better understanding of the large-scale changes taking place in the ionosphere during the collapse and are not directly related to the generation of kilometer scale irregularities.

We shall next discuss the behavior of the ion velocity components around midnight, investigate their origin, and determine their special characteristics in relation to the generation of kilometer scale irregularities. The Arecibo ion velocity components parallel and perpendicular to the magnetic field in the  $F$  region obtained on April 19–20 are shown in Figure 7, the uncertainties in the measurements ( $\sim 20 \text{ m/s}$ ) being shown in our diagram [Harper and Ganguly, 1977]. The velocities at any particular time are those obtained by averaging over five or six of the individual altitude measurements at intervals of approximately 30 km between 200-km and 490-km altitude. Only those measurements with the best signal-to-noise ratios were chosen. The velocities then are not at constant altitude but tend to follow the  $F$  layer peak. Two large fluctuations are seen between 2300 and 0100 hours when  $V_{\parallel}$ , the component of ion velocity parallel to the magnetic field, and  $V_{\perp}$  are seen to be anticorrelated and in opposite directions. Polarization electric fields give rise to such anticorrelated velocities as discussed by Behnke and Hagfors [1974]. A comparison of Figures 3 and 7 shows that the positive phase of  $V_{\parallel}$  between 2300 and 2400 LT is associated with an upward movement of  $h_m$ , while the negative phase is associated with the rapid downward movement as is to be expected. Vasseur [1969] and Rishbeth [1970] have shown that  $V_{\parallel}$  is the sum of a plasma diffusion term  $V_d$  and a neutral wind term  $V_n$ . Taking upward velocities as positive

$$V_{\parallel} = V_d + V_n = V_d + U \cos I \quad (2)$$

where  $U$  is the horizontal wind speed in the magnetic meridian (positive equatorward) and  $I$  is the dip angle ( $50^\circ$  for Arecibo). Rishbeth [1970] has further shown that for a large downward drift, the diffusion velocity is small and  $V_{\parallel} \sim V_n$ . At 0100 AST,  $V_{\parallel}$  in Figure 7 is  $-45 \text{ m s}^{-1}$ . Thus at this time the poleward wind  $U$  is of the order of  $60 \text{ m s}^{-1}$ , which is probably an upper limit because we have neglected  $V_d$ .

We draw special attention to the fact that  $V_{\perp}$  changes from a southward to northward direction near midnight. In addition, we have shown that a steep density gradient is generated during the midnight collapse. As was mentioned earlier, the Ramey station detected a sudden onset of scintillations at this time. To determine the total electric field configuration during the scintillation event, we present the zonal component of the ion drift  $V_{Ez}$  in Figure 8. In the midlatitude  $F$  region this is caused by a north-south electric field. The southward electric field, giving rise to an eastward drift, changes sign just prior to midnight, when a westward drift is seen. This is a fairly regular occurrence in all seasons at Arecibo [Fukao et al., 1979; Ganguly et al., 1981]. The magnitude of the westward drift is somewhat larger than usual and is probably related to the magnetically disturbed conditions prevailing on the night of April 19–20. Combining Figures 7 and 8, we find that at midnight the ion drift has westward and northward field-perpendicular components that are equivalent to northward and eastward electric fields, respectively.

In summary, then, the midnight collapse observed at Arecibo is probably related to a northward neutral wind. We have also shown that under the conditions favorable for the development of a polarization electric field, the neutral wind can give

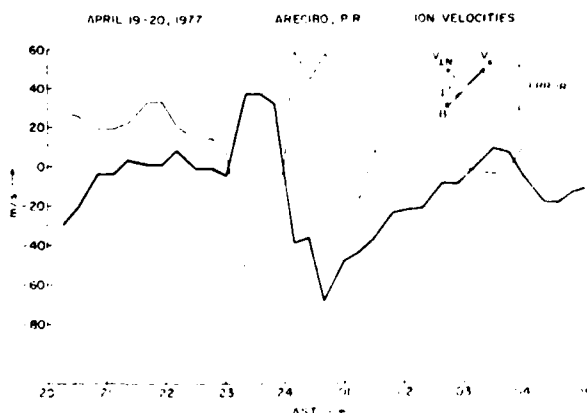


Fig. 7. Ion velocity parallel and perpendicular to the magnetic field observed at Arecibo on April 19–20, 1977.

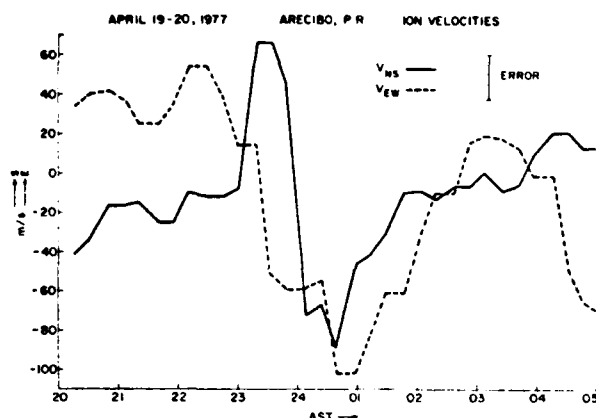


Fig. 8. The north-south and east-west components of ion velocity at Arecibo on April 19-20, 1977.

rise to anticorrelated  $V_{||}$  and  $V_{\perp}$ , as shown in Figure 7. During the collapse, the plasma drift in the vertically downward direction increases with altitude, so that plasma pileup occurs in the bottomside ionosphere resulting in an increase of the bottomside electron content. Scintillations are observed in conjunction with the midnight collapse in an environment of a steep density gradient and northward and westward field-perpendicular ion velocities.

#### b. Data of November 16-17, 1976

A similar set of measurements as those discussed above was available for the night of November 16-17, 1976. The Ramey TEC behavior shown in Figure 9 has a smaller increase of approximately one-half of a TEC unit centered at 2200 AST and another larger increase of 1 TEC unit centered at 0300 AST. The TEC behavior is very similar to the average December 1976 picture shown in Figure 6 of Kersley *et al.* [1980]. As was discussed previously for the April 19-20 event, this apparent postmidnight TEC increase observed by Kersley *et al.* [1980], as well as in Figure 9, is obtained as a result of the midnight collapse and the associated plasma pileup at low altitudes, as determined from the radar measurements shown in Figure 10. A moderately large scintillation event of 6-dB peak-to-peak fluctuation was observed at 0200 hours in conjunction with the collapse-generated gradient. On comparison with the maximum density measured by the Arecibo radar in Figure 10, it is evident that both TEC increases obtained with a constant mean field factor have clear, unambiguous counterparts in  $N_m$ . While the first increase occurs at the earlier time of 2120 AST at Arecibo, the second, larger increase is centered at 0300 AST, the time of a similar increase at Ramey. Thus considering the geometry of these observations shown in Figure 1, one obtains the signature of an equatorward propagating wave in the premidnight hours, the velocity of propagation being only about 50 m/s if the direction is due north-south. As on the night of April 19-20, 1977, it is not possible to determine the delay in the larger postmidnight increase at the two stations, which, according to  $h_m$  behavior, is obviously due to the midnight collapse.

The ion velocities in the meridional plane on the night of November 16-17 show a more complicated behavior than that observed on April 19-20, with several large-scale oscillations being evident in Figure 11. It is interesting to note that scintillations are associated with the second oscillation for which  $V_{\perp N}$  is positive (after 0100 AST), a situation that we found

was necessary for small-scale irregularity generation on the night of April 19-20. However, when Figures 10 and 11 are combined, then it becomes evident that the first positive oscillation of  $V_{\perp N}$  after midnight does not have any density gradient associated with it, while the second such oscillation has the collapse-associated density gradient occurring simultaneously. The east-west drift pattern on this date has not been shown. However, it is found that the drifts reversed from eastward to westward near midnight, so that the scintillation event was also associated with a northward electric field similar to the situation prevailing on April 19-20.

#### c. Data of March 16-17, 1977

Finally, we shall present the correlated observations of TEC/SI and radar velocity measurements on a night when no small-scale irregularities were observed near Arecibo. Figure 12 shows the TEC behavior with the usual sunset decay observed beyond 1800 AST and no major wavelike perturbations or steep gradients being present throughout the night. No scintillations were recorded. The  $F$  region peak density and height measurements made by the Arecibo radar that night are shown in Figure 13. The features to note are the delayed midnight collapse at 0200 AST and the rather gentle nature of the collapse with  $h_m$  falling 100 km in 3 hours, followed by a very weak  $N_m$  increase near 0400. The gentle nature of the collapse leaves a barely recognizable signature on the TEC measurements in the form of the small increase near 0400, in contrast to that shown in Figures 2 and 9, where the faster plasma pileup led to much more prominent increase of  $N_m$  and sharper associated gradients. The ion drift velocities  $V_{||}$  and  $V_{\perp N}$  for the night are shown in Figure 14. The  $V_{\perp N}$  is weakly negative up to 0300 AST, beyond which the direction changes over to being slightly positive. Thus on this night no predominant northward drifts (i.e., eastward electric field) or appreciable density gradients were observed near Arecibo in conjunction with the midnight collapse, as was the case on the other nights discussed earlier.

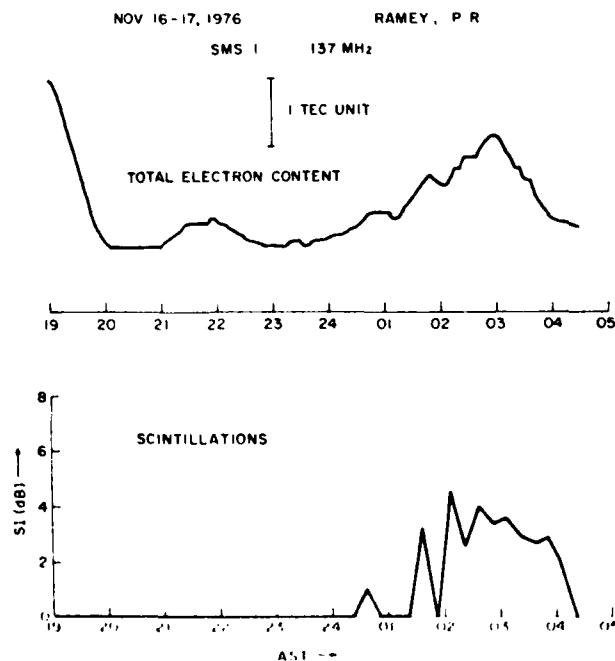


Fig. 9. Same as in Figure 2 for November 16-17, 1976

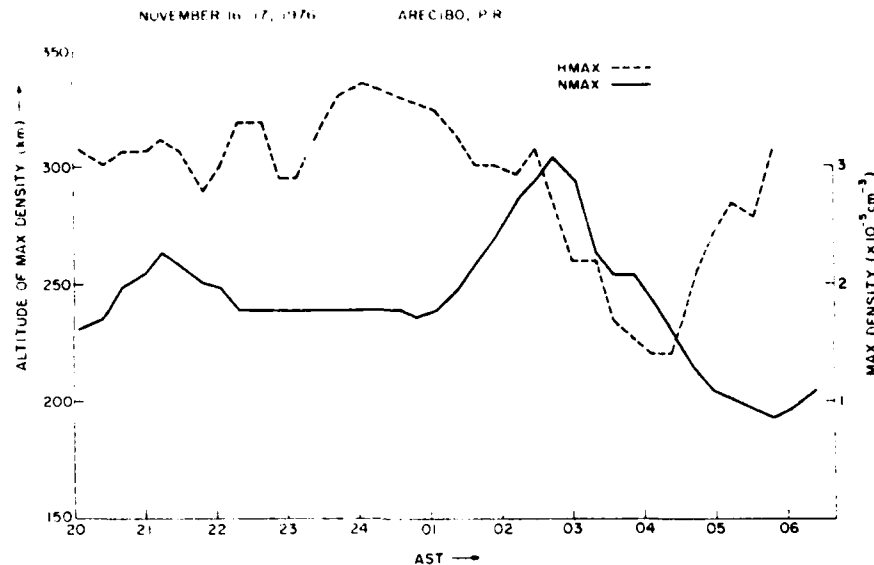


Fig. 10. Variation of  $H_{\max}$  and  $N_{\max}$  deduced from Arecibo incoherent scatter radar measurements on November 16-17, 1976.

#### 4. DISCUSSION

The coordinated radar and TEC/scintillation measurements on the basis of the limited data set available have shown the association of the kilometer scale irregularities with the existence of a northward component of the ion drift and a moderately sharp density gradient in the  $F$  region. The northward component of the ion drift is, of course, due to an eastward electric field in the  $F$  region. Ganguly *et al.* [1981] have provided evidence for the origin of this electric field. For instance, following the arguments for a polarization electric field in the  $F$  region given by Rishbeth [1971], they show that the temporal variation of  $V_{\perp N}$  as measured at Arecibo is well approximated by the temporal variation of  $N_m U_N \sin I$ , where  $N_m$  is the maximum density of the  $F$  region and  $U_N \sin I$  is the field perpendicular component of the northward neutral wind  $U_N$ ,  $I$  being the magnetic dip. Now the product  $N_m U_N$  is the most likely candidate that will cause temporal variations in the field perpendicular ion current, which is generated by the polarization electric field. According to Ganguly *et al.* [1981], since the temporal variation of  $V_{\perp N}$  closely follows the north-

ward neutral wind variation, the polarization field in the  $F$  region would have to be the dominant cause of nighttime electric fields near Arecibo. These polarization electric fields can be maintained because the conducting  $E$  layer is separated from the  $F$  layer by the low-density valley region, which acts as a resistive medium [Klevans and Imel, 1978]. If, on the other hand, the penetration of the magnetospheric electric field is responsible for the eastward electric field observed, then a delay of several hours is expected in the response of the neutral wind because the ion drag time constant in the  $F$  region is a few hours at night [Rishbeth *et al.*, 1978].

Given the association of the small-scale irregularities with drifts and gradients, the  $E \times B$  gradient drift instability [Reid, 1968] would seem to be a strong candidate. For this instability to be operative, one would require a density gradient that is parallel to the ion drift. This drift is found to be northward during the scintillation events. The horizontal density gradient, we have seen, is caused by the midnight collapse. Though our own two closely spaced stations could not detect any northward propagation of the collapse, the airglow measurements of Sobral *et al.* [1978] and Herrero and Meriwether

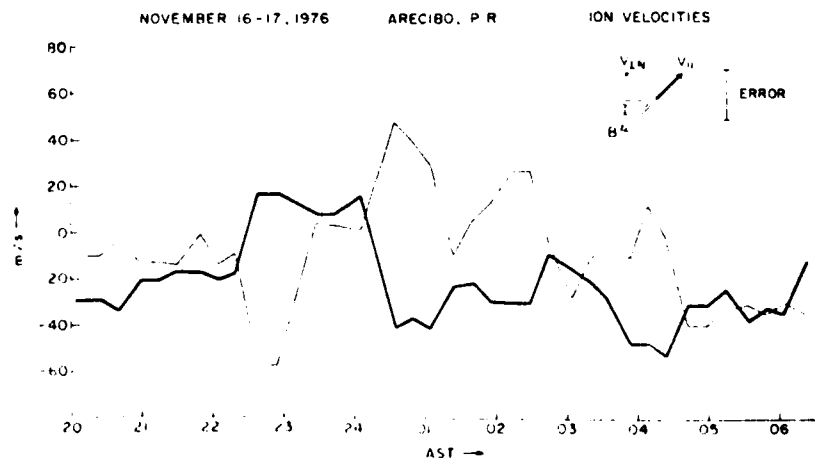


Fig. 11. Same as in Figure 7 for November 16-17, 1976.

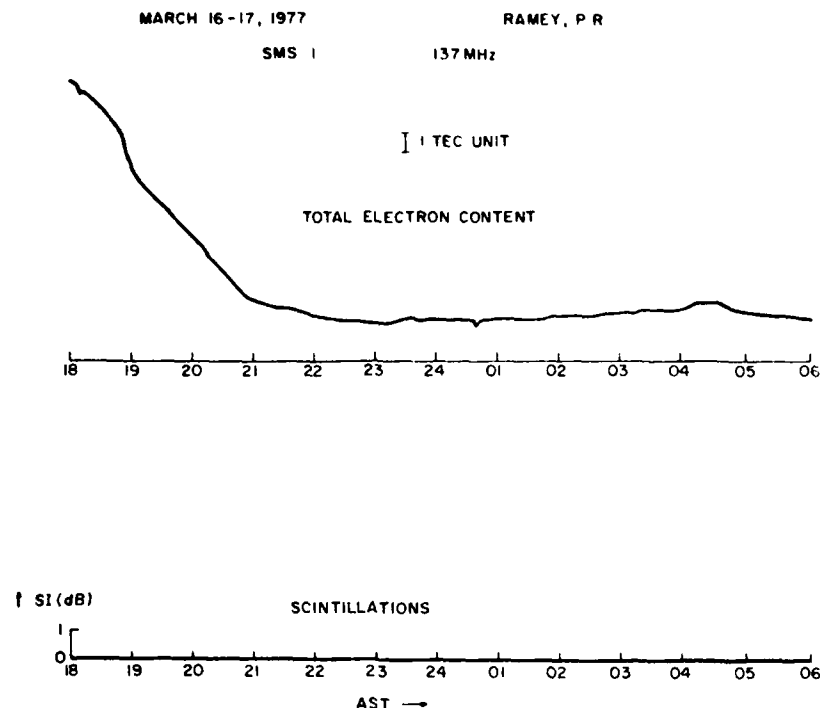


Fig. 12. Same as in Figure 2 for March 16-17, 1977.

[1980] covering a much larger area have conclusively proved that the collapse moves from south to north. We believe that this northward propagating collapse generates a northward directed density gradient, thus fulfilling the requirements of the gradient drift instability. What kind of growth times are to be expected? *Linson and Workman* [1970] have shown that in the *F* region the expression for the typical growth time of the instability, which is independent of the wavelength, is simply given by  $d/V_{\perp}$ , where  $d$  is the gradient scale length and  $V_{\perp}$  is the ion drift in the same direction. From the radar measurements we find that just prior to the onset of irregularities, the field-perpendicular gradient scale is on the order of 50 km near the *F* peak in the bottomside. This figure is obtained by converting the temporal variation of the ion densities at the same altitude to a spatial variation by considering the ion velocity, which is  $60 \text{ m s}^{-1}$  in a field perpendicular direction

(corresponding to an eastward electric field of  $2.2 \text{ mV m}^{-1}$ ). Thus the growth time becomes on the order of 15 min.

The velocity measurements, as pointed out in section 2, are obtained with a time resolution of 45 min. *Behnke* [1979], on the other hand, determined much larger ion drifts with a continuously rotating antenna mode developed earlier by *Hagfors and Behnke* [1974] and a time averaging of only 15 s. He obtained drifts as large as  $175 \text{ m s}^{-1}$  and  $470 \text{ m s}^{-1}$  corresponding to eastward electric fields of  $6.5 \text{ mV m}^{-1}$  and  $17.2 \text{ mV m}^{-1}$ , respectively. We have also found occasional evidence of large northward ion drifts in ion drift meter data from the AE-E satellite (data courtesy of W. B. Hanson and J. P. McClure) near the location of Arecibo in the postmidnight hours, which we plan to discuss in a forthcoming paper. Ion drifts of the order of  $250 \text{ m s}^{-1}$  were measured with an averaging over 3 s of data. If a value of  $250 \text{ m s}^{-1}$  is used for the drift, then the

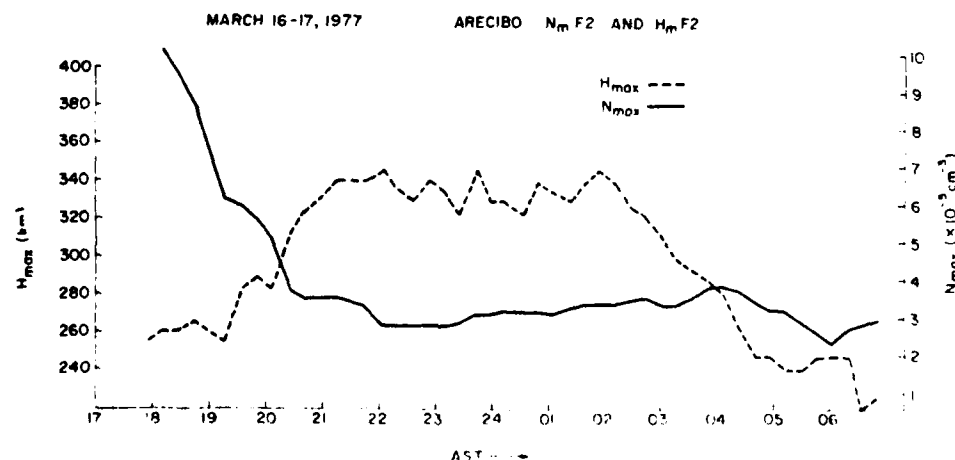


Fig. 13. Same as in Figure 10 for March 16-17, 1977.



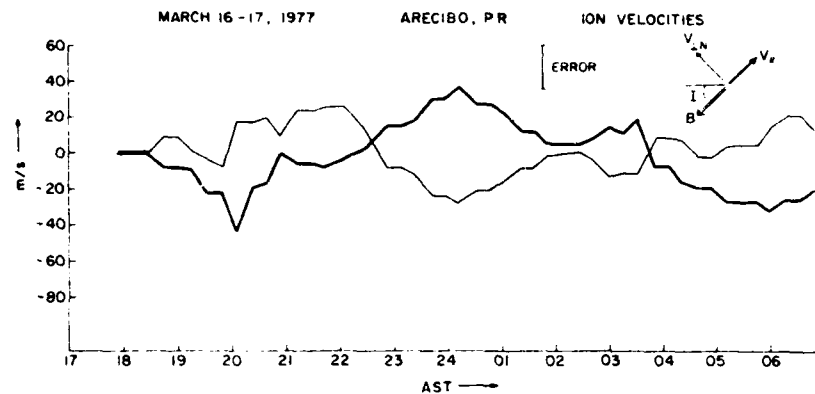


Fig. 14. Same as in Figure 7 for March 16-17, 1977.

growth time may be shortened to approximately 3 min, which is probably more consistent with the rather abrupt onset of scintillations.

A further discussion of the configuration of the electric fields during scintillation events is necessary to determine whether the so-called Perkins instability [Perkins, 1973] can be invoked to explain our measurements. It may be recalled that this instability was invoked by Behnke [1979] for an explanation of his observations at Arecibo. Perkins showed that the commonly observed equilibrium in which the nighttime  $F$  layer is supported by  $E \times B$  drifts is unstable if, in addition to the supporting eastward electric field, a northward component of the electric field exists. Further, in Perkins' derivation of the linear growth rate an equilibrium was taken where both the field line integrated Pedersen conductivity and field line integrated ion number density were assumed to have no horizontal gradients. As pointed out in section 3, the scintillation events on both April 19-20, 1977, and November 16-17, 1976, were observed during a period of eastward and northward electric fields in the ionosphere, in keeping with the necessary conditions for the Perkins instability. However, we have also determined that besides the above electric field configuration, a zero-order horizontal density gradient is essential for the generation of kilometer scale irregularities.

More suitable for comparison with the present set of observations is, therefore, the modification of the Perkins mechanism suggested by Scannapieco *et al.* [1975]. This model starts with the same dynamical equations developed by Perkins but assumes an initial equilibrium that has a long wavelength variation of the integrated Pedersen conductivity in the eastward direction. Thus this mechanism is of the  $E \times B$  type. It is also more suitable for comparison with data, as the authors follow the evolution of the instability into the nonlinear regime. The authors show that the perturbations (about the above equilibrium) whose wave vectors are in the north-south direction will grow, provided the north-south electric field is large enough, and give rise to irregularity structures in the nonlinear state that are sheetlike and more aligned in the east-west direction. These authors, as well as S. L. Ossakow (private communication, 1980) further claim that a long wavelength variation in conductivity in the north-south direction (such as we see in the present situation) will act equally well, provided the east-west field is large enough, giving rise to structures with alignment more in the north-south direction.

The important point to note from their numerical simulation (done for a station with a dip of  $45^\circ$ , nearly equal to that

of Arecibo) is the growth of smaller scale structures ( $\sim 1$  km) at late times ( $\sim 5$  min) from their initial large-scale structures (approximately tens of kilometers). This shows that there is a cascading of energy from long wavelength modes to shorter wavelength modes, as well as the development of axially asymmetric irregularity structures. While our scintillation data are consistent with the simulation growth times, unfortunately, our one station geostationary satellite measurements are unable to shed further light on irregularity orientation, and spaced receiver measurements of scintillations are necessary to test this important prediction. Thus on the whole, our current set of observations tends to favor the  $E \times B$  type instability over the Perkins instability for an explanation of the kilometer scale irregularities at midlatitudes.

As a further point of interest, we wish to emphasize that the midnight collapse takes place even on nights when no scintillations are observed. Indeed, vertical velocity data for the night of March 16-17, 1977 (when no kilometer scale irregularities were observed, as shown in Figure 11) were used by Harper [1979] to prove the tidal origin of the collapse. It seems that the rate of collapse that effectively controls the magnitude of the gradient and the simultaneous presence of northward directed ion drifts are important factors. This also explains the relatively sparse occurrence of large scintillation events, although Nelson and Cogger [1971] determined that the collapse occurs during 80% of the nights at Arecibo.

These large but sporadic scintillation events are observed on geomagnetically quiet as well as on disturbed nights. The night of April 19-20 was disturbed and the other two nights discussed were quiet. While it is true that in this instance the magnetically disturbed night showed the largest activity, we have seen many other cases of large scintillation events on quiet nights. Unfortunately, radar data are not available for those nights. It is also necessary to assess the role of waves in sharpening the gradients associated with the midnight collapse. Further coordinated observations of radar, TEC, scintillation, airglow, and AE-E in situ measurements are planned to study in depth the complex interrelationships of winds and waves, drifts and gradients in the creation of plasma instabilities in the midlatitude ionosphere.

**Acknowledgments.** We wish to thank J. Aarons for his interest and encouragement. The vector velocity measurements at Arecibo were conducted with the help of R. M. Harper. The first two authors acknowledge the assistance of H. D. Craft and the staff of the Arecibo Observatory and thank J. C. G. Walker and H. Rishbeth for useful discussions. The work at Emmanuel College was supported partially

by National Science Foundation grant ATM 78-25264. The National Astronomy and Ionosphere Center is operated by Cornell University under contract with the National Science Foundation.

The Editor thanks R. A. Behnke and R. T. Tsunoda for their assistance in evaluating this paper.

# REFERENCES

- Basu, S., OGO 6 observations of small-scale irregularity structures associated with subtrough density gradients, *J. Geophys. Res.*, **83**, 182, 1978.
- Behnke, R., *F* layer height bands in the nocturnal ionosphere over Arecibo, *J. Geophys. Res.*, **84**, 974, 1979.
- Behnke, R. A., and T. Hagfors, Evidence for the existence of nighttime *F* region polarization fields at Arecibo, *Radio Sci.*, **9**, 211, 1974.
- Behnke, R. A., and R. M. Harper, Vector measurements of *F* region ion transport at Arecibo, *J. Geophys. Res.*, **78**, 8222, 1973.
- Eis, K. E., J. A. Klobuchar, and C. Malik, On the installation, operation, data reduction, and maintenance of VHF electronic polarimeters for total electron content measurements, *Tech. Rep. AFGL-TR-77-0130*, Air Force Geophys. Lab., Hanscom Air Force Base, Mass., 1977.
- Fujita, M., T. Ogawa, and K. Koike, 1.7 GHz scintillation measurements at midlatitude using geostationary satellite beacon, *J. Atmos. Terr. Phys.*, **40**, 963, 1978.
- Fukao, S., T. Sato, I. Kimura, and R. M. Harper, Seasonal mean structure of the nighttime *F2* region over Arecibo, *J. Atmos. Terr. Phys.*, **41**, 1205, 1979.
- Ganguly, S., R. Behnke, and B. A. Emery, Electric fields in the *F* region at Arecibo, submitted to *J. Geophys. Res.*, 1981.
- Hagfors, T., and R. Behnke, Measurements of three-dimensional plasma velocities at the Arecibo Observatory, *Radio Sci.*, **9**, 89, 1974.
- Harper, R. M., Nighttime meridional neutral winds near 350 km at low to mid-latitudes, *J. Atmos. Terr. Phys.*, **35**, 2023, 1973.
- Harper, R. M., A semidiurnal tide in the meridional wind at *F* region heights at low latitudes, *J. Geophys. Res.*, **84**, 411, 1979.
- Harper, R. M., and S. Ganguly, Description of the 19/129 Arecibo data, *Technical Manual*, Arecibo Observatory, Arecibo, Puerto Rico, 1977.
- Hedin, A. E., H. G. Mayr, C. A. Reber, N. W. Spencer, and G. R. Carignan, Empirical model of global thermospheric temperature and composition based on data from the OGO 6 quadrupole mass spectrometer, *J. Geophys. Res.*, **79**, 215, 1974.
- Herrero, F. A., and J. W. Meriwether, Jr., 6300-Å airglow meridional intensity gradients, *J. Geophys. Res.*, **85**, 4191, 1980.
- Kersley, L., J. Aarons, and J. A. Klobuchar, Nighttime enhancements in total electron content near Arecibo and their association with VHF scintillations, *J. Geophys. Res.*, **85**, 4214, 1980.
- Klevans, E. H., and G. Imel, *E* region coupling effects on the Perkins spread *F* instability, *J. Geophys. Res.*, **83**, 199, 1978.
- Linson, L. M., and J. B. Workman, Formation of striations in ionospheric plasma clouds, *J. Geophys. Res.*, **75**, 3211, 1970.
- Mahajan, K. K., and O. P. Saxena, Continuous measurements of nighttime electron concentration profiles and estimation of neutral wind velocities at Arecibo, *J. Geophys. Res.*, **81**, 3165, 1976.
- Mathews, J. D., and R. M. Harper, Incoherent scatter radar observations of spread *F* producing ionospheric structures at Arecibo, *J. Atmos. Terr. Phys.*, **34**, 1119, 1972.
- Mayr, H. G., J. Harris, N. W. Spencer, A. E. Hedin, L. E. Wharton, H. S. Porter, J. C. G. Walker, and H. C. Carlson, Jr., Tides and the midnight temperature anomaly in the thermosphere, *Geophys. Res. Lett.*, **6**, 447, 1979.
- Mitra, S. K., *The Upper Atmosphere*, p. 339, The Asiatic Society, Calcutta, 1952.
- Nelson, G., and L. L. Cogger, Dynamical behavior of the nighttime ionosphere at Arecibo, *J. Atmos. Terr. Phys.*, **33**, 1711, 1971.
- Perkins, F., Spread *F* and ionospheric currents, *J. Geophys. Res.*, **78**, 218, 1973.
- Reid, G. C., The formation of small-scale irregularities in the ionosphere, *J. Geophys. Res.*, **73**, 1627, 1968.
- Rishbeth, H., Field aligned plasma velocity in the *F* region, *J. Atmos. Terr. Phys.*, **32**, 413, 1970.
- Rishbeth, H., The *F* layer dynamo, *Planet. Space Sci.*, **19**, 263, 1971.
- Rishbeth, H., and O. K. Garriott, *Introduction to Ionospheric Physics*, p. 73, Academic, New York, 1969.
- Rishbeth, H., S. Ganguly, and J. C. G. Walker, Field-aligned and field-perpendicular velocities in the ionospheric *F2* layer, *J. Atmos. Terr. Phys.*, **40**, 767, 1978.
- Scannapieco, A. J., S. R. Goldman, S. L. Ossakow, D. L. Book, and B. E. McDonald, Theoretical and numerical simulation studies of midlatitude *F* region irregularities, *NRL Memo. Rep. 3014*, Naval Research Lab., Washington, D. C., 1975.
- Sinno, K., and M. Kan, Midlatitude ionospheric scintillations of VHF radio signals associated with peculiar fluctuations of Faraday rotation, *J. Atmos. Terr. Phys.*, **40**, 503, 1978.
- Sobral, J. H. A., H. C. Carlson, D. T. Farley, and W. E. Swartz, Nighttime dynamics of the *F* region near Arecibo as mapped by airglow features, *J. Geophys. Res.*, **83**, 2561, 1978.
- Spencer, N. W., G. R. Carignan, H. G. Mayr, H. B. Niemann, R. F. Theis, and L. E. Wharton, The midnight temperature maximum in the earth's equatorial thermosphere, *Geophys. Res. Lett.*, **6**, 425, 1979.
- Titheridge, J., Determination of ionospheric electron content from the Faraday rotation of geostationary satellite signals, *Planet. Space Sci.*, **20**, 353, 1972.
- Vasseur, G., Dynamics of the *F* region observed with Thomson-scatter, I, Atmospheric circulation and neutral winds, *J. Atmos. Terr. Phys.*, **31**, 397, 1969.
- Walker, J. C. G., Midnight pressure bulge, in *Proceedings of Sixth International Symposium on Equatorial Aeronomy*, Aguadilla, Puerto Rico, 1980.
- Whitney, H. E., J. Aarons, and C. Malik, A proposed index for measuring ionospheric scintillations, *Planet. Space Sci.*, **17**, 1069, 1969.
- Wright, J. W., Horizontal drifts accompanying large vertical motions of the nocturnal *F* region, *Planet. Space Sci.*, **19**, 1327, 1971.

(Received February 6, 1981;  
revised April 12, 1981;  
accepted April 13, 1981.)

SPATIAL VARIABILITY OF TOTAL ELECTRON CONTENT  
IN THE EASTERN MEDITERRANEAN REGION

HAIM SOICHER  
Center for Communications Systems  
US Army Communications - Electronics Command  
Fort Monmouth, NJ 07703

JOHN A. Klobuchar  
Ionospheric Physics Branch  
Air Force Geophysics Laboratory  
Hanscom AFB, MA 01731

PATRICIA H. DOHERTY  
Emmanuel College  
Boston, MA 02115

### ABSTRACT

Faraday rotation observations were conducted at Haifa, Israel ( $32.87^{\circ}\text{N}$ ,  $35.09^{\circ}\text{E}$ ) and Athens, Greece ( $37.97^{\circ}\text{N}$ ,  $23.72^{\circ}\text{E}$ ) during the maximum phase of the current solar cycle using the VHF beacon of the SIRIO satellite. The subionospheric points (at 420 km) are ( $29.9^{\circ}\text{N}$ ,  $27.9^{\circ}\text{E}$ ) and ( $34.5^{\circ}\text{N}$  and  $18.4^{\circ}\text{E}$ ) and the subionospheric L-shell values are 1.24 and 1.37, respectively. Expected latitudinal and local time differences in total electron content (TEC) for the two locales are observed. However, the Haifa data are characterized by generally occurring, seasonally independent, large post-sunset electron content maxima which are absent for the Athens data. Furthermore, the post-sunset increases would appear to be a solar maximum phenomenon as they are not observed during the minimum phase of the solar cycle. The post-sunset increases are attributed to electron fluxes arriving from the equatorial regions along the magnetic lines of force. The correlation coefficients of hourly TEC at the Haifa/Athens locales exhibit a seasonally independent diurnal variation with minimum values at night and maximum values generally at the end of the buildup phase of TEC variation. The daytime ratios of the standard deviation of TEC to the average TEC are generally seasonally independent and behave quite similarly at the two locales with daytime values below  $\sim 25\%$ .

## INTRODUCTION

Total electron content (TEC) measurements were made at Haifa, Israel (Soicher et al, 1982) ( $32.87^{\circ}\text{N}$ ,  $35.09^{\circ}\text{E}$ ) and Athens, Greece ( $37.97^{\circ}\text{N}$ ,  $23.72^{\circ}\text{E}$ ) by monitoring the polarization rotation of VHF transmission from the geostationary SIRIO Satellite which is located at  $15^{\circ}\text{W}$ . The subionospheric points (i.e. the coordinates of the point at which the path from the satellite to the observation station intersects a mean ionospheric altitude of 420 km) for the Haifa and Athens locales are ( $29.9^{\circ}\text{N}$ ,  $27.9^{\circ}\text{E}$ ) and ( $34.5^{\circ}\text{N}$ ,  $18.4^{\circ}$ ), respectively; the invariant latitudes are  $26.2^{\circ}$  and  $31.4^{\circ}$ , respectively; the magnetic dip angles are  $41.8^{\circ}$  and  $48.4^{\circ}$ , respectively; and the L-shell values are 1.24 and 1.37, respectively. The ionospheric characteristics observed are considered to be those which are prevalent at the subionospheric points rather than at the locations of the receiving apparatus. The beacon frequency of SIRIO used in the observations was 136.14 MHz.

The transmission from the satellite was continuous except for an occasional deliberate shut down of the satellite beacon for power conservation requirements. Occasional interference and loss of power at the receiver site have also caused some data gaps.

At any one location, TEC is a quantity that is observed to vary diurnally, from day to day, seasonally, with the phase of the 11 year solar cycle, and in response to ionospheric disturbances. The data here was taken during the maximum phase of the current solar cycle, (cycle 21, which is a relatively high one in comparison to other cycles), and thus the TEC values represent maximum expected values in this region of the world.

### THE DATA

The superimposed diurnal variation of 15-minute TEC values, normalized to the vertical direction, grouped in monthly intervals for the calendar year 1980 at the Haifa and Athens locations are shown in Figs 1 and 2, respectively. The monthly averages of the TEC data for the same months are displayed in Figs 3 and 4, respectively.

At both locations the daytime TEC maximizes at the equinoxes (the spring (vernal) equinox has larger absolute TEC values than the autumnal equinox), and minimizes at the summer periods.

At both locations the electron content increases rapidly after local sunrise. The rate of increase is quite steep for the equinoctial and winter periods and significantly slower in the summer period. After reaching a diurnal maximum the TEC begins to decrease fairly rapidly. However, the Haifa TEC data are characterized by generally-occurring seasonally-independent large, post-sunset increases which last for two to three hours. These increases are generally absent for the Athens data. For Haifa, the TEC, after reaching a diurnal maximum, begins to decrease fairly rapidly. Following the maximum, TEC may gradually decay to reach a minimum just prior to the next sunrise. On many days, however, TEC may reach a secondary maximum quite dramatically. The peak of the secondary enhancement occurs at about 1800 UT, i.e. about an hour or so after local sunset. The post sunset TEC increase is observed at most seasons but is most pronounced in the late equinoctial and winter periods. For Athens the TEC secondary increase is rarely observed, and after the diurnal maximum is reached the TEC gradually decays to its minimum value.

Some of the gross characteristics of TEC are similar at both locations. For example the sharply lower daytime TEC values on June 27, 1980 and the sharply larger TEC daytime values on September 9, 1980 are common to both locations in comparison to adjacent days. However, some of the less obvious variations (e.g. travelling ionospheric disturbances) are unique to the individual location.

On the monthly average curves the post-sunset increase is averaged out, but a change of slope is noticeable in the Haifa data (Fig 3), while it is totally absent for the Athens data (Fig 4).

For comparison purposes TEC data for November 1975 taken at Haifa using the VHF signal of the geostationary ATS6 Satellite which was located at  $35^{\circ}\text{E}$  is shown in Figure 5. The period of observation was near the minimum phase of the solar cycle. The geographic subionospheric point was at  $30.1^{\circ}\text{N}$ ,  $35.1^{\circ}\text{E}$ ; the invariant latitude is  $26.4^{\circ}$ ; the magnetic dip is  $42.7^{\circ}$ ; and the L-shell value is 1.25. The solar cycle variation of TEC is expressed by the near 5:1 ratio in maximum TEC values during 1980 as compared to 1975. The 1980 post-sunset maximum is absent for the 1975 data, however there are indications of morning maxima in the 1975 data.

The hourly averages of TEC at Haifa and Athens for the equinoctial, summer and winter periods are shown in Figure 6. During the winter and spring equinox the Haifa TEC values are always larger than the corresponding Athens values. During the fall equinox the Haifa values are larger than the Athens values at all times except the pre-dawn period and the initial decay period after the diurnal maximum. During the summer, Athens values are larger than the corresponding Haifa values except during the dawn hours. While it is expected that the lower latitude ionosphere observed from Haifa will exhibit a higher TEC than the one

observed from Athens, due to higher solar zenith angles, the summer data are surprising.

The day-to-day variability of TEC is clearly exhibited by the superposed diurnal curves of Figures 1 and 2. The variability is best described by the standard deviation of the daily TEC values from the average monthly values. Of more practical significance is the ratio of the standard deviation to the mean TEC values as a function of time. Such ratios are plotted for the various seasons for the Haifa and Athens locales in Figure 7. It is seen that during the daytime the ratios are reasonably constant, independent of location and season, and rarely attain values above ~25%. During the night the ratios behave more erratically and are much higher in value. This suggests that there is an irreducible ionospheric variability which, upon normalization by the mean TEC, will be less by day than by night.

Using the smoothed hourly values of TEC from the Haifa and Athens stations, shifted to corresponding local times, correlation coefficients for the two locales were calculated for seasonally representative months as a function of universal time (Fig 8). The error bars represent 95 percent confidence limits, assuming a Gaussian distribution of values about the mean. The correlation coefficients exhibit a seasonally independent diurnal variation with minimum values at night and a steep increase towards maximum values generally at the end of the buildup phase of TEC variation. The general trend is for the coefficient to gradually decline after reaching the maximum, although some variability is observed.

Another approach is to cross correlate, between the two stations, the TEC values over continuous time intervals and the variability of TEC values from their monthly mean contours. By calculating the coefficient for the variabilities, rather than for the actual values of TEC, any possible influence of the different diurnal contour shapes of TEC is eliminated. The correlation is done for TEC values and variabilities during three time intervals; 00-04 UT, 00-24 UT and 1600-2200 UT.



The first time intervals represents the nighttime, the second represents the full diurnal period, while the third represents the time period during which the post-sunset maximum occurs in Haifa. The results are shown in Table I.

As expected, the correlation coefficients for the actual continuous TEC values are always higher than the corresponding TEC-variability coefficients. As with the smoothed hourly correlation coefficients the nighttime correlations are low in comparison to other diurnal intervals. The influence of the 24-hour term is seen in the high correlation of the TEC values for the time intervals 0000-2400. The correlation coefficients are affected significantly when the 24-hour term is removed by correlating the TEC variabilities. For the time periods 1600-2200, when the post-sunset maxima generally occur, the correlation coefficients for the TEC-variability are always lower than the corresponding ones for the full diurnal periods, except during the month of June when the post-sunset phenomenon is not prevalent.

#### DISCUSSION AND CONCLUSIONS

The large post-sunset enhancements in TEC observed at Haifa are due to the "fountain effect" pattern of plasma motion from the equatorial regions along the magnetic lines of force. In the equatorial region polarization fields produce at sunset large upward drifts of electrons, resulting in a rapid lifting of the F layer and massive horizontal flow of plasma along the field lines. (Rishbeth, 1977; Wu 1972). A post-sunset enhancement in upward  $\vec{E} \times \vec{B}$  drift, which is a characteristic feature during solar cycle maximum periods (Anderson and Klobuchar 1983), is primarily responsible for the increase in TEC at Haifa between about 1600 to 2000 UT. Bottomside  $f_oF_2$  observations indicate that the "equatorial anomaly" (i.e. low values of critical frequency at the magnetic equator compared to those at latitudes approximately 15-20 degrees away from the magnetic equator), during sunspot maximum, may extend to  $40^\circ$  magnetic dip angle in the Asian sector

(Rao & Malthotra, 1964). Further, the anomaly is most pronounced from about 2000-2200 local time in the northern latitudes. Bottomside and topside soundings of the equatorial anomaly (Rush et al, 1969) along the 75°W longitude, indicate that during solar maximum the maximum development of the anomaly occurs at ~2000 LT during winter and equinoxes & at ~1700 LT in summer. During years of declining solar activity the maximum development of the anomaly shifts to 1300-1500 LT.

The behavior of the TEC at Haifa vis-a-vis the post-sunset increase or its absence, thus complements  $f_oF_2$  data of the development of the equatorial anomaly in terms of its latitude extent, seasonal and solar phase development structure. The absence of the post-sunset ionospheric structure at Athens, a relatively close location to Haifa, indicate that density peaks may be relatively narrow in extent with resulting strong spatial density gradients.

The ratio of the standard deviation of TEC about its monthly mean to TEC appears independent of season and of geographic location, and during daytime is always below ~25%. This daytime ratio is similar to those observed at other temperate and high latitudes (Soicher & Gorman, 1980).

The relatively high day-to-day variability of TEC during nighttime appears to contribute to the low correlation between the Haifa and Athens TEC at that time intervals. The correlation coefficient increases steeply with time during the buildup phase of the TEC. This is indicative that production through photoionization is the dominant process and affects the TEC increases at both locations in similar manner. The subsequent decline of the correlation coefficient is indicative of the local processes which affect the TEC structure and its variability differently at the two locales.

#### ACKNOWLEDGEMENT

The authors wish to thank Z. Houminer and A. Shuval, Israel Committee for Space Research, Haifa, Israel under whose guidance the Haifa data were taken, and the personnel from the USAF Air Weather Service Detachment 3 of the 2nd Weather Wing for the data from Athens.

TABLE I

MONTH (1980) → TIME PERIOD ↓	APRIL	JUNE	OCTOBER	DECEMBER
0000-0400	.41 (.14)	.33 (.20)	.36 (.18)	.40 (.42)
0000-2400	.84 (.49)	.76 (.49)	.88 (.51)	.89 (.52)
1600-2200	.86 (.46)	.66 (.48)	.84 (.36)	.94 (.46)

Correlation coefficient of TEC values (and variabilities from monthly means) for different time intervals for seasonally representative months.

## FIGURES

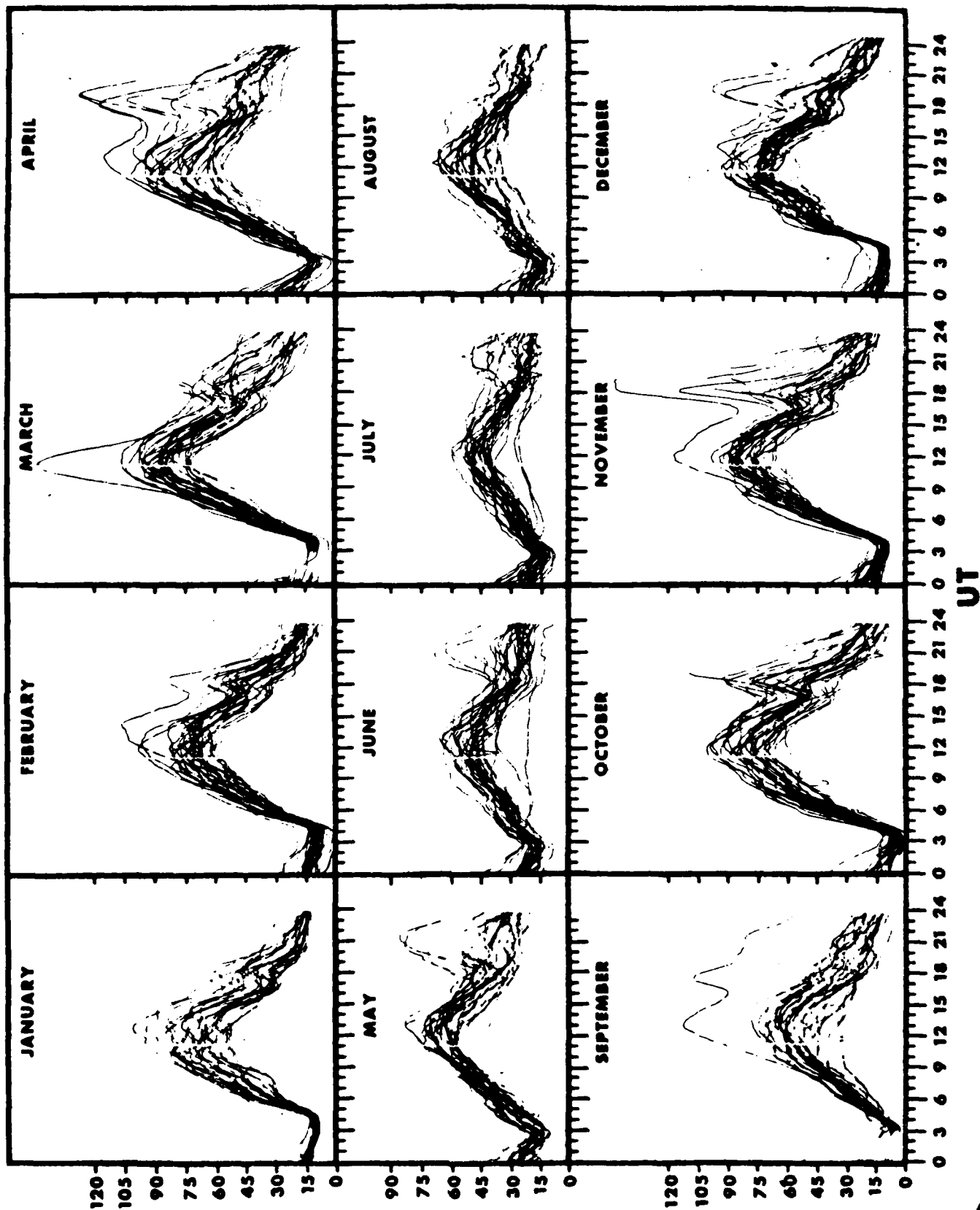
1. Superimposed diurnal variations of total electron content (TEC) for Haifa, Israel, for January through December 1980 versus time in UT. 1 TEC unit =  $10^{16}$  el m<sup>-2</sup>.
2. same as Figure 1 but for Athens Greece.
3. Monthly average variation of TEC in Haifa, Israel, for January through December 1980.
4. Same as Figure 3 but for Athens, Greece.
5. Same as Figure 1 but for November, 1975.
6. Hourly averages of TEC at Haifa, Israel, and Athens, Greece for the equinoctial, summer, and winter periods during 1980.
7. The diurnal variations of the ratio (in percent) of the monthly standard deviation of TEC to the hourly average of TEC at Haifa, Israel and Athens, Greece, for various seasons during 1980.
8. Correlation coefficients vs time of day for smoothed hourly values of TEC at Haifa, Israel and Athens, Greece for seasonally representative months.

## REFERENCES

- Anderson, D.M. and J.A. Klobuchar (1983), "Pre-midnight Enhancements in Total Electron Content at Ascension Island", Proceedings of the International Symposium on "Beacon Satellite Studies of the Earth's Environment", February 7-11, 1983, New Delhi, India (In the press)
- Rao C.S.R. and Malthotra (1964), "A Study of Geomagnetic Anomaly During IGY", J. Atmos. Terr. Phys., 26 (11) 1095.
- Rishbeth, H. (1973), "Dynamics of the Equatorial F-Region", J. Atmos. Terr. Phys., 39, 1159.
- Rush, C.M., S.V. Rush, L.R. Lyons, and S.V. Venkateswaran (1969), "Equatorial Anomaly During a Period of Declining Solar Activity", Radio Science, 4,9, 829.
- Soicher, H., Z. Houminer, and A. Shuval, (1982), "Total Electron Content Structure in the Middle East", Radio Science, 17, 6, 1623.
- Soicher, H. and F.J. Gorman (1980), "Variability of Total Electron Content at Temperate and High Latitudes", Proceedings of the COSPAR/URSI Symposium on "Scientific and Engineering Uses of Satellite Radio Beacons", Warsaw, Poland, May 19-23, 1980, pp 91-98.
- Wu M.F. (1972), "On the Effect of the Vertical Drift in the Equatorial F-Region", Radio Science, 7,12,1079.

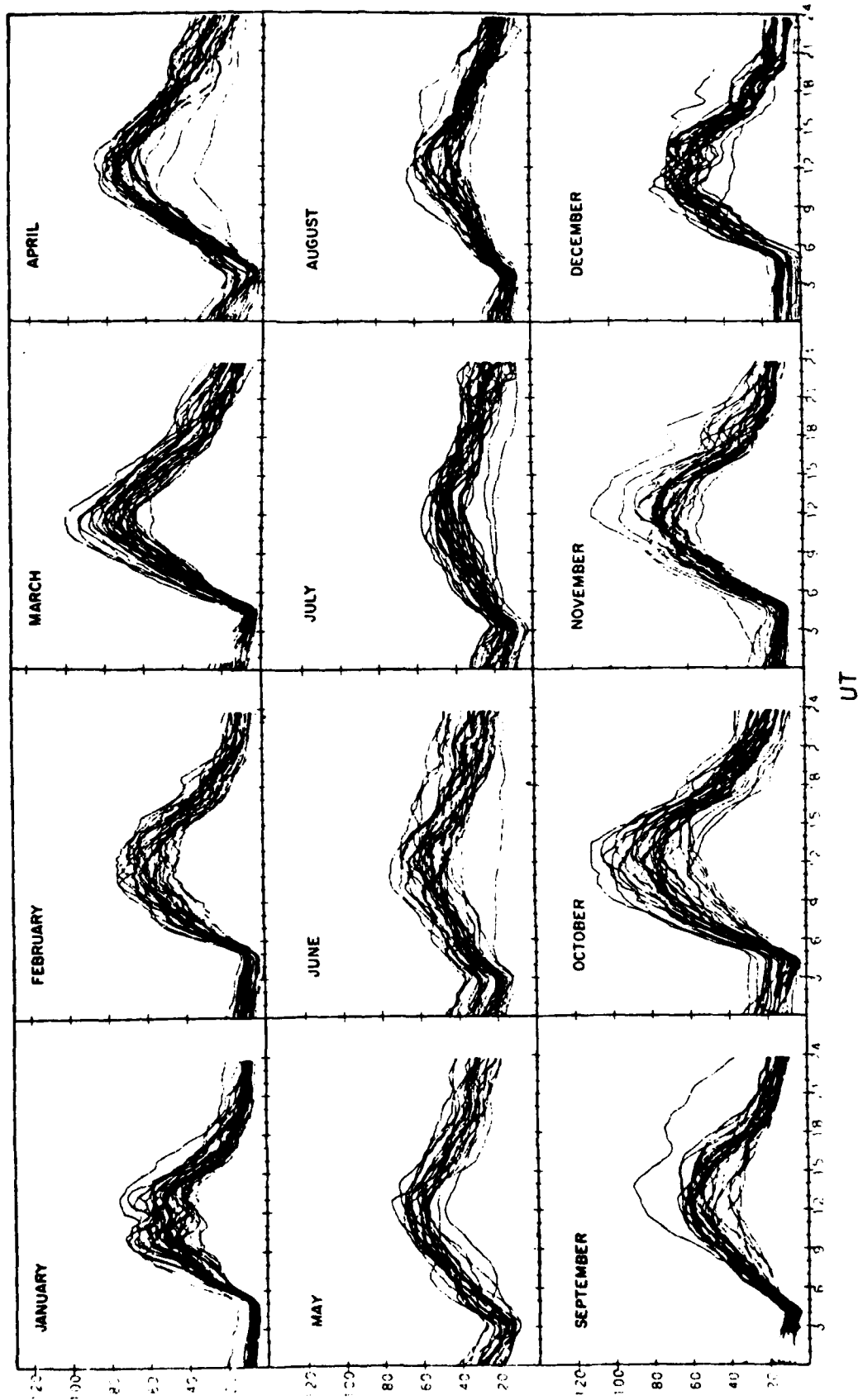
# TEC UNITS

## HAIFA ISRAEL 1980



# ATHENS GREECE 1980

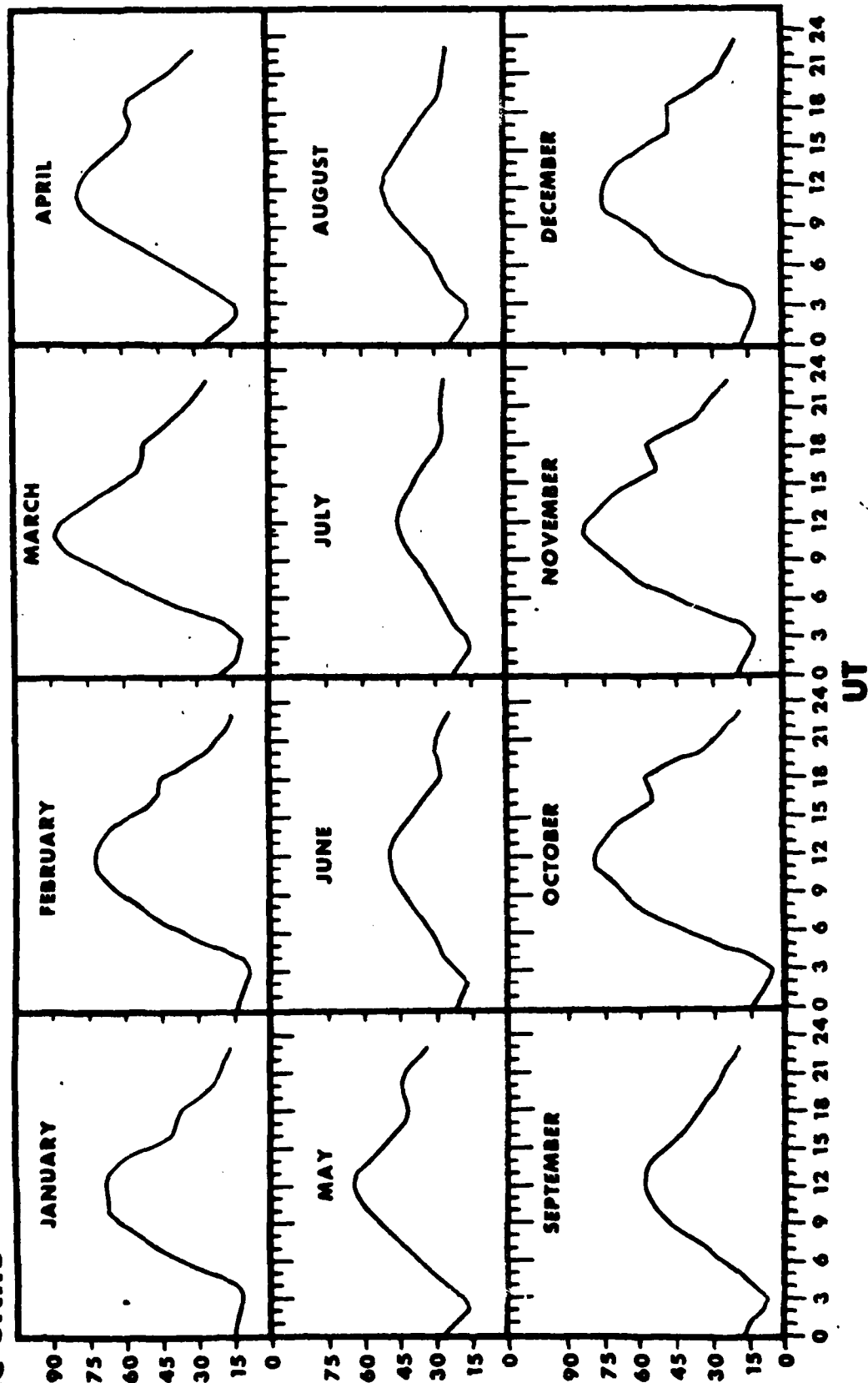
TEC UNITS



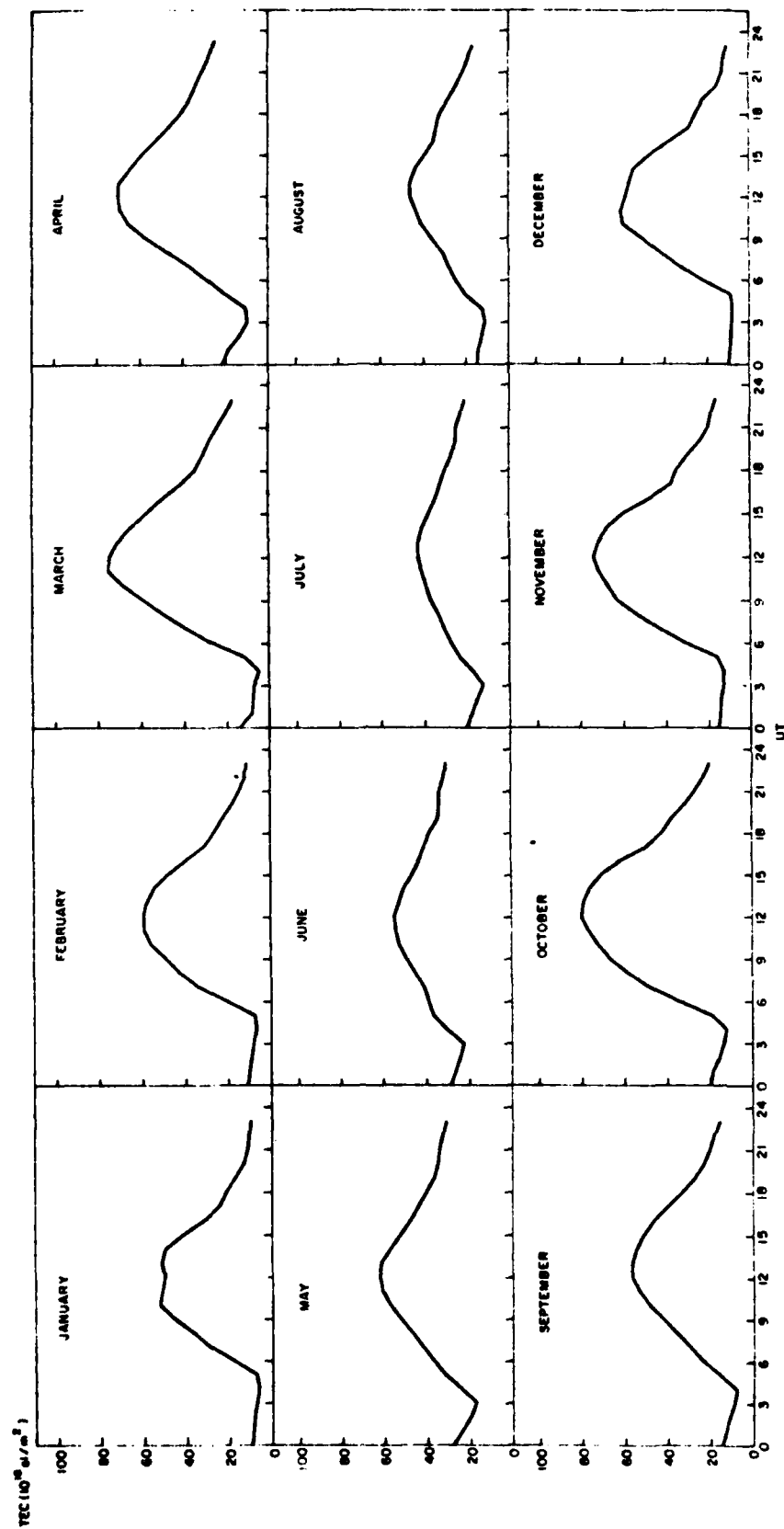


# HAIFA ISRAEL 1980

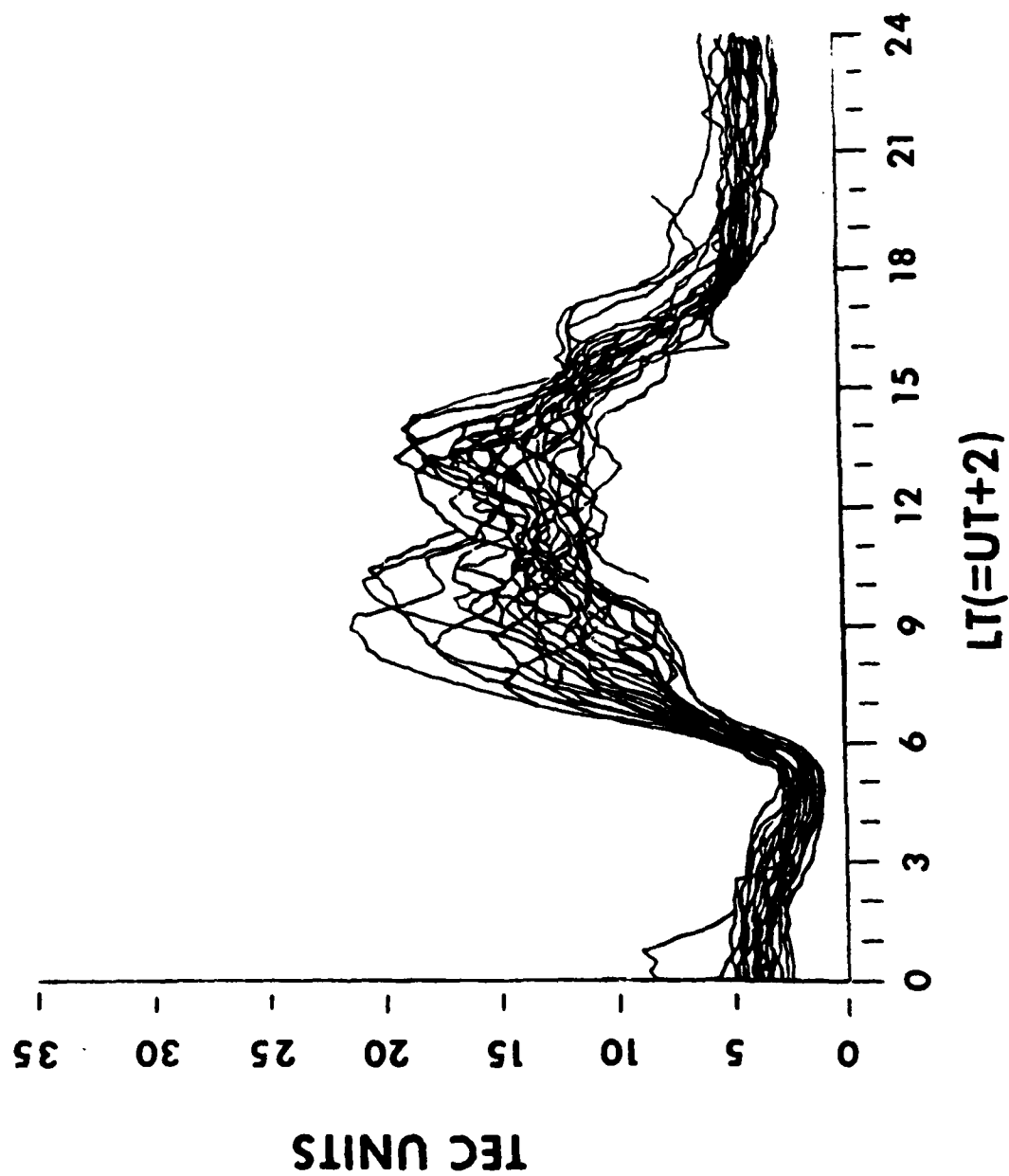
TEC UNITS



# ATHENS GREECE 1960

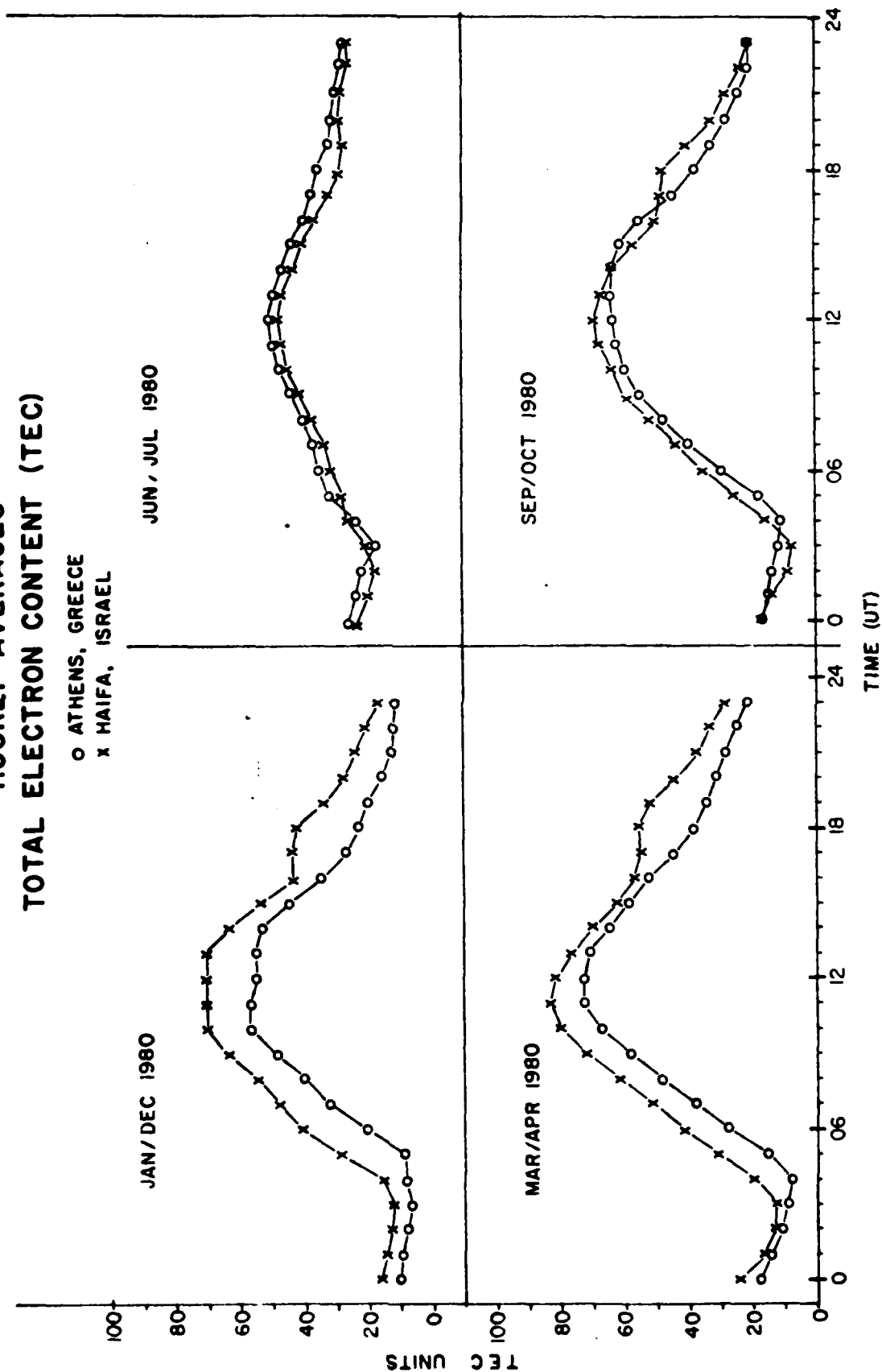


**SATELLITE ATS-6 140 MHZ BEACON**  
**NOVEMBER 1975**  
**HAIFA, ISRAEL**



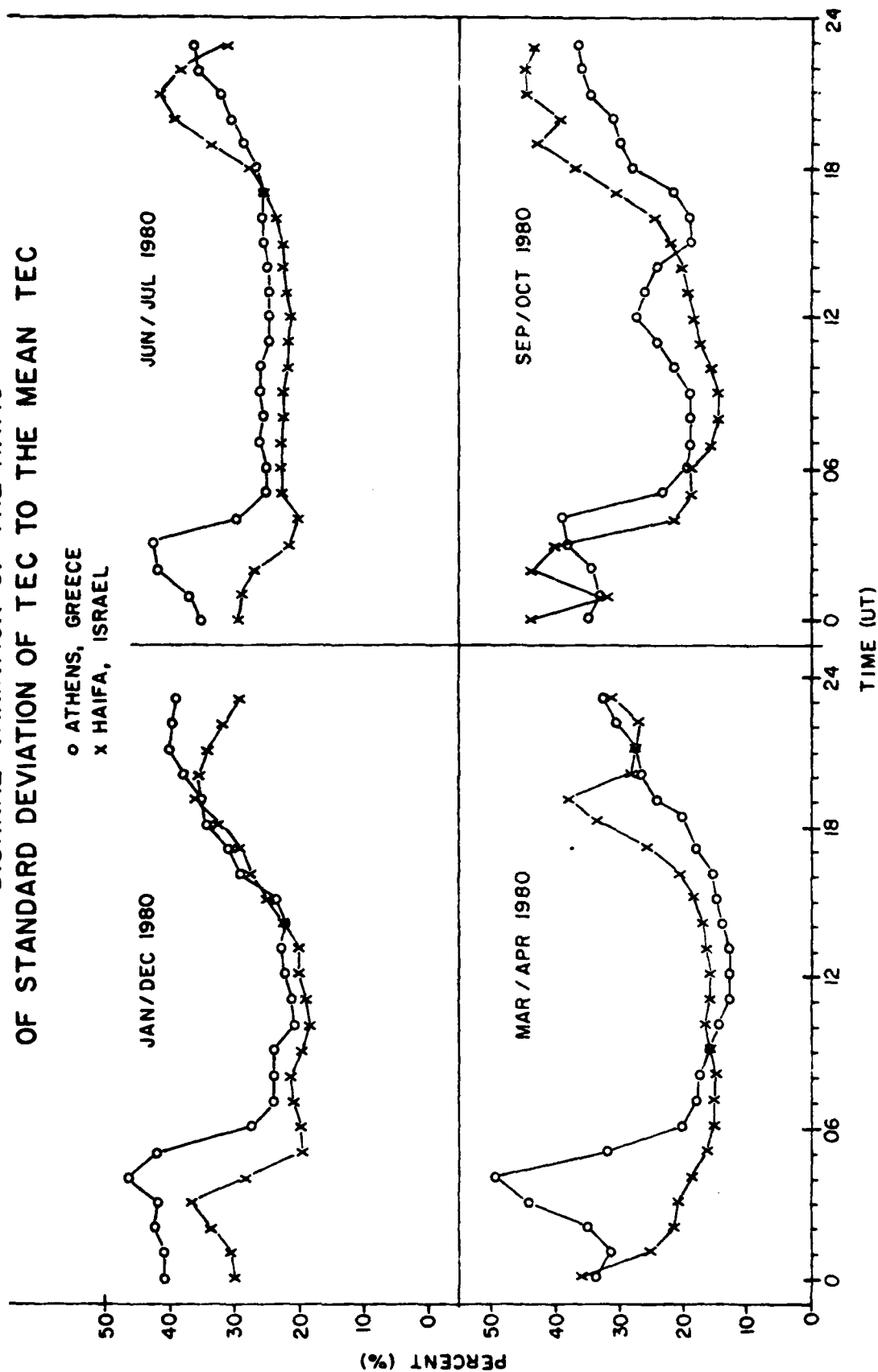
# HOURLY AVERAGES TOTAL ELECTRON CONTENT (TEC)

○ ATHENS, GREECE  
× HAIFA, ISRAEL

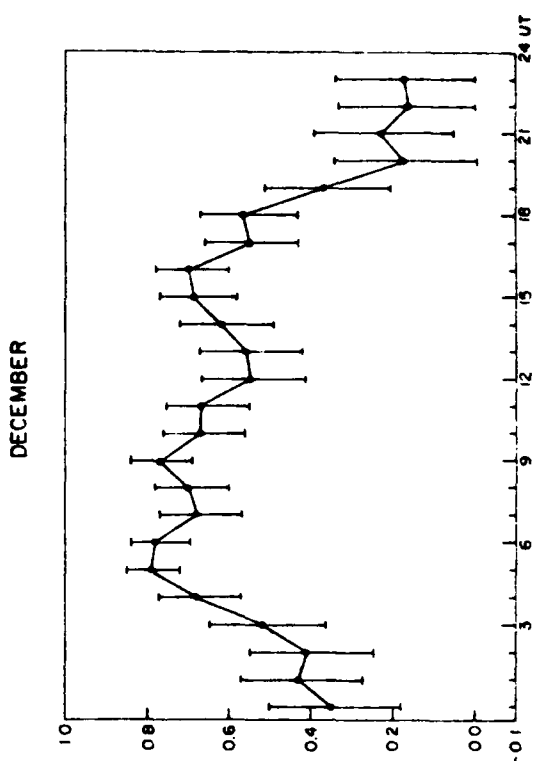
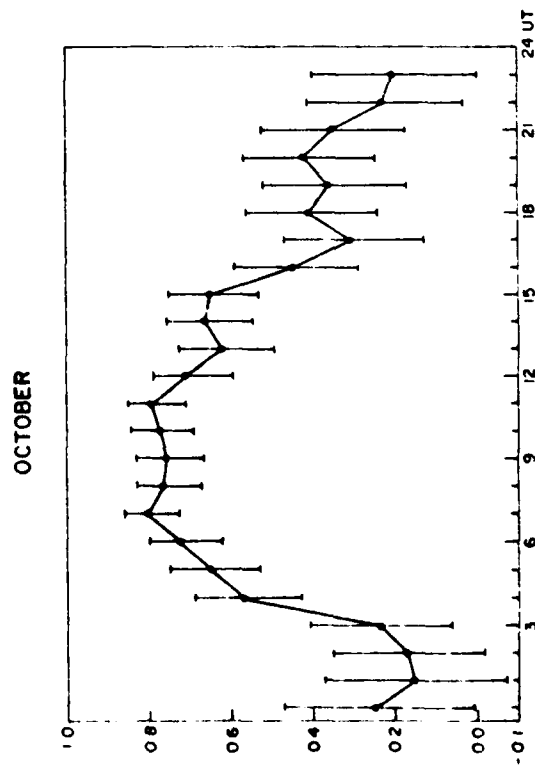
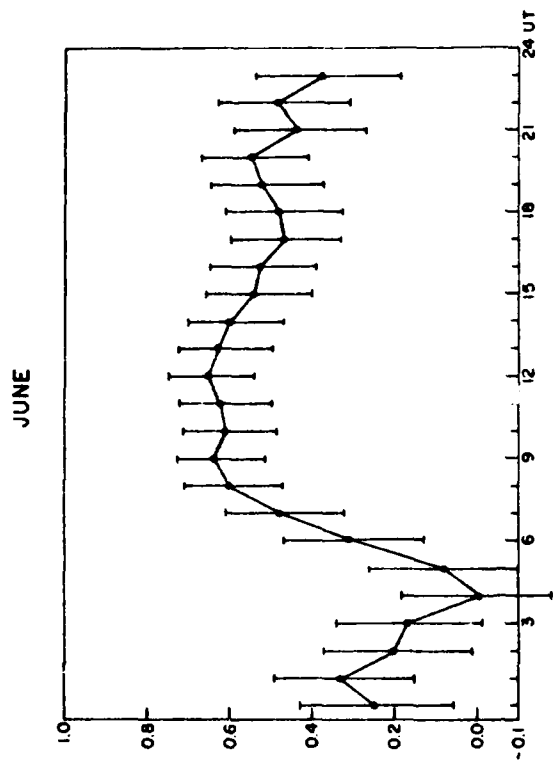
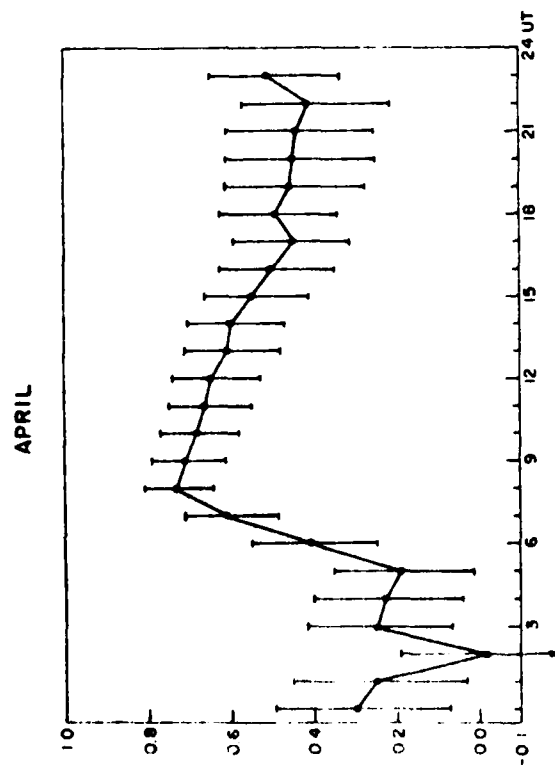


# DIURNAL VARIATION OF THE RATIO OF STANDARD DEVIATION OF TEC TO THE MEAN TEC

o ATHENS, GREECE  
x HAIFA, ISRAEL



# ATHENS VS. HAIFA CORRELATION COEFFICIENT VS. TIME OF DAY 1980



AD-A141 236

MODELLING OF IONOSPHERIC IRREGULARITIES AND TOTAL  
ELECTRON CONTENT(U) EMMANUEL COLL BOSTON MASS PHYSICS  
RESEARCH DIV S BASU ET AL. DEC 83 AFGL-TR-84-0032

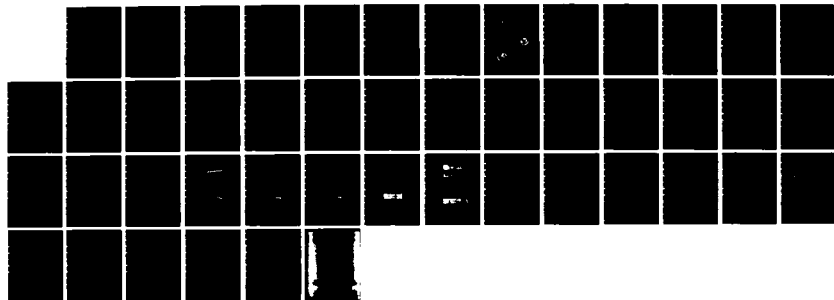
2/2

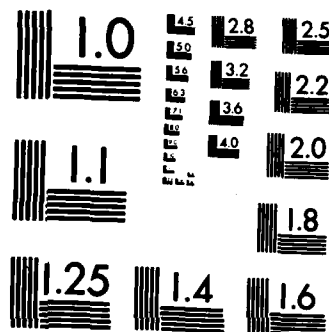
UNCLASSIFIED

F19628-81-K-0011

FFG 4/1

NL





MICROCOPY RESOLUTION TEST CHART  
NATIONAL BUREAU OF STANDARDS-1963-A



# THE ROLE OF IN-SITU MEASUREMENTS IN SCINTILLATION MODELLING

Sunanda Basu  
Santimay Basu  
Emmanuel College  
Boston, MA 02115

W.B. Manson  
University of Texas at Dallas  
Richardson, TX 75080

## ABSTRACT

Satellite borne in-situ measurements of irregularity amplitude have been very useful in providing the general features of the global F-region irregularity morphology. Thus, the conflicting equatorial scintillation observations obtained from greatly separated ground stations could be organized in the framework of a longitudinal variation of irregularity occurrence. Similarly, for the current study, high inclination satellite data have been utilized to delineate the essential morphological features of the polar cap irregularity environment. The lack of a significant diurnal and magnetic control of the irregularity morphology within the low solar flux northern winter polar cap ( $\Lambda > 80^\circ\text{N}$ ) distinguishes this region from the auroral oval regime. Scintillation results from a polar cap station during the winter season in years of high and low solar flux can be explained on the basis of in-situ observations of irregularity amplitude coupled with the variation of ambient density. A polar orbiting communication system sensitive to phase perturbations may observe large differences in the phase to amplitude scintillation ratio as it traverses through the auroral oval (with its possible magnetic E-W sheet-like irregularity anisotropy) and into the polar cap with its sun-aligned arc system. The current status of scintillation modelling is such that information on the gross variations of the electron density deviation and anisotropy seem to be more important than subtle changes of irregularity spectrum and layer thickness.

## 1. INTRODUCTION

Ground-based measurements over two decades have established the broad morphological features of three major scintillation regions, two covering the auroral ovals and polar caps and the third one approximately centered on the magnetic equator (Aarons, 1975). However, the detailed morphology has remained unknown because of some obvious handicaps, namely, the limited number of ground stations, the unavailability of suitable sources of VHF-UHF transmissions at certain longitudes and the existence of large ocean surfaces. Satellites carrying out in-situ observations of irregularity parameters present a viable alternative for mapping the irregularity morphology at both high and low latitudes. While only the high latitude morphology was studied by Dyson (1969) and Sagalyn et al. (1974), Clark and Raitt (1976) studied global irregularity morphology over an eighteen-month period. Basu et al. (1976) and Basu and Basu (1980) confined their attention to equatorial morphology only. However their major objective was to convert the observed irregularity morphology into estimated phase and amplitude scintillation models using other realistic model parameters. The resulting models showed in a rather dramatic fashion the longitudinal control of equatorial scintillations during the solstices. Apparently conflicting ground-based scintillation data from far-flung stations (Taur, 1973; Aarons, 1977) could readily be fitted into the synoptic picture of the worldwide equatorial scintillation occurrence pattern that emerged from the in-situ data.

The availability of data from the AE-D satellite with its inclination of  $90^\circ$  provided an ideal platform for the extension of such modelling efforts to the high latitude environment. Since little scintillation data is available from polar cap stations (Aarons et al., 1981) the in-situ model would be able to provide much needed information for global scintillation modelling efforts such as undertaken by Fremouw et al. (1980). Unfortunately, most of the AE-D data base is limited to a 3-month period around the northern winter solstice during 1975-76. Thus the model will be appropriate for northern winter under sunspot minimum conditions. The paucity of the data also prevents us from

studying the seasonal-cum-longitudinal behavior of auroral scintillations discussed earlier by Basu (1975) and Basu and Aarons (1980).

## 2. MODEL DEVELOPMENT

The ion-drift-meter data obtained from the AE-D satellite have been used for the modelling effort. The drift meter provides the ion density (or electron density for charge neutrality) every 1/16 sec ( $\sim 500$  m) along the orbital track as a function of position and magnetic local time of the satellite as shown by the solid line in Figure 1 which represents a typical AE-D pass through the noontime cusp, polar cap and nighttime auroral oval regions. From these samplings the rms irregularity amplitude  $\Delta N/N$  is computed over 3 secs of data (approximately 20 km of path length perpendicular to the magnetic field) at intervals of 8 secs as shown by the open circles. The first object of the modelling process is to determine the average irregularity amplitude as a function of magnetic activity, invariant latitude, and magnetic local time. The irregularity amplitude may be a function of altitude so that separate groupings of the data were made as a function of satellite altitude as well.

The next step is to convert the observed morphology into an estimated model of phase and amplitude scintillations. Scintillations are, of course, proportional to the integrated electron density deviation along the ray path (Rufenach, 1975). In order to estimate this a model of the ambient density  $N$  and irregularity layer thickness  $L$  are necessary. We further assumed that for propagation studies where only the total integrated effect along the ray path is considered, it is probably quite realistic to assume that the irregularity layer thickness is the same as the slab thickness of the ionosphere under similar geophysical conditions. The ITS-78 model (Llewellyn and Bent, 1973) with suitable updating for sunspot cycle and season was used to determine  $N$  and  $L$  values as a function of position and local time. Combining the observed rms  $\Delta N/N$  values with  $N$  derived above the morphology of  $\Delta N$  was obtained.

In the framework of diffraction theory under the limit of weak scattering, the irregularity morphology can be translated into models of phase and amplitude scintillations. The equations for the determination of  $\sigma_\phi^2$ , the phase variance, and  $S_4$ , the second central moment of intensity are taken from Rino (1979). Rino (1979) derived the equations for a variable three-dimensional spectral index  $p$  of the irregularities. However, the equations take on a simplified form if  $p$  is assumed to be 4 which was the most commonly observed spectral index by in-situ techniques (Dyson et al., 1974; Phelps and Sagalyn, 1976). With  $p=4$ , these equations are

$$\begin{aligned}\langle \sigma_\phi^2 \rangle^2 &= \frac{1}{2^3 \pi^3} (r_e \lambda)^2 (L \sec \theta) G C_s (v_{eff} \tau)^2 \\ S_4 &= \frac{1}{2} (r_e \lambda)^2 (L \sec \theta) C_s \left( \frac{\lambda z \sec \theta}{4\pi} \right) F\end{aligned}\tag{1}$$

where

- $r_e$  - classical radius of the electron ( $2.8 \times 10^{-15}$  m)
- $\lambda$  - radio wavelength
- $L$  - irregularity layer thickness
- $\theta$  - ionospheric zenith angle
- $C_s$  - strength of turbulence =  $2^3 \pi \langle \Delta N \rangle^2 \left( \frac{2\pi}{\lambda_o} \right)$
- $\lambda_o$  - outer scale ( $\sim 20$  km, determined by data interval)
- $G, F$  - geometrical parameters for field aligned irregularities
- $z$  - reduced distance of center of irregularity layer
- $v_{eff}$  - effective scan velocity
- $\tau$  - detrend interval

It is important to note in the above equations that in a power law environment with a large outer scale, the data segment over which the rms  $\Delta N/N$  is computed effectively sets an outer scale for modelling purposes. The strength of turbulence  $C_s$  will thus also depend on the length of the data segment used. Further, while the  $S_4$  index can be uniquely determined in terms of irregularity and anisotropy parameters, the phase scintillation also depends on the detrend interval over which the phase variance is computed and the effective scan velocity of the ray path across the iso-correloids of electron density. For this modelling effort we considered a detrend interval of 10 secs to make the results compatible with those of the Wideband satellite (Fremouw et al., 1978). For the determination of the effective scan velocity we considered a simple orbital geometry shown in Figure 2. The satellite beacon was assumed to be orbiting in the magnetic meridian plane at an altitude of 1000 km. The projected velocity at F region heights was considered to be  $3 \text{ km sec}^{-1}$  in the magnetic N-S direction with no component of velocity in the magnetic E-W direction. The modelling was done for an overhead geometry. Three kinds of irregularity anisotropies were considered. In the nighttime auroral oval magnetic L-shell aligned E-W sheets were used (Martin and Aarons, 1977; Rino et al., 1978) while in the daytime sub-auroral region field-aligned rods were used

(Fremouw et al., 1980) in keeping with earlier experimental observations. However, no data exists on anisotropy characteristics either in the daytime auroral oval or in the entire polar cap region. Considering the nature of the arc system (Shepherd, 1979), we made the assumption that in the daytime auroral oval the irregularity anisotropy is also in the form of E-W sheets whereas in the polar cap the sun-aligned arc system (Lassen, 1979; Weber and Buchau, 1981) could be associated with N-S sheets. In Section 4, we shall present some results of phase and amplitude scintillation modelling based on such composite irregularity characteristics.

### 3. HIGH-LATITUDE IRREGULARITY MORPHOLOGY

In Figure 3a, we show the average irregularity morphology observed in the Northern Hemisphere as a function of invariant latitude and magnetic local time for quiet magnetic conditions ( $K_p < 3.5$ ) obtained between October 22 - December 31, 1975. The irregularity map was obtained by sorting the AE-D data of rms  $\Delta N/N$  (expressed as a percentage) in  $5^\circ$  wide invariant latitude and 4 hour magnetic local time boxes and determining the average value of  $\Delta N/N$ . The  $80^\circ$ - $90^\circ$  invariant latitude range was combined into one box. For Figure 3a, the data was confined to the time periods when AE-D was between 200-400 km while Figure 3b shows the morphology when AE-D was above 400 km altitude. The highest altitude attained by AE-D was approximately 1400 km so that Figure 3b represents the altitude range between 400-1400 km.

The most striking difference between Figures 3a and b is the difference in irregularity amplitudes in the nighttime auroral oval. In this region ( $65$ - $80^\circ$  latitude) the high altitude data shows much larger amplitudes while in the polar cap region of open field lines ( $>80^\circ$  latitude) the irregularity amplitudes seem to be independent of altitude. The diurnal variation within the polar cap is quite small with the largest irregularities being observed at midday and smallest at midnight. The sharp irregularity boundary at  $75^\circ$  latitude at the equatorward edge of the cusp in the noon sector is another noteworthy feature of these two maps. In addition, the high altitude data shows an asymmetry between the morning and afternoon sectors of the cusp with the morning sector irregularities being larger. Figure 3b is remarkably similar to the map of small scale transverse magnetic disturbances determined by the Triad satellite at 800 km altitude (Saflekos et al., 1978) if we keep in mind the differences in the way the data were sorted in each study.

The irregularity morphology observed during disturbed magnetic conditions ( $K_p > 3.5$ ) is shown in Figure 3c. Because of the smaller amount of data, an altitude separation was not feasible. The nighttime auroral oval shows a pronounced broadening. However irregularity amplitudes do not attain the large values observed in Figure 3b probably because of both altitudinal and latitudinal smearing. There is a definite equatorward motion of both the nighttime auroral oval and the dayside cusp.

### 4. MODEL OF PHASE AND AMPLITUDE SCINTILLATIONS

As mentioned in Section 2, the observed morphology of rms  $\Delta N/N$  in the high latitude region can be converted to equivalent phase and amplitude scintillation models by using a model of maximum F-region densities to obtain the magnitude of  $\Delta N$ . Figures 4A and B show maps of electron density deviation  $\Delta N$  generated by combining the ITS-78 model of densities for the sunspot conditions pertaining to November and December, 1975 with the irregularity amplitudes obtained in the AE-D study presented in Section 3. Figure 4a was determined by combining all the data used in the preparation of Figures 3a and b with the density model while Figure 4b was obtained from Figure 3c and the density model.

The point to note from Figure 4a is the persistence (even in  $\Delta N$ ) of most of the features found in  $\Delta N/N$ . Thus the polar cap still shows a relatively small diurnal variation with the maximum electron density deviation being observed in the daytime. The cusp is a region of high  $\Delta N$  while the nightside auroral oval expectedly shows much larger electron density deviations than observed at the same latitudes in the daytime.

Following the procedure outlined in Section 2, Figure 4a is converted into models of  $\sigma_\phi$  and  $S_4$  by using a composite of three different types of irregularity anisotropy in various sectors of the high latitude region. Only the low  $K_p$  data set is used for scintillation models because of the better data coverage. The assumed form of the irregularity anisotropy in the different MLT and invariant latitude sectors are as follows. E-W sheets (10:10:1 with larger dimensions along the field and in the magnetic E-W direction) have been assumed over the nighttime and daytime auroral ovals ( $60^\circ$ - $80^\circ$  latitude between 18 MLT to 06 MLT and  $75^\circ$ - $80^\circ$  latitude between 06 MLT to 18 MLT). Over the polar cap also, E-W sheets have been assumed except for the noontime and midnight sectors (10-14 MLT and 22-02 MLT) where N-S sheets (10:10:1 with larger dimensions along the field and in the magnetic N-S direction) are considered. In the sub-auroral region ( $60^\circ$ - $75^\circ$  latitude between 06-18 MLT) irregularities in the form of field-aligned rods (with 10:1 ratio) have been assumed. As outlined in Section 2, the irregularity layer thickness has been derived from the slab thickness obtained from ITS-78. These values usually range between 200 and 250 km.

Figure 5a shows the resultant model for amplitude scintillation index ( $S_4$ ) at 137 MHz under overhead propagation conditions. The non-uniform scaling of  $\Delta N$  values shown in Figure 4a to  $S_4$  index in Figure 5a arises from variations in the form of anisotropy and magnetic dip. The model developed for sunspot minimum conditions yields values of  $S_4 < 0.5$  which thus conform to the weak scatter limit.

The model of rms phase deviation, shown in Figure 5b, corresponds to the reception of 137 MHz signal on the ground from a beacon satellite orbiting in the magnetic meridian plane, with a scan velocity of 3 km/sec at F region heights. The detrend interval for rms phase deviation has been chosen to be 10 sec. It should be noted that in the presence of irregularity anisotropy the rms phase deviation is not only dictated by the electron density deviation ( $\Delta N$ ) but is markedly controlled by the scan velocity with respect to the irregularity axes. In the present model, the scan velocity of the satellite has been considered to be very large compared to the irregularity drift. However, in the general case, the scan velocity of the ray path relative to the irregularity motion needs to be considered. From Figure 5b, the marked effect of the anisotropy with respect to the satellite motion may be noted. For the assumed alignment of the orbital track with the magnetic meridian, the rms phase deviation ( $\sigma_\phi$ ) is accentuated in regions where the anisotropy is in the form of E-W sheets. For example, the high levels of  $\sigma_\phi$  in the daytime cusp region arises not only from high  $\Delta N$  values in this region but is due to the N-S orbital motion in a region where the irregularity anisotropy is assumed to be in the form of E-W sheets. This is again demonstrated in the polar cap where the  $\sigma_\phi$  values are deemphasized in the noon and midnight sectors where N-S sheets are considered and are accentuated in the afternoon and post-midnight sectors where E-W sheets have been assumed to exist. From an observational standpoint, the form of the anisotropy can thus be obtained from the ratio of  $\sigma_\phi$  and  $S_4$  (Fremouw, 1980). For a satellite orbiting in the magnetic meridian, this ratio ( $\sigma_\phi/S_4$ ) is largest where E-W sheets occur, intermediate where the anisotropy is in the form of magnetic field aligned rods and is minimum where N-S sheets exist.

In Figures 6a and 6b, models for  $S_4$  and  $\sigma_\phi$  at 250 MHz are shown for identical forms of irregularity anisotropy and constraints of satellite orbit. As is to be expected, the general patterns are similar to those of Figures 5a and 5b with the values of  $\sigma_\phi$  and  $S_4$  reduced at the higher frequency in accordance with the frequency scaling laws appropriate for a 3-dimensional irregularity spectral index of 4.

#### 5. COMPARISON WITH SCINTILLATION DATA

To determine the effectiveness of the in-situ modelling process presented in the last section, it is important to compare the model with actual ground-based scintillation data. A suitable data base for the comparison with Figure 5a was available at the Air Force Geophysics Laboratory. This was the Narssarssuaq ATS-3 scintillation data obtained during the winter of 1975-76 for which the ionospheric intersection point was  $64^\circ\Lambda$ . This data formed part of the high latitude morphology published earlier (Basu and Aarons, 1980) and is shown in Figure 7a for quiet magnetic conditions. Little diurnal variation is observed with maximum  $S_4$  observed being .22 near midnight. Now if the geometrical factor for ATS-3 observations at  $20^\circ$  elevation is computed for E-W sheets with axial ratios of 10:10:1 and compared with the overhead geometrical factor at the same location for the same anisotropy then a factor of 2.6 enhancement is obtained at the low elevation angle point. Thus the nighttime values shown in Figure 7a when scaled down by a factor of 2.6 are found to be quite consistent with the modeled values close to 0.1. Similar arguments are true for the daytime values.

Rino and Matthews (1980) in their Figure 10 have shown the median  $S_4$  values at 137 MHz as a function of magnetic latitude for the winter of 1976-77 obtained with the Wideband satellite in the nighttime auroral region. Our model was done for the winter of 1975-76 but the sunspot numbers during the two succeeding winters were quite similar. There is good agreement between the model and scintillation observations if one disregards the geometrical enhancement region of the Wideband satellite data. The phase scintillation is more difficult to compare because of the idealized orbit chosen for the study.

In the polar cap little data is available for comparison. The only available data during quiet sunspot years is at 250 MHz from Thule, Greenland for the period August-October, 1975. The subionospheric latitude coverage is  $82^\circ$ - $90^\circ$  CG latitude. Even though the geometrical factors are not accurately known for this data set (Aarons et al., 1981) and the periods do not match exactly with the model, we exhibit the  $S_4$  indices obtained at Thule in Figure 7b to show that the modelled values of 0.15 to 0.2 in the polar cap are at least of the right order of magnitude as the data.

#### 6. CONCLUSIONS

The satellite in-situ irregularity measurements provide a direct measurement of electron density deviation ( $\Delta N$ ) parameter which can be used to derive models for amplitude and phase scintillations. In view of the insufficient coverage of ground scintillation observations caused by either the absence of suitable ground locations or satellites, the usefulness of in-situ probing with unlimited latitude and longitude coverage cannot be overemphasized. The evaluations made in the previous

section show that scintillation models based on the quantitative measure of electron density deviation ( $\Delta N$ ) by satellites at high latitudes provide realistic estimates. They also provide a synoptic picture over the northern polar cap which is almost impossible to achieve with ground-based measurements. We have thus been able to provide models of both equatorial and high latitude amplitude and phase scintillations from in-situ data.

It should, however, be mentioned that our current efforts are based on satellites whose primary function was not concerned with irregularity measurements at F region heights for scintillation modelling. As such, the restrictions imposed on satellite altitude, time of transit, etc., limited this data base. A dedicated satellite performing such measurements at F-region altitudes with suitable orbital characteristics will be an ideal vehicle for the development of a world-wide model of phase and amplitude scintillations.

#### ACKNOWLEDGMENTS

We wish to thank J. Aarons and H.E. Whitney for making the scintillation data available to us and for many helpful discussions. We thank J. Noonan and N. Scotti for assistance with computer programming.

The work at Emmanuel College was partially supported by NASA Grant NSG 5419 and AFGL Contract F19628-81-K-0011.

#### REFERENCES

- Aarons, J., AFCRL Report No. TR-75-0135, Air Force Cambridge Research Laboratories, Hanscom AFB, MA 01731, 1975.
- Aarons, J., *Antennas Propagat.*, AP-25, 729, 1977.
- Aarons, J., J.P. Mullen, H.E. Whitney, A.L. Johnson and E.J. Weber, *Geophys. Res. Lett.*, 8, 1981 (in press).
- Basu, S., *J. Geophys. Res.*, 80, 4725, 1975.
- Basu, S. and J. Aarons, *Radio Sci.*, 15, 59, 1980.
- Basu, S. and S. Basu, *Cospar Symposium Series*, 8, 189, 1980.
- Basu, S., S. Basu and B.K. Khan, *Radio Sci.*, 11, 821, 1976.
- Clark, D.H. and W.J. Raitt, *Planet. Space Sci.*, 24, 873, 1976.
- Dyson, P.L., *J. Geophys. Res.*, 74, 6291, 1969.
- Dyson, P.L., J.P. McClure and W.B. Hanson, *J. Geophys. Res.*, 79, 1497, 1974.
- Fremouw, E.J., *J. Atmos. Terr. Phys.*, 42, 775, 1980.
- Fremouw, E.J., R.L. Leadabrand, R.C. Livingston, M.D. Cousins, C.L. Rino, B.C. Fair and R.A. Long, *Radio Sci.*, 13, 167, 1978.
- Fremouw, E.J., J.M. Lansing and D.A. Miller, Report No. PD-NW-81-237R, Physical Dynamics Inc., Bellevue, WA 98009, 1980.
- Lassen, K., *Geophys. Res. Lett.*, 6, 777, 1979.
- Llewellyn, S.K. and R.B. Bent, Report No. AFCRL-TR-73-0657, Air Force Cambridge Research Laboratories, Hanscom AFB, MA 01731, 1973.
- Martin, E. and J. Aarons, *J. Geophys. Res.*, 82, 2717, 1977.
- Phelps, A.D.R. and R.C. Sagalyn, *J. Geophys. Res.*, 81, 515, 1976.
- Rufenach, C.L., *Radio Sci.*, 10, 155, 1975.
- Rino, C.L., *Radio Sci.*, 14, 1135, 1979.
- Rino, C.L., R.C. Livingston and S.J. Matthews, *Geophys. Res. Lett.*, 5, 1039, 1978.
- Shepherd, G., *Rev. Geophys. Space Phys.*, 17, 2017, 1979.

Rino, C.L. and S.J. Matthews, J. Geophys. Res., 85, 4139, 1980.

Saflekos, M.A., T.A. Potemra and T. Iijima, J. Geophys. Res., 83, 1493, 1978.

Sagaly, R.C., M. Smiddy and M. Ahmad, J. Geophys. Res., 79, 4252, 1974.

Weber, E.J. and J. Buchau, Geophys. Res. Lett., 8, 125, 1981.

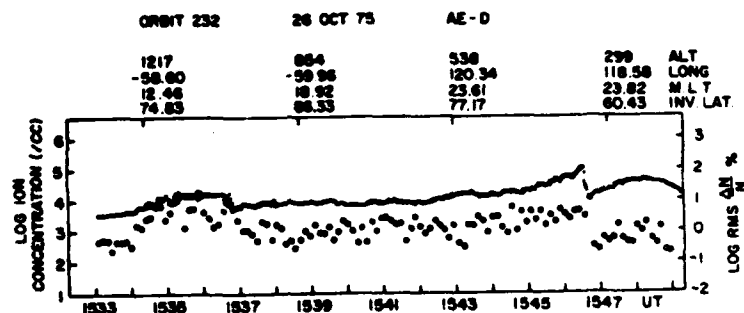
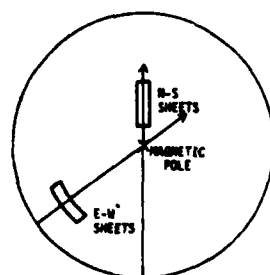


Figure 1. Ion concentration and irregularity amplitude (open circles) obtained by the ion drift meter on AE-D satellite. The altitude (ALT), longitude (LONG) and invariant latitude (INV. LAT.) of the satellite as a function of magnetic local time (MLT) and universal time (UT) are indicated on the diagram.



OVERHEAD SCINTILLATION MODEL FOR SPECIAL SATELLITE ORBIT AND IRREGULARITY CHARACTERISTICS

- SATELLITE HEIGHT: 1000 km
- SATELLITE LOCATION: OVERHEAD
- ORBIT: ALIGNED WITH MAGNETIC MERIDIAN
- EFFECTIVE SCAN VELOCITY: 3 km/sec
- OFFEND INTERVAL: 10 sec
- IRREGULARITY GEOMETRY:
  1. FIELD ALIGNED ROD
  2. E-W SHEETS
  3. N-S SHEETS

Figure 2. The idealized orbital geometry of the satellite and the irregularity anisotropy considered in the model are illustrated.

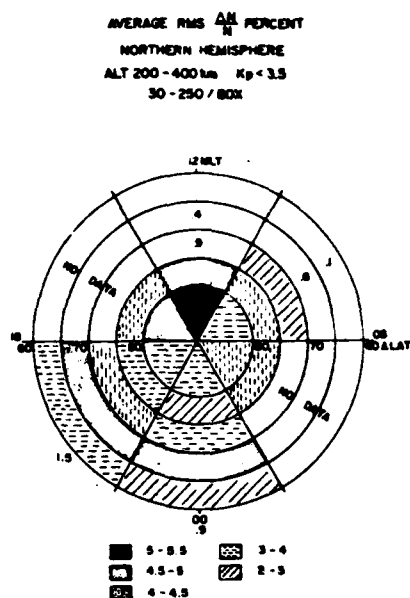


Figure 3a. Variation of the average irregularity amplitude as a function of the invariant latitude and magnetic local time under magnetically quiet conditions obtained from the AE-D satellite in the altitude interval of 200-400 km. The different tones correspond to different irregularity amplitudes expressed in percentage.

Figure 3b. Same as in Figure 3a except for the satellite altitude interval of 400-1400 km.

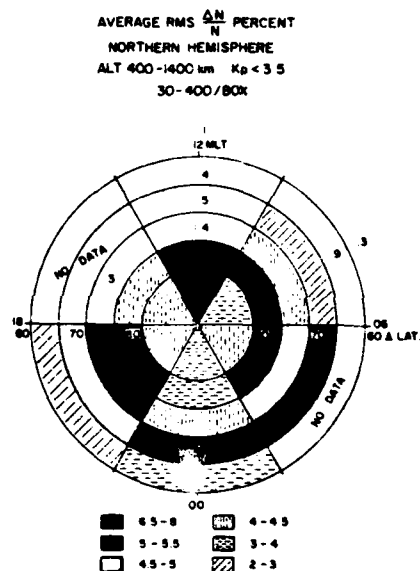
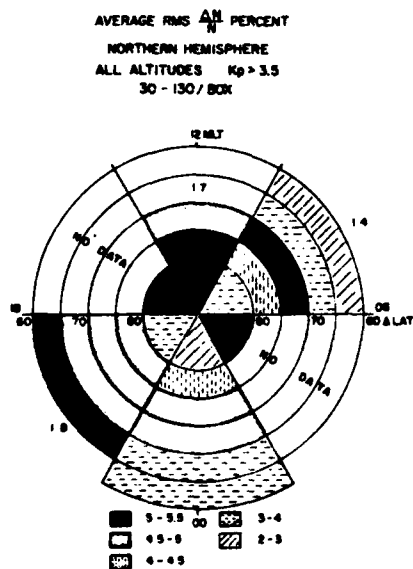


Figure 3c. Variation of the average irregularity amplitude with magnetic local time and invariant latitude under magnetically disturbed conditions ( $K_p > 3.5$ ) considering all data obtained between 200-1400 km altitude.

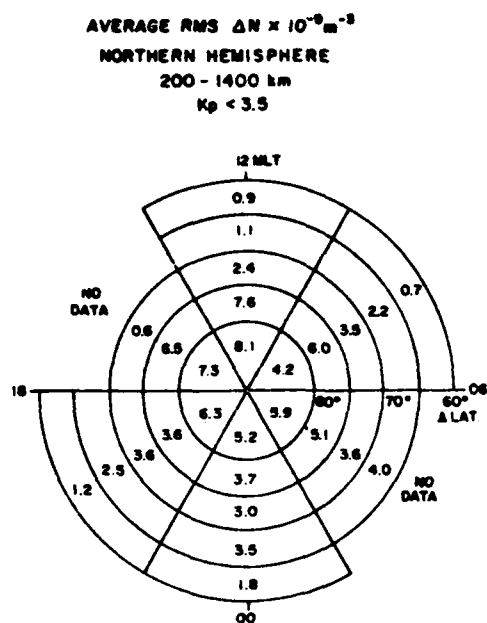


Figure 4a. Morphology of electron density deviation ( $\Delta N$ ) in units of  $10^9 \text{ m}^{-3}$  under magnetically quiet conditions.

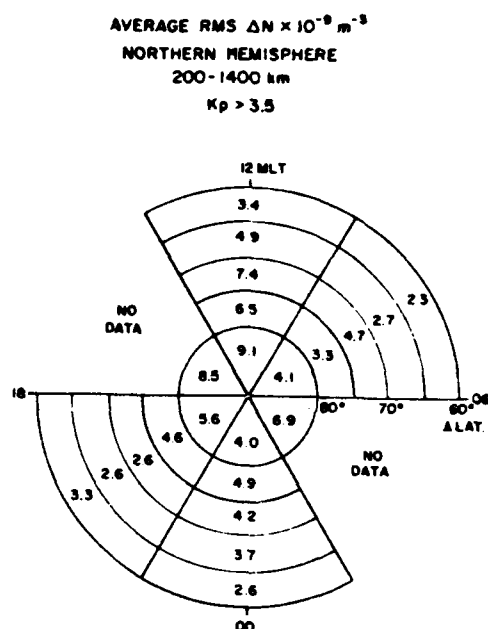


Figure 4b. Same as in Figure 4a for magnetically disturbed conditions.

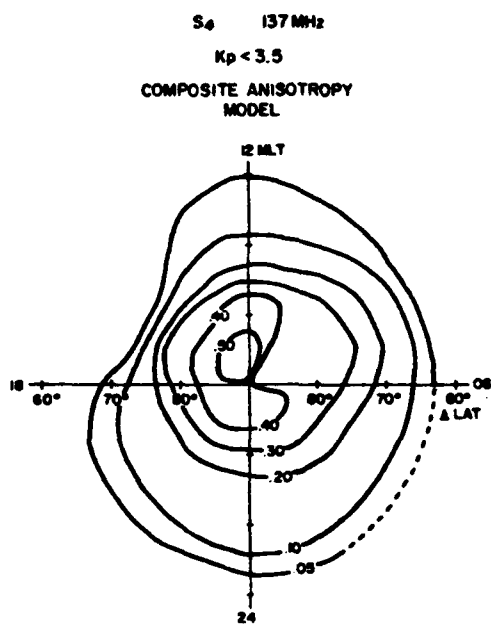


Figure 5a. Model of intensity scintillation ( $S_4$ ) at 137 MHz under magnetically quiet conditions.

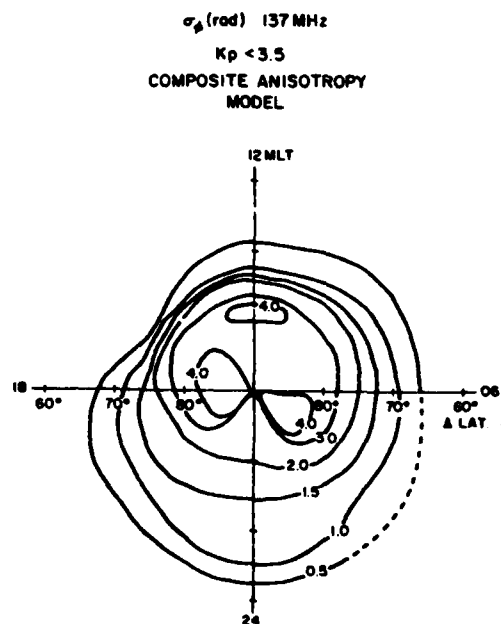


Figure 5b. Model of rms phase scintillation at 137 MHz valid for a beacon satellite orbiting at 1000 km altitude over the magnetic meridian. A composite form of anisotropy (see text) and detrend interval of 10 sec are used.



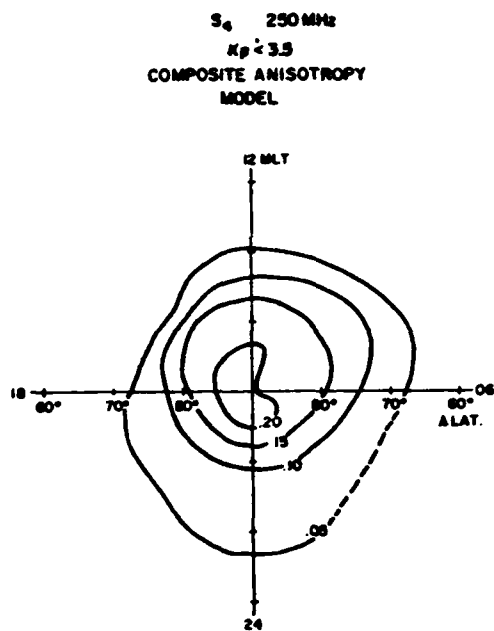


Figure 6a. Same as in Figure 5a except for 250 MHz.

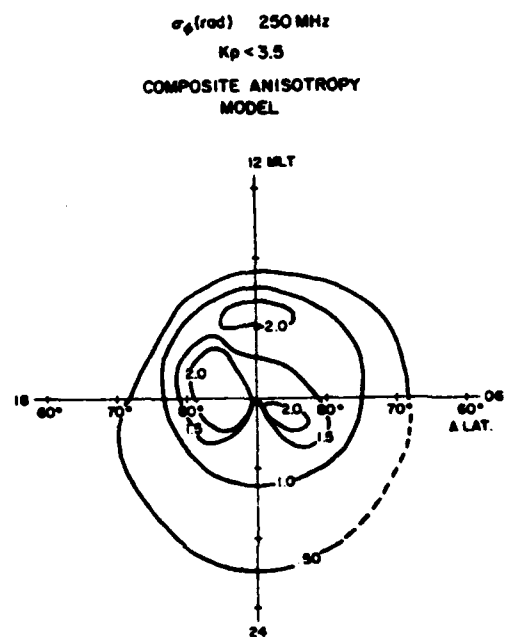


Figure 6b. Same as in Figure 5b except for 250 MHz.

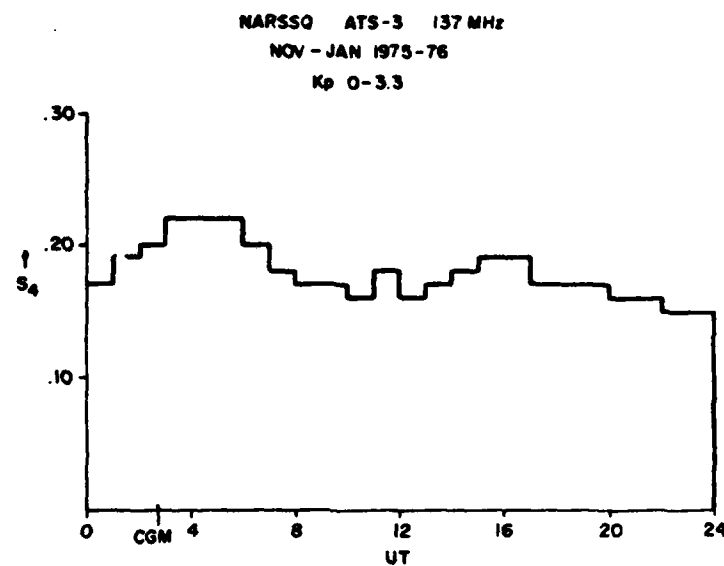


Figure 7a. Average value of intensity scintillation index ( $S_4$ ) using ATS-3 at 137 MHz observed at Narssarssuaq for magnetically quiet conditions during Nov-Jan 1975-76.

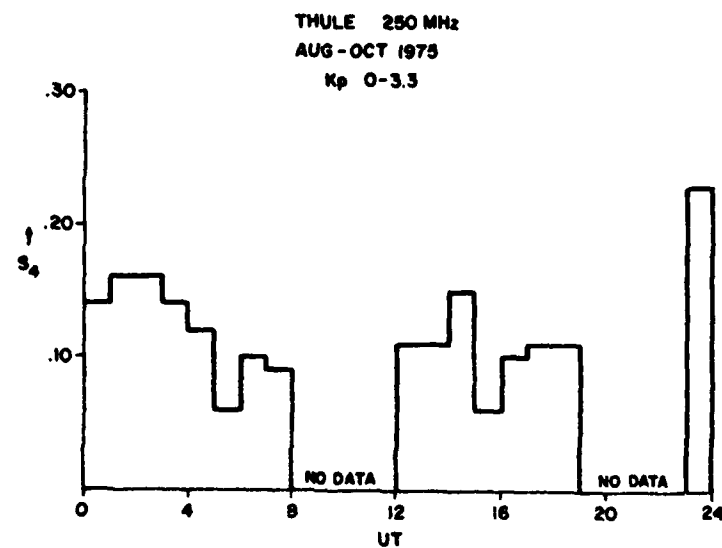


Figure 7b. Average value of Intensity scintillation Index ( $S_4$ ) at 250 MHz observed at Thule for magnetically quiet conditions during Aug-Oct, 1975.

## Coordinated measurements of low-energy electron precipitation and scintillations/TEC in the auroral oval

Sunanda Basu, Eileen MacKenzie, and Santimay Basu

Emmanuel College

H. C. Carlson, D. A. Hardy, and F. J. Rich

Air Force Geophysics Laboratory

R. C. Livingston

SRI International

(Received November 7, 1982; accepted April 20, 1983.)

A case study of coordinated observations of low-energy ( $< 500$  eV) electron precipitation in the auroral oval from DMSP F2 and phase and amplitude scintillations from Goose Bay, using a geostationary satellite transmitting at 244 MHz, is presented. The precipitation event took place during the expansion phase of an intense evening substorm, when the equatorward boundary of the diffuse aurora reached 59° invariant latitude. Particularly large phase scintillations ( $> 10$  radians for fluctuation frequencies  $> 0.0067$  Hz) were found to be well correlated with intense fluxes ( $> 10^4$  particles  $(\text{cm}^2 \text{ s sr})^{-1}$ ) of precipitated low-energy electrons. Total electron content and magnetometer measurements indicate that the onset of the precipitation event was about 10 min prior to the DMSP pass. Within this time scale, the ionization generated in the *F* region could reach the topside so that the thermal sensor on board the DMSP satellite was able to measure a factor of 2-3 density enhancement at 840 km. The latitudinal width of these density structures is consistent with that of *F* region blobs observed at Chatanika. The gradient scale length measured in the topside was only 30 km, which was probably responsible for the fast growth rate of the scintillation-producing irregularities. The phase to amplitude scintillation ratio changed rather drastically compared to quiet magnetic times, however, implying that increased convection velocities during these magnetic disturbances were partially responsible for the enhanced phase scintillation.

### 1. INTRODUCTION

The ubiquitous nature of high-latitude irregularities has been well established by measurements employing a variety of techniques including scintillations [Basu and Aarons, 1980; Aarons *et al.*, 1981; Rino and Matthews, 1980] and in situ sampling of electron density irregularities [Dyson, 1969; Sagalyn *et al.*, 1974; Clark and Raitt, 1976; Basu *et al.*, 1981] and electric fields [Maynard and Heppner, 1970; Kelley and Mozer, 1972]. Recently, Kelley *et al.* [1982] have proposed that soft-particle precipitation at the poleward edge of the auroral oval is the primary source of the structured *F* region plasma in the auroral ionosphere. They further point out that

transport of these irregularities augmented by plasma instabilities gives rise to the observed irregularity distribution throughout the polar cap and auroral oval regions. Evidence for transport was obtained from the measurements of Vickrey *et al.* [1980], who showed that the large-scale irregularities ( $\geq 10$  km) or plasma "blobs" observed with the Chatanika radar convect with the background field and, because of their very long lifetimes [Vickrey and Kelley, 1982], can be transported to great distances from where they were produced.

It is the object of this paper to provide a case study of the formation of a plasma blob by low-energy ( $< 500$  eV) electron precipitation near the equatorward edge of the auroral oval during the expansion phase of an intense evening substorm and to describe the associated propagation effects. While the precipitation of such soft electron fluxes at the pole-

Copyright 1983 by the American Geophysical Union

Paper number 3S0630  
0048-6604/83/0035-0630\$08.00

The U.S. Government is authorized to reproduce and sell this report. Permission for further reproduction by others must be obtained from the copyright owner.

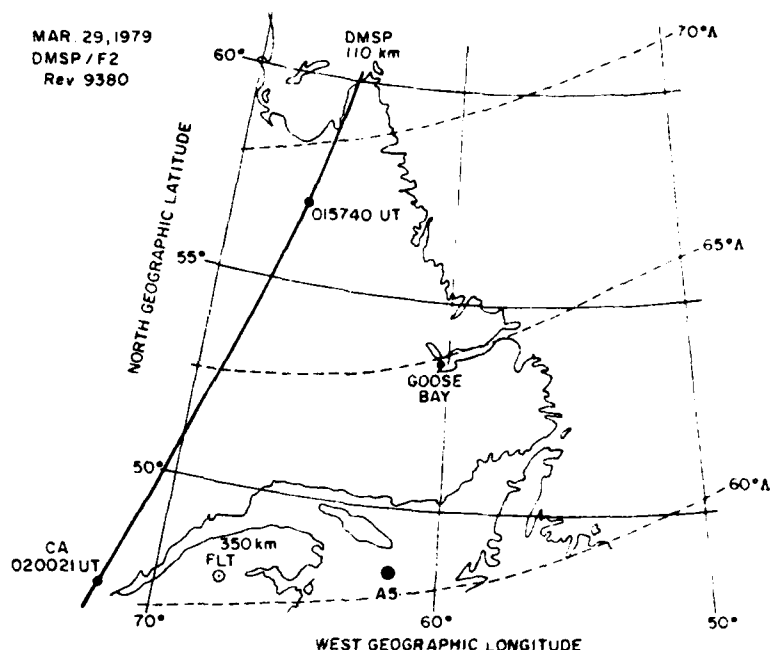


Fig. 1. The DMSP/F2 satellite track projected along the magnetic field line to 110 km for orbit 9380, from which particle data was obtained for the March 29, 1979, study. This track is just 3° to the west of the Fleetsat 350 km subionospheric intersection. The ATS 5 subionospheric intersection is also shown.

ward edge of the auroral oval is well documented in the literature (cf. *Fejer and Kelley [1980], Kelley et al. [1982]*, and references therein), the existence of such intense fluxes rather deep within the plasma-sheet is less well known. *Tanskanen et al. [1981]*, using DMSP data, were the first to discuss such events in detail, although *Deehr et al. [1976]* did note their existence earlier. We shall show that such a precipitation event monitored by the DMSP satellite also caused a concomitant increase of the background thermal density by a factor of 2–3 at an altitude of 820 km, bounded by regions of sharp plasma density gradients. Coordinated magnetometer and total electron content measurements showed that the precipitation event was a long-lasting one ( $\sim 10$  min), which enabled the effect of the precipitation in the *F* region to be transmitted to the topside. We also provide evidence that medium scale irregularities ( $\sim 1$  km and larger) which were responsible for causing phase and amplitude scintillations, intensified within a very short time scale ( $\sim 1$  min), thereby suggesting that plasma instabilities could grow on the sharp topside gradients.

It is of some interest to note that the phase and amplitude scintillations for this study were obtained at Goose Bay, Labrador, by utilizing the 244 MHz

transmissions of the Fleetsat satellite parked at  $100^\circ\text{W}$ . The method of obtaining phase scintillation measurements using a geostationary source, as well as the diurnal and seasonal statistics, have been dealt with in a recent report [*Basu et al., 1982*] and will not be repeated here. The important point to emphasize is that the scale-length coverage of phase scintillations for a fixed detrend interval is dependent on the E-W drift velocity. This is contrary to the situation when an orbiting satellite, such as Wideband, is the source of the transmissions. In such cases, particularly at high latitudes, the scale-length coverage is dictated by the effective velocity of the satellite [*Fremouw et al., 1978*] and is generally independent of the ionospheric drift. We shall show later that enhanced ionospheric drifts during the substorm under study contributed to a relatively larger increase of the phase scintillations as compared to the intensity scintillations.

## 2. DMSP ENERGETIC PARTICLE AND THERMAL DENSITY DATA

The particle data used are those obtained from DMSP-F2 satellite in the evening MLT sector during a period of substorm activity. DMSP F2 is a three-axis stabilized satellite in a nearly sun-synchronous,

circular orbit at an altitude of 820 km. The orbital period is 101 min; the nominal inclination is  $99.1^\circ$ . At launch the orbit was centered near the 0700–1900 meridian, but it is subject to a very slow precessional drift toward later local times, as is the case in the present situation. The specific satellite orbit under study, 9380 ( $\sim 0200$  UT, March 29, 1979), when mapped to 110 km altitude along magnetic field lines, passed just  $3^\circ$  to the west of the Fleetsat ionospheric intersection point (intersection between the 350 km ionospheric height and the propagation path from Goose Bay to Fleetsat), as shown in Figure 1. Since visual auroras occur at 110 km, the DMSP track is routinely mapped to 110-km height, whereas a 350-km intersection is more relevant when *F* region propagation effects are being studied, such as with Fleetsat transmissions.

The DMSP pass occurred during a period of southward turning of the interplanetary magnetic field ( $B_z$ , negative) as shown in Figure 2, which caused a series of substorms as observed from the auroral electrojet index (*AE*) data. The *AE* index looks rather smooth as the hourly values have been plotted, in keeping with the resolution of the  $B_z$  data. The middle panel of Figure 2 shows that the planetary index *Kp* was 6 at the time of the pass. On a more local level, the DMSP pass occurred about 8 min after the onset of a 400  $\gamma$  negative bay, which started at 0152 UT on the Goose Bay magnetogram shown in Figure 3. Unfortunately, the auroral photographs corresponding to this orbit are not available. However, it is expected that at such disturbed times, the statistical auroral oval should be in the vicinity of the Fleetsat intersection point [Basu et al., 1982].

The DMSP particle detectors have been described in detail by Hardy et al. [1979]. Briefly, the particle detector on DMSP/F2 consists of two curved-plate electrostatic analyzers that measure the fluxes of electrons in 16 energy channels between 50 eV and 20 keV once per second. The apertures of the analyzers always face toward local vertical so that at auroral and polar cap latitudes they detect precipitating rather than backscattered and trapped electrons. One analyzer covers the energy range from 50 eV to 1 keV with a geometric factor of  $4 \times 10^{-4}$  cm<sup>2</sup> sr and a  $\Delta E/E$  of 10%. The other analyzer covers the energy range from 1 to 20 keV with a geometric factor of  $10^{-3}$  cm<sup>2</sup> sr and a  $\Delta E/E$  of 12%. The large geometric factors insure that the flux level for the electrons in the diffuse aurora is well above the detector's sensitivity [Tanskanen et al., 1981].

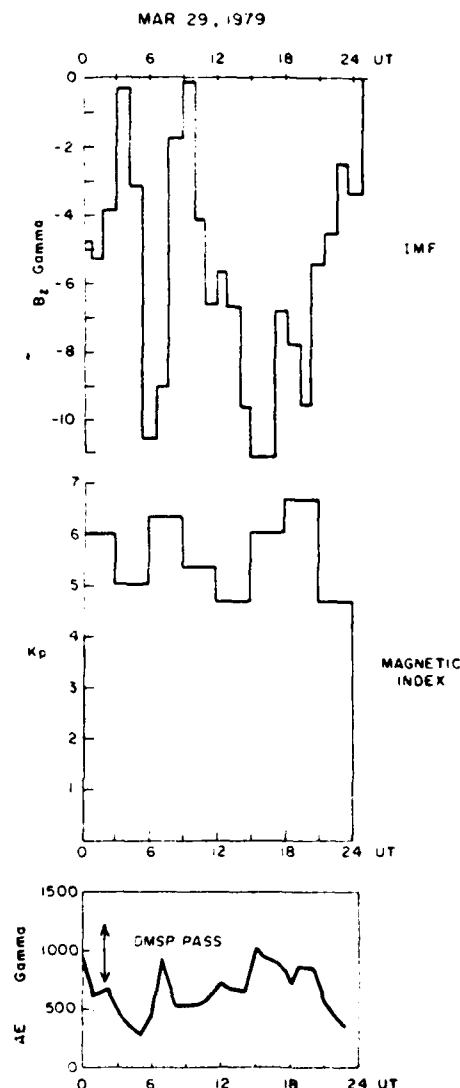


Fig. 2. The interplanetary magnetic field  $B_z$ , planetary magnetic index *Kp*, and auroral electrojet index *AE* data for March 29, 1979. The time of the DMSP/F2 pass is indicated.

The energetic-electron measurements over the evening portion of the auroral oval for this orbit are shown in Figure 4, and the point of closest approach to the latitude of the Fleetsat intersection at 0200:21 UT is identified as CA. In this figure, the particle data are plotted as JTOT, the directional integral flux (cm<sup>2</sup> s sr)<sup>-1</sup> in the bottom panel; JETOT, the directional energy flux [keV(cm<sup>2</sup> s sr)<sup>-1</sup>] on the middle panel; and EAVE, the average energy in keV in the top panel. The scale for EAVE is linear. These quantities are plotted as functions of universal time (UT), the geographic coordinates of the satellite

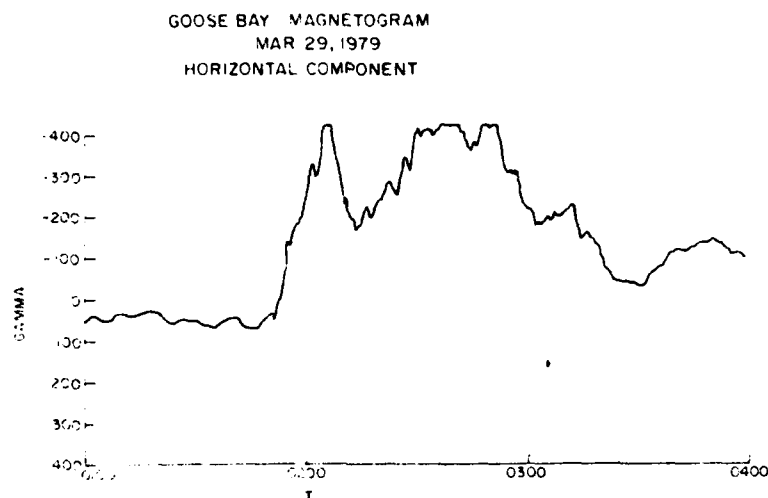


Fig. 3. The horizontal component of the Goose Bay magnetogram on March 29, 1979, showing a 400  $\gamma$  negative bay starting at 0152 UT.

(GLAT and GLON), the corrected geomagnetic latitude [Whalen, 1970] of the satellite mapped along the magnetic field line to 110 km (MLAT) and the magnetic local time (MLT). The poleward and equatorward boundaries of the oval were defined on the basis of JTOT exceeding the level of the polar rain or background, respectively [Gussenhoven *et al.*, 1981]. On this basis the equatorward boundary of the aurora in the evening sector is at  $59^\circ\Lambda$  (at the 110 km level), which for  $K_p = 6$  matches well the empirical relationship  $\Lambda_{CGM} = 71.2 - 2.1 K_p$  developed by Gussenhoven *et al.* [1981] for the northern hemisphere evening boundary. The difference between the corrected geomagnetic latitude  $\Lambda_{CGM}$  and invariant latitude  $\Lambda$  is less than  $0.5^\circ$  in this longitude sector (J. A. Whalen, private communication, 1982).

From Figure 4, we see that the Fleetsat intersection is within the evening precipitation region. Moreover, from the nature of the average energy of the precipitating fluxes ( $\sim 4$  keV), we infer that the intersection point is within the region of the diffuse aurora. In the absence of simultaneous DMSP photographs, it is difficult to establish the exact width of the diffuse aurora, but based on the shape of the electron spectra and their average energy, it is likely that the entire latitude range spanned by the satellite between 0159 and 0201 UT can be considered to be within the diffuse auroral precipitation region. Within that interval, at least two relatively narrow regions of significant integral number flux enhancements are observed in conjunction with decreases of the average energy (0200 : 15 and 0200 : 40 UT). The

electron number flux and the energy flux show significant fluctuation in the two regions, reaching values as high as  $\sim 8 \times 10^9$  electrons  $(\text{cm}^2 \text{ s sr})^{-1}$  and  $\sim 3 \times 10^9$  keV  $(\text{cm}^2 \text{ s sr})^{-1}$ , respectively. The average energy of this particle population is  $\sim 400$  eV for the first region. It can also be seen from Figure 4 that the average energy is  $\sim 1$  keV for the second region. The surrounding regions have typical energies of the order of 3 keV. We shall further discuss the particle characteristics near the first region (0200 : 15 UT) of low average energy, which is closest to the Fleetsat intersection point.

To compare the particle spectra in the vicinity of the point of closest approach with that in the diffuse aurora, we present two plots each showing 10 differential energy spectra for 10 successive seconds starting at 0159 : 50 and 0200 : 10 in Figures 5a and 5b, respectively. The first one (Figure 5a, which actually has nine spectra, the one for 0159 : 52 UT being unavailable) obtained poleward of the Fleetsat intersection, when taken in conjunction with the relevant portion of Figure 4, shows smooth variations in JTOT, JETOT, and EAVE and a quasi-thermal type of spectrum. The EAVE reaches a maximum value of 5 keV at 0159 : 52 UT. Quite a drastic change in spectral shape occurs in Figure 5b, particularly during 0200 : 10–0200 : 16 UT. There is a large increase in flux at the lower energies with a corresponding decrease in flux at the higher energies leading to a severe reduction in the average energy as mentioned earlier. Further, low-energy peaks in the range 100–600 eV are found to be superimposed on

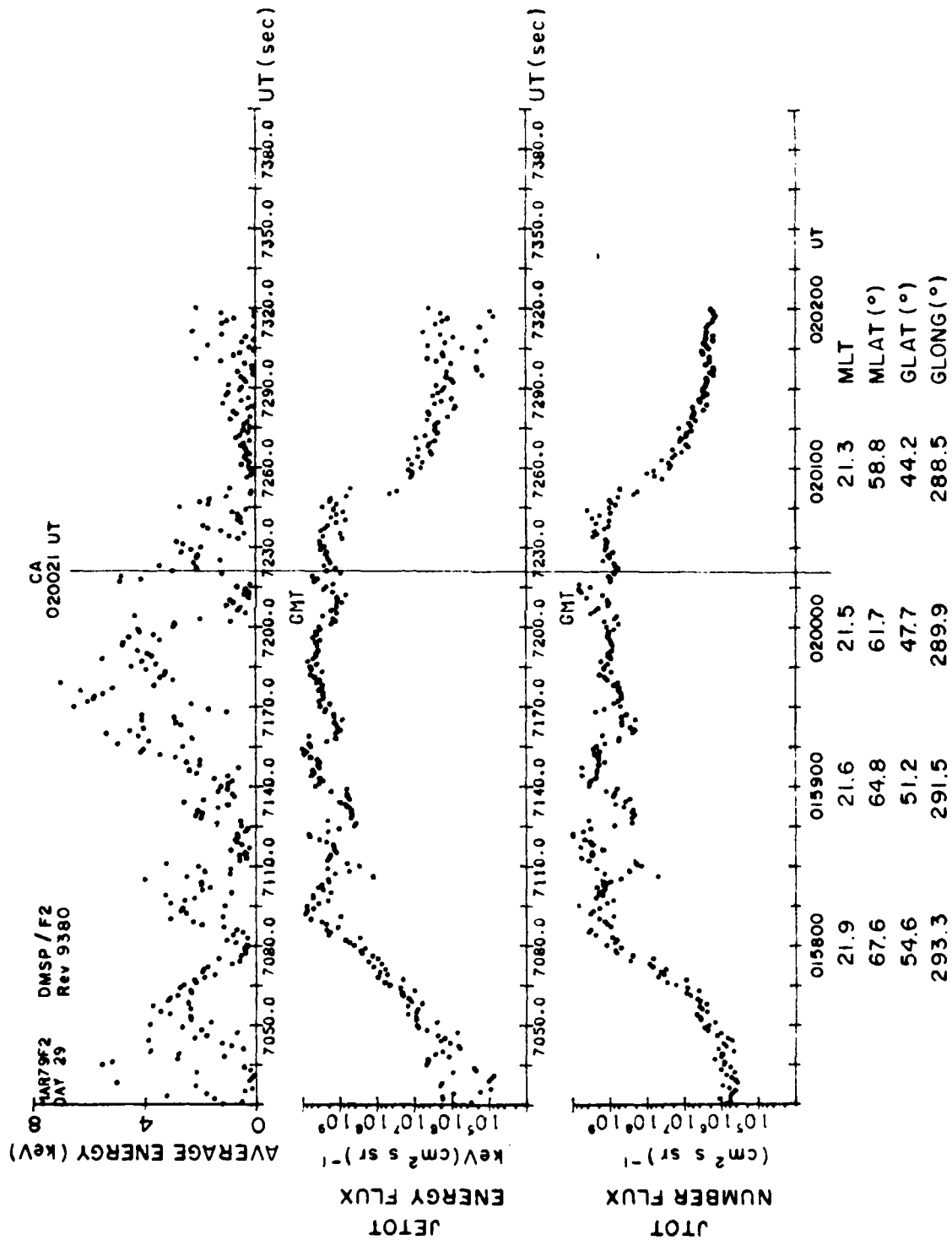


Fig. 4. View of the evening auroral oval precipitation region for orbit 9380 on March 29, 1979 (0157 0202 UT). Point of closest approach to the auroral oval intersection latitude is marked as CA at 0200:21 UT.

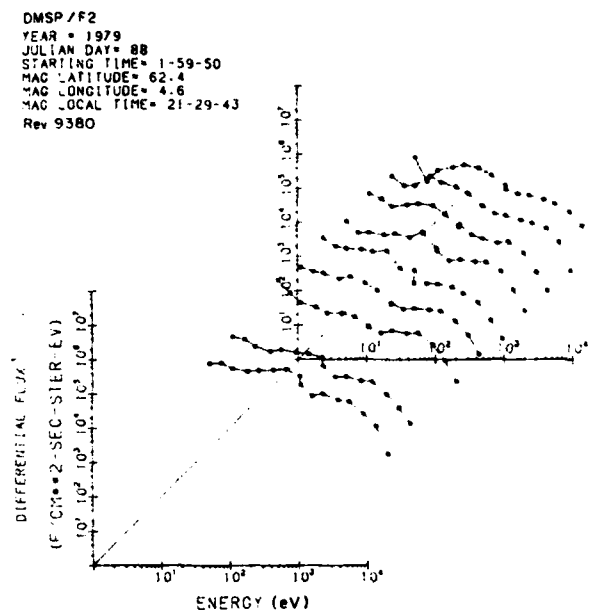


Fig. 5a. Ten differential energy spectra for ten successive seconds of DMSP precipitating electron data taken from orbit 9380 on March 29, 1979, poleward of the Fleetsat intersection between 0159:50 and 0159:59 UT showing smooth variations in JTOT, JETOT, and EAVE and a quasi-thermal spectrum (Note that spectrum for 0159:52 UT is missing.)

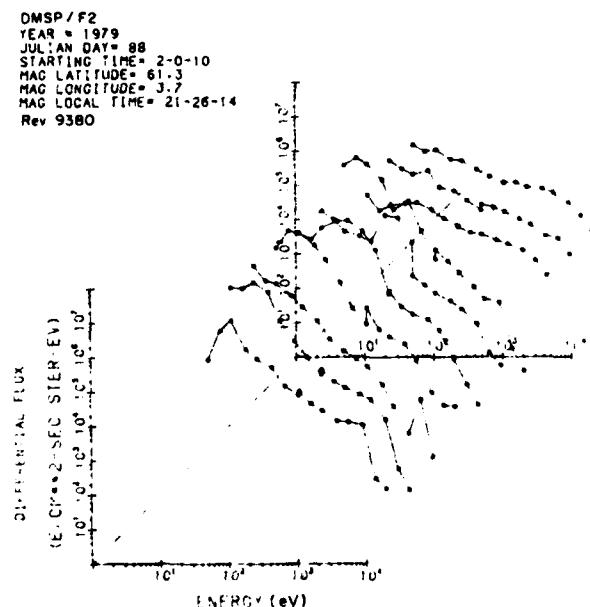


Fig. 5b. Same as in Figure 5a but showing decrease in high energy flux and increase in lower energies between 0200:10 and 0200:19 UT.

the basically quasi-thermal background distribution. Such spectra were also shown by *Tanskanen et al.* [1981] to exist in a similar region of the nighttime auroral oval.

Figures 5c and 5d shed further light on the differences between spectra shown in Figures 5a and 5b. In Figure 5c the single differential flux spectrum from Figure 5a corresponding to 0159:50 UT is replotted. In addition, histograms are superimposed to show the percentage of the total number flux  $R'$  and total energy flux  $R$  that is being carried within each channel of the detector. The plot shows that outside the region of low-energy electron enhancement, most of the flux and the vast majority of the energy in the electrons are being carried by particles with energies exceeding 1 keV, i.e., particles that would produce effects primarily in the E layer of the ionosphere [Whalen, 1981]. By contrast, the spectrum in Figure 5d for the first enhancement region indicates that the electrons in the part of the spectrum peaked at  $\sim 400$  eV are now carrying most of the particle and energy flux and thus will have their primary effect in the F region ionosphere. The number flux into the ionosphere at this time is as large as  $8 \times 10^9$  electrons

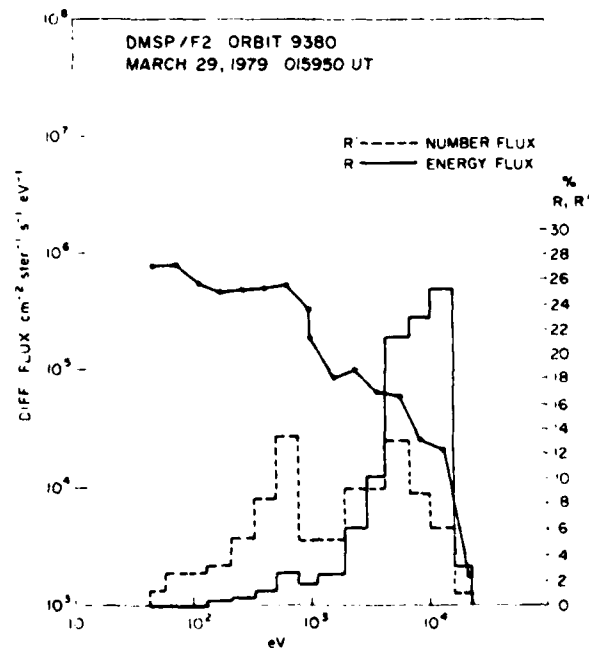


Fig. 5c. One-second differential electron flux at 0159:50 UT on March 29, 1979, to the north of the Fleetsat intersection point.  $R$  (solid line) is the relative directional energy flux per energy channel.  $R'$  (dashed line) is the relative directional number flux per energy channel.



( $\text{cm}^2 \text{ s sr}^{-1}$ ), carrying an energy of 5 ergs ( $\text{cm}^2 \text{ s sr}^{-1}$ ). Ninety percent of this flux is composed of electrons with energies  $< 500 \text{ eV}$  and 65% with energies  $< 300 \text{ eV}$ .

To study the latitudinal variation of this low-energy component, we show in the lower panel of Figure 6a a plot of the differential flux of the lowest energy channel, namely, 47 eV, as a function of the position of the satellite in corrected geomagnetic coordinates. (The next three higher energy channels, ranging in energy from 73 eV to 173 eV, show a similar latitudinal pattern and are not shown here.) The flux values are obtained once per second, i.e., at a spatial resolution of approximately 7 km. On the upper panel, we display the thermal ion density data obtained at 820 km altitude by the planar retarding potential analyzer on board the DMSP/F2 satellite described by Smiddy *et al.* [1978] and by Rich *et al.* [1980]. The ion densities shown in this figure have been plotted at the rate of one point per second, which is the same resolution as that of the lower energy electron data. Figure 6b, on the other hand, shows the data points plotted at their highest resolu-

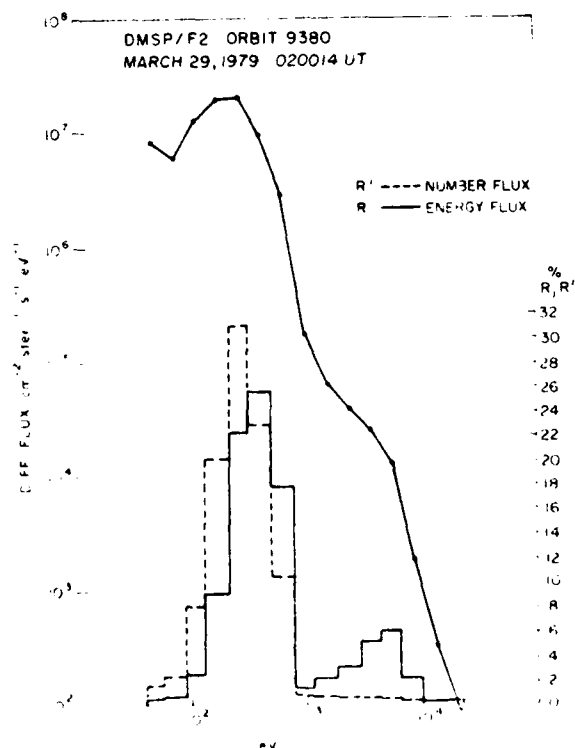


Fig. 5d. One-second differential electron flux at 020014 UT on March 29, 1979, obtained within the soft precipitation region near the FleetSat intersection point. Same format as in Figure 5c.

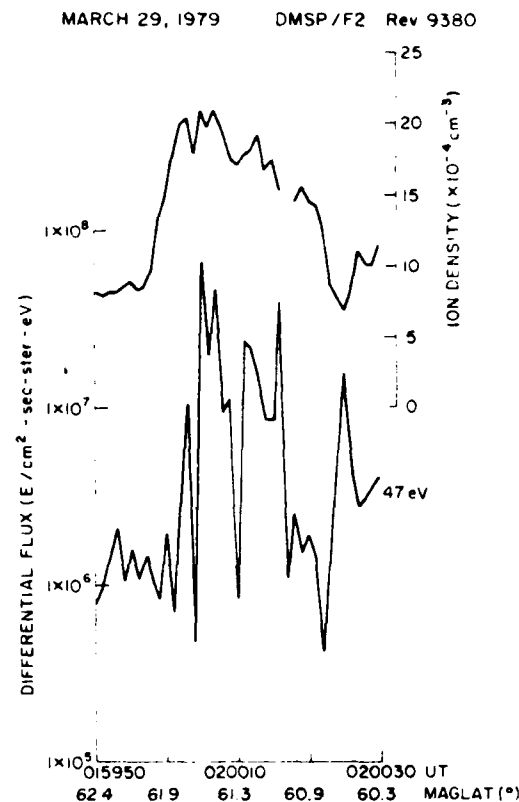


Fig. 6a. Simultaneous measurements of the differential flux at 47 eV and ion density at 840 km from DMSP/F2 for orbit 9380 on March 29, 1979. Note the sharp density gradients associated with the soft-particle precipitation.

tion, namely, seven per second, i.e., at a spatial separation of approximately 1 km since the velocity of the spacecraft is  $7 \text{ km s}^{-1}$ . This enables us to observe the in situ density structure existing at 820 km at scale lengths  $\sim 1 \text{ km}$ , which is responsible for the enhanced scintillations to be discussed in the next section. It should be mentioned here that although the absolute density measurements of the DMSP sensor may only be accurate to 25–50% (with the measured values being usually on the high side), the relative variation in density is obtained with an accuracy of 2%. Thus an accurate idea can be obtained regarding small-scale density structure and gradients.

The ion density shows a factor of  $\sim 3$  enhancement in association with the low-energy flux increase over a latitudinal interval of 61° to 61.8°. The width of the density enhancement is somewhat larger, however, extending both poleward and equatorward of the flux increase by 0.2° on each side. This is the first time that a comparison has been made between data

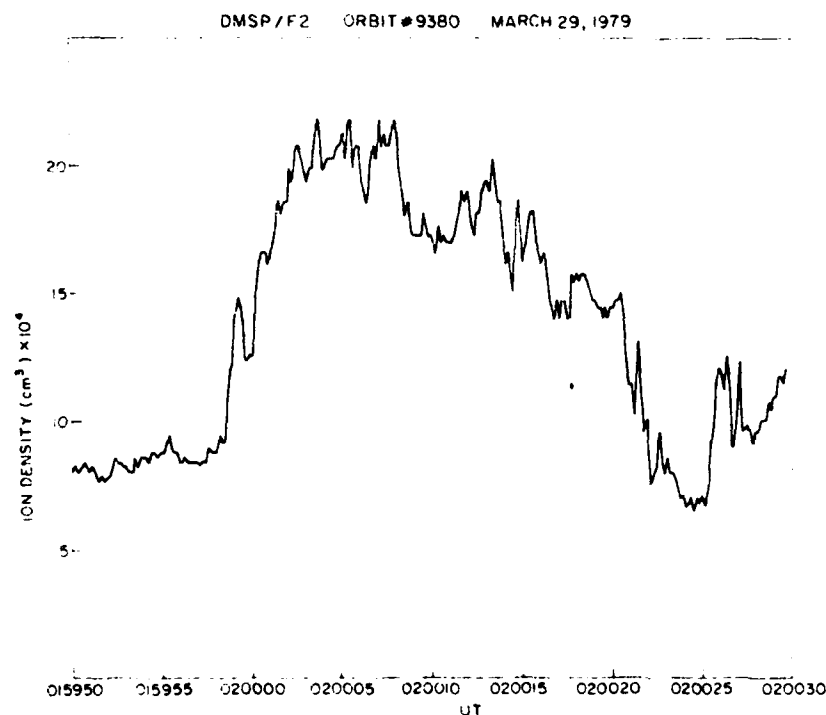


Fig. 6b. High spatial resolution ( $\sim 1$  km) measurements of the ion density from DMSP for orbit 9380 during the precipitation event shown in Figure 6a.

obtained with the particle detectors and the thermal sensors on the DMSP satellite. The width of the density enhancement is reminiscent of the *F* region blobs observed at Chatanika [Vickrey *et al.*, 1980]. Rather steep density gradients are observed on both the poleward and equatorward edges of the enhancement. The implication of these gradients and the time scale needed to observe the topside density enhancements will be discussed in section 4.

### 3. TEC PHASE AND AMPLITUDE SCINTILLATIONS

Measurements of total electron content (TEC) from Goose Bay obtained using the polarimeter technique and transmissions from ATS 5 at 137 MHz and shown in Figure 7 exhibit significant enhancement of TEC at 0152 UT, which is about 8 min prior to the passage of the DMSP satellite through the same latitude region. These measurements refer to a subionospheric position of 48.34°N and 61.91°W.

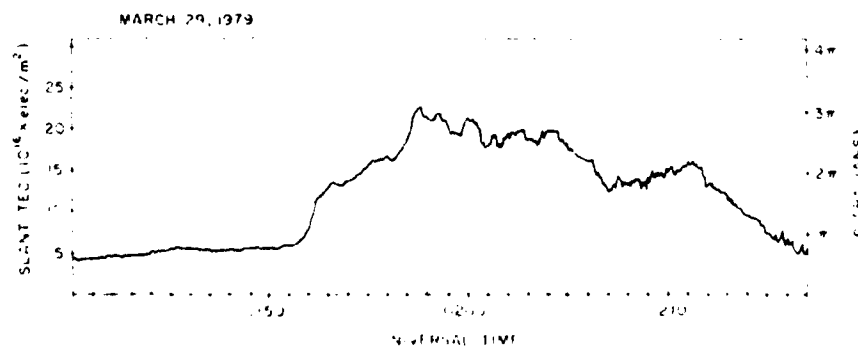


Fig. 7. Total electron content (TEC) measurements from the ATS 5 satellite measured at Goose Bay, Labrador, on March 29, 1979, showing onset of TEC increase at approximately 0152 UT.

GOOSE BAY MAR. 29, 1979

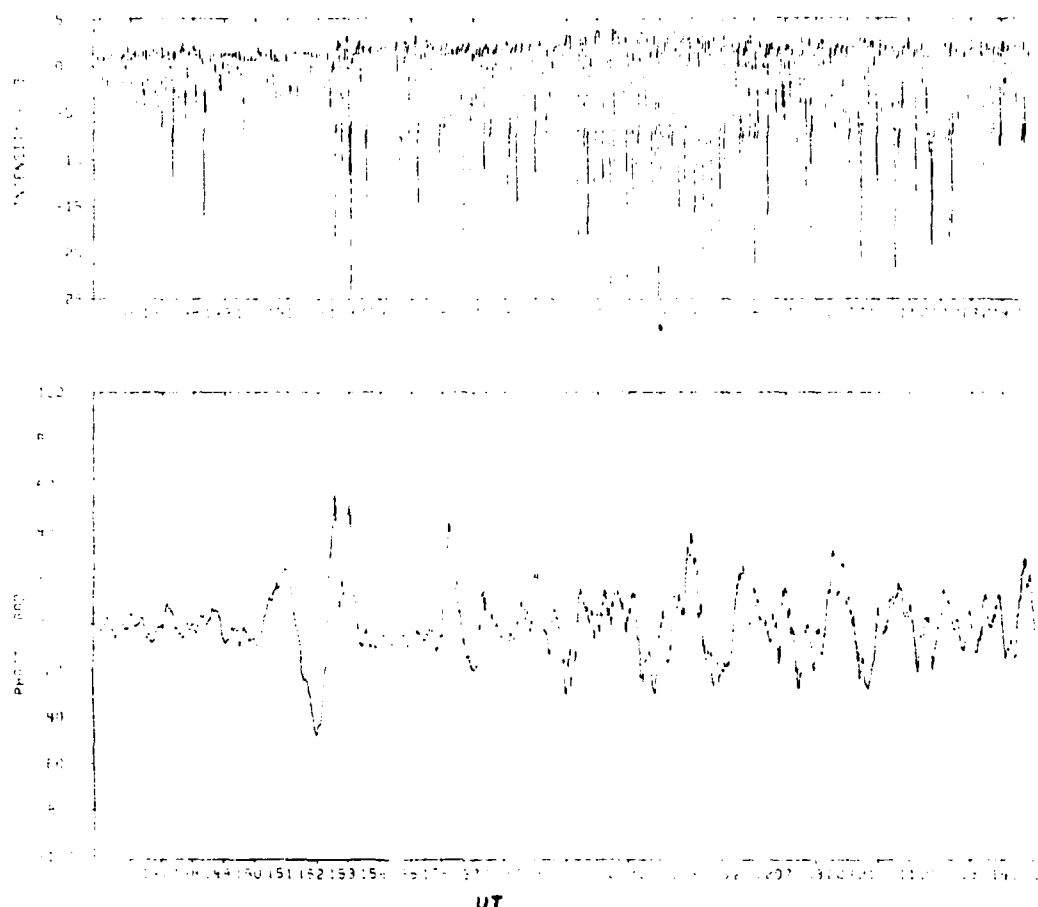


Fig. 8. Time record of 244 MHz phase and amplitude fluctuations, detrended with a filter cutoff of 0.0067 Hz, of the Fleetsat signal at Goose Bay on March 29, 1979.

which is close to the latitude of the equatorward edge of the density enhancement discussed in the last section. It is important to note that the TEC enhancement is observed at the time of onset of a negative bay in the Goose Bay magnetogram, as shown in Figure 3. The TEC enhancement reaches its peak value at 0158 UT, which is very close to the time of the DMSP pass. It is also necessary to note that the polarimeter observations were made at an elevation angle of  $30^\circ$ . Thus the vertical content increase is approximately a factor of 2 less than that shown in Figure 7 and amounts to 10 TEC units (i.e.,  $10 \times 10^{12} \text{ el cm}^{-2}$ ).

The time record of phase and amplitude fluctuations of the Fleetsat signal at 244 MHz after detrending with a filter cutoff of 0.0067 Hz for the same period, shown in Figure 8, exhibits a large in-

crease in both quantities at almost exactly the time of the TEC increase registered by ATS 5. A similar situation was discussed by Aarons [1976] for the October 31, 1972, storm. Since the ionospheric intersection points of ATS 5 and Fleetsat are separated by 6° of longitude, it is obvious that low-energy electrons were precipitating in the vicinity of 60°A over a relatively wide swath of longitudes. The almost simultaneous response of the magnetogram (which is a signature of ionospheric currents and their motion) and phase and amplitude scintillations (which respond to ionospheric irregularities) to the particle influx raises important questions regarding irregularity generation mechanisms and growth times for large-amplitude irregularities. We shall discuss some of these questions in the next section.

The time history of amplitude and phase scintil-

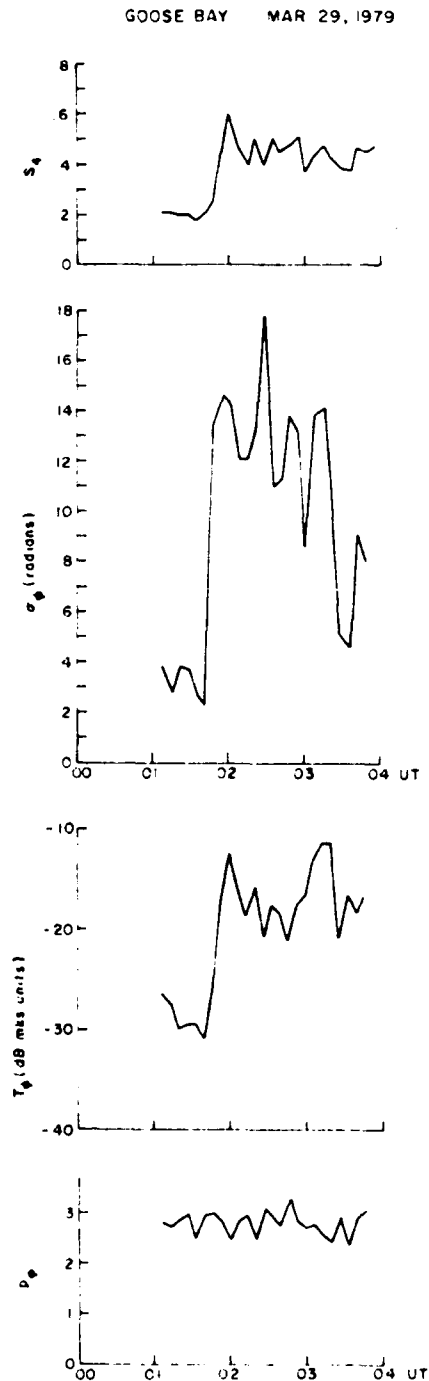


Fig. 9. The intensity and phase scintillation parameters  $S_4$ ,  $\sigma_\phi$ ,  $T_\phi$ , and  $p_\phi$  of the 244-MHz Fleetsat signal at Goose Bay on March 29, 1979 (0100–0400 UT). The parameters are explained in the text.

lation indices,  $S_4$  and  $\sigma_\phi$ , during a 3-hour period commencing at 0100 UT on March 29, 1979, is shown in Figure 9. Corresponding phase spectral strength parameter  $T_\phi$  and slope  $p_\phi$ , as defined by Fremouw *et al.* [1978], are shown in the lower two panels. The rather dramatic increase of  $\sigma_\phi$  at 0150 UT from 2 to 14 radians is accompanied by a three-fold increase in amplitude scintillation index from 0.2 to 0.6. If we assume that the above range of  $S_4$  index is approximately within the weak scatter limit, then we can study the variation of the  $\sigma_\phi/S_4$  ratio prior to 0150 UT and thereafter. While the average value of this ratio is 14 before the onset of severe phase scintillations, the average doubles to 28 between 0152 UT and 0325 UT. The ratio is given by [Rino, 1979; Fremouw, 1980]

$$\frac{\sigma_\phi^2}{S_4^2} = \frac{1}{(v - \frac{1}{2})C(v)} \frac{G}{F} \frac{(V_e \tau_c)^{2v-1}}{(\lambda z \sec \theta 4\pi)^{v-1/2}}$$

where

- $v = p_\phi/2$ ,  $p_\phi$  phase spectral index;
- $C(v)$  a constant dependent on  $v$  only ( $= 16\pi^3$  for  $v = 1.5$ );
- $G, F$  geometrical factors for phase and amplitude scintillations;
- $V_e$  effective velocity at which the density contours of equal correlation in the ionosphere cuts across the radio propagation path;
- $\tau_c$  detrend period (i.e., reciprocal of filter cutoff frequency, which is 0.0067 Hz in this case);
- $\lambda$  radio wavelength;
- $z$  effective "reduced height" of the irregularities [Briqas and Parkin, 1963];
- $\theta$  incidence angle.

In the above expression, since the geometry remains constant for geostationary satellite observations and if we make the assumption that  $v$  remains constant and is approximately 1.5 (as may be noted from panel 4 of Figure 9), then we find that  $\sigma_\phi/S_4$  is directly proportional to  $V_e$  for a constant detrend period  $\tau_c$ . Chatanika drift measurements during substorms have shown large increases in the E-W ion drifts (i.e., of the meridional electric field) at the same invariant latitudes as these measurements [Foster *et al.*, 1981]. Thus the greater relative enhancement of phase scintillations, when compared to amplitude scintillations, is probably caused by larger E-W drifts in response to enhanced magnetospheric electric fields during substorms.

Another method of investigating the variation of the effective drift velocity is to study the spectra of

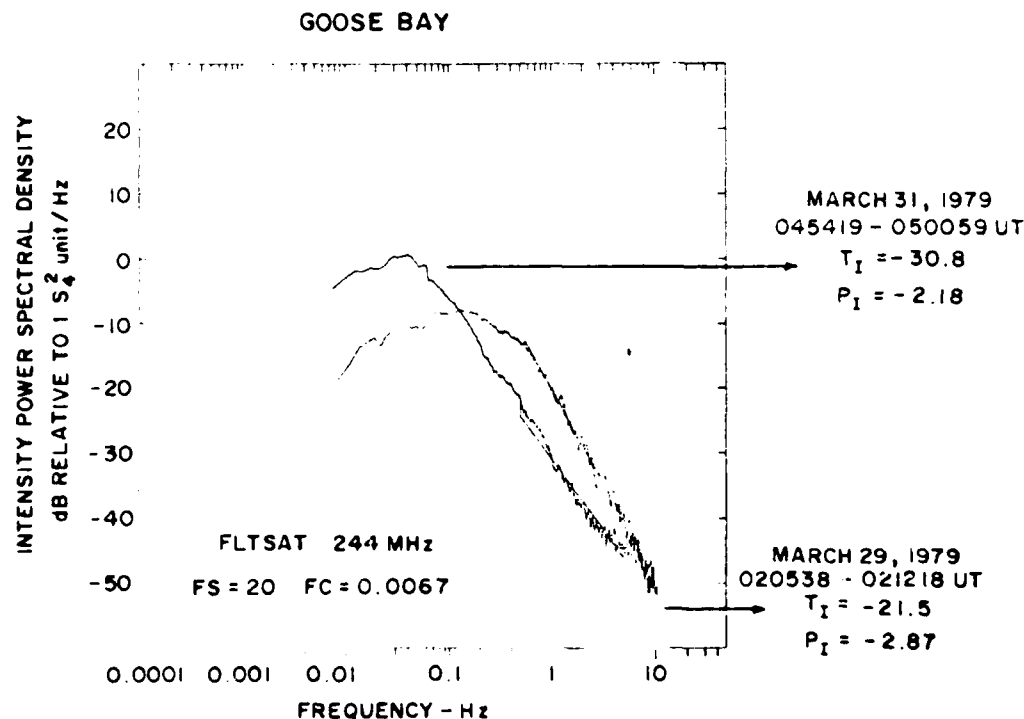


Fig. 10. Power spectra of amplitude scintillations on March 29, 1979, between 0205:38 and 0212:18 UT with  $S_4 = 0.46$  and  $\sigma_p = 14$  rad and on March 31, 1979, between 0454:19 and 0500:59 UT with  $S_4 = 0.51$  and  $\sigma_p = 2.5$  rad, showing very different values of the Fresnel frequency and thereby indicating an increase in the drift velocity during magnetic storms. (Note that  $p_p$  is determined by linear least squares fit to the spectrum between 0.5 and 50 Hz.)

amplitude fluctuations. It is well known that for weak amplitude fluctuations ( $S_4 \leq 0.5$ ), the roll-off point on the spectrum (i.e., the point at which the falloff of power spectral densities begins) can be related to the Fresnel frequency,  $f_F = V_e(\pi\lambda z)^{-1/2}$ , where  $V_e$  is the effective ionospheric drift,  $\lambda$  is the radio wavelength, and  $z$  is the distance between the ionospheric irregularities and the receiver [Singleton, 1974]. Thus if the viewing geometry remains constant, then the Fresnel frequency is directly proportional to the ionospheric drift velocity. In Figure 10, we show the amplitude spectrum obtained on March 29, 1979, at 0205:38 UT during the substorm event under study. The amplitude spectrum obtained on March 31, 1979, at 0454:19 UT, when magnetic activity had subsided, is superposed for comparison. The two spectra correspond to very similar levels of the  $S_4$  index. The average  $\sigma_p/S_4$  ratio is 4 for the March 31 data shown in Figure 10 and for contiguous data samples, as discussed in section 5 of the work of Basu *et al.* [1982]. We have already mentioned that the  $\sigma_p/S_4$  ratio of the March 29 data

shown in Figure 10 is 28. Thus there is a factor of 7 difference in the  $\sigma_p/S_4$  ratios corresponding to the two amplitude spectra shown in Figure 10. We do indeed find a great difference in the spectral character of the two samples. The March 31 sample has a Fresnel frequency of 0.04 Hz, whereas the March 29 data shows a roll-off between 0.2 to 0.3 Hz, a factor of 5–7 higher than the former. In view of the direct proportionality of the Fresnel frequency to the drift velocity, we have further evidence that increased drifts contributed to the increase in the  $\sigma_p/S_4$  ratio during the magnetic disturbances observed on March 29, 1979.

Before concluding this section, we wish to comment on some subtle differences between the two spectra shown in Figure 10 from the propagation point of view. The major differences between the two spectra are related to the high-frequency roll-off rates and a somewhat broader Fresnel maximum in the March 29 spectrum. The depression of the power spectral density in the low-frequency region of the March 29 spectrum relative to the March 31 spec-

trum is, in our opinion, apparent rather than real. In contrast to the March 31 spectrum, the March 29 spectrum did not achieve the noise floor level at 10 Hz, and, as a result, the alignment of the power spectral densities at 10 Hz for the two spectra in Figure 10 caused the differences at the low-frequency end. The high-frequency roll-off rates and broader Fresnel maximum as depicted by the March 29 spectrum are usually obtained when strong scattering is encountered [Basu and Whitney, 1983]. The fact that these features are present in the sample having an  $S_4$  index of 0.5 and, therefore, corresponding to the weak scatter domain, may be explained as follows. The higher roll-off rate may be attributed to higher spectral index of the irregularities of electron density in the ionosphere on March 29 as compared to March 31. Further, the broadening of the Fresnel maximum on March 29 may be a result of the irregularities moving with a distributed velocity rather than with a uniform motion [Lotova, 1981]. Such velocity dispersion is known to occur in the solar wind [Lotova and Chashei, 1981] and may have a counterpart in the ionosphere, particularly on days with large drift velocities such as March 29, 1979.

#### 4. DISCUSSIONS

The unique feature of the case study described in sections 2 and 3 stems from the fact that the low-energy electron precipitation was intense enough to cause (1) a large topside density enhancement, which could be measured by the DMSP satellite in a time scale of 10 min, and (2) an integrated effect throughout the  $F$  region, which was registered by the polarimeter. The only other report on "the birth of a blob" in a similar time scale, by Muldrew and Vickrey [1982], described a small enhancement of 15% in the  $F$  region peak density in response to a possible keV electron precipitation. Most earlier model studies, however, such as those by Roble and Rees [1977] and Whitteker [1977], have shown that the time scale for density increases to take place in the  $F$  region is of the order of 30 min to 1 hour. The major difference between these earlier model studies and the present case is in the magnitude of the number flux and energy flux into the ionosphere. Roble and Rees [1977] consider a flux of  $3.12 \times 10^9$  electrons ( $\text{cm}^2 \text{ s}^{-1}$ ) of mean energy 200 eV and an energy input of 1 erg ( $\text{cm}^2 \text{ s}^{-1}$ ) into the ionosphere. Whitteker [1977] uses an energy input that is only 0.28 ergs ( $\text{cm}^2 \text{ s}^{-1}$ ). We have mentioned in conjunction with Figure 5d

that the number flux in the ionosphere during the particle precipitation event in this study is  $8 \times 10^9$  electrons ( $\text{cm}^2 \text{ s}^{-1}$ ) with an energy input of 5 ergs ( $\text{cm}^2 \text{ s}^{-1}$ ), a full 90% of the electrons having energy  $< 500$  eV. No pitch angle information is available from DMSP, but recent observations using the P78-1 satellite shows that such soft fluxes, which are embedded in the diffuse aurora, are usually confined to a half width of approximately  $40^\circ$  (D. A. Hardy, private communication, 1982). Hence we consider the total influx of particles to be  $8 \times 10^9$  electrons ( $\text{cm}^2 \text{ s}^{-1}$ ). Tanskanen et al. [1981] also provided evidence for the existence of such intense low-energy fluxes at the equatorward edge of the auroral oval during substorms. These were even seen on consecutive passes of the DMSP satellite.

We provide in this paragraph an order-of-magnitude estimate of the density enhancement that may be expected if a particle precipitation event of the above magnitude lasts for 10 min. The simplest order of magnitude estimate can be obtained by considering that if an energy flux of  $3 \times 10^{12}$  eV ( $\text{cm}^2 \text{ s}^{-1}$ ) or 5 ergs ( $\text{cm}^2 \text{ s}^{-1}$ ) is incident on the ionosphere in the region of the enhancement (as represented by Figure 5d) and the energy needed to produce an ion-electron pair is 35 eV [Rees, 1963], then one obtains 120 s as the time needed to produce a vertical TEC increase of 10 TEC units (as observed in Figure 7). If, further, one assumes that 50% of the  $\text{O}^+$  ions (which have the largest scattering cross section) are lost due to recombination [Whitteker, 1977], then a time scale less than 5 min is obtained. This is a lower bound on the time, since it is well known that if the incoming electrons have energies  $< 500$  eV, the above computation is not very realistic as the energy required to create an ion-electron pair is much larger than 35 eV used in the computations [Banks and Kockarts, 1973].

Mantas and Walker [1976] considered specifically the precipitation of soft electrons  $\leq 100$  eV into the ionosphere. They found that such incident fluxes are stopped in the altitude region between 300 and 400 km, where they deposit most of their energy. They considered various loss processes, including elastic backscattering, loss of degraded primaries and newly produced secondaries, and arrived at a figure of 1.71 for the electron thermalization rate per unit incident flux of monoenergetic electrons at 100 eV. Since 65% of the number flux shown in Figure 5d have energies less than 300 eV, we used the above thermalization rate to determine that  $1.4 \times 10^{10}$  el ( $\text{cm}^{-2}$ ) are pro-

duced per unit time. Thus a time of 700 s is necessary to buildup a content of 10 TEC units. This latter order-of-magnitude estimate is surprisingly close to the observed time of approximately 10 min required for the TEC enhancement.

It has been shown earlier that steep gradients were found at the boundaries of the enhanced density region. Both the poleward and equatorward edges have horizontal density gradient scale lengths as small as 30 km at the 820 km altitude of observations. The latitude of the equatorward boundary is in close proximity to the intersection latitudes of both the polarimeter and scintillation measurements. The phase and amplitude scintillations were found to intensify within a matter of 1–2 min of the onset of the TEC enhancement. If we consider the TEC increase to be a good indicator of the buildup of the soft-precipitation-induced gradient in the *F* region, then we can postulate a short growth time of 1–2 min for the generation of kilometer-scale irregularities.

It is unfortunate that no simultaneous electric field or field-aligned current measurement is available, which would have allowed us to distinguish between the current convective instability [Ossakow and Chaturvedi, 1979] and the  $\mathbf{E} \times \mathbf{B}$  instability [Simon, 1963; Linson and Workman, 1970] as the generation mechanism of the scintillation-producing irregularities. We have mentioned above that the scintillation and TEC measurements refer to the latitude of the equatorward edge. At this edge, the gradient is directed poleward and would be stable to the usual  $\mathbf{E} \times \mathbf{B}$  instability, as the zonal electric field is generally found to be westward at this time of the night [Evans et al., 1979; Vickrey et al., 1980; Robinson et al., 1982]. However, the entire density enhancement region shown in Figure 6 is embedded in the diffuse auroral precipitation region as shown in Figure 4. It is well known that downward field-aligned Birkeland currents are found in such regions (cf. recent review by Saffkeos et al. [1982] and references therein). Thus it is quite possible that large Birkeland currents are destabilizing what appears to be a stable  $\mathbf{E} \times \mathbf{B}$  instability configuration.

A problem arises in the matter of growth rates. Keskinen et al. [1980], doing a numerical simulation of the analytical formulation of the current convective instability by Ossakow and Chaturvedi [1979], found growth times  $\sim 10^3$  s for the fastest growing mode, using a gradient scale length of 20 km on the assumption of a westward *E* field of 10 mV/m when augmented by a large Birkeland current of 8  $\mu\text{A}$

$\text{m}^{-2}$ . Now, this growth time seems to be an order of magnitude too long to match the observations. On the other hand, Keskinen and Ossakow [1982] found that even if a much smaller field-aligned current of 1  $\mu\text{A} \text{ m}^{-2}$ , which is more in accord with measurements, was used to further destabilize the already gradient-drift unstable poleward edge, then growth times  $\sim 10^2$  s may be obtained. Our current set of measurements clearly is more in tune with the latter computation. It is interesting to note that recent work has shown that a beam of 100 eV particles such as we have here does not appreciably affect the growth rate of the current convective instability [Chaturvedi and Ossakow, 1983].

Thus our data would seem to indicate the possible existence of a fluctuating zonal electric field with alternating eastward and westward components of the order of 10 mV/m, as was measured by the Chatanika radar in the vicinity of an auroral arc [de la Beaujardiere et al., 1977]. Such fluctuating electric fields also are observed in the vicinity of auroral forms by the ion-drift meter on the AE-D satellite (W. B. Hanson, private communication, 1982). Since growth times are short and, once created, the kilometer-scale irregularities have long lifetimes [Vickrey and Kelley, 1982], such a fluctuating zonal electric field of the right polarity could drive the poleward gradient unstable. The computation of a short growth time neglects the effect of *E* region conductivity, which may affect this growth time substantially (R. T. Tsunoda and J. F. Vickrey, unpublished manuscript, 1982). Further studies are necessary to determine the effect of *E* region Pedersen conductivity within such soft precipitation zones.

It is also possible that these irregularities are created directly by structured low-energy particle precipitation and irregular field-aligned currents. There is some suggestion of the former effect evident in Figures 6a and 6b. It is hoped that the forthcoming HILAT satellite [Fremouw et al., 1983] with its complement of instruments, including a drift meter and magnetometer and much higher spatial resolution of the particle measurements, will allow a more definitive determination of the generation mechanism of the scintillation-producing irregularities associated with *F* region density enhancements or "blobs."

**Acknowledgments.** The scintillation program at Goose Bay is under the able direction of H. E. Whitney. We thank E. J. Weber and J. A. Whalen for helpful discussions. The AISC polarimeter data were kindly made available to us by J. A. Koebuch. M. D. Cousins was responsible for the phase scintillation instrumenta-

tion. The ISEE 3 interplanetary magnetic field data were obtained from the National Space Science Data Center. The AE indices were obtained from the World Data Center C2 for Geomagnetism in Kyoto University Japan. This work was partially sponsored by the Air Force Office of Scientific Research. The work at Emmanuel College was supported by AFGL contract F19628-81-K-0011.

## REFERENCES

- Aarons, J., High-latitude irregularities during the magnetic storm of October 31 to November 1, 1972, *J. Geophys. Res.*, **81**, 661, 1976.
- Aarons, J., J. P. Mullen, H. E. Whitney, A. L. Johnson, and E. J. Weber, UHF scintillation activity over polar latitudes, *Geophys. Res. Lett.*, **8**, 277, 1981.
- Banks, P. M., and G. Kockarts, *Aeronomy*, part A, p. 214, Academic, New York, 1973.
- Basu, S., and J. Aarons, The morphology of high-latitude VHF scintillation near 70°W, *Radio Sci.*, **15**, 59, 1980.
- Basu, S., and H. E. Whitney, The temporal structure of intensity scintillations near the magnetic equator, *Radio Sci.*, **18**, 263, 1983.
- Basu, S., S. Basu, and W. B. Hanson, The role of in-situ measurements in scintillation modelling, paper presented at Ionospheric Effects Symposium, Nav. Res. Lab., Arlington, Va., 1981.
- Basu, S., S. Basu, R. C. Livingston, E. MacKenzie, and H. E. Whitney, Phase and amplitude scintillation statistics at 244 MHz from Goose Bay using a geostationary satellite, *Rep. AFGL-TR-82-0222*, Air Force Geophys. Lab., Bedford, Mass., 1982.
- Briggs, B. H., and I. A. Parkin, On the variation of radio star and satellite scintillation with zenith angle, *J. Atmos. Terr. Phys.*, **25**, 339, 1963.
- Chaturvedi, P. K., and S. L. Ossakow, Effect of an electron beam on the current convective instability, *J. Geophys. Res.*, **88**, 4119, 1983.
- Clark, D. H., and W. J. Raitt, The global morphology of irregularities in the topside ionosphere as measured by the total ion current probe on ESRO-4, *Planet. Space Sci.*, **24**, 873, 1976.
- Deehr, C. S., J. D. Winningham, F. Yasuhara, and S.-I. Akasofu, Simultaneous observations of discrete and diffuse auroras by the ISIS 2 satellite and airborne instruments, *J. Geophys. Res.*, **81**, 5527, 1976.
- de la Beaujardiere, O., R. Vondrak, and M. Baron, Radar observations of electric fields and currents associated with auroral arcs, *J. Geophys. Res.*, **82**, 5051, 1977.
- Dyson, P. L., Direct measurements of the size and amplitude of irregularities in the topside ionosphere, *J. Geophys. Res.*, **74**, 6291, 1969.
- Evans, J. V., J. M. Holt, and R. H. Wand, Millstone Hill incoherent scatter observations of auroral convection over  $60^\circ \leq A \leq 75^\circ$ , 1. Observing and data reduction procedures, *J. Geophys. Res.*, **84**, 7059, 1979.
- Fejer, B. G., and M. C. Kelley, Ionospheric irregularities, *Rev. Geophys. Space Phys.*, **18**, 401, 1980.
- Foster, J. C., J. R. Dougan, and G. S. Stiles, Ionospheric convection and currents in the midnight sector on November 8, 1979, *J. Geophys. Res.*, **86**, 2143, 1981.
- Fremouw, F. J., Geometrical control of the ratio of intensity and phase scintillation indices, *J. Atmos. Terr. Phys.*, **42**, 775, 1980.
- Fremouw, F. J., C. L. Rino, J. F. Vickrey, D. A. Hardy, R. E. Hufman, E. J. Rich, C. I. Meng, K. A. Potocki, T. A. Potemra, W. B. Hanson, R. A. Heelis, and L. A. Wittwer, The HILAT program, *Eos Trans. AGU*, **64**, 163, 1983.
- Fremouw, F. J., R. L. Leadabrand, M. D. Cousins, C. L. Rino, B. C. Fair, and R. A. Long, Early results from the DNA Wideband satellite experiment—Complex-signal scintillation, *Radio Sci.*, **13**, 167, 1978.
- Gussenhoven, M. S., D. A. Hardy, and W. J. Burke, DMSP F2 electron observations of equatorward auroral boundaries and their relationship to magnetospheric electric fields, *J. Geophys. Res.*, **86**, 768, 1981.
- Hardy, D. A., M. S. Gussenhoven, and A. Huber, The precipitation electron detectors (SSJ 3) for the block 5D flights 2-5 DMSP satellites: Calibration and data presentation, *Rep. AFGL-TR-79-0210*, Air Force Geophys. Lab., Bedford, Mass., 1979.
- Kelley, M. C., and F. S. Mozer, A satellite survey of vector electric fields in the ionosphere at frequencies of 10-500 Hz. 1. Isotropic, high-latitude electrostatic emissions, *J. Geophys. Res.*, **77**, 4158, 1972.
- Kelley, M. C., J. F. Vickrey, C. W. Carlson, and R. Torbert, On the origin and spatial extent of high-latitude F region irregularities, *J. Geophys. Res.*, **87**, 4469, 1982.
- Keskinen, M. J., and S. L. Ossakow, Nonlinear evolution of plasma enhancements in the auroral ionosphere. 1. Long wavelength irregularities, *J. Geophys. Res.*, **87**, 144, 1982.
- Keskinen, M. J., S. L. Ossakow, and B. E. McDonald, Nonlinear evolution of diffuse auroral F region ionospheric irregularities, *Geophys. Res. Lett.*, **7**, 573, 1980.
- Linson, L. M., and J. B. Workman, Formation of striations in ionospheric plasma clouds, *J. Geophys. Res.*, **75**, 3211, 1970.
- Lotova, N. A., Temporal scintillation spectra with allowance for the solar-wind velocity distribution: Theory, *Geomagn. Aeron.*, **21**, 447, 1981.
- Lotova, N. A., and I. V. Chashei, Temporal spectra of scintillations with allowance for the jet structure of the solar wind, *Sov. Astron.*, **24**, 192, 1980.
- Mantas, G. P., and J. C. G. Walker, The penetration of soft electrons into the ionosphere, *Planet. Space Sci.*, **24**, 409, 1976.
- Maynard, N. C., and J. P. Heppner, Variations in electric fields from polar orbiting satellites, in *Particles and Fields in the Magnetosphere*, edited by B. McCormac, p. 247, D. Reidel, Hingham, Mass., 1970.
- Muldrew, D. B., and J. F. Vickrey, High-latitude F region irregularities observed simultaneously with ISIS 1 and the Chatanika radar, *J. Geophys. Res.*, **87**, 8263, 1982.
- Ossakow, S. L., and P. K. Chaturvedi, Current convective instability in the diffuse aurora, *Geophys. Res. Lett.*, **6**, 332, 1979.
- Rees, M. H., Auroral ionization and excitation by incident energetic electrons, *Planet. Space Sci.*, **11**, 1209, 1963.
- Rich, F., M. Smiddy, R. C. Sagalyn, W. J. Burke, P. Anderson, S. Bredesen, and W. P. Sullivan, In-flight characteristics of the topside ionospheric monitor (SSIF) on the DMSP satellite flight 2 and flight 4, *Rep. AFGL-TR-80-0152*, Air Force Geophys. Lab., Bedford, Mass., 1980.
- Rino, C. I., Power-law phase screen model for ionospheric scintillation. 1. Weak scatter, *Radio Sci.*, **14**, 1135, 1979.
- Rino, C. I., and S. J. Matthews, On the morphology of auroral zone radio wave scintillation, *J. Geophys. Res.*, **85**, 4139, 1980.



- Robinson, R. M., R. R. Vondrak, and T. A. Potemra, Electrodynamical properties of the evening sector ionosphere within the Region 2 field-aligned current sheet, *J. Geophys. Res.*, **87**, 731, 1982.
- Roble, R. G., and M. H. Rees, Time-dependent studies of the aurora: Effects of particle precipitation on the dynamic morphology of ionospheric and atmospheric properties, *Planet. Space Sci.*, **25**, 991, 1977.
- Saflekos, N. A., R. E. Sheehan, and R. L. Carovillano, Global nature of field-aligned currents and their relation to auroral phenomena, *Rev. Geophys. Space Phys.*, **20**, 709, 1982.
- Sagalyn, R. S., M. Smiddy, and M. Ahmed, High-latitude irregularities in the topside ionosphere based on ISIS 1 thermal probe, *J. Geophys. Res.*, **79**, 4552, 1974.
- Simon, A., Instability of a partially ionized plasma in crossed electric and magnetic fields, *Phys. Fluids*, **6**, 382, 1963.
- Singleton, D. G., Power spectra of ionospheric scintillations, *J. Atmos. Terr. Phys.*, **36**, 113, 1974.
- Smiddy, M., R. C. Sagalyn, W. P. Sullivan, P. J. L. Wildman, P. Anderson, and F. Rich, The topside ionosphere plasma monitor (SSIE) for the block 5D flight 2 DMSP satellite, *Rep. AFGL-TR-78-0071*, Air Force Geophys. Lab., Bedford, Mass., 1978.
- Tanskanen, P. J., D. A. Hardy, and W. J. Burke, Spectral characteristics of precipitating electrons associated with visible aurora in the premidnight oval during periods of substorm activity, *J. Geophys. Res.*, **86**, 1379, 1981.
- Vickrey, J. F., and M. C. Kelley, The effects of a conducting E layer on classical F region cross-field plasma diffusion, *J. Geophys. Res.*, **87**, 4461, 1982.
- Vickrey, J. F., C. L. Rino, and T. A. Potemra, Chatanika TRIAD observations of unstable ionization enhancements in the auroral F region, *Geophys. Res. Lett.*, **7**, 789, 1980.
- Whalen, J. A., Auroral oval plotter and monograph for determining corrected geomagnetic local time, latitude and longitude for high latitudes in the northern hemisphere, *Rep. AFCRL-TR-70-0422*, Air Force Geophys. Lab., Bedford, Mass., 1970.
- Whalen, J. A., General characteristics of the auroral ionosphere, in *Physics of Space Plasmas, SPI Conf. Proc. Repr. Ser.*, vol. 4, edited by T. S. Chang, B. Coppi, and J. R. Jasperse, Scientific Publishers, Cambridge, Mass., 1981.
- Whitaker, J. H., The transient response of the topside ionosphere to precipitation, *Planet. Space Sci.*, **25**, 773, 1977.
- S. Basu, S. Basu, and E. MacKenzie, Emmanuel College, Boston, MA 02115.
- H. C. Carlson, D. A. Hardy, and F. J. Rich, Air Force Geophysics Laboratory, Hanscom Air Force Base, Bedford, MA 01731.
- R. C. Livingston, SRI International, Menlo Park, CA 94025.

ARTIFICIAL IRREGULARITIES GENERATED BY IONOSPHERIC HEATING AND  
THEIR EFFECTS ON TRANSIONOSPHERIC PROPAGATION

Santimay Basu and Sunanda Basu  
Emmanuel College  
Boston, MA 02115

S. Ganguly  
Department of Space Physics  
Rice University  
Houston, TX 77001

J.A. Klobuchar  
Air Force Geophysics Laboratory  
Hanscom AFB, MA 01731

C.M. Rush  
U.S. Department of Commerce  
Institute for Telecommunication Sciences  
Boulder, CO 80303

ABSTRACT

The results of 250 MHz scintillations observed during ionospheric heating in both the overdense (heater frequency below the critical frequency) and the underdense (heater frequency above the critical frequency) cases with the high-power high frequency transmitter at Platteville, Colorado are discussed. In the overdense case, strong irregularities are found to be excited promptly within a few seconds giving rise typically to scintillations in the range of 3-6 dB at 244 MHz. In the underdense case of heating, on the other hand, weak irregularities are usually excited after some delay and are found to cause 1-3 dB scintillations in the 244 MHz - 249 MHz frequency range, although one 10 dB scintillation event was encountered on a field aligned propagation path. The temporal structures of scintillations in the two cases of heating are found to be very different, with slow fadings dominating the scintillation structure in the underdense case. The spatial structures of irregularities generated in the two cases of heating are discussed from power spectral studies of scintillations and measurements of irregularity drift speed from spaced receiver scintillation observations.

Observations of radio star and satellite scintillations associated with ionospheric heating by the use of the newly constructed facility at Arecibo are also discussed. Radio star measurements were conducted at 50 and 430 MHz while geostationary satellite observations with three spaced receivers were made at 250 MHz. These preliminary measurements indicate discrete 'clumping' of irregularities near the center of the heated volume and a weak wavelength dependence of scintillations.

INTRODUCTION

It has been established that high power high frequency radio waves reflected from the ionosphere can not only introduce the expected modification of electron gas temperature and number density near the altitude of reflection (Gordon et al., 1971; Utlaut and Cohen, 1971), but can also give rise to a variety of physical phenomena related to non-linear plasma physics (for comprehensive reviews see Perkins et al., 1974; Carlson and Duncan, 1977; Fejer, 1979; Gurevich, 1978). Among the various manifestations of plasma instabilities induced by the heating experiments, the generation of artificial spread-F was one of the most striking and immediate experimental results (Utlaut et al., 1970; Utlaut and Violette, 1972; Wright, 1973). The generation mechanism of long wavelength (~1 km) field aligned irregularities remained obscure for quite sometime and is now attributed either to thermal self-focusing (Perkins and Valeo, 1974; Thome and Perkins, 1974) or to stimulated Brillouin scattering (Cragin and Fejer, 1974). The substantial level of the spectral intensity of km-scale

Irregularities were subsequently demonstrated from the observations of scintillations of VHF/UHF signals received from radio stars and satellites through the artificially heated ionospheric volume (Rufenach, 1973; Pope and Fritz, 1974; Bowhill, 1974). Bowhill (1974) performed scintillation measurements with both geostationary and orbiting satellites and established the field-aligned nature of the irregularities, their transverse scale size and drift velocity. In all the above studies, the heater wave frequency was below the critical frequency of the F region. Recently, Basu et al (1980) have performed scintillation measurements on the ground and on the moving platform of an aircraft with geostationary satellites when the heating transmitter was operated at a frequency both below and above the critical frequency of the F region.

In the overdense case of heating (heater frequency below the critical frequency), they noted a prompt excitation of the irregularities causing as large as 10 dB scintillations at 250 MHz. On the other hand, in the underdense case when the heater frequency was about 15% higher than the critical frequency, they observed a delayed and often sporadic onset of long period scintillations not generally exceeding 3 dB at 250 MHz. Perkins and Goldman (1981) have recently considered a theory of self-focusing instability in an underdense ionosphere and have predicted the generation of sheet-like irregularities aligned with the magnetic meridian that could have given rise to the scintillation effects discussed above.

In the present paper, we shall utilize our earlier geostationary satellite scintillation observations (Basu et al., 1980) performed in conjunction with ionospheric heating at Platteville for a study of the spectral characteristics of scintillations in the overdense and underdense cases of heating. We shall also discuss our recent results of radio star and satellite scintillation measurements in conjunction with ionospheric heating at the newly constructed facility at Arecibo.

#### EXPERIMENTAL DETAILS

The experimental details and the geometry of scintillation observations performed in conjunction with the heating transmitter at Platteville are outlined in Basu et al. (1980) and will not be repeated here. During December 1980, radio star and satellite scintillation measurements were conducted at Puerto Rico by using the newly constructed h.f. heating facility at Arecibo. Figure 1 shows the extent of the central heated region at 200 km altitude above the heating facility as limited by the estimated half power beam circle at 5 MHz (35 km E-W and 70 km N-S). Each of the four transmitters were operated at 75 kw power level during the period of observation. Ordinary mode heating was performed during the period of observation. The intersections of the ionospheric height of 200 km with the ray paths from the Roosevelt Roads Naval Station to the LES-9 satellite are shown in Figure 1. The subionospheric (200 km) tracks of several radio sources, namely Taurus, 3 C 166 and 3 C 210 as viewed by the 1000 ft radio telescope at Arecibo are shown in Figure 2. Radio star scintillation data were acquired during the meridian transit of these sources. The LES-9 satellite scintillation measurements were performed at 249 MHz with three spaced receiving systems. Scintillation measurements with Taurus were performed at 50 MHz with the 1000 ft reflector at Arecibo. The 50 MHz receiving system was kindly placed at our disposal by Dr. J. Röttger of Max Planck Institute, Lindau, West Germany. The other radio sources were observed with the 430 MHz receiving system of the Arecibo Observatory.

#### OBSERVATIONAL RESULTS

Figure 3a shows a 15 minute scintillation data segment that was obtained at Carpenter, Wyoming by the use of 249 MHz transmissions of LES-8 satellite on March 13, 1980. The heater at Platteville was operated at 9.9 MHz with ordinary mode polarization and the critical frequency of the F region was 10.3 MHz. The normalized second central moment ( $S_4$ ) of intensity scintillations was 0.37. Figure 3b shows the corresponding scintillation spectrum. The high frequency roll off starts at a frequency of about 0.2 Hz and the slope of the roll off portion corresponds to a frequency ( $f$ ) dependence of  $f^{-2.5}$ . The observed slope is shallower as compared to the spectral slope of natural scintillations at midlatitudes. It should be noted that detectable spectral intensity is obtained at several Hz in the case of overdense heating.

In Figure 4a we show a sample of 249 MHz scintillation observed at Carpenter, Wyoming on March 13, 1980 during an underdense heating cycle. The heater frequency was 9.9 MHz during this cycle while the critical frequency of the F region was 7.9 MHz. The quasi-periodic fluctuations are reminiscent of naturally occurring scintillations caused by ionization gradients. Figure 4b shows the corresponding scintillation spectrum which indicates that the spectral power is concentrated below about 0.3 Hz with a very sharp high frequency roll-off.

Figure 5a illustrates another scintillation data sample acquired at Carpenter, Wyoming on March 13, 1980. The heater frequency was 9.9 MHz and the critical frequency was 8.5 MHz during this underdense heating period. Figure 5b shows the corresponding power spectrum. Spectral power is concentrated over the low frequency band and a very shallow slope ( $f^{-1.5}$ ) is obtained over the roll-off portion. The comparison between the spectra obtained under two different kinds of heating

indicates that while spectral power exists up to several Hz in the overdense case, almost all the power is confined to frequencies below 1 Hz in the underdense case.

We shall now examine the results of satellite and radio star scintillation measurements that have been performed at Puerto Rico in conjunction with ionospheric heating (on December 22, 1980). Sustained heating cycles over several hours were maintained during this test in contrast to the 15-minute or shorter duration of heating cycles employed at Platteville.

Figure 6 shows 249 MHz scintillations observed at Roosevelt Roads station during an overdense heating cycle. The heater at Arecibo was operated at 5.1 MHz and radiated ordinary mode polarization. The ray path to the satellite intersected the western fringe of the half power beam circle as shown in Figure 1. Scintillation index of 2.5 dB corresponding to the  $S_4$  index of about 0.15 was obtained.

Figure 7 shows scintillations observed with the Taurus radio source at 50 MHz during an overdense heating period. A peak to peak fluctuation of 3.7 dB corresponding to  $S_4$  index of 0.21 is obtained.

Figure 8 shows scintillations observed with radio source 3 C 166 at 430 MHz during another overdense heating period. Maximum scintillation activity of about 0.8 dB was recorded. If we compare the scintillation levels obtained with Taurus and 3 C 166 at 50 MHz and 430 MHz respectively, a very weak frequency dependence ( $f^{-.5}$ ) of scintillation is obtained. It should be emphasized, however, that the above comparison is not strictly valid since the measurements were not simultaneous. However, we make the assumption that steady state heating conditions were achieved and the background ionosphere did not change greatly during the fifty-minute delay between the two sets of observations.

Figure 9 shows the weak and slow variations of signal intensity of 3 C 210 at 430 MHz when the heater frequency was marginally higher than the critical frequency. Such variations of signal intensity were recorded briefly during underdense heating as was the case also at Platteville.

The interesting differences of the irregularity characteristics in the underdense and overdense cases of heating as discussed in this report needs further study. We plan to perform similar experiments with ground based and airborne instruments at Arecibo later this year.

#### ACKNOWLEDGMENTS

The authors wish to thank J. Carroll and E.J. Violette for the operation of the Platteville facility and A. Veldhuis and D. Albino for the operation of the Arecibo heating facility. The assistance of H.D. Craft and the staff of the Arecibo Observatory are gratefully acknowledged. Special thanks are due to J.M. Goodman for providing necessary support at Roosevelt Roads Naval Station and to C. Ferioli for help with the observations.

The National Astronomy and Ionosphere Center is operated by Cornell University under contract with the National Science Foundation. The work at Emmanuel College was partially supported by NSF grant ATM78-25264 and AFGL contract F19628-81-K-0011.

#### REFERENCES

- Basu, S., S. Basu, A.L. Johnson, J.A. Klobuchar and C.M. Rush, Preliminary results of scintillation measurements associated with ionosphere heating and possible implications for the solar power satellite, Geophys. Res. Lett., **7**, 609, 1980.
- Bowhill, S.A., Satellite transmission studies of spread-F produced by artificial heating of the ionosphere, Radio Sci., **9**, 975, 1974.
- Carlson, H.C. and L.M. Duncan, HF excited instabilities in space plasmas, Radio Sci., **12**, 1001, 1977.
- Cragin, B.L. and J.A. Fejer, Generation of large-scale field-aligned irregularities in ionospheric modification experiments, Radio Sci., **9**, 1071, 1974.
- Fejer, J.A., Ionospheric modification and parametric instabilities, Rev. Geophys. Space Phys., **17**, 135, 1979.
- Gurevich, A.V., "Nonlinear Phenomena in the Ionosphere", Springer Verlag, New York, 1978.
- Gordon, W.E., H.C. Carlson and R.L. Showen, Ionospheric heating at Arecibo: First tests, J. Geophys. Res., **76**, 7808, 1971.

- Perkins, F.W., C. Oberman and E.J. Valeo, Parametric instabilities and ionospheric modification, J. Geophys. Res., 79, 1478, 1974.
- Perkins, F.W. and E.J. Valeo, Thermal self-focusing of electromagnetic waves in plasma, Phys. Rev. Lett., 32, 1234, 1974.
- Perkins, F.W. and M.V. Goldman, Self-focusing of radio waves in an underdense ionosphere, to be published in J. Geophys. Res., 1981.
- Pope, J.H. and R.B. Fritz, Observations of artificially produced scintillations using satellite transmissions, J. Geophys. Res., 79, 1074, 1974.
- Rufenach, C.L., Radio scintillation of stellar signals during artificial ionospheric modification, J. Geophys. Res., 78, 5611, 1973.
- Thome, G.D. and F.W. Perkins, Production of ionospheric striations by self-focusing of intense radio waves, Phys. Rev. Lett., 32, 1238, 1974.
- Utlaut, W.F., E.J. Violette and A.K. Paul, Some ionosonde observations of ionospheric modification by very high power high-frequency ground-based transmission, J. Geophys. Res., 75, 6429, 1970.
- Utlaut, W.F. and Cohen, Modifying the ionosphere with intense radio waves, Science, 174, 245, 1971.
- Utlaut, W.F. and E.J. Violette, Further observations of ionospheric modification by a high-powered HF transmitter, J. Geophys. Res., 77, 6804, 1972.
- Wright, J.W., Kinesonde observations of ionosphere modification by intense electromagnetic fields from Platteville, Colorado, J. Geophys. Res., 78, 5622, 1973.

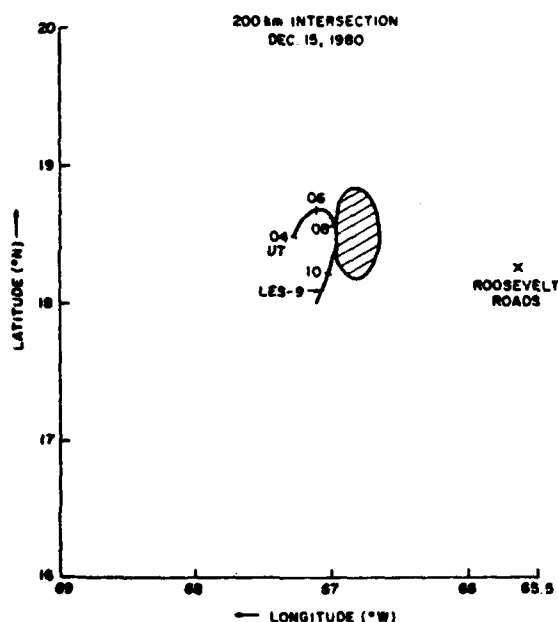


Figure 1. Geometry of observations of the LES-9 geostationary satellite from the Roosevelt Roads Naval Station in conjunction with the ionospheric heating at Arecibo in December, 1980.

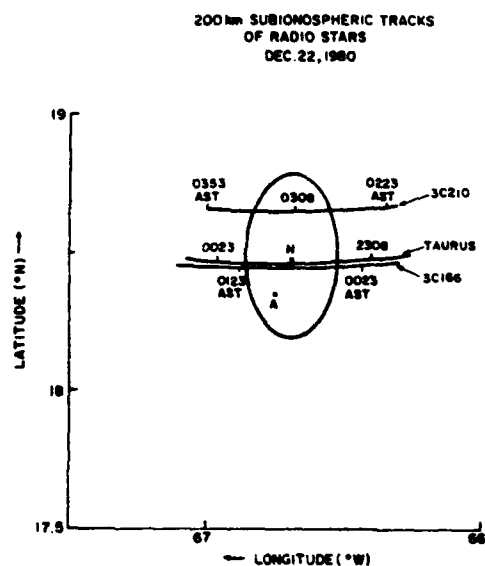


Figure 2. Subionospheric (200 km) tracks of Taurus, 3 C 166 and 3 C 210 as viewed by the Arecibo 1000 ft radio telescope (A) with the heater (H) on December 22, 1980.

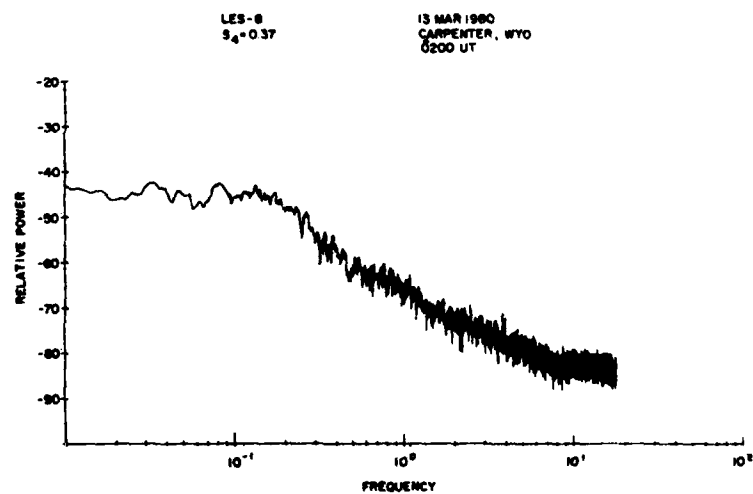
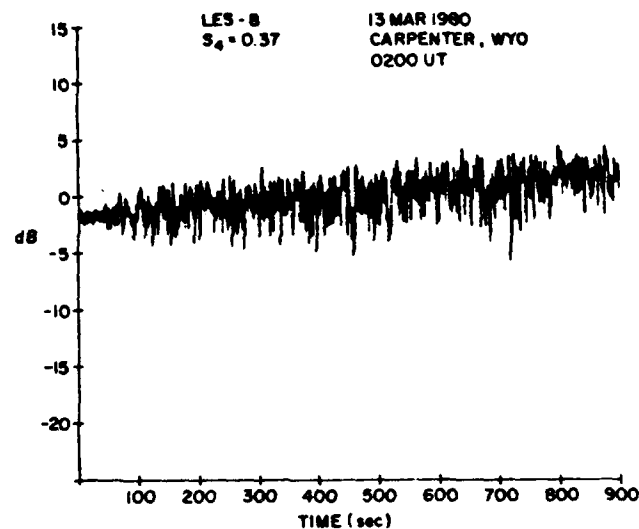


Figure 3a and b. A 15-min sample of scintillations from LES-8 at 249 MHz observed at Carpenter, Wyoming on March 13, 1980 during overdense heating and its corresponding spectrum

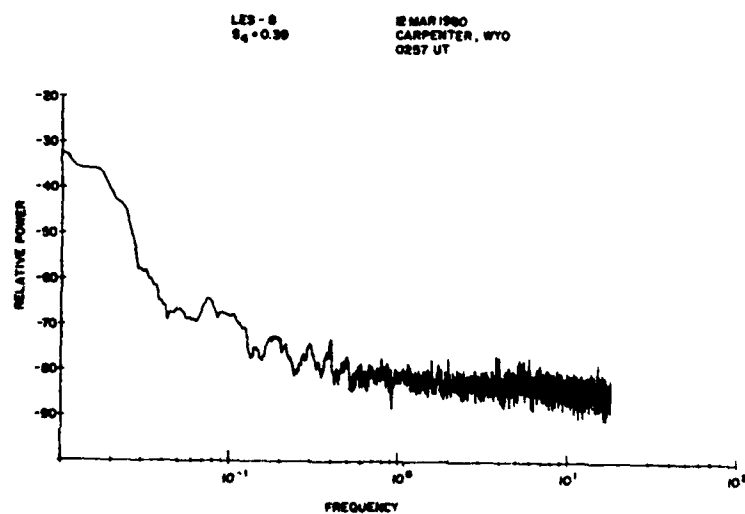
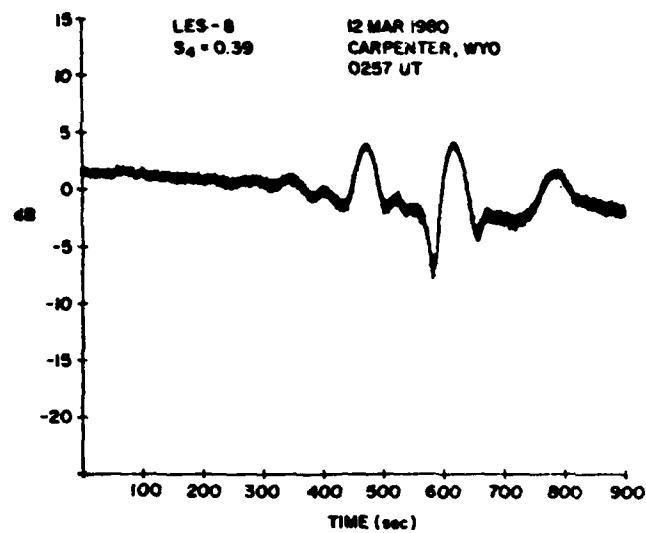


Figure 4a and b. A 15-min sample of scintillations from LES-8 at 249 MHz observed at Carpenter, Wyoming on March 13, 1980 during underdense heating and its corresponding spectrum

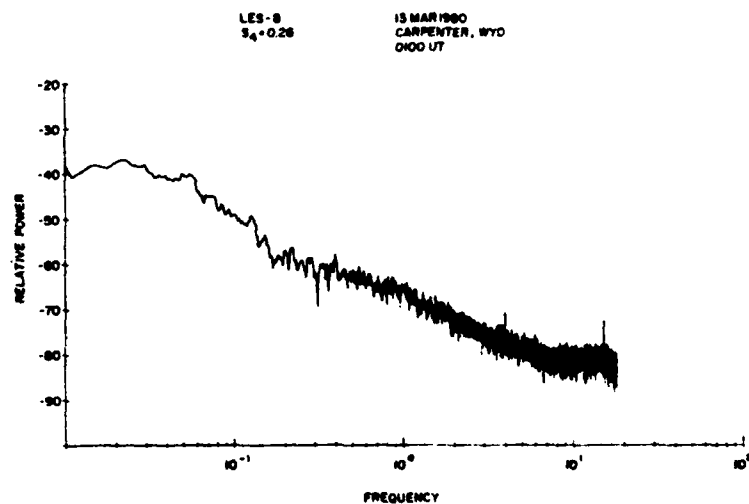
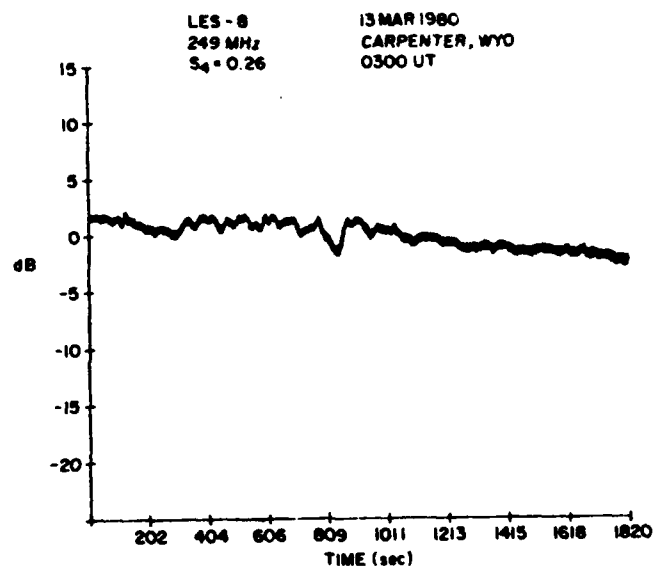


Figure 5a and b. A 15-min sample of scintillations from LES-8 at 249 MHz observed at Carpenter, Wyoming on March 13, 1980 during underdense heating and its corresponding spectrum



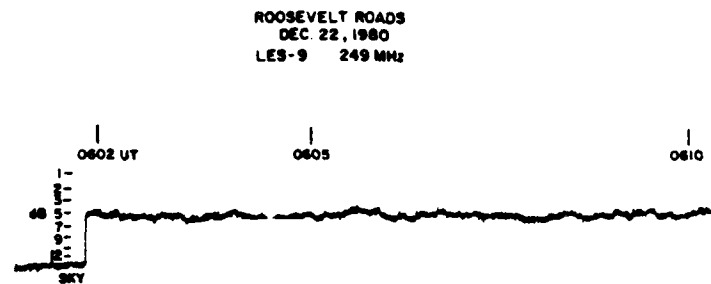


Figure 6. Scintillations from LES-9 at 249 MHz observed at Roosevelt Roads, P.R. on December 22, 1980 during overdense heating at Arecibo

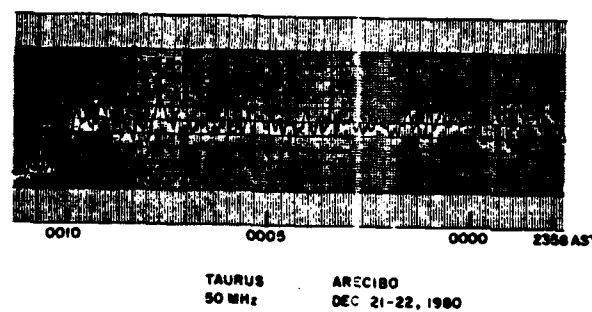


Figure 7. Scintillations at 50 MHz using Taurus radio source at Arecibo during overdense heating on December 22, 1980

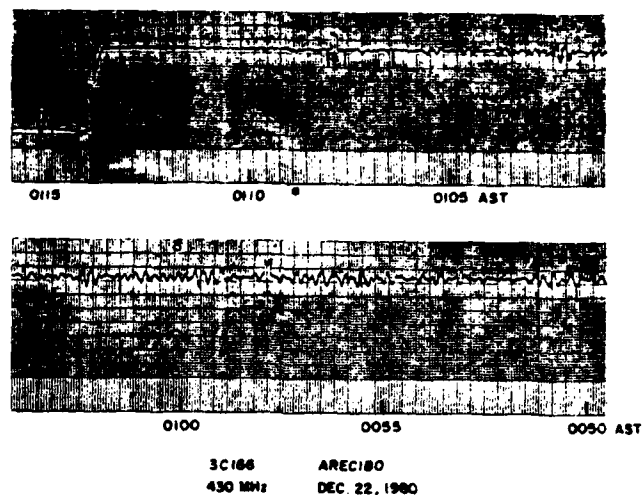


Figure 8. Scintillations at 430 MHz using 3 C 166 at Arecibo during overdense heating on December 22, 1980

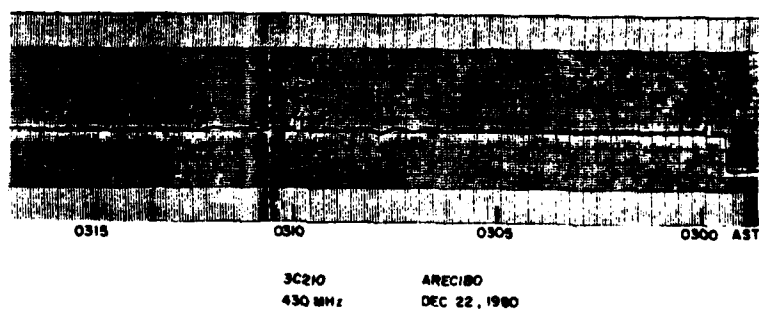


Figure 9. Scintillations at 430 MHz using 3 C 210 at Arecibo during marginally underdense heating on December 22, 1980

# Coordinated Study of Subkilometer and 3-m Irregularities in the *F* Region Generated by High-Power HF Heating at Arecibo

SANTIMAY BASU AND SUNANDA BASU

*Emmanuel College*

S. GANGULY AND W. E. GORDON

*Department of Space Physics, Rice University*

High-power high-frequency transmitters near Arecibo were used to generate artificial ionospheric irregularities in the *F* region. Radio star scintillation observations at 430 MHz were performed at Arecibo Ionospheric Observatory with the 305-m antenna, and radar backscatter measurements at 50 MHz were simultaneously made from Guadeloupe Island to probe the subkilometer and 3-m irregularities in the heated volume. Scintillation studies indicate a low-frequency modulation of the faster intensity fluctuation structure. By the use of plasma drift data this low-frequency temporal structure translates to spatial dimensions of 1–2 km. The frequency of the modulation envelope is found to be controlled by the heater power and is related to the dominant irregularity wavelength generated by the self-focusing instability. Scintillation spectra imply a steep power law index of  $-5$  in the scale length range of about 300 m to 150 m and a shallow index of  $-2$  at less than 150 m. The steep power law index may arise from an aperture averaging effect of the large 305-m antenna at Arecibo. Simultaneous measurements of 430-MHz scintillations and 50-MHz radar backscatter from field-aligned striations were performed to show that subkilometer irregularities can be generated by both *O* and *X* mode heating whereas the 3-m irregularities are excited only by the *O* mode heating, as is predicted by the theories of self-focusing and parametric instability. The width of the 50-MHz echo Doppler spectra is observed to be very narrow, only  $\sim 2$ –3 Hz, and independent of the background plasma drift, implying that the frequency bandwidth of the scattered signal is probably controlled by the instability process.

## INTRODUCTION

High-power high-frequency radio transmitters operated from the ground have been successfully used to excite various types of plasma instabilities in the ionosphere. In terms of these instability mechanisms it has been possible to explain the generation of irregularities of electron density spanning a scale length range of tens of centimeters to a few kilometers [Carlson and Duncan, 1977; Fejer, 1979, and references therein].

In this paper we present the first study of the characteristics of field-aligned subkilometer and meter scale irregularities of electron density that were generated simultaneously within a common ionospheric volume above Arecibo by the use of the newly constructed ionospheric modification facility at Islote, Puerto Rico. The generation of meter scale and subkilometer irregularities is attributed to very different plasma instability mechanisms. The field-aligned meter scale irregularities of electron density that give rise to VHF radar backscatter are explained in terms of the dissipation of parametrically excited Langmuir waves [Perkins, 1974; Lee and Fejer, 1978] or the thermal coupling between the Langmuir waves repeatedly scattered by a growing striation [Inhester *et al.*, 1981]. On the other hand, the generation of kilometer scale irregularities, which cause radio wave scintillations [S. Basu *et al.*, 1980, and references therein], is attributed to some type of self-focusing instability [Perkins and Valeo, 1974; Fejer, 1973; Goldman, 1974; Craquin *et al.*, 1977]. In view of the very different instability mechanisms involved in the two cases, the characteristics of meter and kilometer scale irregularities are distinctly different. However, mutual interactions are expected through the effects of the irregularities of electron density on the high-frequency radio wave that drives both instabilities.

In view of the above, a combination of irregularity diagnostic experiments was planned during September 22–26, 1981, when the ionosphere above Arecibo was modified by the high-power radio transmitters at the Islote heating facility. On two nights the Arecibo incoherent scatter facility was used to obtain information on background ionospheric parameters such as electron density, electron and ion temperatures, and vector plasma drifts. The plasma parameters and drifts were measured to help the interpretation of airglow, digital ionosonde, and scintillation measurements made by the airborne ionospheric observatory of the Air Force Geophysics Laboratory [S. Basu *et al.*, 1982]. The heater-induced modifications detected by the moving platform are being studied carefully, and these results will not be discussed in this paper.

As mentioned earlier, the major objective of the paper is the study of heater-generated irregularities of different scale lengths. The subkilometer irregularities were studied by the radio star scintillation technique at 430 MHz using the 305-m reflector on the nights of September 24–25, 1981, and September 26–27, 1981. On the latter night the meter scale irregularities were simultaneously detected by means of a coherent backscatter radar at 50 MHz operated from the island of Guadeloupe. We study the effects of wave polarizations of the heater on the generation and decay of subkilometer and meter scale irregularities. In addition, we present a detailed study of the temporal structure of scintillations and discuss the implications of a low-frequency modulation observed in the data. The Doppler spectra of the 50-MHz backscattered signal are found to be a good indicator of the background plasma drifts. These spectra are found to be rather narrow, the width being independent of the ambient drifts.

## RESULTS

Figure 1 illustrates the geometry of the observations. The location of the Arecibo HF heating facility at Islote is shown

Copyright 1983 by the American Geophysical Union.  
Paper number 3A1336.  
0148-0227/83/003A-1336\$05.00

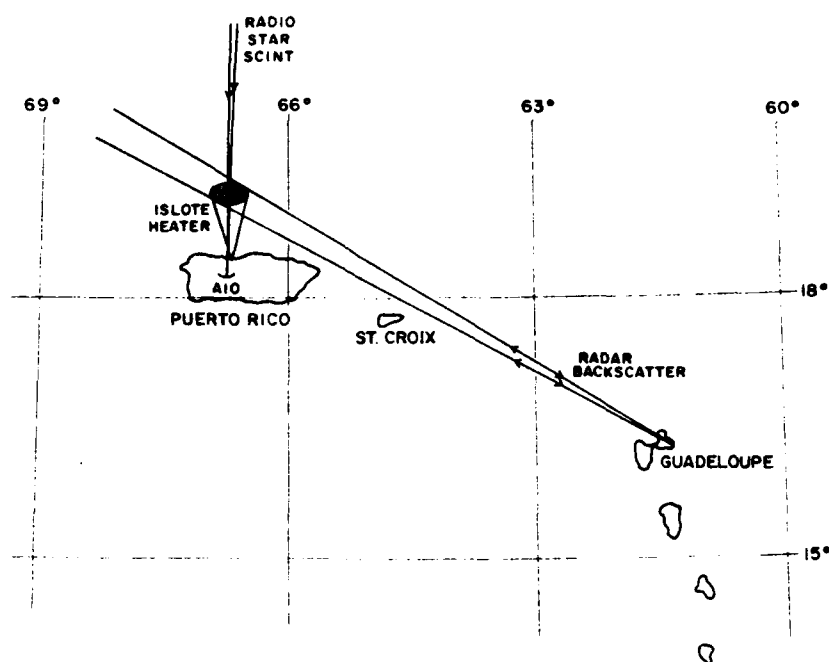


Fig. 1. Geometry of scintillation and radar observations.

in the diagram. It is at an azimuth of  $33^\circ$  and at a distance of 17 km from the Arecibo Ionospheric Observatory (AIO). The HF antenna system consists of a broadside array of 32 log-periodic antennas which gives rise to a main lobe with a half-power beam area of 20 km (E-W)  $\times$  40 km (N-S) at an altitude of 250 km for a frequency of 5 MHz [Gordon and Dobelman, 1982]. Considering only the nearest grating lobes, we estimate that at 5 MHz a power density of about  $50 \mu\text{W}/\text{m}^2$  is obtained at 250 km for a total transmitter power of 300 kW and radiation efficiency of 50%. All the experiments involved "overdense" heating with the heater operating CW at a frequency lower than the penetration frequency and the radiated wave polarization corresponding primarily to the ordinary mode (left circular) except during certain sessions when the extraordinary mode (right circular) was employed. The 305-m radio telescope at the observatory was used to track a variety of

radio sources through the heated volume corresponding to the main lobe. Figure 1 also shows the Guadeloupe station from which 50-MHz radar backscatter measurements were performed. A nominal pulse width of  $25 \mu\text{s}$  with the interpulse period varying between 1.3 and 1.9 ms was employed in the radar system. The data were analyzed in five slant range bins each of width 15 km covering the altitude interval 150 to 283 km near the heater site. It should be noted that the radar line of sight becomes orthogonal to the earth's magnetic field at an altitude of about 254 km above the heater site and consequently the backscattered power becomes maximum when heating is performed at this altitude.

Figure 2 shows the time sequence of ionospheric heating, the heater frequency, and the polarization modes employed on the two nights, September 24–25 and September 26–27, 1981. It also shows the time variation of the altitude of the enhanced

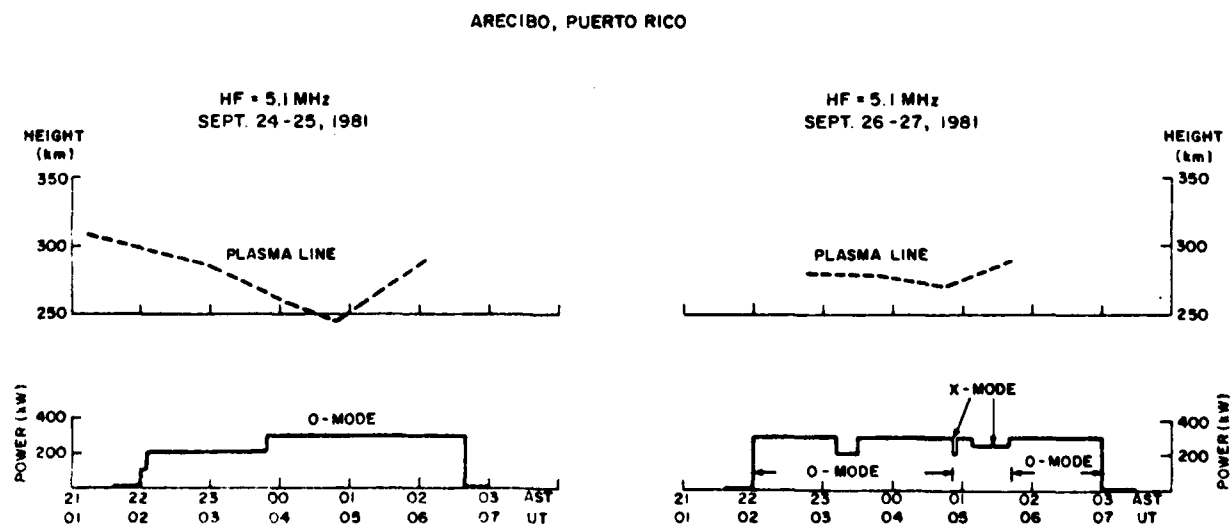


Fig. 2. Time history of Arecibo heater operations and plasma line altitude on September 24–25 and September 26–27, 1981.

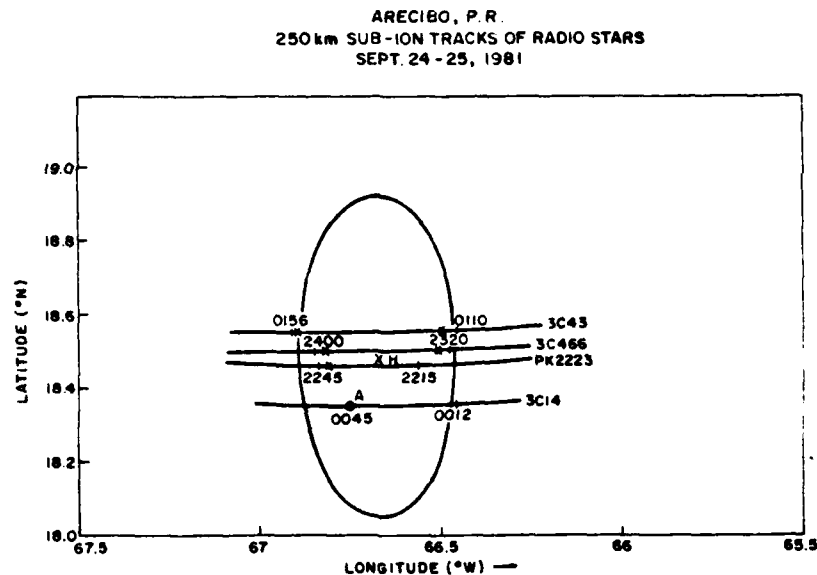


Fig. 3. Subionospheric tracks of radio sources through the heated volume for September 24-25, 1981.

plasma line determined by the incoherent scatter radar. It may be noted that on September 24-25 the height of the plasma line decreased by about 50 km, signifying the occurrence of the so-called midnight collapse, i.e., the phenomenon of the rapid drop of the height of the maximum ionization density in the *F* region [Su. Basu *et al.*, 1981, and references therein], whereas on September 26-27 the plasma line height remained nearly constant at 275 km around midnight, which indicates an absence of the collapse phenomenon.

The intersection of the propagation path from the Arecibo Observatory (A) to a variety of radio sources with the ionospheric height of 250 km, known as the subionospheric position, was obtained. The subionospheric positions of these radio sources at different Atlantic standard times (AST) marked along the tracks are shown in Figure 3. The crosses marked on each track signify the start and end of the mini-

mum detectable level (5%) of intensity scintillations at 430 MHz. On two tracks, the onset of scintillations could not be marked because of an insufficient time interval between the successive transits of radio stars. The elliptic area of dimension 50 km E-W and 100 km N-S centered about the heater location (H) covers the zone of 430-MHz scintillations indicated by the crosses. Since the half-power beam dimension is approximately 20 km  $\times$  40 km, we conclude that the dimension of the irregularity zone exceeds the half-power beam dimension by a factor of 2 to 3. It should be mentioned that if the median altitude of the irregularities corresponds to the 250-km altitude of the enhanced plasma line, the Fresnel zone radius of scintillation measurements corresponds to 420 m. Thus 430-MHz scintillations yield the distribution of the dominant 400-m irregularity scale length. A slight asymmetry between the start and end locations of scintillation with re-

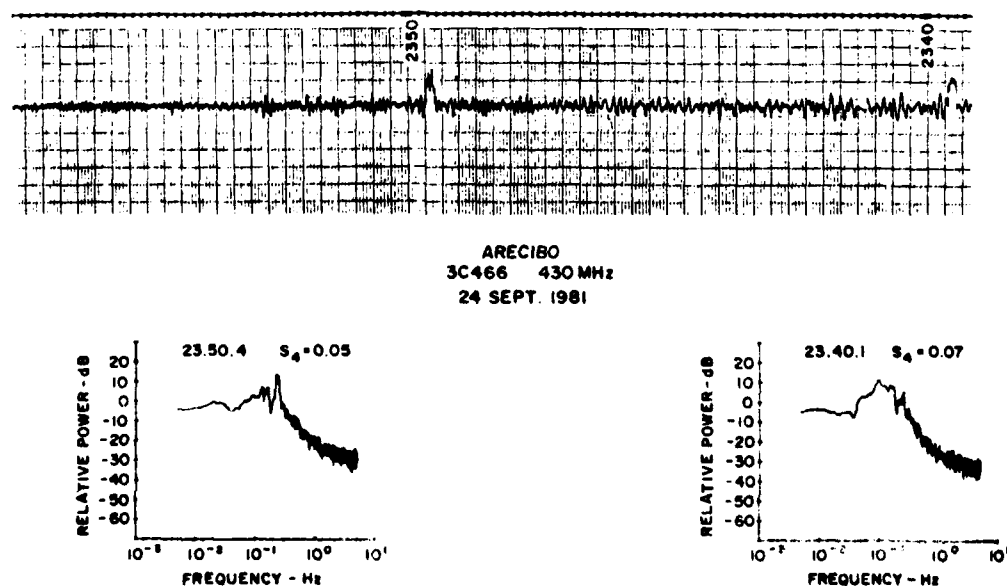


Fig. 4. Heater-induced 430-MHz intensity scintillation data using 3C466 and corresponding spectra for two levels of heater power.

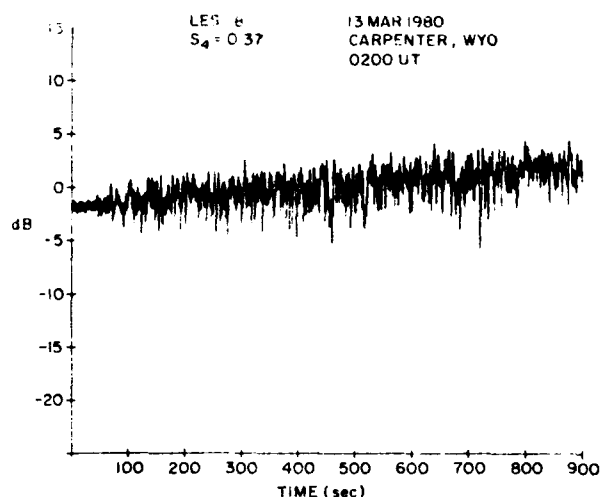


Fig. 5a. Temporal structure of 244-MHz scintillations from LES-8 obtained with the Platteville heater on March 13, 1980.

spect to the heater may be noted for the radio star 3C43. The westward extension of the irregularities is about 3 km, which can be explained if we assume a decay time of 3 min and a typical westward plasma drift of approximately 15 m/s at Arecibo in the postmidnight time frame.

Figure 4 shows one short section of the temporal structure of scintillations observed at 430 MHz from the radio source 3C466. The sudden jumps in the record immediately prior to 2340 and 2350 AST are due to 21°K calibration pulses superposed on the radio star signal. In the lower panel, intensity scintillation spectra over 7-min intervals starting at 2340 AST and 2350 AST are shown. The  $S_4$  index, or the normalized second central moment of signal intensity [Briggs and Parkin, 1963], is indicated in both spectra. From a close examination of the top panel it is found that the fast fluctuations are modulated by a low frequency. Prior to 2347 AST this low-frequency modulation period is about 50 s (corresponding to a spatial wavelength of 1.5 km for an assumed horizontal drift of 30 m/s). Afterward, the time period decreases to about 45 s, a decrease by a factor of 1.1. The sudden decrease of the modulation period could be related to an increase of the transmitter power from 200 kW to 300 kW. It is interesting to

note that as the low-frequency modulation period decreases with increasing transmitter power, the small-scale irregularities also become more intense as clearly demonstrated by the increased power spectral density at a frequency of 0.2 Hz in the 2350 AST spectrum.

The spectra of radio star scintillations at 430 MHz illustrated in the bottom panels of Figure 4 indicate a steep spectral roll-off ( $f^{-5}$ ) immediately above the Fresnel maximum followed by a slower roll-off ( $f^{-2}$ ) at higher frequencies. By identifying the Fresnel frequency with the first roll-off point in the spectrum and knowing the height of the diffraction screen (which can be identified with the height of the enhanced plasma line), it is possible to make an approximate conversion of the frequency scale to the spatial scale. On the basis of this conversion, it is found that the steep roll-off portion of the spectra corresponds to the irregularity scale length range of 300–150 m, so that the change in the spectral slope occurs at a scale length of about 150 m. Similar forms of spectra characterized by two spectral indices have been reported by Getmantsev *et al.* [1976] and Erukhimov *et al.* [1977, 1979] from intensity scintillation observations and more recently by Livingston [1983] from phase scintillation measurements. There exist, however, considerable differences between these observations regarding the spectral indices of the two components and the scale length at which the break in slope occurs. In contrast to the two-component spectra, the results of S. Basu *et al.* [1981] pertaining to the observations along the magnetic field line indicated a single-component high-frequency roll-off of approximately  $f^{-2.5}$  to  $f^{-3.5}$  above the Fresnel maximum. An example of such scintillation and its spectra obtained at Platteville with a geostationary satellite is shown in Figures 5a and 5b. The spectral index in this case is found to be  $-2.5$ . We shall discuss later the possible implications of the two-component spectra illustrated in Figure 4.

On the night of September 26–27, 1981, simultaneous 50-MHz radar backscatter measurements from Guadeloupe and 430-MHz scintillation measurements at Arecibo were performed. Figure 6 shows a section of 430-MHz radio star scintillation data obtained at Arecibo along with the relative power of the 50-MHz radar backscatter in different range intervals received at Guadeloupe from the 3-m field-aligned density striations generated above the heated volume. The

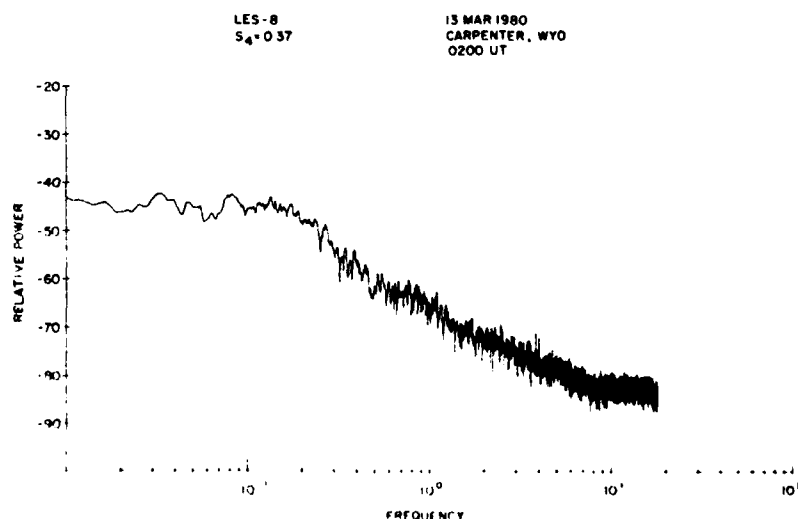


Fig. 5b. Intensity scintillation spectrum corresponding to data shown in Figure 5a.

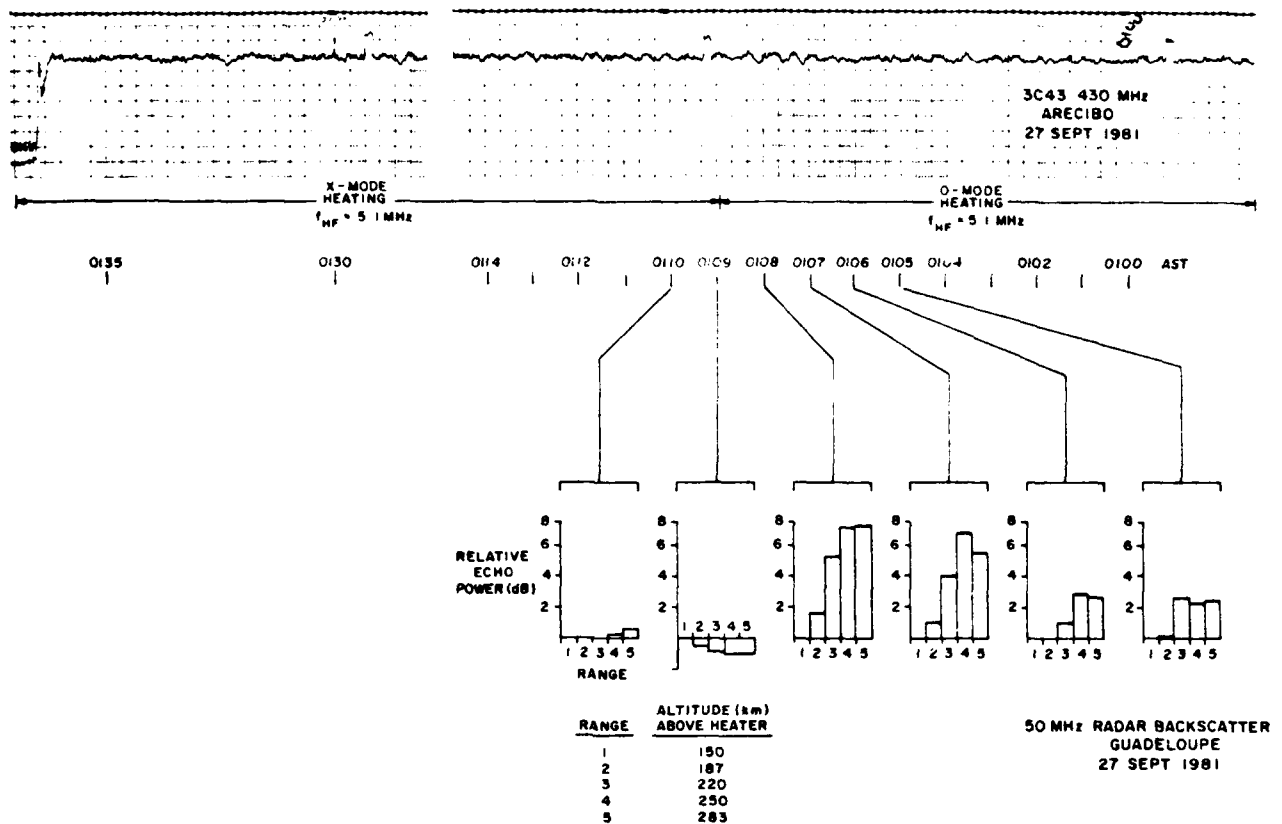


Fig. 6. Intensity scintillations at 430 MHz (top panel) and simultaneous 50-MHz radar observations during switching of wave polarization from O mode to X mode at 0109 AST.

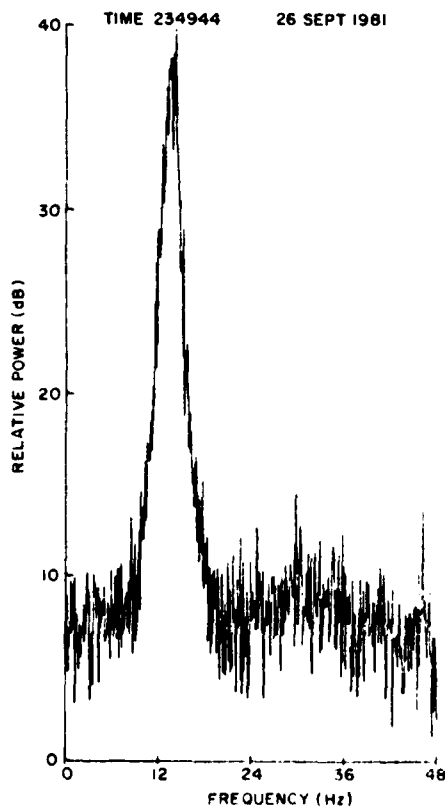


Fig. 7a. Doppler spectra of 50-MHz backscatter from heater-induced field-aligned striations obtained at 2349:44 AST on September 26, 1981.

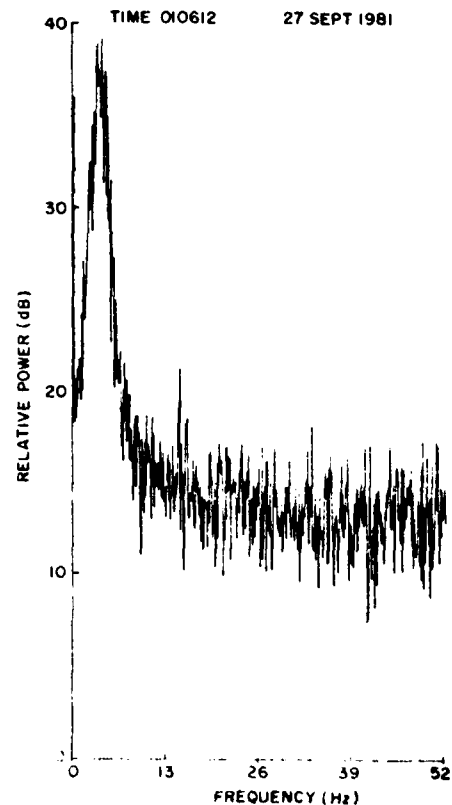


Fig. 7b. Same as in Figure 7a except for 0106:12 AST on September 27, 1981.

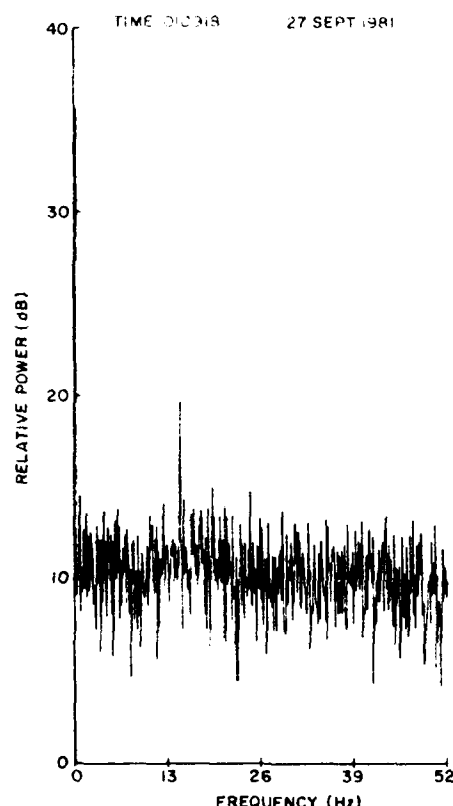


Fig. 7c. Same as in Figure 7a except for 0109:18 AST on September 27, 1981.

successive histograms in the bottom frame indicate a fluctuation of 50-MHz echo power. In view of the elongation of 3-m irregularities along the magnetic field, the strength of the backscattered signal is expected to be maximum when the ionospheric heating is performed at an altitude of 254 km which, as mentioned before, satisfies the orthogonality criterion of radar observations from Guadeloupe. From Figure 6 it may be noted that echo power is indeed maximum between ranges 4 and 5, corresponding to an altitude interval of 250–280 km. Simultaneous incoherent scatter radar measurements indicated that the altitude of the enhanced plasma line at this time was 275 km. At 0109 AST the wave polarization was changed from *O* mode to *X* mode. Prompt quenching of the 50-MHz backscattered power is noted at all ranges, but scintillations continued through the switching of wave polarization and persisted for the duration of *X* mode heating. This established that the subkilometer irregularities causing scintillations can be excited by both *O* and *X* modes as was established for artificial spread *F* [Utlaut and Violette, 1974].

Figure 7a shows the Doppler spectrum of the 50-MHz backscattered signal from striations. Similar measurements had been made earlier in conjunction with heating experiments at Platteville and Guadeloupe [Fialer, 1974; Minkoff and Kreppel, 1976; Duncan and Gordon, 1977; Ecklund et al., 1981]. The Doppler shift corresponds to a radial drift of 3-m irregularities at 40 m/s toward Guadeloupe. The width ( $e^{-1}$ ) of the Doppler spectra is observed to be very narrow, only 2.3 Hz. Figures 7b and 7c show the Doppler spectral sequence prior to and after the switching of wave polarization from *O* mode to *X* mode. Figure 7b when compared to Figure 7a shows a reduction in the line of sight velocity to 10 m/s. In Figure 7c the Doppler echo has disappeared as a consequence

of the switching of the heater wave polarization from *O* to *X* mode at 0109 AST. Table 1 lists the results of echo Doppler spectral analysis on the night of September 26–27, 1981. It may be noted that the drift of the striations varied from 40 m/s to 10 m/s and remained radial toward Guadeloupe (i.e., eastward). The persistence of an equatorward plasma drift around midnight did not allow any midnight collapse to occur on this night, as noted earlier. It should also be mentioned that the  $e^{-1}$  width of the Doppler spectra also listed in Table 1 varies between only 2 and 3 Hz, implying extreme aspect sensitivity even when the background drift varies by a factor of 4. The bandwidth of the Doppler spectra is thus independent of the variation of the background plasma drift.

We studied the rate of decay of the 50-MHz backscattered signal when the wave polarization of the heater was changed from the ordinary to the extraordinary mode. In Figure 8 we show the time variation of echo power from a slant range of 690 km, corresponding to an altitude of 250 km above the heater, expressed in decibels above the power received outside the heated volume at a range of 645 km. Each data point represents an average over a 0.1-s time interval. An abrupt fall of echo power after 0051:40 may be noted when *O* to *X* mode switching was performed. In view of an inherent signal fluctuation with a period of about 0.5 s during the *O* mode heating, it is difficult to obtain a precise value of the  $e$ -folding time, for the decay. However, we may conclude that the  $e$ -folding time of 3-m field-aligned striations is of the order of 1 to 2 s rather than tens of seconds as reported by Minkoff and Kreppel [1976].

## DISCUSSIONS

The most interesting feature of our radio star scintillation measurements at Arecibo during ionospheric heating is the detection of a low-frequency modulation envelope of the fast scintillation structure. We showed that the period of the envelope modulation is 4–5 times the dominant fading period of scintillations. Since the dominant fading period of 430-MHz scintillations corresponds to an irregularity scale length of about 400 m, the spatial dimension of the envelope modulation is estimated to be about 1.5–2 km. Since such spatial dimensions are larger than the Fresnel zone, they cannot affect the scintillation structure through a diffractive process. However, we can explain the temporal structure of scintillations if we consider that the heater wave field intensity is spatially

TABLE 1. Results of 50-MHz Doppler Spectral Observations September 26–27, 1981

Time, AST	Radial Drift Toward South, m/s	Width of Doppler Spectra, Hz
2338	39	2.1
2343	41	2.1
2348	42	2.3
2353	41	2.3
0012	34	2.1
0017	37	2.5
0022	33	2.7
0027	30	2.1
0034	30	2.3
0039	27	2.4
0051	18	1.7
0056	16	2.0
0100	13	2.0
0106	10	2.2



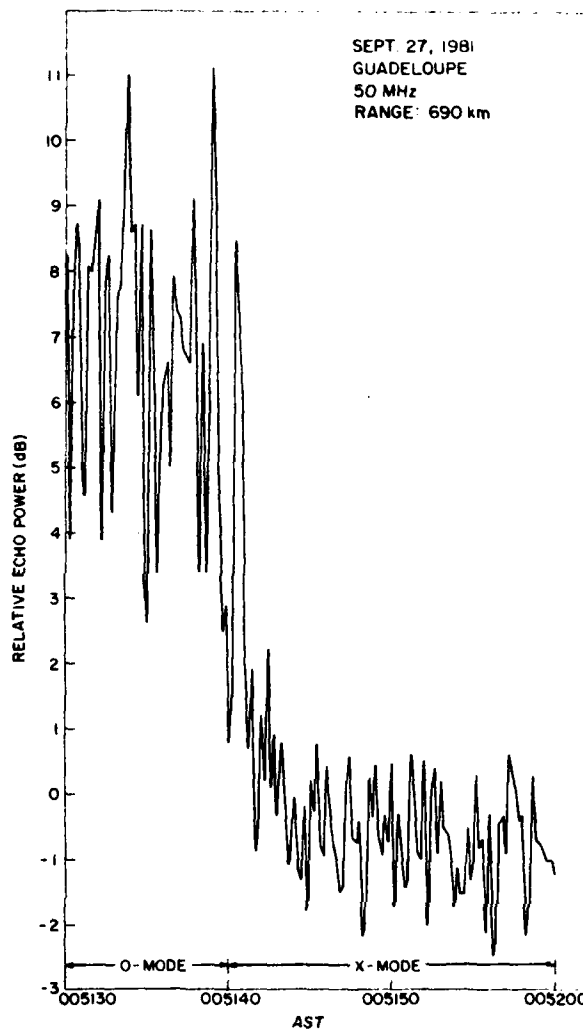


Fig. 8. Decay of 50-MHz backscattered power when wave polarization switched from *O* mode to *X* mode at 0051:40 AST on September 27, 1981.

modulated at kilometer scales through the self-focusing instability [Perkins and Valeo, 1974; Cragin et al., 1977], generating a series of "hot" spots where small-scale irregularities develop through a cascading process and are convected across the propagation path. Such a signature of large-scale spatial modulation of enhanced plasma line intensity was first detected by Duncan and Behnke [1978] at Arecibo. Recently, Farley et al. [1983] used simultaneous satellite in situ and radar data at Arecibo during ionospheric heating and established that the kilometer scale variations of electron density do indeed cause variations of similar scale in plasma line intensity. We showed that the period of the large-scale modulating structure in scintillations varies in response to a variation of heater power, as is expected from the self-focusing instability theories of both Perkins and Valeo [1974] and Cragin et al. [1977]. However, the former theory predicts that the dominant wave number should vary as the square root of the threshold power density while the latter predicts a variation proportional to the fourth root of power density. Our observations indicated that an increase of power density by a factor of 1.5 results in a decrease of irregularity wavelength by a factor of 1.1, which follows almost exactly the predictions of Cragin et al. [1977]. It should, however, be pointed out that the theoretical predic-

tions pertain to the linear theory whereas the observations presumably represent nonlinear conditions (L. M. Duncan, private communication, 1983). It is interesting to note that Farley et al. [1983] have also calculated the threshold power density from measurements of background plasma parameters and the dominant irregularity wavelength and found better agreement with the theory of Cragin et al. [1977]. We intend to test the two theories in future experiments by changing the power density over a wider range and observing the change in the period of the modulation envelope.

From a determination of scintillation index ( $S_4$ ) defined as the normalized second central moment of signal intensity it is possible to determine the irregularity amplitude  $\Delta N/\bar{N}$ , where  $\Delta N$  is the rms electron density deviation and  $\bar{N}$  the average electron density. We observed a maximum scintillation index of  $S_4 = 0.07$  at 430 MHz during the meridian transit of 3C466 on September 24, 1981. At this time the heater transmitted an *O* mode wave at 5.1 MHz, the transmitter output was 200 kW, and the height of the plasma line measured after the transit was 258 km. We assumed that the irregularity layer height was also 258 km; the irregularity layer thickness was 100 km [Livingston, 1983; J. Buchau and L. F. McNamara, private communication, 1983]; and the outer scale of turbulence was 2 km, corresponding to the low-frequency envelope modulation of the scintillation structure and the power law index of scintillation spectra as 4. By using the weak scatter theory as developed by Rino [1979], we found that the  $S_4$  index of 0.07 at 430 MHz corresponds to an irregularity amplitude of  $\Delta N/\bar{N} = 1.4\%$  if the irregularities are in the form of rods with an axial ratio of 5:1:1, the elongation corresponding to the direction of the magnetic field. If, instead, the irregularities are assumed to be sheets oriented parallel to the magnetic meridian, the irregularity amplitude required to cause the same level of scintillation is reduced. Since Duncan and Behnke [1978] observed a somewhat longer correlation length in the magnetic meridian plane as compared to the magnetic E-W direction, sheetlike irregularities in the meridian with axial ratios of 5:2:1 seem to be more appropriate. For 5:2:1 sheets an irregularity amplitude of  $\Delta N/\bar{N} = 1\%$  is sufficient to cause the same level of scintillation ( $S_4 = 0.07$ ). This estimate is within a factor of 2 of the measurement of irregularity amplitude by the Atmosphere Explorer E satellite [Farley et al., 1983]. A more careful measurement of irregularity anisotropy by spaced receiver scintillation observations is necessary. This is because of its importance in resolving differences between existing theories of self-focusing instabilities as pointed out by Farley et al. [1983].

The general form of radio star scintillation spectra observed at Arecibo having two spectral indices is substantiated by other observations of heater-induced scintillations [Erukhimov et al., 1977, 1979; Livingston, 1983]. The two-component spectrum may be qualitatively explained by considering a source region of limited altitude extent having a wide range of irregularity scale sizes with a shallow spectral index as well as the varying efficiency with which the irregularities of different scale lengths in the source region can map along the magnetic field [Farley, 1959, 1960]. In view of the fact that the large-scale irregularities are able to map more efficiently out of the source region than the small-scale irregularities, the integrated electron density deviation will be larger at the large-scale length end, giving rise to the observed steeper slopes. On the other hand, the steepness of spectral slope may arise as a result of smoothing caused by the large 305-m diameter reflec-

the irregularities. These will result in a marked attenuation of the diffracted field at spatial dimensions corresponding to half the diameter of the reflector. Since the Fresnel dimension of 430-MHz scintillation is about 400 m, the useful part of the scintillation spectrum is affected by the antenna smoothing effect. During December 23, 1980, we could make radio star scintillation measurements at a lower frequency utilizing the 46.8-MHz radar system of Max-Planck-Institut für Aeronomie (courtesy J. Röttger) temporarily stationed at Arecibo. The scintillation spectra again exhibited a steep slope between the spatial dimensions of about 300 m and 150 m, implying that the diameter of the antenna aperture dictates the range of spatial dimensions where the attenuation of power spectral density occurs rather than the antenna beam width which is frequency dependent and different at 430 MHz and 46.8 MHz. Recently, Farley *et al.* [1983] have discussed the spatial filtering effect of the Arecibo antenna on radar observations of the temporal structure of the enhanced plasma line during heating experiments.

Simultaneous 50-MHz radar backscatter and scintillation measurements provided an opportunity to study the coexistence of subkilometer and 3-m field-aligned irregularities during *O* mode heating. The quenching of small-scale field-aligned striations when the heater wave polarization is changed from *O* mode to *X* mode reconfirms that the striations are a consequence of parametric decay instability. Since the large-scale irregularities are attributed to differential heating of the electrons by a beat wave arising from the incident and scattered electromagnetic waves [Farley *et al.*, 1983], polarization of the heater wave is expected to have no effect on these irregularities. On the other hand, the field-aligned meter scale density striations, generated by the plasma turbulence resulting from parametrically excited Langmuir waves, are expected only during the *O* mode heating. This is because the extraordinary wave for which the angular frequency  $\omega > \omega_p + \frac{1}{2}\omega_H$  (where  $\omega_p$  is the plasma frequency and  $\omega_H$  the gyrofrequency) cannot parametrically excite Langmuir waves [Fejer, 1979].

As mentioned earlier, it is difficult to provide an accurate estimate for the decay time of 3-m field-aligned irregularities because of the presence of large-amplitude short-period ( $\sim 0.5$  s) fluctuations. It seems, however, that an outer bound for the e-folding time of about 1–2 s is fairly representative of our observations. This estimate is considerably shorter than 8 s obtained by Minkoff and Kreppel [1976]. The discrepancy becomes even more pronounced when one considers that these authors studied 95-cm irregularities through their 157-MHz observations. It may be mentioned that cross-field diffusion time varies directly as the square of the irregularity wavelength. We also mention here that small-scale striations exhibited a long-period modulation of the order of a minute, which is being analyzed and compared with similar modulation of scintillations.

We also determined that the 50-MHz Doppler spectra are very narrow and their bandwidths are independent of the magnitude of the ambient plasma drift. The extremely narrow width probably signifies that it is controlled by the generation mechanism rather than ionospheric drift, as predicted by theory [Lee and Fejer, 1978; Inhester *et al.*, 1981].

**Acknowledgments.** We thank the scientific and flight crew of the Air Force Geophysics Laboratory airborne ionospheric observatory for their support during these observations. We acknowledge useful discussions with M. J. Griffin, J. A. Fialer, and R. C. Foss,

A. Coster, A. Frey, and J. Dobelman for help with the radar data acquisition and processing. We also acknowledge the assistance of D. Campbell, A. Veldhuis, and the staff of the Arecibo Observatory. The work at Emmanuel College was supported by National Science Foundation (NSF) grant ATM-811130 and Air Force Geophysics Laboratory contract F19628-81-K-0011. The work at Rice University was supported by NSF grant ATM-8116046. The National Astronomy and Ionosphere Center is operated by Cornell University under contract with the National Science Foundation.

The Editor thanks B. Cragin and R. C. Livingston for their assistance in evaluating this paper.

## REFERENCES

- Basu, S., Su. Basu, A. L. Johnson, J. A. Klobuchar, and C. M. Rush, Preliminary results of scintillation measurements associated with ionospheric heating and possible implications for the solar power satellite, *Geophys. Res. Lett.*, **7**, 609, 1980.
- Basu, S., Su. Basu, S. Ganguly, J. A. Klobuchar, and C. M. Rush, Artificial irregularities generated by ionospheric heating and their effects on transionospheric propagation, *Proceedings of Symposium on the Effect of the Ionosphere on Radiowave Systems*, p. 72, Naval Research Laboratory, Alexandria, Va., 1981.
- Basu, S., Su. Basu, E. J. Weber, J. G. Moore, J. Buchau, S. Ganguly, W. E. Gordon, M. C. Lee, R. C. Livingston, B. W. Reinisch, and R. A. Behnke, Multitechnique probing of the artificially modified ionosphere over Arecibo, paper presented at National Radio Science Meeting, U.S. Natl. Comm. for URSI, Boulder, Colo., January 1982.
- Basu, S., S. Basu, S. Ganguly, and J. A. Klobuchar, Generation of kilometer scale irregularities during the midnight collapse at Arecibo, *J. Geophys. Res.*, **86**, 7607, 1981.
- Briggs, B. H., and I. A. Parkin, On the variation of radio star and satellite scintillation with zenith angle, *J. Atmos. Terr. Phys.*, **25**, 339, 1963.
- Carlson, H. C., Jr., and L. M. Duncan, HF excited instabilities in space plasmas, *Radio Sci.*, **12**, 1001, 1977.
- Cragin, B. L., J. A. Fejer, and E. Leer, Generation of artificial spread *F* by a collisionally coupled purely growing parametric instability, *Rad. Sci.*, **12**, 273, 1977.
- Duncan, L. M., and R. A. Behnke, Observations of self-focusing electromagnetic waves in the ionosphere, *Phys. Rev. Lett.*, **41**, 998, 1978.
- Duncan, L. M., and W. E. Gordon, Ionosphere: microwave beam interaction study, report, Rice Univ., Houston, Tex., September 1977.
- Ecklund, W. L., D. A. Carter, and B. B. Balsley, Gradient drift irregularities in mid-latitude sporadic *E*, *J. Geophys. Res.*, **86**, 858, 1981.
- Frukhimov, L. M., E. E. Mityakova, E. N. Myasnikov, S. V. Polyakov, A. V. Rakhlin, and V. M. Sinelnikov, Spectra of artificial ionospheric irregularities at different heights, *Radio Phys. Quantum Electron.*, Engl. Transl., **20**, 1246, 1977.
- Frukhimov, L. M., V. I. Kovalev, A. M. Lerner, E. N. Myasnikov, I. N. Poddel'skii, and A. V. Rakhlin, Spectrum of large scale artificial inhomogeneities in the *F* layer, *Radio Phys. Quantum Electron.*, Engl. Transl., **22**, 888, 1979.
- Farley, D. T., A theory of electrostatic fields in a horizontally stratified ionosphere subject to a vertical magnetic field, *J. Geophys. Res.*, **64**, 1225, 1959.
- Farley, D. T., A theory of electrostatic fields in the ionosphere at nonpolar geomagnetic latitudes, *J. Geophys. Res.*, **65**, 869, 1960.
- Farley, D. T., C. LaHoz, and B. G. Fejer, Studies of the self-focusing instability at Arecibo, *J. Geophys. Res.*, **88**, 2093, 1983.
- Fejer, J. A., Generation of large-scale field-aligned density irregularities in ionospheric heating experiments, *AGARD Conf. Proc.*, **138**, 1, 1973.
- Fejer, J. A., Ionospheric modification and parametric instabilities, *Rev. Geophys. Space Phys.*, **17**, 135, 1979.
- Fialer, P. A., Field-aligned scattering from a heated region of the ionosphere—Observations at HF and VHF, *Radio Sci.*, **9**, 923, 1974.
- Getmantsev, G. G., I. M. Frukhimov, E. E. Mityakova, N. A. Mityakov, N. M. Prytkov, V. O. Rapoport, and V. A. Cherepovitskii, Certain results of investigating ionospheric irregularities induced by powerful radio emission using background reception of satellite signals, *Radio Phys. Quantum Electron.*, Engl. Transl., **19**, 354, 1976.
- Goldman, M. V., Field-aligned instability due to stimulated scattering of intense radio waves from diffusion quasi-modes, *Radio Sci.*, **9**, 1077, 1974.

- Gordon, W. E., and J. A. Dobelman, Comparison of measured and calculated antenna patterns for the Islote heater, report, Rice Univ., Houston, Tex., 1982.
- Inhester, B., A. C. Das, and J. A. Fejer, Generation of small-scale field-aligned irregularities in ionospheric heating experiments, *J. Geophys. Res.*, **86**, 9101, 1981.
- Lee, M. C., and J. A. Fejer, Theory of short-scale field-aligned density striations due to ionospheric heating, *Radio Sci.*, **13**, 893, 1978.
- Livingston, R. C., Heater-generated intermediate-scale irregularities: Spatial distribution and spectral characteristics, *Radio Sci.*, **18**, 253, 1983.
- Minkoff, J., and R. Kreppel, Spectral analysis and step response of radio frequency scattering from a heated ionospheric volume, *J. Geophys. Res.*, **81**, 2844, 1976.
- Perkins, F. W., A theoretical model for short-scale field-aligned plasma density striations, *Radio Sci.*, **9**, 1065, 1974.
- Perkins, F. W., and E. J. Valeo, Thermal self-focusing of electromagnetic waves in plasmas, *Phys. Rev. Lett.*, **32**, 1234, 1974.
- Rino, C. L., A power law phase screen model for ionospheric scintillation, I. Weak scatter, *Radio Sci.*, **14**, 1135, 1979.
- Utlaut, W. F., and E. J. Violette, A summary of vertical incidence radio observations of ionospheric modification, *Radio Sci.*, **9**, 895, 1974.
- Santimay Basu and Sunanda Basu, Emmanuel College, 400 The Fenway, Boston, MA 02115.
- S. Ganguly and W. E. Gordon, Department of Space Physics, Rice University, Houston, TX 77001.

(Received May 9, 1983;  
revised August 5, 1983;  
accepted August 9, 1983.)

## DNA Distribution List

Berkeley Research Assoc.  
Attn: Clifford W. Prettie  
P.O. Box 983  
Berkeley, CA 94701

ESL, Inc.  
Attn: J. Marshall  
495 Java Drive  
Sunnyvale, CA 94086

Def. Nuclear Agency  
Attn: STTL Tech. Library  
Washington, D.C. 20305

Mission Research Corp.  
Attn: R. Bogush  
735 State St.  
Santa Barbara, CA 93101

Naval Research Lab.  
Attn: Dr. John Goodman  
Code 4110  
Washington, D.C. 20375

Dr. J. Aarons  
Boston University  
Boston, MA 02215

Major G. Wortham  
AFGWC/WSE  
Offutt AFB, NE 68113

Lt. P. Styczek  
SACCA/CSS  
Offutt AFB, NE 68113

Ed Skomal  
Aerospace Corp.  
Box 92957  
Los Angeles, CA 90009

Allen L. Johnson  
Air Force Avionics Lab  
AFAL/AAAI  
Wright Patterson AFB  
Ohio 45433

Dow Evelyn  
Def Nuclear Agency/RAAE  
Washington, D.C. 20305

Major L. Wittwer  
Def Nuclear Agency/RAAE  
Washington, D.C. 20305

Major R. Sutton  
SD/YKX  
P.O. Box 92960  
Worldway Postal Center  
Los Angeles, CA 90009

Dr. H. Soicher  
US Army Communication Res. and  
Development Commons  
Fort Monmouth, NJ 07703  
(DRDCO-COM-RH-4)

SRI International  
333 Ravenswood Ave.  
Menlo Park, CA 94025  
Attn: C. Rino

SRI International  
333 Ravenswood Ave.  
Menlo Park, CA 94025  
Attn: R. Livingston

Physical Dynamics, Inc.  
P. O. Box 3027  
Bellevue, WA 98009  
Attn: E.J. Fremouw

Dr. K. Davies  
NOAA  
Boulder, CO 80302

Dr. H. Mullaney  
Code 427  
Dept. of the Navy  
Office of Naval Research  
Arlington, VA 22217

Dr. George Millman  
General Electric Co.  
Building 9, Room 46  
Court Street Plant  
Syracuse, NY 13201

Prof. K.C. Yeh  
University of Illinois  
Dept. of Electric Engineering  
Urbana, IL 61801

Dr. Warren Brown  
Sandia Lab  
ORG 314  
Albuquerque, NM 87185

Dr. C.H. Liu  
60 Electrical Engineering Building  
University of Illinois  
Urbana, IL 61801

Dr. S. Ossakow  
Plasma Dynamics, Code 7750  
U.S. Naval Research Lab  
Washington, D.C. 20390

Dr. Phil McClure  
U. of Texas at Dallas  
Richardson, TX 75080

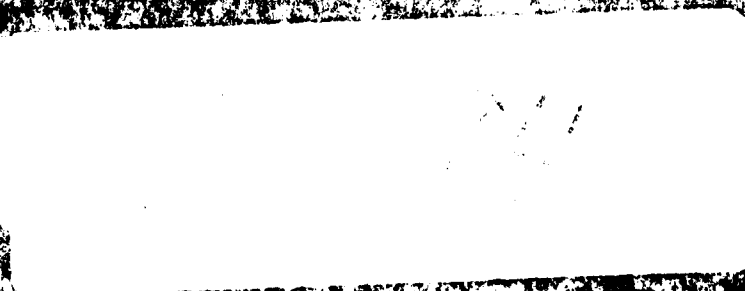
Prof. H.G. Booker  
Dept. of Applied Physics  
U. of Calif. at San Diego  
La Jolla, CA 92037

Prof. Michael Kelley  
Dept. of Elect. Engineering  
Cornell University  
Ithaca, NY 14850

Prof. W.B. Hanson  
U. of Texas at Dallas  
Richardson, TX 75080

END

FILMED



DYNAMIC